VILNIUS UNIVERSITY

Džiugas
JABLONSKAS

Nonlinear Dielectric Susceptibility Studies in $Pb(Mg_{1/3}Nb_{2/3})O_3$-based Relaxor Ferroelectrics

DOCTORAL DISSERTATION

Physical Science,
Physics (02P)

VILNIUS 2018

The dissertation has been developed during the years 2014 – 2018 in Vilnius university.

Supervisor – prof. dr. Robertas Grigalaitis (Vilnius university, Physical sciences, physics – 02P).

Dissertation is defended in the open session of defend council:

Chairman – prof. dr. Gintaras Valušis (Center for Physical Sciences and Technology, physics – 02P).

Members:

doc. dr. Edvardas Kazakevičius (Vilnius University, physical sciences, physics – 02P);

doc. dr. Valdemaras Aleksa (Vilnius University, physical sciences, physics – 02P);

prof. habil. dr. Saulius Balevičius (Vilnius University, physical sciences, physics – 02P);

prof. dr. Artūras Jukna (Vilnius Gediminas Technical University, physical sciences, physics – 02P).

Dissertation is defended in the open session in the Council of Physics of Vilnius University on 27th of September, 2018 at 14 o‘clock in auditorium 815 at faculty of physics, Vilnius university.

Address: Saulėtekio av. 3, Vilnius, Lithuania.

VILNIAUS UNIVERSITETAS

Džiugas
JABLONSKAS

Netiesinio dielektrinio jautrio tyrimai $Pb(Mg_{1/3}Nb_{2/3})O_3$ šeimos feroelektriniuose relaksoriuose

DAKTARO DISERTACIJA

Fiziniai mokslai,
fizika (02P)

VILNIUS 2018

Disertacija rengta 2014 – 2018 metais Vilniaus universitete.

Mokslinis vadovas – Prof. Dr. Robertas Grigalaitis (Vilniaus universitetas, fiziniai mokslai, fizika – 02P).

Disertacija ginama viešame gynimo tarybos posėdyje:

Pirmininkas – prof. dr. Gintaras Valušis (Fizinių ir technologijos mokslų centras, fiziniai mokslai, fizika – 02P).

Nariai:

doc. dr. Edvardas Kazakevičius (Vilniaus universitetas, fiziniai mokslai, fizika – 02P);

doc. dr. Valdemaras Aleksa (Vilniaus universitetas, fiziniai mokslai, fizika – 02P);

prof. habil. dr. Saulius Balevičius (Fizinių ir technologijos mokslų centras, fiziniai mokslai, fizika – 02 P);

prof. dr. Artūras Jukna (Vilniaus Gedimino technikos universitetas, fiziniai mokslai, fizika – 02 P).

Disertacija ginama viešame Fizikos mokslo krypties tarybos posedyje 2018 m. rugsėjo mėn. 27 d. 14 val. Vilniaus universiteto fizikos fakulteto 815 auditorijoje.

Adresas: Saulėtekio al. 3, Vilnius, Lietuva.

TABLE OF CONTENTS

ABBREVIATIONS

COR – chemically ordered region;

CW – Curie – Weiss;

FH – field heating;

LB – linear birefringence;

MPB – morphotropic phase boundary;

PE – paraelectric phase;

PLMN – $Pb(Mg_{1/3}Nb_{2/3})O_3 – 0.02La(Mg_{2/3}Nb_{1/3})O_3$;

PMN – $PbMg_{1/3}Nb_{2/3}O_3$;

PMN-xPT – $(1\text{-}x)PbMg_{1/3}Nb_{2/3}O_3\text{-}xPbTiO_3$;

PMT – $Pb(Mg_{1/3}Ta_{2/3})O_3$;

PNR – polar nano region;

PT – $PbTiO_3$;

PZ – $PbZrO_3$;

PZN – $Pb(Zn_{1/3}Nb_{2/3})O_3$

RF – relaxor ferroelectric;

RP – relaxor state;

SNR – signal to noise ratio;

SRBRF – Spherical Random Bond Random Field model;

TEM – transition electron microscopy;

TO – transverse optical;

VF – Vogel – Fulcher;

ZFC – zero-field cooling;

ZFH – zero-field heating.

INTRODUCTION

Research of relaxor ferroelectrics is an attractive field. These materials are known to be among the best piezoelectrics for application reasons. However, this work is dedicated for a fundamental research of relaxor ferroelectrics. It is mainly focused on a research of macroscopic properties of $Pb(Mg_{1/3}Nb_{2/3})O_3$ based relaxor ferroelectrics. $Pb(Mg_{1/3}Nb_{2/3})O_3$ is named as the canonical relaxor ferroelectric by many authors. However, it happened historically, because it was one of the first relaxor ferroelectrics found. Since the beginning of the research of $Pb(Mg_{1/3}Nb_{2/3})O_3$ there were many debates if it has a phase transition or not. It does show anomalies in temperature dependence of refraction index, dielectric permittivity, velocity of sound, etc. However, clear structural changes of lattice were not observed, by microscopic research techniques, as the structure remains averagely cubic in broad temperature range. Furthermore, since the beginning of research of relaxor ferroelectrics, there were attempts to apply Landou-Ginzburg-Devonshire phenomenological theory of phase transitions on temperature behavior of $Pb(Mg_{1/3}Nb_{2/3})O_3$. As well, there were attempts to write different theoretical models onto the unique behavior of relaxor ferroelectrics. It is widely accepted, that polar nano regions are responsible for the unique behavior of relaxor ferroelectrics. Those are regions of tens of nanometers of size, which depends on temperature, pressure and various additions in the crystal. Within one region all dipoles tends to orient the same direction, so sometimes polar nano regions are interpreted as superdipoles or dipole clusters, that may have flipping, breathing or both dynamical properties in electric field and non-zero temperature. Polar nano regions appear in the relaxor ferroelectrics due to an internal disordered charge distribution. However, universal theoretical model of relaxor ferroelectrics is still not found and after each attempt many debates and rhetorical questions remain.

This work contributes to the knowledge of $Pb(Mg_{1/3}Nb_{2/3})O_3$ based relaxor ferroelectrics. It confirms that enhancing chemically ordered regions do

not weaken relaxor behavior or promote a spontaneous phase transition. In order to find out more about relaxor ferroelectrics in general and to analyze them from a different perspective a non-linear susceptometer was built. The measurement method allows to measure temperature behavior of higher order susceptibilities of material without influencing internal electric fields of the sample. That method may give useful data on phase transitions occurring in the material. As well, it is more sensitive to changes of dipolar dynamics of the sample. Thanks to this unique measurement technique a phase transition was found in $0.83Pb(Mg_{1/3}Nb_{2/3})O_3 - 0.17PbTiO_3$ single crystal. As well, it opened new perspective of observation of dipolar dynamics of Mn-doped $0.9Pb(Mg_{1/3}Nb_{2/3})O_3 - 0.1PbTiO_3$ ceramics. $PbTiO_3$ is normal ferroelectric material and many authors try to find occurrence of phase transition threshold of relaxor – normal ferroelectric solid solutions, that is called morphotropic phase boundary. This region of phase diagram is important for application reasons, as solid solutions of this specific mixture has best piezoelectric and tunability properties.

Finally, this work definitely gives contribution to fundamental knowledge of $Pb(Mg_{1/3}Nb_{2/3})O_3$ based relaxor ferroelectrics. Furthermore, it opens doors to a different perspective to these materials, by introducing a variant of non-linear susceptometer and various application examples of it.

2.1 GOALS AND TASKS OF THE WORK

The main goal of the work is to improve current fundamental knowledge of $Pb(Mg_{1/3}Nb_{2/3})O_3$ – based relaxor ferroelectrics, which can be branched into following tasks:

1. Perform linear dielectric spectroscopy of $0.98Pb(Mg_{1/3}Nb_{2/3})O_3 - 0.02La(Mg_{2/3}Nb_{1/3})O_3$ single crystal and compare it with properties of pure $Pb(Mg_{1/3}Nb_{2/3})O_3$ single crystal. Perform calculations of distributions of relaxation times of both crystals that help to find correlation between behavior of polar nano regions and La-doping.

2. Create a computer controlled non-linear susceptometer. That is unique and new measurement method. Based on non-linear susceptibility response useful data on phase behavior and collective behavior of dipoles of material may be derived.
3. Find out, if there is a phase transition in $0.83Pb(Mg_{1/3}Nb_{2/3})O_3 - 0.17PbTiO_3$ single crystal.
4. Find out the influence of Mn-doping on $0.9Pb(Mg_{1/3}Nb_{2/3})O_3 - 0.1PbTiO_3$ ceramics.

2.2 STATEMENTS OF THE DOCTORAL THESIS

1. It is necessary to calibrate a phase shift between current and voltage caused by measurement equipment, in order to obtain precise results in higher frequencies of non-linear susceptometer.
2. There is an occurrence of phase transition in $0.83Pb(Mg_{1/3}Nb_{2/3})O_3 - 0.17PbTiO_3$ single crystal from relaxor to normal ferroelectric phase.
3. Mn-doping of $0.9Pb(Mg_{1/3}Nb_{2/3})O_3 - 0.1PbTiO_3$ ceramics causes pinning of polar nano regions.
4. Significant increase of chemically ordered regions in $Pb(Mg_{1/3}Nb_{2/3})O_3$ single crystal, due to La-doping, does not reduce relaxor ferroelectric behavior and does not lead to an occurrence of spontaneous phase transition.

2.3 SCIENTIFIC NOVELTY

Dielectric spectra in frequencies higher than 1 MHz in broad temperature range of $0.98Pb(Mg_{1/3}Nb_{2/3})O_3 - 0.02La(Mg_{2/3}Nb_{1/3})O_3$ was presented for the first time. Distribution of relaxation times of $0.98Pb(Mg_{1/3}Nb_{2/3})O_3 - 0.02La(Mg_{2/3}Nb_{1/3})O_3$ was presented for the first time. Obtained results on comparison of $Pb(Mg_{1/3}Nb_{2/3})O_3$ and $0.98Pb(Mg_{1/3}Nb_{2/3})O_3 - 0.02La(Mg_{2/3}Nb_{1/3})O_3$ single crystals led to confirmation that increase of size of chemically ordered regions does not promote a phase transition.

Non-linear susceptometer is great tool for characterizing phase transitions in materials. It helps to unambiguously recognize the order of a phase transition. Furthermore, non-linear response of the material is more sensitive to changes in motions of dipoles. Overall, all the features of the non-linear susceptometer makes it a valuable tool in investigations of relaxor ferroelectrics – materials that have anomalies in physical parameters, due to complex dipolar evolution, which provoke scientific discussions about the occurrence of the spontaneous phase transitions. Hence, the unique variant of non-linear susceptometer was constructed. The unique software was programmed. Innovative phase shift calibration procedure was included into the system. Furthermore, this susceptometer uses the digital data acquisition module for a signal generation and data acquisition, while other authors use a separate signal generator. It is worth to mention, that non-linear susceptometers are not available commercially.

Non-linear dielectric spectroscopy on poled and non-poled samples of $0.83Pb(Mg_{1/3}Nb_{2/3})O_3 - 0.17PbTiO_3$ was performed for the first time. Non-linear susceptometer helped to distinguish a phase transition in $0.83Pb(Mg_{1/3}Nb_{2/3})O_3 - 0.17PbTiO_3$. Non-linear dielectric spectroscopy on Mn-doped $0.9Pb(Mg_{1/3}Nb_{2/3})O_3 - 0.1PbTiO_3$ ceramics was performed for the first time. Pinning of polar nano regions due to Mn addition was reported.

2.4 PUBLICATIONS

1. D. Jablonskas, R. Grigalaitis, J. Banys, A. A. Bokov, Z.-G. Ye, Broadband dielectric spectra in $PbMg_{1/3}Nb_{2/3}O_3$ crystals with chemical ordering modified by La doping, *Appl. Phys. Lett.*, vol. **107**, Issue 14, p. 142905, 2015, doi: 10.1063/1.4932656.
2. D. Jablonskas, M. Ivanov, R. Grigalaitis, J. Banys, Implementation of an improved non-linear susceptometer, *Ferroelectrics*, vol. **513**, Issue 1, p. 32-37, 2017, doi: 10.1080/00150193.2017.1350071.

3. Š. Svirskas, D. Jablonskas, V. Samulionis, S. Kojima, J. Banys, Is there a spontaneous ferroelectric phase transition in $0.83PbMg_{1/3}Nb_{2/3}O_3$-$0.17PbTiO_3$ single crystal?, *J. All. Comp.*, vol. **748**, p. 127-133, 2018, doi: 10.1016/j.jallcom.2018.03.130.
4. Š. Svirskas, D. Jablonskas, V. Samulionis, A. Kuprevičiūtė, J. Banys, S. J. Chin, T. McNally, Effect of $Mo_6S_3I_6$ nanowires on dielectric properties of poly(ε-caprolactone), *Phys. stat. sol. (a)*, vol. **210**, Issue 11, p. 2272-2277, 2013, doi: 10.1002/pssa.201329313.
5. D. Jablonskas, S. Lapinskas, S. Rudys, M. Ivanov, J. Banys, Full-wave finite space model of open-ended coaxial line for dielectric spectroscopy of liquids, *Rev. Sci. Instrum.*, vol. **88**, Issue 8, p. 084703, 2017, doi: 10.1063/1.4991312.
6. D. Jablonskas, M. Ivanov, J. Banys, G. A. Giffin, S. Passerini, Dielectric spectroscopy of Pyr_{14}TFSI and Pyr_{12O1}TFSI ionic liquids, *Electrochim. Acta*, 2018, doi: 10.1016/j.electacta.2018.04.104.

2.5 PRESENTATIONS AT THE CONFERENCES

D. Jablonskas, R. Grigalaitis, Z.-G. Ye, A. A. Bokov, „Dielectric properties of $0.98Pb(Mg_{1/3}Nb_{2/3})O_3 - 0.02La(Mg_{2/3}Nb_{1/3})O_3$ crystal,“ in 39th Lithuanian national physics conference, Vilnius, Lithuania, p. 99, 6-8 October (2011)

D. Jablonskas, R. Grigalaitis, J. Banys, Z.G. Ye, A.A. Bokov, „Dielectric Properties of 0.98Pb(Mg1/3Nb2/3)O3 – 0.02La(Mg2/3Nb1/3)O3 Crystal,“ International conference „Functional materials and nanotechnologies”, Riga Latvia, p.143, 17-20 April, (2012).

D. Jablonskas, R. Grigalaitis, Z. - G. Ye, A. A. Bokov, „Dielectric properties of 0.98Pb(Mg1/3Nb2/3)O3 – 0.02 La(Mg1/3Nb2/3)O3 crystal,“ 55th Scientific conference for young students of physics and

natural sciences Open Readings 2012, Vilnius, Lithuania, p 84, 28 – 31 March, (2012).

D. Jablonskas, J. Banys, R. Grigalaitis, Z. – G. Ye, A. A. Bokov, „Dielectric properties of $0.98Pb(Mg_{1/3}Nb_{2/3})O_3$-$0.02La(Mg_{2/3}Nb_{1/3})O_3$ crystal," ISAF ECAPD PFM, Aveiro, Portugal, p. 480 - 481, 9 – 13 July (2012).

D. Jablonskas, A. Kupreviciute, S. Svirskas, V. Samulionis, J. Banys, T. McNally, „ Broadband dielecttric spectroscopy and ultrasonic investigations of composites of poly(ε-caprolactone) and $Mo_6S_3I_6$ nanowires," 56th Scientific conference for young students of physics and natural sciences Open Readings 2013, Vilnius, Lithuania, p 155, 20 – 23 March, (2013).

D. Jablonskas, A. Kupreviciute, S. Svirskas, V. Samulionis, J. Banys, T.McNally, „Broadband dielecttric spectroscopy and ultrasonic investigations of composites of poly(ε-caprolactone) and $Mo_6S_3I_6$ nanowires," FM&NT-2013, Tartu, Estonia, p 19, 21 – 24 April (2013).

D. Jablonskas, S. Svirskas, V. Samulionis, J. Banys, T. McNally, „Dielectric and ultrasonic investigations of composites of poly(ε-caprolactone) and $Mo_6S_3I_6$," 40th Lithuanian national physics conference, Vilnius, Lithuania, p. 47, 10 - 12 June (2013).

D. Jablonskas, R. Grigalaitis, J. Banys, Z. – G, Ye, A. A. Bokov, H. N. Tailor, „Distribution of relaxation times of $Pb(Mg_{1/3}Nb_{2/3})O_3$ – $La(Mg_{2/3}Nb_{1/3})O_3$ crystal," International workshop on realxor ferroelextrics, Saint Petersburg, Russia, p. 179 – 180, 1 – 6 July (2013).

D. Jablonskas, R. Grigalaitis, J. Banys, Z. - G. Ye, A. A. Bokov, „Distribution of relaxation times of $Pb(Mg_{1/3}Nb_{2/3})O_3$ – $La(Mg_{2/3}Nb_{1/3})O_3$ crystal," 13th International Meeting on Ferroelectricity (IMF-13), Kraków, Poland, p.373 - 374, 1 – 6 September (2013).

D. Jablonskas, S. Lapinskas, S. Rudys, M. Ivanov, J. Banys, "Multimode finite space model for open – ended coaxial line dielectric spectroscopy," DYPROSO XXXIV, Vienna, Austria, p. 84, 15 – 19 September (2013).

D. Jablonskas, M. Ivanov, J. Banys, V. Trepakov, M. Makarova, A. Dejneka, „Microwave Dielectric Measurements of Mn-Doped Perovskite-Type $SrTiO_3$ nanopowders," Joint International Symposium RCBJSF – 2014 - FM&NT, Riga, Latvia, p. 179, 29 September – 2 October (2014).

A. A. Bokov, D. Jablonskas, R. Grigalaitis, J. Banys, Z. – G. Ye, „Multiple relaxation and characteristic temperatures in $PbMg_{1/3}Nb_{2/3}O_3$:La relaxor ferroelectric crystals," in Fundamental physics of ferroelectrics 2015, Knoxville, TN, USA, p. 55 – 56, 25 - 28 January (2015).

D. Jablonskas, S. Lapinskas, S. Rudys, M. Ivanov, J. Banys, „Full-Wave Finite Space Model of Open-Ended Coaxial Line for Dielectric Spectroscopy of Fluids and Powders," in 41st Lithuanian national physics conference, Vilnius, Lithuania, p. 188, 17 – 19 June (2015).

D. Jablonskas, S. Lapinskas, S. Rudys, M. Ivanov, J. Banys, „Full-Wave Finite Space Model of Open-Ended Coaxial Line for Dielectric Spectroscopy of Fluids and Powders," 13th European meeting on Ferroelectricity, Porto, Portugal, p. P2_5, 28 June – 3 July (2015).

D. Jablonskas, S. Lapinskas, S. Rudys, M. Ivanov, R. Grigalaitis, J. Banys, „Full – wave finite space model of open – ended coaxial line for dielectric spectroscopy of fluids anf powders," COST Action IC1208 Joint 6th Management Committee Meeting, Budapest, Hungary, p.3, 3 – 4 September (2015).

J. Banys, A. Sakanas, C. E. Ciomaga, L. Curecheriu, V. Buscaglia, M. M. Vijatović Petrovic, R. Grigalaitis, M. Ivanov, S. Svirskas, D. Jablonskas, L. Mitoseriu, J. D. Bobic, B. D. Stojanovic, S. Kamba,

„Multiferroic Composites,“ Joint 13th International Symposium RCBJSF – international workshop on relaxor ferroelectrics, Matsue, Japan, p. 17, 19 – 23 June (2016).

D. Jablonskas, M. Ivanov, R. Grigalaitis, J. Banys, “Implementation of an improved non-linear susceptometer,” Joint 13th International Symposium RCBJSF – international workshop on relaxor ferroelectrics, Matsue, Japan, p. 23, 19 – 23 June (2016).

D. Jablonskas, M. Ivanov, J. Banys, G. A. Giffin, S. Passerini, „Dielectric Spectroscopy of Pyr_{14}TFSI and Pyr_{12O1}TFSI Ionic Liquids,” in Joint IEEE ISAF ECAPD PFM, Darmstadt, Germany, p. 19, 21-25 August (2016).

D. Jablonskas, M. Ivanov, J. Banys, G. A. Giffin, S. Passerini, “Dielectric Spectroscopy of Pyr_{14}TFSI and Pyr_{12O1}TFSI Ionic Liquids,” LUP IV, Palanga, Lithuania, p. 68, 5 – 9 September (2016).

J. Banys, S. Svirskas, D. Jablonskas, S. Lapinskas, S. Rudys, R. Grigalaitis, „Measurement of electrical properties of materials at microwaves,“ 6th Seminar Properties of ferroelectric and superionic systems, Uzhhorod, Ukraine, p. 8, 17 – 18 November (2016).

D. Jablonskas, M. Ivanov, S. Lapinskas, S. Rudys, J. Banys, „Versatile coaxial line method for dielectric spectroscopy of fluids,“ Modern Multifunctional Materials and Ceramics, Vilnius, Lithuania, p. 14, 19 – 20 April (2017).

D. Jablonskas, M. Ivanov, J. Banys, G. A. Giffin, S. Passerini, ”Static dielectric permittivity of Pyr_{14}TFSI and Pyr_{12O1}TFSI ionic liquids,” FM&NT-2017, Tartu, Estonia, p 97, 24 – 27 April (2017).

D. Jablonskas, M. Ivanov, R. Grigalaitis, J. Banys, “Application of non-linear susceptibility measurement method to ferroelectric materials,” FM&NT-2017, Tartu, Estonia, p 151, 24 – 27 April (2017).

D. Jablonskas, M. Ivanov, R. Grigalaitis, J. Banys, “Investigation of non-linear susceptibility or some relaxor ferroelectrics”, International Meeting on Ferroelectricity, San Antonio, TX, USA (2017).

2.6 AUTHORS CONTRIBUTION

The broadband dielectric spectroscopy of pure $Pb(Mg_{1/3}Nb_{2/3})O_3$ and $0.98Pb(Mg_{1/3}Nb_{2/3})O_3 - 0.02La(Mg_{2/3}Nb_{1/3})O_3$ single crystals was made by the author, as well as the data analysis of dielectric spectra and calculations of distributions of relaxation times, which were published in scientific publication and many conferences.

The author is the main creator of the non-linear susceptometer. The programming, modeling and testing of the susceptometer was carried out by the author with consultations with doc. M. Ivanov. All non-linear susceptibility measurements are performed by the author. Presentations and publication on non-linear susceptometer were prepared by the author. The author contributed with the non-linear susceptibility data to publication on PMN-0.17PT single crystal.

Furthermore, the author is the main creator of equipment for dielectric spectroscopy of liquids, which was made according the theoretical model of dr. S. Lapinskas. All the results of dielectric spectroscopy of powders and liquids were carried out by the author.

OVERVIEW

3.1 PHYSICAL PHENOMENA OF RELAXOR FERROELECTRICS

A definition of relaxor ferroelectric (RF) is rather vague. It is conventional to use a series of physical characteristics in order to define this family of materials. Hence, RF is a material that has [1]:

1) Anomalously high and broad peak of dielectric permittivity. In earlier literature it is called „diffused“;

2) The peak of dielectric permittivity shifts towards higher temperatures with increase of frequency. Such behavior is caused by wide distribution of relaxation times;

3) The anomaly in temperature dependence of dielectric permittivity is not related to any structural phase transition. Furthermore, the average structure of RFs remains the same throughout the wide temperature range, within which the anomaly is observed.

The responsibility for such behavior is credited to polar nano regions (PNRs) – regions of sizes of tens of nanometers that consist of many strongly correlated dipoles. PNRs are often interpreted as large dipoles. It is believed, that PNRs appear in temperatures below characteristic temperature T_B – Burns temperature. T_B is much higher than the temperature T_m that corresponds to anomaly of dielectric permittivity [2]. For this reason, it is usual to use definition of relaxor state (RP) that is different from the paraelectric phase (PE), however the average structure of lattice remains the same [1]. Throughout this work only perovskite structure RFs are considered, however there are other structure materials that show behavior similar to RFs, e.g. tetragonal tungsten bronze structure ($Sr_xBa_{1-x}Nb_2O_6$ [3], $Ca_xBa_{1-x}Nb_2O_6$ [4], etc.).

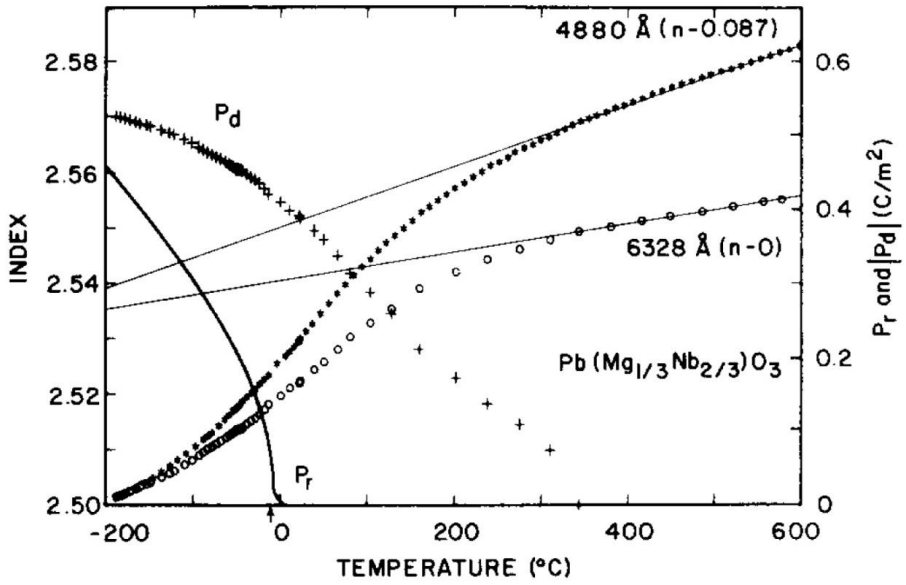

Figure 3.1.1 The indices of refraction at 6328 Å (o) and at 4880 Å (*). P_d – is the local polarization, P_r – is the reversible spontaneous polarization [5].

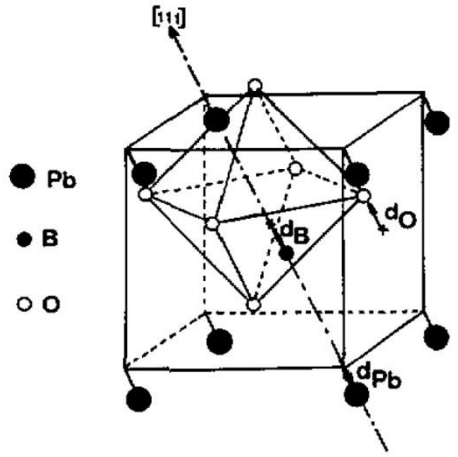

Figure 3.1.2 Rhombohedral structure of the locally polar nanoregions at 5 K [6]. The atomic shifts consists of Pb and Mg/Nb antiparallel shifts against the oxygen atoms along a [111].

The canonical RF is considered to be $PbMg_{1/3}Nb_{2/3}O_3$ (PMN). In early works of Burns et al. [2,5] the so called Burns temperature T_B of PMN was determined by measuring temperature dependence of refraction coefficient $n(T)$. At this characteristic temperature (which is much higher than the temperature of maximum of dielectric permittivity T_m) $n(T)$ starts to deviate away from the linear dependence on temperature (Figure 3.1.1). In ordinary perovskite ferroelectric materials $n(T)$ variation becomes proportional to the

square of spontaneous polarization below a phase transition temperature T_C [2]. Similar result was observed in PMN below T_B. This result led to conclusion that T_B indicates the appearance of PNRs, which supposed to be responsible for specific behavior of RF materials. “These results can be explained by the appearance of small regions of crystal having polarization. This polarization would exist on the scale of several unit cells rather than macroscopic dimensions. The local fields in the small volume due to the particular arrangement of atoms and defects cause the local distortion of the atoms and determine the volume of distortion and the direction of polarization” [2]. “Just below T_B, polarization develops in local regions, of the order of several unit cells in size that are richer in Nb^{5+} ions than the average chemical formulae. As the temperature is lowered these regions can grow and other regions, less rich in Nb^{5+} ions can also develop a polarization.” [5].

The X-ray and neutron diffraction experiment showed that at the temperature of 5 K the orthorhombic symmetry is as probable as rhombohedral symmetry in PMN perovskite structure. As well, it showed two sources of polarity, i.e. the atomic shifts and polar phase existence. The atomic shifts consists of Pb and Mg/Nb antiparallel shifts against the oxygen atoms along a [111] (or a [110]) axis [6] (Figure 3.1.2). These atomic shifts contribute to polarity of the crystal, but that is not the only contribution to polarity. Additionally, polar phase was determined within a crystal. The length of polar correlation was found to be ≈ 100 Å, and a definition of PNRs introduced, i.e. zones within the crystal of ≈ 100 Å, in which the average polarization is different from zero. Polarization intensity may vary in PNRs and the polar direction may differ from one PNR to another. However, the observed phenomena are valid for two models [6]:

1) The crystal is made of islands of polar ordered nano domains (first phase) immersed inside a disordered paraelectric host lattice (second phase).

2) The crystal is made of a pavement of polar nano domains (first phase). Taking into account that the interdomain regions may be more important than the domain size, the interdomain volume cannot be neglected (second phase).

Hence, finding the correct model of RF remains an open question.

Transmission electron microscopy (TEM) experiment at room temperature conducted by Z. Xu et al. [7] on $PbTiO_3$ (PT) doped PMN, showed the clear existence of polar nano structures within the sample, that supposed to be PNRs. Furthermore, it was shown that it is possible to control the size and distribution of these polar structures with variation of concentration of dopant. In this case, 0.9PMN-0.1PT shows existence of PNRs of average size of 50 Å, while in sample of 0.8PMN-0.2PT had PNRs of sizes up to 100 – 150 Å at room temperature [7]. Still, there might be structural difference of polar nano structures and surrounding matrix. Hence, it is worth analyzing the local structure of RFs.

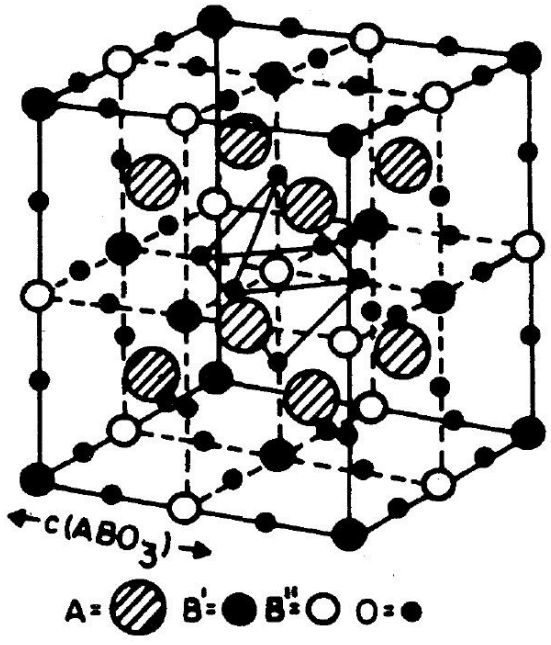

Figure 3.1.3 The F-centered ordering of B-site cations in $Pb(B'_{1/2}B''_{1/2})O_2$ [8].

PMN belongs to ABO_3 perovskite family branch of complex lead based perovskites. In a cubic perovskite structure, the A-cations occupy the corner positions of the cube, the B-cations occupy the body center position, and the

oxygen anions are situated at the face-centered positions [8]. Lead based perovskite means, that A-site is occupied solely by Pb^{2+}-cations. Complex perovskite means, that B-site is occupied by one of two cations interchangeably. General formula of such compounds may be written as $Pb(B'_xB''_{1-x})O_3$ (Figure 3.1.3). There are two cases of x distinguished. In case of $x = 1/2$ the structure is called stoichiometric, because B-site order results in average valence of +4, and the case of PMN, where $x = 1/3$, is called non-stoichiometric, because average valence is less than +4 [8,9]. According to TEM studies, complex lead perovskites were classified to groups according the scale of the ordering of B-site cations. Group I – perovskites possessing no detectable order (< 2 nm); group II – ordered with long coherency (≥ 100 nm); III – ordered, but on a nanoscale or short coherency (2 – 5 nm). The cations are said to be ordered when nearest neighbors on the B-sublattice are unlike and next nearest neighbors are similar [8]. However, clear explanation on why short coherency in B site of PMN gives RF behavior is required.

Mehmet A. Akbas et al., conducted X-ray diffraction and TEM experiments on as sintered and annealed pure $Pb(Mg_{1/3}Ta_{2/3})O_3$ (PMT) and $PbZrO_3$ (PZ) doped PMT ceramics. Dark field TEM images of pure PMT in the as-sintered form (1225° C, 1 h) confirmed that the microstructure is similar to the PMN-type systems and contains 2 – 3 nm ordered domains that are dispersed in a disordered matrix [10,11]. After a heat treatment at 1325° C for 45 h, it was observed that domain size increased significantly to ≈ 10 nm and the sample was at least 70 % ordered. Multiple annealing attempts to get larger ordered domain sizes on pure PMT proved to give no better results. In contrast, 0.95PMT-0.05PZ after normal sintering (1225° C) had ≈ 20 % of sample volume ordered in very small, ≈ 2 – 3 nm domains. However, after high-temperature annealing (1325 °C, 48 h), ≈ 95 % of the sample was ordered in domains that approach 100 nm. Because the RF effect is related to the degree of cation order, the structure changes that are induced by high-temperature heat treatments might be expected to modify the dielectric response of the PMT-PZ

solid solutions. Although, dielectric data of annealed PMT-PZ showed small reduction of the magnitude (≈ 13 %) and shift of 7° C of permittivity maximum. This result clearly showed that nano level ordering and compositional segregation are not necessary requirements for relaxor behavior in the PMN type perovskites [10]. RF characteristics of PMT-PZ and other PMN-type systems are directly attributable to the random distribution of the magnesium and tantalum cations (and zirconium) on the B' positions of the 1:1 ordered structure. In case of PMN, the perovskite structure is $Pb(B'_{1/2}B''_{1/2})O_3$, where B" position is solely occupied by Nb^{5+}-cation and B' position is occupied by random distribution of 2:1 of Mg^{2+} and Nb^{5+}. The final structure can be written as $Pb[(Mg^{2+}_{2/3}Nb^{5+}_{1/3})_{1/2}(Nb^{5+})_{1/2}]O_3$. And so the "random site" model for structure of RFs was born.

So far, it is agreed that, PMN has PNRs, which appear at T_B, because of structural disorder. The relaxor behavior, as well as PNRs, remains down to temperatures of 5 K, despite the volume fraction of induced by annealing ordered regions within the sample. This brings us to the discussion of temperature evolution of PNRs.

Xu et al., performed a high resolution diffuse neutron scattering on PMN single crystal [12]. Their experiment took part in wide temperature range, i.e. 10 K – 650 K. It allowed them to observe measurable diffuse scattering intensity at 400 K. Temperature dependence of the real-space correlation length ξ, which is a direct measure of the length scale of the static PNRs, allowed to observe, that the PNRs are small when they first appear at high temperatures, with average size of 15 Å. At low temperatures the length scale of the PNRs reaches ≈ 65 Å. Furthermore, below 300 K small PNRs merge together forming large clusters of PNRs. Previous experiments of Wakimoto et al. [13] showed that the transverse optic (TO) mode phonon become over damped near the zone center at temperature of 600 K, which is roughly the temperature at which PNRs start to appear. Conclusion follows that the PNRs may originate from the condensation of the soft TO mode. However, the soft

mode extends to much lower temperatures than T_m in PMN [13]. The phase below T_m is believed to be recently discovered phase *X* [14,15], which exhibits an average cubic structure. However, unlike conventional ferroelectric phase transition, no macroscopic lattice distortion has been observed. Diffuse neutron scattering experiment led to interpretation that at Burns temperature T_B, the soft TO phonon mode becomes over damped near the zone center and formation of PNRs starts. PNRs form with polarization along <111> directions. The number and size of PNRs increases with cooling. At T_m, a large scale overall „freezing" of PNRs occurs. Small PNRs start to merge into larger ones and total volume of PNRs increasing. The soft-mode lifetime increases below T_m and the over damping near the zone center disappears. A macroscopic polar phase without lattice distortion establishes. Below T_m PNRs grow slowly with cooling. However, if the coupling between the PNRs and surrounding lattice is not sufficiently strong, as is the case of pure PMN, then the energy barrier created by the uniform phase shift would prevent the PNRs merging further and forming macroscopic lattice distortions. The resulting phase have average cubic structure, but with embedded (rhombohedrally) polarized PNRs [12,13,16–18].

The PMN RF temperature behavior picture was improved by Dkhil et al. The team performed acoustic emission radiation experiments on PMN and other RFs [19]. He found an anomaly at temperature $T^* \approx 500$ K, which surprisingly was observed in various lead based RFs. Additionally, they performed XRD experiment and obtained a temperature dependence of lattice parameter. Two distinct changes were detected on the lattice parameter above 400K: T_B was found out to be associated with a weak change in slope and the most interestingly – the appearance of a plateau below T^* was observed. Experiments with various RF compounds revealed, that despite the difference of T_B, T^* remains the same. Furthermore, it was found out, that T_B and T^* are independent on the B-site cation ordering, as well as independent on amount of dopant PT in PMN crystal. Authors claim, that temperature T^* should be

associated with lead cations and/or oxygen network. Lead is known to be responsible for the main polarization in lead-based relaxors [20]. Hence, at *T** polar nanoclusters become static and marks beginning of static correlation of nanoclusters, that leads to anomalous behavior of RFs [19].

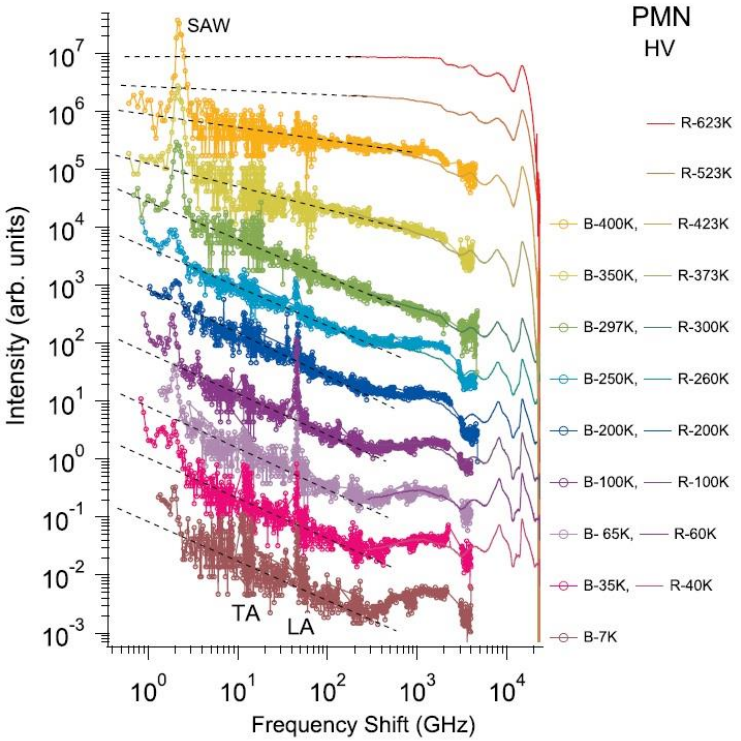

Figure 3.1.4 Temperature variation of power law light-scattering spectrum in PMN. The open circles that are connected by lines represent the spectra recorded by a tandem FP (Brillouin spectra), and the solid lines are the spectra recorded by a triple diffraction monochromator. The temperatures of the Brillouin and Raman spectra (indicated as B- and R-, respectively, in the legend) are not exactly the same, and differ by as much as 10% [21].

Very interesting observation was published by Koreeda et al. The scientists performed a light-scattering spectroscopy experiment on PMN single crystals. The frequency range of their experiment covered the Rayleigh, Brillouin, and Raman scattering regimes [21]. They found out, that intensity spectrum starts to show a power law component in temperatures < 623 K (in log-log scale) in frequency range < 1 THz, which spans more than 3 decades. The tilting of the spectrum increases with decrease of temperature. At temperatures < 200 K slope of intensity spectrum remains constant (Figure 3.1.4) The emergence of the power-law spectra suggests that there is a wide

distribution of relaxation times and the spectrum can be expressed as superposition of many Lorentzians. The conclusion was derived that the existence of a power-law distribution of relaxation times, directly suggests that there is a structural self-similarity [22], which is commonly known as fractal.

J. Hlinka stressed certain contrast to the widely accepted RF behavior. He made an observation that the very basic and famous concepts like PNRs or morphotropic phase boundary are vividly debated in the scientific community and their precise meaning is still questioned [23]. Other authors expressed worries about the meaning of the Burns temperature [24] and about the very existence of PNRs as static entities [25]. J. Hlinka remarks three most important properties of PMN RF. Firstly, symmetry remains cubic even below the freezing temperature ($T_F \approx 220$ K), unless it is cooled in relatively strong external electric field (over 2 – 3 kV/cm) [26]. Secondly, the occurrence of the shift of dielectric permittivity maximum towards the higher temperatures with increase of measurement frequency. This change is rather well described by the Vogel – Fulcher law and indicates some kind of polarization fluctuations undergoing a glass-like freezing [19]. Thirdly, anomalous temperature dependence of refractive index at Burns temperature ($T_B \approx 630$ K of PMN) [5]. He suggests an explanation of behavior of PMN without using the concept of PNRs. The quadric deviation from the paraelectric reference of the refraction index may be caused by enhancement of the amplitude of the soft mode fluctuations, which typically occur in THz range. The occurrence of shift of dielectric maximum, alternatively, may be caused by the dynamics of a dense system ferroelectric domain walls. However, one has to assume that the domains are of nanometric size or domain walls are fractal with dimensions at the nano scale. Such distribution of domains, may prevent the macroscopic change of the structure, as it may provoke laminate structure with planar ferroelastic twin walls extending over macroscopic dimensions [23]. These observations truly highlight the fundamental interest of RFs and give a request for further scientific work on physics of the material family.

3.2 MACROSCOPIC PROPERTIES OF RELAXOR FERROELECTRICS

Above is reviewed the variety of experiments performed on RFs in order to find out the origins of their unique behavior. No less important are experiments of dielectric spectroscopy on RFs. Moreover, this work is the mostly concentrated on dielectric response of PMN based RFs. Hence, below are briefly overviewed interesting works on research of macroscopic properties of RFs.

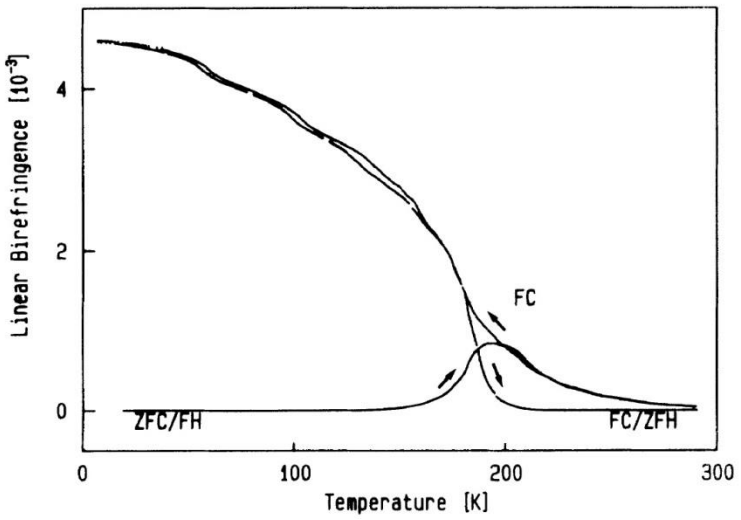

Figure 3.2.1 Temperature dependence of the linear birefringence in the (001) plane of PMN induced by an electric field E = 3.3 kV/cm along [110] [26]

Optical experiments conducted by Westphal et al. [26] showed interesting results. They measured temperature dependence of linear birefringence (LB) of PMN crystal in three different regimes: 1) field heating after zero-field cooling (ZFC/FH) with E = 3.3 kV/cm in temperature range of 5 to 300 K; 2) field-cooling (FC) down to 5 K with E = 3.3 kV/cm; 3) subsequent ZFH again up to 300 K (Figure 3.1.1). At $T \leq 160$ K the system appears completely frozen. Zero LB in ZFC/FH curve indicates a random distribution of spontaneously polarized domains and their complete immobility. On the other hand, nearly perfect coincidence of the large induced LB upon FC and subsequent ZFH shows the thermal stability of the polarized state once frozen in. As well, authors performed time dependence measurements of LB, which allowed them

to suppose, that the temporal behavior of the LB describes growth of a percolating paraelectric cluster within the homogeneously polarized single domain, which is stochastically pinned to the RF distribution. Very probably the paraelectric cluster is fractal as its growth is described by power law. Authors claim, that the most convincing piece of evidence for the ferroelectric nature of PMN is the observation of an extra peak in the dielectric permittivity when applying an ordering field to the domain state (Figure 3.2.2). The clear difference can be observed between ZFC an FH curves. Very clearly the field of 4 kV/cm induces net, albeit broadened, peaks at temperature of ≈ 212 K. They are superimposed on the usual broad background. This is a consequence of partial poling of the network of nonpercolating ferroelectric clusters, that supposed to appear at T_B [5].

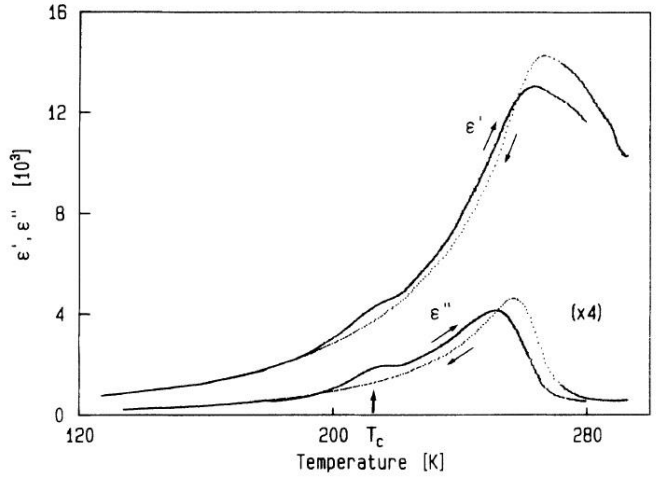

Figure 3.2.2 Dielectric permittivity measured at 10^3 Hz upon zero-field cooling and successive field heating with E = 4 kV/cm as indicated by arrows [26]

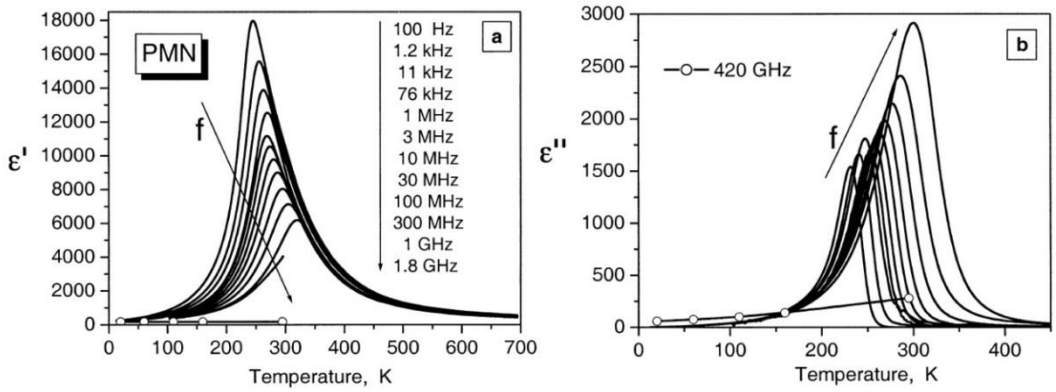

Figure 3.2.3 Temperature dependence of dielectric permittivity of PMN single crystal [27]

V. Bovtun et al. investigated dielectric properties of PMN single crystal in wide temperature and frequency range [27]. The obtained results show typical RF behavior (Figure 3.2.3), i.e. low-frequency dielectric permittivity ε^* is very high and diffused $\varepsilon'(T)$ is observed at T_m, i.e. the peaks of $\varepsilon'(T)$ and $\varepsilon''(T)$ move towards higher temperatures on increasing frequency. The nearly temperature independent (below 300 K) value $\varepsilon' = 175$ at 420 GHz proves that phonon contribution is much lower than the low-frequency maximum $\varepsilon'(T_m)$. Dielectric dispersion takes place in the whole investigated frequency range and in a broad temperature region both below and above T_m [27].

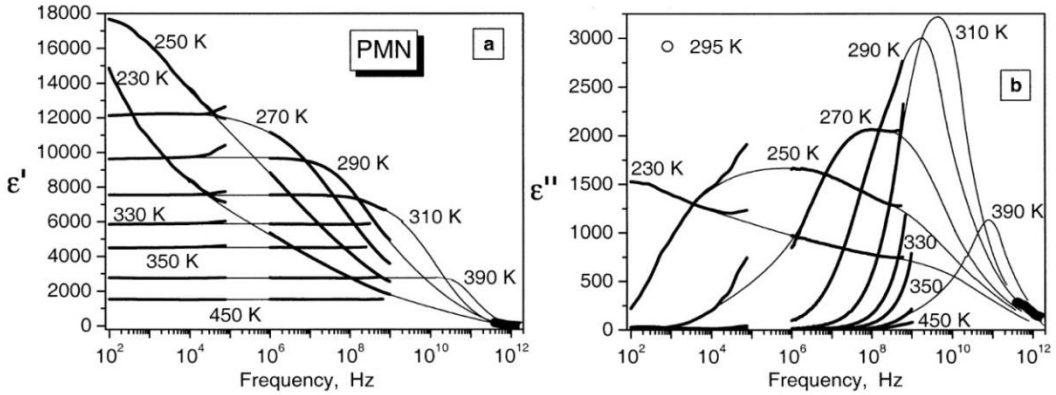

Figure 3.2.4 Frequency dependence of dielectric permittivity of PMN single crystal. Thick lines correspond to the experimental data, thin lines are guides for eye [27]

Authors obtained the relaxational dielectric dispersion clearly of non-Debye type and it could be characterized by a wide distribution of the relaxation times (Figure 3.2.4). The distribution is very wide below 200 K and

becoming narrower on increasing temperature. By means of spectroscopy in Terahertz range authors found one of the components of the central mode (that supposed to split below the Burns Temperature and further split into two components at the room temperature) at 30 cm^{-1} (≈1 THz) for all temperatures below room temperature. The mode was assigned to a transverse acoustic phonon absorption induced by the presence of the polar nano-clusters, enhanced by the doubling of unit-cell volume of the local cluster structure. Second component of the central mode is observed in the frequency range 100 Hz – 1.8 GHz. It broadens anomalously on cooling and two overlapping dispersion regions can further be distinguished between 210 K and 290 K (hence asymmetric $\varepsilon''(f)$ dispersion). The higher frequency component dominates below 200 K, where it develops into a frequency-independent loss. The lower-frequency component exhibits such temperature dependence, that its mean relaxation time obeys Vogel-Fulcher law with freezing temperature $T_f \approx$ 200 K [27].

The authors claim, that obtained results support a concept of polar nanoclusters within RFs. The concept tells that the dominant mechanism of this dynamics is reversal (flipping) of polar clusters and fluctuations of polar-cluster volume (breathing). Presumably, the microwave dispersion close to T_B is due to the cluster dipole flipping. The interactions among polar clusters cause freezing of the local dipole moments when approaching T_f , preventing any cluster flipping in weak fields below T_f . Consequently, only the breathing mechanism contributes to dielectric response below T_f, and is responsible for the frequency-independent dielectric loss. The broad distribution of relaxation times stems from structural inhomogeneities (Mg^{2+} and Nb^{5+}) in the perovskite B-sites, which cause random fields and broad distribution of activation energies for highly anharmonic hopping of Pb atoms. The distribution width should be comparable with the mean barrier height [27].

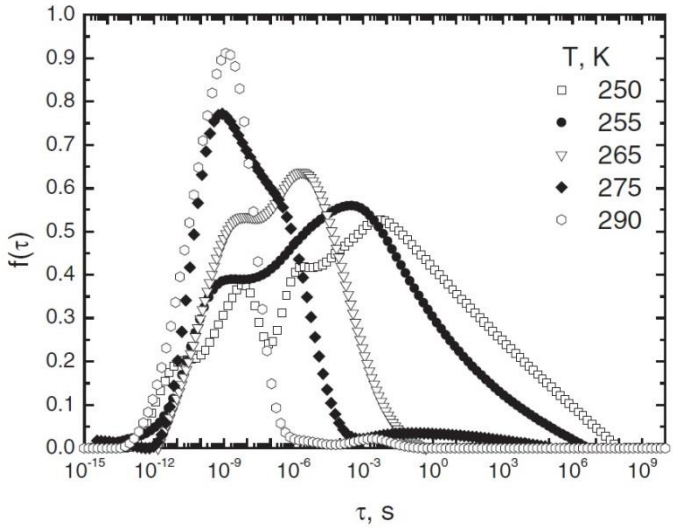

Figure 3.2.5 Relaxation time distribution function of PMN for different temperatures [28]

In the framework of the general scheme described above, two observed relaxational contributions to the central mode can be assigned to the cluster breathing mechanism (low-temperature dispersion characterized by frequency independent loss) and to the cluster flipping mechanism (high temperature relaxation). Results show tendency of all central-mode contributions (relaxational and the THz component) to merge into the TO_1 soft mode upon heating at T_B [27].

R. Grigalaitis et al. performed a dielectric spectroscopy of PMN single crystal in frequency range of 20 Hz to 3 GHz and wide temperature range [28]. Obtained dielectric data allowed deriving distributions of relaxation times (Figure 3.2.5). The idea was that relaxation process in PMN is the ensemble of independent Debye-like processes. The distribution of relaxation times broadens and shifts to the region of longest relaxation times with decrease of temperature to 290 K. Below 290 K the distribution becomes asymmetrical what indicate that contribution of the polar nanoregions to the total dielectric permittivity of PMN increases significantly. Here we can distinguish between dynamics of polar nanoregions and surrounding glassy matrix which contribute mainly to the shortest edge of the relaxation time distribution function and is nearly temperature independent.

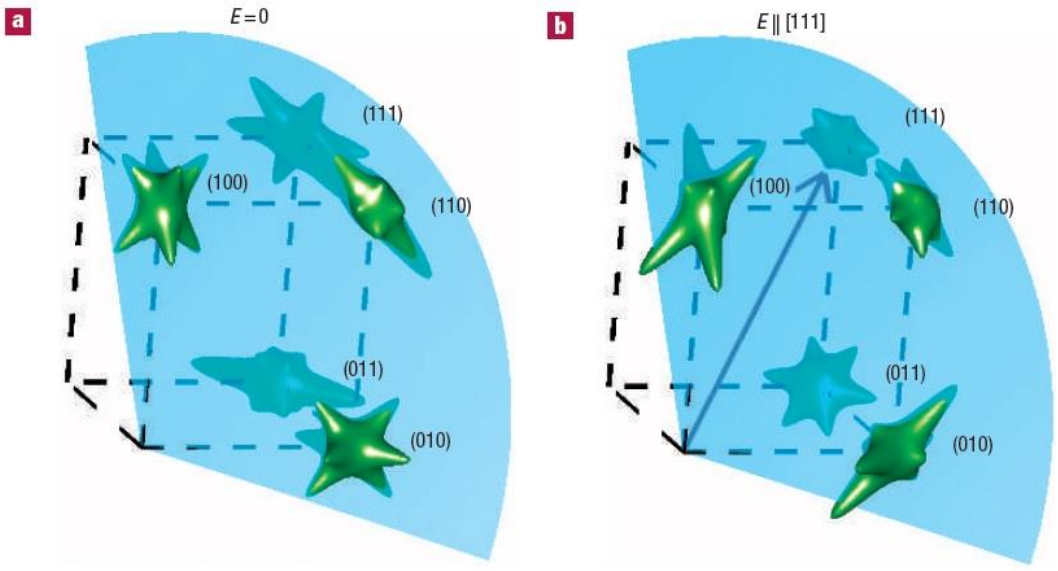

Figure 3.2.6 Schematic of the three-dimensional diffuse-scattering distribution from PZN. Plotted in the three-dimensional reciprocal space around (100), (110), (111), (010) and (011) reciprocal lattice points for **a**, E = 0, and **b**, E along [111]. In **b**, the diffuse rods along the [110], [101] and [011] directions are enhanced [29].

G. Xu et al. performed a X-ray diffraction experiment on $Pb(Zn_{1/3}Nb_{2/3})O_3$ (PZN) single crystal in 0 and 20 kV/cm (along [111]) external electric field. The observed differences are shown in (Figure 3.2.6). The interesting phenomenon observed is that diffuse scattering from PNRs with polarizations perpendicular to the external electric field has been enhanced, in contrast to conventional expectations to have local dipole moments aligned along the external electric field [29]. Authors suggest that the electric field affects the PNRs indirectly, through 'poling' the lattice environment the PNRs live in. In the paraelectric cubic phase above T_C, all the <110> directions are equivalent so that PNRs will be populated equally among all <110> polarizations. In the ferroelectric phase below T_C, domains of rhombohedral symmetry develop with polarizations along the <111> directions. The cubic symmetry is broken in each of these <111> domains, so that PNRs with different <110> polarizations are no longer equally favored in these environments. However, this preference cannot be observed in the macroscopic level without an external electric field because one always can observe only the average effect of all ferroelectric domains with different

<111> polarizations. An external field along [111] can help increase the volume of the lattice environment (ferroelectric domains) polarized along the [111] direction or even induce a single domain state, and introduce a clean scheme to understand the configuration of PNRs in a polarized environment. The results indicate that the PNRs are favored to grow in polarizations perpendicular to that of the surrounding lattice [29].

Dielectric measurements of poled sample in 20 kV/cm electric field highlighted the following features: 1) The almost non-dispersive permittivity in low-temperature range. 2) The dielectric anomaly associated with the diffuse ferroelectric phase transition at $T_C \approx 375$ K is more pronounced. 3) The typical relaxor behavior persists in the temperature range above the transition. These results indicate that electric field does enhance the ferroelectric order in the low-temperature phase. However, this is not achieved by realigning the PNRs to be along the field. Instead, macroscopic ferroelectric domains with polarizations along [111] develop and are enhanced by the electric field, whereas the PNRs persist in these domains [29].

The authors conclude that their findings uncover the preference of PNRs to have polarizations orthogonal to that of the lattice environment they reside in. That may be a key factor preventing them from dissolving into the ferroelectric phase. This is an extremely interesting and rare situation where a stable short-range (polar) order persists in a long-range ferroelectric order with the polarizations of the two orders being perpendicular to each other. This situation may be general in all perovskite relaxor systems [29].

X. Zhao et al. performed dielectric spectroscopy of PMN single crystals of [111], [110] and [100] cuts with constant bias electric field. Upon FC with electric field applied along the <111> direction, a sharp dielectric anomaly was detected at 222 K under E = 3 kV/cm, indicating a first-order phase transition. With the field increased to 5 kV/cm, the dielectric anomaly occurred at a higher temperature, 238 K, and became broader. At a still higher field of 7.5 kV/cm, the dielectric anomaly immersed into the broad dielectric peak around

T_m [30]. When the field was applied along the <110> direction, much weaker dielectric anomalies were detected at 197 K under 3.0 kV/cm and 222 K under 5.0 kV/cm. At the field level of 7.5 kV/cm, a dielectric anomaly can be barely detected at 232 K. For the [100] crystal platelet, no apparent anomaly was observed on the relative permittivity vs. *T* curves under 3.0, 5.0, or 7.5 kV/cm. However, anomalies did appear on the tg(δ) vs *T* curves at 204 K under 5.0 kV/cm, and 215 K under 7.5 kV/cm [30].

Field-heating tests were conducted under the same field levels. For the [111] crystal, an anomaly associated with the ferroelectric to relaxor transition upon heating occurred at 230 K under 3.0 kV/cm and 242 K under 5.0 kV/cm, and immerses into the dielectric peak under 7.5 kV/cm. For the [110] platelet, the transition occurred at 222 K under 3.0 kV/cm, 230 K under 5.0 kV/cm, and 238 K under 7.5 kV/cm. For the [100] platelet, the phase transition can barely be detected from the dielectric loss curve at 218 K under 3.0 kV/cm, but is clearly observed at 226 K under 5.0 kV/cm and at 229 K under 7.5 kV/cm [30].

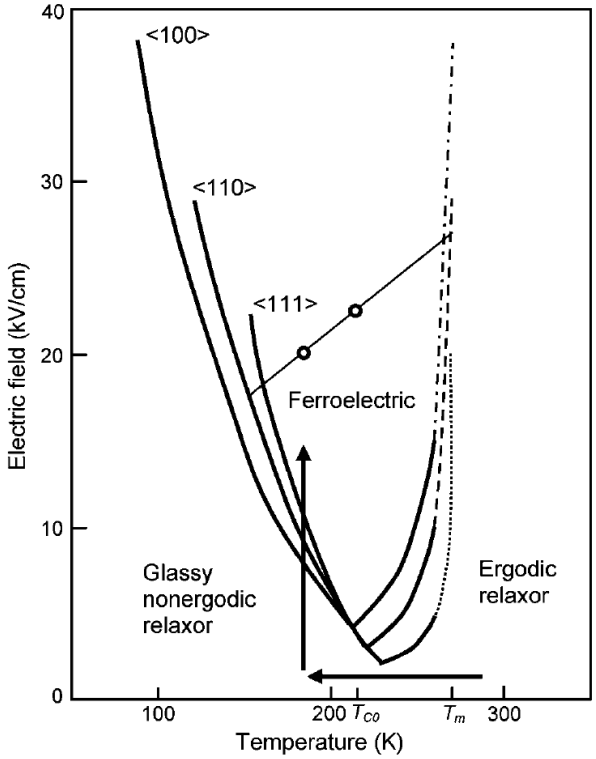

Figure 3.2.7 The *E-T* phase diagrams of PMN single crystal [30].

Along with polarization hysteresis measurements, authors derived a U-shaped phase diagram (Figure 3.2.7). The Curie temperature T_C (the upper boundary of the U-shaped region) and the lower boundary of the U-shaped region are shifted to lower temperatures in the crystal under field directions in the sequence of <111>, <110>, and <100>. The electric field along the <111> and <100> directions trigger only the relaxor cubic to ferroelectric rhombohedral phase transition. Fields along the <110> direction with a magnitude around 20 kV/cm trigger a further ferroelectric rhombohedral to ferroelectric orthorhombic transition after the initial relaxor cubic to ferroelectric rhombohedral transition [30]. Authors suggest that the mechanisms of the field-induced transformation to the ferroelectric phase from the glassy nonergodic relaxor phase and from the ergodic relaxor phase are different. In the former case the motions of the boundaries between polar nanoregions are the main origin. In the latter case the flipping of the dipole moments of the polar nanoregions are involved. The behavior is explained in terms of the two-stage kinetic model of the first-order phase transitions in compositionally disordered crystals [30,31].

R. Pirc and R. Blinc attempted to describe nonlinear dielectric response in framework of Spherical Random Bond Random Field model (SRBRF) [32]. In a system with average cubic symmetry the phenomenological relation between the applied electric field E_μ (μ = 1, 2, 3) and polarization P_μ can be written, assuming small amplitudes, as a power series

$$P_1 = \chi_1 E_1 - \chi_{122} E_1 \left(E_2^2 + E_3^2\right) - \chi_{111} E_1^3 + \ldots \qquad (3.2.1)$$

The inverse relation:

$$E_1 = a_1 P_1 + a_{122} P_1 \left(P_2^2 + P_3^2\right) + a_{111} P_1^3 + \ldots \qquad (3.2.2)$$

Comparing the above two relations yields:

$$a_1 = \frac{1}{\chi_1}; \quad a_{122} = \frac{\chi_{122}}{\chi_1^4}; \quad a_{111} = \frac{\chi_{111}}{\chi_1^4} \qquad (3.2.3)$$

Here χ_1 is the linear susceptibility and χ_{122}, χ_{111}, etc. the third-order nonlinear susceptibilities. For a field $\boldsymbol{E}$||[111] and $P_1 = P_2 = P_3 = P$ equations (3.2.1) and (3.2.2) simplify to:

$$P = \chi_1 E - \chi_3 E^3 + ... \qquad (3.2.4)$$

$$E = a_1 P - a_3 P^3 + ... \qquad (3.2.5)$$

where $\chi_3 = 2\chi_{122} + \chi_{111}$ and

$$a_3 = \frac{\chi_3}{\varepsilon_0^3 \chi_1^4} \qquad (3.2.6)$$

The same relations formally hold for an isotropic system.

Experimentally, χ_3 can be determined, for example, by measuring the third-harmonic non-linear response to an oscillating external field in zero-bias. The scaled non-linear response a_3 is obtained with an assumption, that one has also determined the linear response χ_1 in zero bias. If nonzero-bias field E is applied, one measures the modified field-dependent linear and third-harmonic non-linear responses.

The expression for the linear susceptibility $\chi_1(E)$ is this [32]:

$$\chi_1(E) = \frac{\beta(1-q)}{1-\beta J_0(1-q) + D(E,P)} \qquad (3.2.7)$$

Here $D = 0$, if $E = 0$ and D has to be taken into account, if $E \neq 0$; q – is Edwards – Anderson parameter, $\beta = 1/kT$.

In experiments, χ_1 is s typically measured at some finite frequency ω. Thus a comparison with the predictions of a static theory is not straightforward in view of the strong frequency dispersion observed in relaxor ferroelectrics. Clearly, the results of a static theory are applicable only in the temperature region where frequency dispersion is negligible, namely, at sufficiently high temperatures. A dynamic version of the SRBRF model has not yet been worked out by the authors. The frequency dispersion also plays a role in the temperature dependence of the third-order nonlinear susceptibility χ_3. The scaled non-linear response a_3 is a suitable quantity to be compared with the

static theory. By SRBRF model it is expected to observe divergence of a_3 at freezing temperature T_f in RFs. The divergence should disappear under bias field [32].

A. E. Glazounov and A. K. Tagantsev developed a phenomenological model of a dynamic nonlinear response of RFs, in order to fill the gap between theory and experiment [33]. It aims at describing the frequency dependence of the third harmonics of the polarization, in order to expand the temperature interval, necessary to study freezing phenomena in RFs, towards freezing temperature T_f. The model employs a series expansion of the free energy of the material in terms of macroscopic polarization: $G_1 = \alpha P^2 + \beta P^4 + \ldots$,where α and β are temperature dependent coefficients. This expansion describes macroscopically centrosymmetrical cubic material, which is the case of most of the RFs, including the "classical" example PMN. The expansion (and the following formulas) is written in the scalar form, which corresponds to the case of either a single crystal, where a field and a polarization are directed along the <100> crystal axis, or ceramics with a random orientation of the grains. The term βP^4 in this expansion controls the nonlinear dielectric properties of the material, and higher order non-linear terms are omitted. This assumption may be the case of experiment, where the amplitudes of polarization harmonics, satisfy $P_1 >> P_3 >> P_5\ldots$, which was observed in PMN [34].

For the system, where the dynamic response is controlled by a single relaxation time, such as "normal" ferroelectrics, the equation of motion corresponding to the above expansion can be written as $E = \alpha P + \beta P^3 + \eta \mathrm{d}P/\mathrm{d}t$, or in following form:

$$\tau \frac{dP}{dt} + P = \varepsilon_0 \varepsilon_S \left[E - \beta P^3 \right] \qquad (3.2.8)$$

where relaxation time, $\tau = \eta/\alpha$, and static linear permittivity, $\varepsilon_S = \varepsilon_0/\alpha$. The nonlinear component of the polarization can be found by using response function, $f_p(t) = \exp(-t/\tau)/\tau$, and iterating the following integral equation:

$$P(t) = \varepsilon_0 \varepsilon_S \int_{-\infty}^{t} f_p(t-t')\left[E(t') - \beta P^3(t')\right]dt' \qquad (3.2.9)$$

This method can also be applied to relaxors, if one takes into account their broad spectrum of relaxation times [33]. With a generalized response function, the nonlinear component of the polarization can still be found by iterating (3.2.9) [33].

If an alternating field, $E(t) = E_m\sin(\omega t)$, is applied to the cubic material, the induced polarization is given as a sum of odd frequency harmonics. Since in the model being considered the nonlinear properties are given by the term βP^3 in (3.2.8), we limit ourselves to the first and third harmonics: $P(t) = P_1'\sin(\omega t) + P_1''\cos(\omega t) + P_3'\sin(3\omega t) + P_3''\cos(3\omega t)$, where the amplitudes of their real, P_1', P_3', and imaginary, P_1'', P_3'', parts satisfy the inequality: $P_3', P_3'' << P_1', P_1''$. The first iteration of (3.2.9) gives well-known expressions for the real and imaginary parts of linear permittivity:

$$\varepsilon_l'(\omega) = \varepsilon_S \int_{-\infty}^{+\infty} \frac{G(\ln\tau)}{1+(\omega\tau)^2}\, d(\ln\tau); \quad \varepsilon_l''(\omega) = \varepsilon_S \int_{-\infty}^{+\infty} \frac{G(\ln\tau)(\omega\tau)}{1+(\omega\tau)^2}\, d(\ln\tau) \qquad (3.2.10)$$

which are defined from the amplitudes of the first harmonics as $P_1' = \varepsilon_1'\varepsilon_0 E_m$ and $P_1'' = -\varepsilon_1''\varepsilon_0 E_m$, respectively. The second iteration yields the amplitudes of the third harmonic as:

$$P_3' = \frac{\beta}{4}\left[\varepsilon_l'^3(\omega)\varepsilon_l'(3\omega)\right]\varepsilon_0^4 E_m^3 \qquad (3.2.11)$$

$$P_3'' = \frac{\beta}{4}\left[\varepsilon_l''(3\omega)\varepsilon_l'^3(\omega) + 3\varepsilon_l''(\omega)\varepsilon_l'^3(3\omega)\varepsilon_l'^2(\omega)\right]\varepsilon_0^4 E_m^3 \qquad (3.2.12)$$

Note that in these equations, β, the permittivity, and the third harmonic also depend upon temperature T [33].

If the model is correct, the nonlinear coefficient β should be frequency independent. However, if the dispersion is present in the experimental results, two possible reasons can be indicated: either this is a true dispersion of β itself, or the dispersion comes from higher order harmonics (i.e. 4th, 5th, etc.). After

performing non-linear polarization measurements on PMN, authors claim, that to the larger part, $\beta(T)$ agreed with the SRBRF model, but it did not exhibit the maximum at the freezing temperature, which is predicted by the model [33].

Two concepts were consistent with the key feature of RFs. One concept described RFs as analogues of dipolar glasses [32], the second claimed that the freezing is considered as a transition into a ferroelectric state broken into nanodomains due to quenched random fields [26,35]. In order to find out more relevant model, J. Dec et al. performed measurements of temperature dependence of scaled third order susceptibility χ_3 in the vicinity of the static freezing temperature, $T_f \approx 220$ K [35]. The measurements of PMN single crystal were performed in the limit of weak *ac* fields, instead of exploiting the *dc* nonlinear effect [36], in order to avoid a possibly induced phase transition into a long range ordered ferroelectric phase transition [35]. The obtained result is shown in Figure 3.2.8. The positive sign of χ_3 may confuse into thinking, that it indicates the second order phase transition, in which case the χ_3 is positive only below T_C. However, authors claim that such behavior originates from quasi-static precursor polarization, which in case of RFs are PNRs [35]. For explanation reasons an expression of the Gibbs free energy is given:

$$G = G_0 + \frac{1}{2}A(T - T_0)P^2 + \frac{1}{4}BP^4 + \frac{1}{6}CP^6 \qquad (3.2.13)$$

where G_0 stands for the free energy at $P = 0$ and A, B, C and T_0 are constants. In the ferroelectric phase the polarization P yields the spontaneous one, P_S, as an order parameter. In case of continuous phase transition $B > 0$ and $C = 0$. Successive differentiations of G in respect of P give a relationship between E and P and finally the susceptibilities [35,37]:

$$\chi_1 = \frac{1}{\varepsilon_0\left[A(T - T_C) + 3BP_S^2\right]} \qquad (3.2.14)$$

$$\chi_2 = -3\varepsilon_0^2 B\chi_1^3 P_S \qquad (3.2.15)$$

$$\chi_3 = \varepsilon_0^3\left(18\varepsilon_0 B^2 \chi_1 P_S^2 - B\right)\chi_1^4 \qquad (3.2.16)$$

In a normal ferroelectric P_S vanishes at $T = T_C$, hence $\chi_2(T \geq T_C) \equiv 0$ and $\chi_3 = -\varepsilon^3_0 B \chi^4_1 < 0$ as measured in systems displaying continuous phase transitions [38,39]. Below T_C, however, where $P^2_S = (A/B)(T_C - T)$ and $\chi_1 = (2\varepsilon_0 A(T_C - T))^{-1}$ one obtains $\chi_3 = 8\varepsilon^3_0 B \chi^4_1 > 0$ as evidenced experimentally [38,39]. Contrastingly, in case of a discontinuous phase transition, where $B < 0$ and $C > 0$, a similar calculation [37] yields $\chi_3 > 0$ at all temperatures, in particular also above T_C, where $\chi_3 = -\varepsilon^3_0 B \chi^4_1 > 0$. Despite the $\chi_3 > 0$ in case of PMN, it does not undergo neither continuous nor discontinuous phase transition accompanied by macroscopic symmetry breaking at T_m.

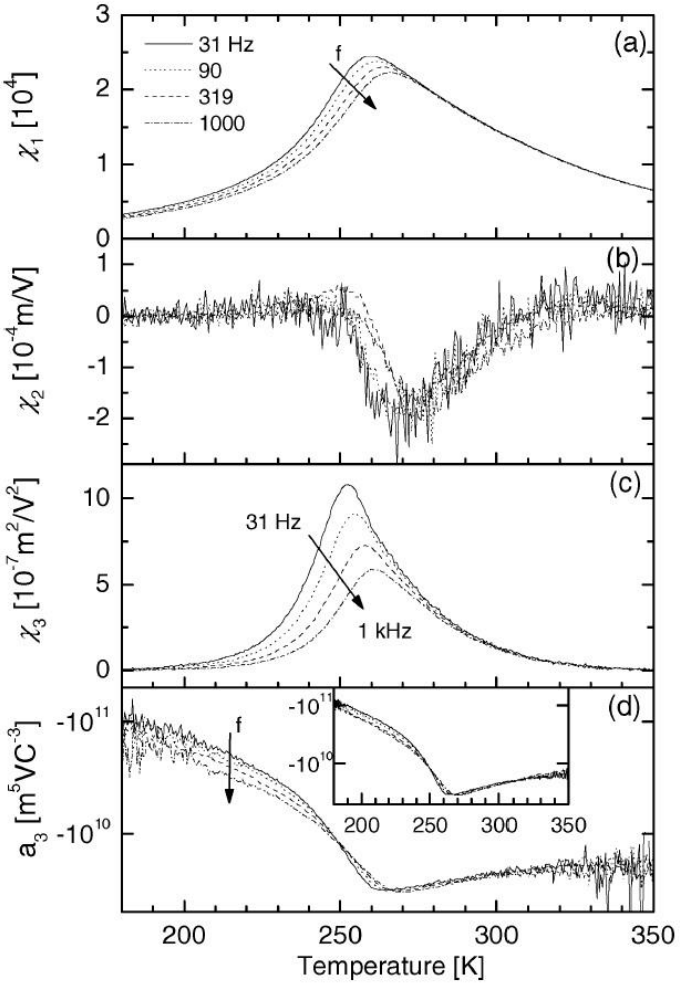

Figure 3.2.8 Temperature dependences of the real parts of the linear (a), second-order (b), and third-order (c) dielectric susceptibilities of a PMN single crystal recorded along the [100] direction and the calculated scaled non-linear susceptibility a_3 (d) [35]

In case of PMN (Figure 3.2.8) the positive sign of χ_3 may result from a positive term $18\varepsilon^4{}_0B^2P^2{}_0\chi^5{}_1$ exceeding the negative one, $-\varepsilon^3{}_0B\chi^4{}_1$. Note that the positive term is sensitive to square of polarization. Hence, it may contribute to χ_3 since P^2 does not average out to zero, while P is expected to do so. However, χ_2 being (sensitive to P) not zero hints at an incomplete averaging out to zero of the average polarization of the PNR subsystem. Both χ_1 and χ_3 do not display any anomalies at T_f, also the scaled non-linear susceptibility a_3 does not exhibit any maximum ($a_3 = \chi_3 / (\varepsilon^3{}_0\chi^4{}_1)$) as predicted by the SRBRF model. Thus, the obtained result does not support the dipolar glass model for PMN-type RFs. On the other hand, the pyroelectric response of PMN allowed the authors to claim that PMN may be considered as system displaying silent (or diluted) ferroelectricity [35].

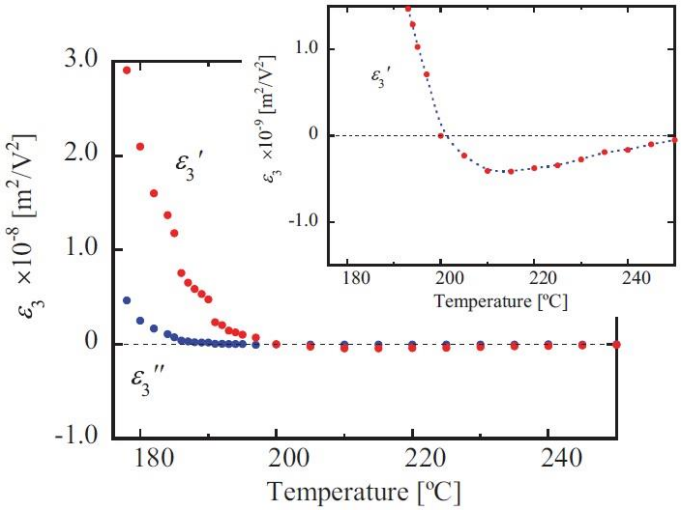

Figure 3.2.9 The temperature dependence of the third-order nonlinear susceptibility at 100 kHz. Inset shows the magnified view near the temperature, where the sign of the real part of the non-linear susceptibility changes [40]

Quite a contrasting result was published by Iwata et al. [40], where is shown temperature dependence of the third order nonlinear dielectric permittivity of $0.92Pb(Zn_{1/3}Nb_{2/3})O_3$-$0.08PbTiO_3$ (PZN-0.08PT) solid solution single crystal (Figure 3.2.9). Authors claim, that their obtained result indicates the occurrence of the first-order phase transition under zero electric field bias in 0.92PZN-0.08PT [40].

The two works discussed above clearly shows the benefits of use of non-linear dielectric permittivity measurements in fundamental research of RF. Overall, throughout the years there were obtained loads of scientific data onto physics of RFs and still, time and time again it proves to be interesting and curiosity driving family of materials, especially in case of fundamental physics. This work provides insight on influence of different dopants to properties of PMN. Namely, La and Mn doping, at first glance, give similar effect onto the properties of PMN, i.e. decrease of dielectric permittivity value. However, this work explains that the mechanism, due to which occurs the reduction of dielectric permittivity, is quite different. Furthermore, a phase behavior of solid solution of 0.83 relaxor PMN and 0.17 ferroelectric PT is analyzed.

EXPERIMENTAL

Dielectric permittivity measurements in frequency range of 10 Hz – 10 MHz were performed with an impedance analyzer HP-4284A. The sample is placed in a cryostat as a dielectric between two parallel capacitor plates. Then, capacity and loss tangent of the system is measured. Complex dielectric permittivity of the material under test may be extracted using the following relationships:

$$\varepsilon' = \frac{(C_m - C_0)d}{\varepsilon_0 S} + 1 \tag{4.1}$$

$$\varepsilon'' = \varepsilon' \operatorname{tg}(\delta) = \frac{C_m \operatorname{tg}(\delta_m) - C_0 \operatorname{tg}(\delta_0)}{C_m - C_0} \tag{4.2}$$

Here C_m and $\operatorname{tg}(\delta_m)$ – capacity and loss tangent of the system with the sample inside, C_0 and $\operatorname{tg}(\delta_0)$ – capacity and loss tangent of the empty system, S – area of the sample touching the parallel capacitor plates, d – thickness of the sample or the distance between capacitor plates, ε_0 – dielectric permittivity of free space.

Dielectric permittivity measurements in frequency range of 1 MHz – 3 GHz were performed with a vector analyzer Agilent 8714 ET. The sample is placed into cryostat formed onto the end of a coaxial waveguide as a capacitive load. The reflectance from the end of the coaxial waveguide, which intersects with a calibration plane, is measured. Coaxial waveguide or coaxial line is broadband, i.e. it has short wavelength (high frequency) limit condition:

$$\lambda > \pi(r_{in} + r_{out}) \tag{4.3}$$

Here r_{in} – a diameter of an internal conductor of the coaxial line, r_{out} – a diameter of an outer conductor of the coaxial line, λ – a wavelength of an electromagnetic wave. The reflectance of this system can be expressed as:

$$R^* = \frac{Z_B^* - Z_0}{Z_B^* + Z_0} \tag{4.4}$$

Here Z_B – an impedance of the load, in our case it is capacitive load, Z_0 – an impedance of the coaxial line (usually it is the same as an impedance of a

port of the vector analyzer and it is ≈ 50 Ω). The capacitive load impedance is well known:

$$Z_B^* = \frac{1}{i\omega C_B^*} \tag{4.5}$$

Complex capacitance can be related with a complex dielectric permittivity with the following relationship:

$$\varepsilon' - i\varepsilon'' = \frac{d}{\varepsilon_0 S}\left(C' - iC''\right) + 1 \tag{4.6}$$

Then combining relationships (4.4), (4.5) and (4.6) real and imaginary parts of complex dielectric permittivity can be expressed:

$$\varepsilon' = \frac{d}{\varepsilon_0 S}\left(\frac{-2R\sin\varphi}{\omega Z_0\left(1 + 2R\cos\varphi + R^2\right)} - C_0\right) + 1 \tag{4.7}$$

$$\varepsilon'' = \frac{d}{\varepsilon_0 S}\frac{1 - R^2}{\omega Z_0\left(1 + 2R\cos\varphi + R^2\right)} \tag{4.8}$$

Here R – is the absolute value of the complex reflectance, φ – is the phase of the complex reflectance.

These expressions of the complex dielectric permittivity are valid only when a condition of quasi-static electromagnetic field within the sample is fulfilled, i.e. the distribution of electromagnetic field within the sample is homogeneous. Hence, the geometric size of the sample has to be much smaller than the length of wave propagating through it. When the frequency is high, the field distribution within the sample is not homogeneous and for disk shaped sample can be expressed as in [41]:

$$E = AJ_0\frac{kr}{\sqrt{\varepsilon'}} \tag{4.9}$$

Here A – is a constant, which is related with the geometry of the sample, r – radius of the disk shaped sample, J_0 – a Bessel function of the first kind and 0th degree, k – is the wavenumber. An assumption can be made, that the radius of the sample is ≈ 10 times smaller than the first root of J_0, then the field within the sample is approximately quasi homogeneous (with 2% error). Then the limit for the radius of disk shaped sample can be expressed as:

$$r \leq \frac{0.24\lambda}{2\pi\sqrt{\varepsilon'}} \tag{4.10}$$

Another matter, which has to be considered for this measurement method, is the calibration of the equipment. The physical connections and the lines are not ideal and they give distortions to the reflectance response. Hence, three loads of known impedance have to be measured in order to obtain the scatter matrix parameters. For this reason the reflectance of open ended line (R = 1, φ = 0°), shorted end line (R = 1, φ = 180°) and standard load (R = 0) are measured. Obtained scatter matrix parameters are used to correct the reflectance of the actual sample.

Dielectric permittivity measurements in frequencies of 35 GHz and 48 GHz were performed using rectangular waveguides. Thin, needle like sample is placed into the special frame, which is shaped as a cross section of the waveguide. So the sample stays perpendicular to the wide walls of the rectangular waveguide in the center. Hence, the inhomogeneity of matter is made in the space, where the electric field of the main mode TE_{10} is the strongest. The electromagnetic wave is generated by a microwave generator. The measurement of a complex transmission T^* and a reflectance R^* are performed with the analyzer Elmika R2400. Complex magnitudes T^* and R^* are dependent on width of the waveguide a, frequency of the generator f, complex dielectric permittivity of the sample ε^* and the radius of the needle shaped sample r. The complex dielectric permittivity of the sample $\varepsilon^*(f)$ can be obtained by solving nonlinear complex equation $\varepsilon^* = f(R^*)$ or $\varepsilon^* = f(T, R)$. The sample reflects all the energy of the electromagnetic wave TE_{01}, if the sample has no loss and the frequency is:

$$f_0 = \frac{c}{2\pi r\sqrt{\varepsilon}} \tag{4.11}$$

The accuracy of the method decreases with the increase of the loss of the sample, especially if $f > f_0$, because the extreme of ε' dependence of the transmission and the reflectance absolute values ($T(\varepsilon')$, $R(\varepsilon')$) becomes more shallow with a limit of horizontal line through wide range of ε' values.

Non-linear susceptibility measurements were performed using a custom made non-linear susceptometer. More details about the susceptometer is given in section **4**. Sample is placed between the flat capacitor plates. The measurements are carried out in frequency range of 100 Hz – 5 kHz. The amplitude of sweep signal is between 0 – 10 V. The field strength then depends on the thickness of the sample. The non-linear susceptibility is obtained as published by Miga et al. [42]. A dielectric material is exposed to the harmonic alternating electric field $E(t)$ at the angular frequency ω:

$$E(t) = E_0 \sin(\omega t) \tag{4.12}$$

Then the polarization P of the sample can be written in general form:

$$P(t) = \varepsilon_0 \sum_{i=1}^{n} \chi_i E^i(t) = \varepsilon_0 \sum_{i=1}^{n} \chi_i E_0^i \sin^i(\omega t) \tag{4.13}$$

Here χ is the scalar susceptibility of the sample.

In this power series both odd and even terms are presented. Usually this series are truncated at the third term (n = 3). Our susceptometer takes into account 5 terms, so this leads to the following expression:

$$P(t) = \varepsilon_0 \sum_{i=0}^{5} \chi_i E_0^i \sin^i(\omega t) = \varepsilon_0 [\frac{3}{8}\chi_4 E_0^4 + \frac{1}{2}\chi_2 E_0^2 + \left(\frac{5}{8}\chi_5 E_0^5 + \frac{3}{4}\chi_3 E_0^3 + \chi_1 E_0\right)\sin(\omega t) -$$
$$-\left(\frac{1}{2}\chi_4 E_0^4 + \frac{1}{2}\chi_2 E_0^2\right)\cos(2\omega t) - \left(\frac{5}{16}\chi_5 E_0^4 + \frac{1}{4}\chi_2 E_0^3\right)\sin(3\omega t) + \left(\frac{1}{8}\chi_4 E_0^4\right)\cos(4\omega t) +$$
$$+\left(\frac{1}{16}\chi_5 E_0^5\right)\sin(5\omega t)] \tag{4.14}$$

It can be seen here, that the polarization of the non-linear material follows not only the fundamental frequency ω of the driving field, but also contains terms of higher harmonics. As a result, the displacement current I, related to the polarization, is given by:

$$I = S\frac{\partial D(t)}{\partial t} \tag{4.15}$$

where $D = \varepsilon_0 E + P$ and S is the surface of the electrode. Based on (4.14), (4.15), one obtains the current as:

$$I(t)=\varepsilon_0 S\omega\left(\frac{5}{8}\chi_5 E_0^5+\frac{3}{4}\chi_3 E_0^3+(\chi_1+1)E_0\right)\cos(\omega t)+\varepsilon_0 S\omega\left(\chi_4 E_0^4+\chi_2 E_0^2\right)\sin(2\omega t)-$$

$$-\varepsilon_0 S\omega\left(\frac{15}{16}\chi_5 E_0^5+\frac{3}{4}\chi_3 E_0^3\right)\cos(3\omega t)-\varepsilon_0 S\omega\left(\frac{1}{2}\chi_4 E_0^4\right)\sin(4\omega t)+$$

$$+\varepsilon_0 S\omega\left(\frac{5}{16}\chi_5 E_0^5\right)\cos(5\omega t) \qquad (4.16)$$

As seen in (4.16) the displacement current contains many harmonic terms. Since each term is linearly dependent on susceptibility χ_i (where i = 1, 2, 3, 4, 5 in our case) one obtains a system of five equations enabling the computation of higher order susceptibilities. After solving this system of equations one obtains:

$$\chi_1=\frac{1}{\varepsilon_0 S\omega}\left(\frac{d}{U_0}\right)(I_1+I_3+I_5)-1$$

$$\chi_2=\frac{1}{\varepsilon_0 S\omega}\left(\frac{d}{U_0}\right)^2(I_2+2I_4)$$

$$\chi_3=\frac{1}{\varepsilon_0 S\omega}\left(\frac{d}{U_0}\right)^3\left(-\frac{4}{3}I_3-4I_5\right)$$

$$\chi_4=\frac{1}{\varepsilon_0 S\omega}\left(\frac{d}{U_0}\right)^4(-2I_4)$$

$$\chi_5=\frac{1}{\varepsilon_0 S\omega}\left(\frac{d}{U_0}\right)^5\left(\frac{16}{5}I_5\right) \qquad (4.17)$$

with $E_0 = U_0/d$, where U_0 – is the amplitude of the driving voltage and d – is the thickness of the sample. Hence, relationships (4.17) enable the calculation of the linear and higher order susceptibilities from measurable physical quantities, i.e. the amplitude of the driving electric field and the amplitudes of the displacement current harmonics. However, above equations are written for nondisipative and nonconductive dielectrics. In order to generalize the equations for lossy and/or weakly conductive dielectrics, one has to replace the existing amplitudes by their complex counterparts thus involving a phase shift of the displacement current harmonics relatively to the

driving voltage. Consequently, the complex linear and non-linear susceptibilities can be calculated. It must be highlighted, that the odd harmonic components of the displacement current I_i for an ideal dielectric (zero loss and nonconductive) are phase shifted by 90° with the driving field while the even components are in phase. If one designates the complex quantities in (4.17) by Ψ_i^*, then the components χ_i' and χ_i" of the linear and nonlinear susceptibilities with odd subscripts (in our case i = 1, 3, 5), may be calculated as:

$$\chi_i' = \mathrm{Im}\left(\Psi_i^*\right), \quad \chi_i'' = \mathrm{Re}\left(\Psi_i^*\right) \tag{4.18}$$

while for even subscripts (in our case i = 2, 4) one should use the relations:

$$\chi_i' = \mathrm{Re}\left(\Psi_i^*\right), \quad \chi_i'' = \mathrm{Im}\left(\Psi_i^*\right) \tag{4.19}$$

Our susceptometer gathers the sample response current as the voltage data in time scale. Then, the fast Fourier transformation (FFT) is used in order to carry out the harmonic analysis of the measured current. However, this spectrum contains additional phase shift, which originates from the equipment. In order to remove this equipment caused phase shift, we perform a phase shift calibration. For this reason we use Solartron 12961 reference capacitance module, that contains a set of four (9.31 pF, 102 pF, 0.999 nF, 10.04 nF) nearly ideal capacitors (linear, no loss), that allows calibrating the whole possible to measure capacitance range. If the calibration capacitor C is driven by the harmonic signal $U^* = Ue^{j\omega t}$, it gives the current:

$$I^* = j\omega CU^* = j\omega CUe^{j(\omega t+\Delta\varphi)} = \omega CUe^{j\left(\omega t+\frac{\pi}{2}+\Delta\varphi\right)} \tag{4.20}$$

here $\Delta\varphi$ – is the phase shift caused by the equipment. If there was no phase shift caused by the equipment, then the ideal current would be:

$$I_{id}^* = \omega CUe^{j\left(\omega t+\frac{\pi}{2}\right)} \tag{4.21}$$

knowing this, it is possible to calculate the calibration coefficient:

$$K^* = \frac{I_{id}^*}{I^*} = \frac{\omega CUe^{j\left(\omega t+\frac{\pi}{2}\right)}}{\omega CUe^{j\left(\omega t+\frac{\pi}{2}+\Delta\varphi\right)}} = \frac{1}{e^{j\Delta\varphi}} \tag{4.22}$$

If a sample is measured, a current response is obtained, which can be expressed as:

$$I^*_{meas} = \omega C_b U e^{j\left(\omega t + \frac{\pi}{2} + \varphi_b + \Delta\varphi\right)} \qquad (4.23)$$

here φ_b – is the phase shift caused by the sample, C_b – is the capacitance of the sample. However, we can see, that $\Delta\varphi$ remains here and spoils the response of the sample. In order to obtain a correct data, we perform a correction with use of the calibration coefficient K^*:

$$I^*_{result} = K^* I^*_{meas} = \omega C_b U \left(\frac{e^{j\left(\omega t + \frac{\pi}{2} + \varphi_b + \Delta\varphi\right)}}{e^{j\Delta\varphi}} \right) = \omega C_b U e^{j\left(\omega t + \frac{\pi}{2} + \varphi_b\right)} \qquad (4.24)$$

We can see that $\Delta\varphi$ disappears from the response after the calibration correction. The calibration coefficients are calculated and stored for each harmonic before the beginning of the measurement procedure.

Temperature measurements in all experiments were performed using multimeter Keithley Integra 2700. Platinum thermo resistor PT100 was used as a temperature sensor for the dielectric spectroscopy in 10 Hz – 1 MHz frequency range and the non-linear susceptibility measurements. Thermo couple of T-type was used for the dielectric spectroscopy with the coaxial line and rectangular waveguides. Wire heater was used for an electrical heating of the cryostats and for the cooling reasons a liquid nitrogen purge was used for all experiments.

Silver paste contacts were used in all experiments. The parallel faces of a sample are polished. After polishing, the sample is washed in acetone and in isopropanol, in an ultrasonic bath. Once the sample is dried, the silver paste is applied onto the one face of the sample. After 10 minutes of drying the silver paste is applied onto the other face. After > 30 minutes of drying, the sample is put into a furnace and heated up to 600°C. The heating rate from room temperature is set to 4 K/min. The sample is kept in the top temperature for ≥ 2 hours. The furnace is then turned off to cool down to a room temperature.

NON-LINEAR DIELECTRIC SUSCEPTOMETER

Linear dielectric spectroscopy or dielectric susceptibility measurements are performed using a small alternating voltage (or electric field) signal. The relationship between a polarization P and an external electric field E, is well known:

$$P = \varepsilon_0 \chi_1 E \qquad (5.1)$$

where ε_0 – electric permittivity of space and χ_1 – the linear electric susceptibility of a dielectric material.

Such relationship is valid, if a condition of a small external electric field applies. In experiments, where a large electric field is introduced, the $P(E)$ relationship is no longer linear and higher order susceptibilities have to be taken into account:

$$P = \varepsilon_0 \left(\chi_1 E + \chi_2 E^2 + \chi_3 E^3 + ... \right) \qquad (5.2)$$

here χ_i – are the non-linear susceptibilities (where i – positive integers). These non-linear components show the non-linear contribution to the polarization [43]. The measurements of the non-linear dielectric susceptibility of polar dielectrics give useful information on phase transitions [44]. Namely, it is possible to unambiguously recognize the type of the phase transition. Ferroelectric systems, which display a continuous or the second order phase transition, have the negative third order susceptibility (χ_3) in paraelectric state and, with decrease of temperature χ_3 changes the sign to positive at the temperature of the phase transition. In case of a discontinuous phase transition or the first order transition the sign of χ_3 is positive and remains unchanged throughout the vicinity of the temperature of the phase transition. So is explained by the theory of Landau-Ginzburg-Devonshire [45,46] and was proved by measurements of Triglycine Sulfate (the second order phase transition) and Barium Titanate (the first order phase transition) [47]. As well, it proves to be a useful tool to investigate essential differences between RFs and dipolar glasses [32,48,49]. A good example are works on PMN [35,50],

that helped to derive a more general model than SRBRF model [32] for behavior of RFs [51]. This model, the Compressible Spherical Dipolar Glass, takes into account the electrical polarization and the fluctuations of the strain tensor.

There are few methods developed, which allow performing the measurements of the non-linear susceptibility [37,42,52,53], but none of them are available commercially. Here are shortly discussed the three most common ones. The first type, has a small voltage bias applied on the sample and additional small alternating signal swept through the frequency range. Then, the bias is increased and frequencies swept again. The nonlinear response is derived from the large amount of obtained data. The drawback of such method is that the long periods of time the sample is placed in the external electric field may induce a phase transition. The second type is combined with the use of lock-in amplifier. The sample is measured with zero biased small alternating signal, which is large enough to observe the nonlinear response, but much smaller than the coercive field of the material. The drawback of such method is that the measurement can be obtained only in one fixed frequency. The third type uses the similar zero biased alternating signal generated by the high quality harmonic signal generator. Although, low noise current amplifier is used instead of lock-in amplifier. It gives the ability to perform the measurements in broader frequency range. However, the drawback of such method is that the whole system needs a single synchronization source, which synchronizes the generation of the voltage signal and data acquisition. Furthermore, with increase of frequency phase distortions occur due to RC filters used in the amplifier.

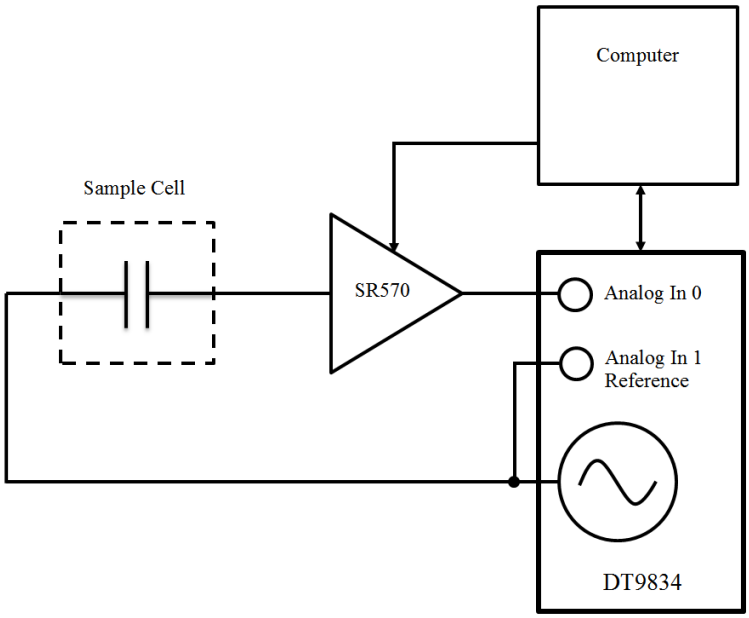

Figure 5.1 Block diagram of non-linear susceptibility measuring system

The concept of our susceptometer is based on the equipment presented by S. Miga, et al. [42] (the third type). Our system consists of (Figure 5.1): Data Translations DT9834 Data Acquisition Module, Stanford Research Systems SR570 Low Noise Current Preamplifier with controllable sensitivity, Computer, Sample Cell. DT9834 module is used to generate a zero biased alternating voltage signal with amplitude, which allows observing the nonlinear response of the sample under test, but it is rather small in comparison with a coercive field of the material of the sample. The signal drives the sample within the sample cell. The current of the sample response is converted to a voltage by SR570 current preamplifier. The *Analog In* channel of DT9834 module is used to gather the measurement data. As well, a separate *Analog In* channel is used to gather the data of the reference signal, which drives the load (sample inside the cell/cryostat). Computer is used to control a sensitivity of SR570 and to perform calculations with the data gathered by DT9834.

The DT9834 does not perform any data analysis. All calculations and data analysis are performed in the computer. The measurement signal is generated in burst of several periods, which begins and ends at the same phase. Such time data allows performing fast Fourier transformation without need to use of window functions. After the transformation an array of spectrum

amplitudes is obtained. The number of element of the array, which contains the amplitude of the harmonic, is found by the following relation:

$$h_n = n\frac{f \cdot L}{f_S} \qquad (5.3)$$

Here n – is the number of harmonic, h_n – is the number of the array element of the spectrum, f – is the main harmonic frequency, L – is the total length of spectrum array, f_S – is the sampling frequency.

The equipment allows performing measurements of samples with capacitances in a range of 10 pF up to 10 nF. The estimated frequency range of an excitation signal is 8 Hz – 10 kHz. The maximum amplitude of the alternating signal is ±10 V. As the sample is put in a separate cryostat, it is possible to perform measurements in a wide temperature range 100 K – 500 K. It is possible to achieve the Signal to Noise Ratio (SNR) of 100 dB (10^5). The specifications and Capabilities of the non-linear susceptometer are summarized in Table 5.1.

Table 5.1 Specifications and capabilities of the non-linear susceptometer

Specifications
500 kHz sampling rate
16 bit DAC/ADC
30 kHz LP RC filter to minimize the quantization noise of generated signal
Variable amplification range
Capabilities
Capacitance range of the sample 10 pF – 10 nF
Maximum amplitude of the generated voltage signal ± 10 V
Wide temperature range (depends on the cryostat used)
Signal to noise ratio up to 100 dB (10^5)
Estimated frequency range or the 1st harmonic 8 Hz – 10 kHz

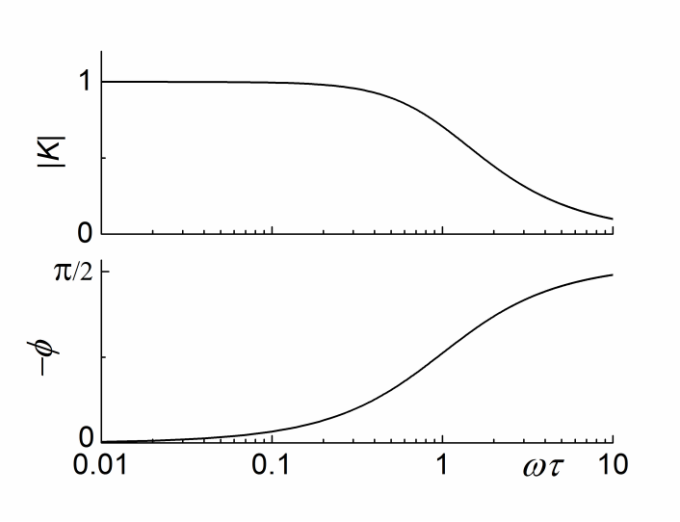

Figure 5.2 Frequency response of a low-pass RC filter.

The displacement current of the sample response is complex and contains a phase shift in respect of the reference signal. This data is used to calculate complex linear and non-linear susceptibilities, as explained in [42] and in part **3**. Here, couple of things should be considered: 1) DT9834 *Analog In* channels do not gather data exactly simultaneously, which is unavoidable, because the device uses semiconductor processor, which does not support real time parallel operations, thus there is an intrinsic delay between any two operations and that results in a phase shift between the measurement signal and the reference signal gathered in separate Analog In channels; 2) SR570 has limited amplification band, i.e. the phase of the amplifier response is flat up to the certain frequency. Furthermore, with an increase of frequency the phase shift increases. The amplification frequency band is limited by RC circuit. The typical frequency response of it is shown in Figure 5.2. As well, the amplifier has different sensitivities with different threshold frequencies. Figure 5.3 shows a temperature dependence of the third order non-linear susceptibility $\chi'_3(T)$ of a sample under test (the sample material is not specified, because here it is not of the primary importance). Data in dots show results after corrections of phase distortions caused by the equipment and lines show the not corrected data. A better picture of the influence of phase distortions to the data of $\chi'_3(T)$ is in Figure 5.4. It shows, that data of the highest frequency has the highest

relative error, which is consistent with the Figure 5.2, i. e. the equipment caused phase shift has more influence to higher frequencies. The jump of relative error in the vicinity of 400 K temperature is related with the switch of the sensitivity of the current preamplifier, as it has discrete sensitivities, which are switched based on the signal level.

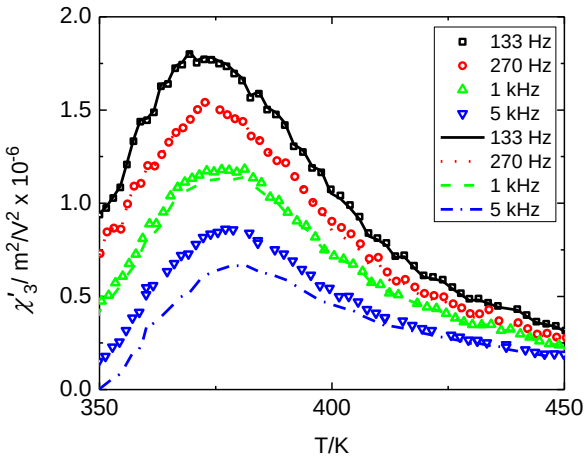

Figure 5.3 Temperature dependence of the third order non-linear susceptibility of sample under test. Dots show data of phase shift calibrated measurement, lines show data of measurement without phase shift calibration. Legend shows the frequency of the main harmonic

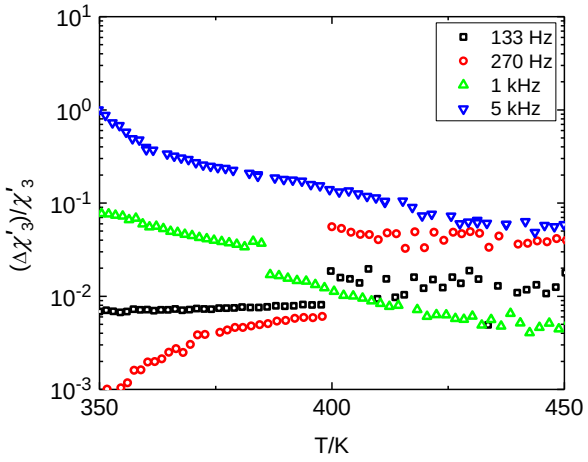

Figure 5.4 Relative error caused by phase distortions to the data of temperature dependence of the third order non-linear susceptibility (Figure 3.2.3). Legend shows the frequency of the main harmonic

The error to data caused by the phase distortions is clear. In order to acquire correct data at higher frequencies it is imperative to take into account the phase shift caused by the equipment. For this reason phase shift calibration is a must. The phase distortions of the system are evaluated by measuring calibration capacitors. We use Solartron 12961 dielectric reference module, which contains four precise linear capacitors of 9.31 pF, 102 pF, 0.999 nF, 10.04 nF capacitances. As well, the calibration signal is of specific shape, it is described by the following:

$$S(f) = \sum_{i=1}^{5} \frac{1}{i} \cos(2\pi i f t + \varphi_i) \qquad (3.2.4)$$

It consists of five harmonics, each harmonic has an amplitude lowered by a number of the harmonic in respect of the first harmonic. This is because the derivative of such signal would have equal amplitudes at every harmonic. And indeed, if we drive the calibration load, which is capacitive, with our voltage calibration signal, the resultant current will have the shape of a derivative of the original voltage signal. Furthermore, the initial phase of each harmonic is chosen such, that the peak/rms ratios of the signal and its derivative would be minimum. This helps to have more efficiently used dynamic range of the signal, i.e. there are less of sharp peaks in short timespans of the signal and the signal is more evenly distributed around the bias. The comparison between the signal, which have zero initial phases of each harmonic, and our specific signal is shown in Figure 5.5 and Figure 5.6. The phase of each harmonic of the calibration signal: $\varphi_1 \approx 0.412$, $\varphi_2 \approx 3.443$, $\varphi_3 \approx 2.859$, $\varphi_4 \approx 3.602$, $\varphi_5 \approx 2.922$. Figure 5.7 shows that in practice the voltage and current signals are of the same shape as shown in Figure 5.6.

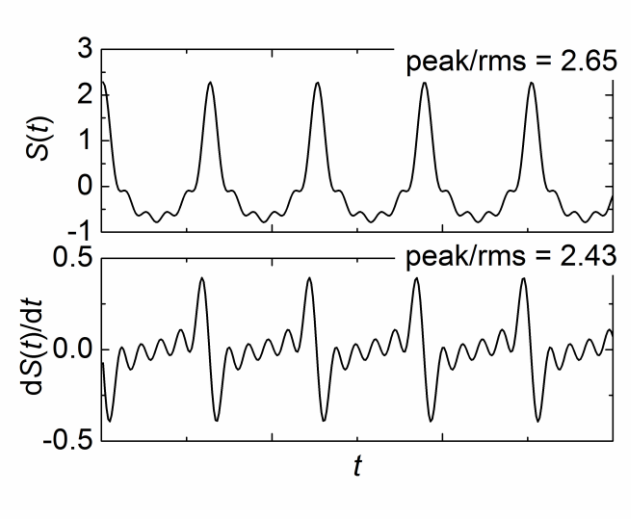

Figure 5.5 Shape of signal of sum of five harmonics and its derivative, where phases of each harmonic are equal

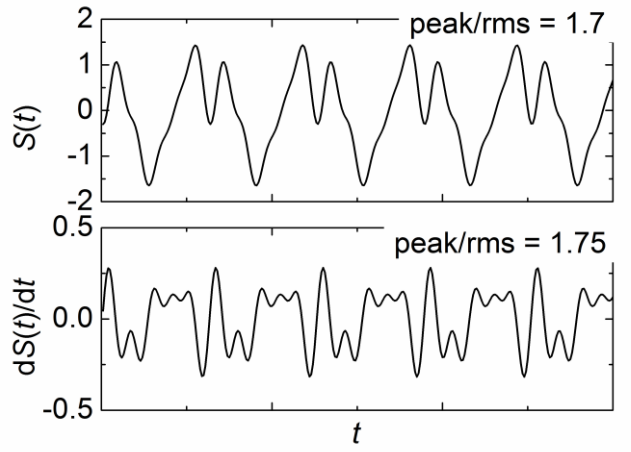

Figure 5.6 Shape of signal of sum of five harmonics and its derivative, where phases chosen to minimize Peak/RMS ratio of signal and its derivative. The phase of each harmonic: $\varphi_1 \approx 0.412$, $\varphi_2 \approx 3.443$, $\varphi_3 \approx 2.859$, $\varphi_4 \approx 3.602$, $\varphi_5 \approx 2.922$

It is important to notice that the amplitudes of higher harmonics of the non-linear response of the sample are quite low and sensitive to noise (Figure 5.8). The noise level of the system is rather low, but additionally, to obtain even better SNR the sample response averaging algorithm is implemented. Thanks to it, we are able to obtain SNR up to 100 dB. Furthermore, it is worth to mention, that our excitation signal, as any digitally created signal, tends to have a quantization noise, which distorts the amplitude of the signal. Although,

our voltage signal is rather linear (DT9834 uses 16 bit DACs and 500 kHz sampling frequency), but the small quantized steps in voltage signal, may give rather large peaks in a current response, if a capacitive load is driven. In order to prevent this uncontrollable phenomenon we use 1st order analog RC low pass filter, which has threshold frequency of 30 kHz, which has a sufficient attenuation of -20 dB per frequency decade to prevent effects of quantization noise of 500 kHz sampling frequency. Moreover, to reduce the quantization distortions of the generated signal we have implemented a dithering. The features mentioned here makes our system capable to measure a non-linear susceptibility of polar dielectrics.

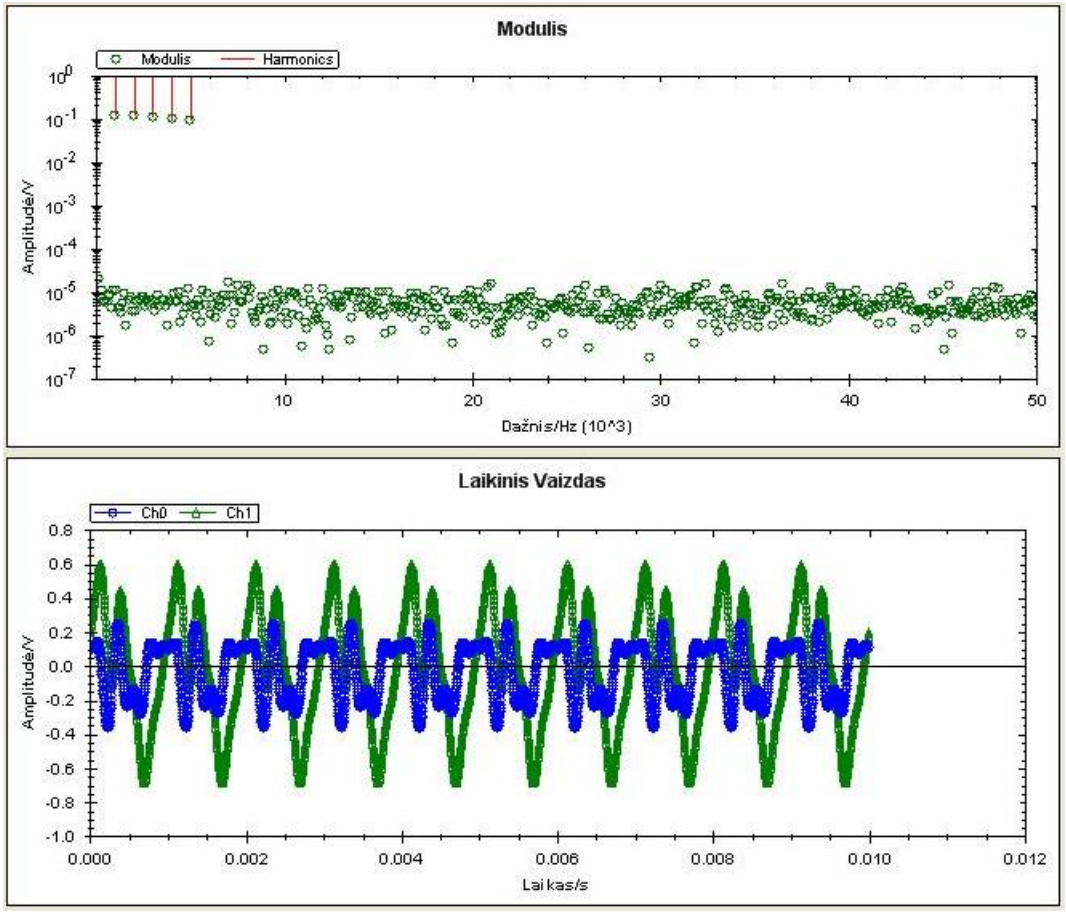

Figure 5.7 Measurement of calibration capacitor of 9.31 pF. The main harmonic frequency is 1 kHz. The higher graph shows spectrum of absolute amplitudes. The sticks are only a guide for eyes to find the five harmonics. The amplitude of each harmonic is the green circle. The lower graph shows the voltage signal (green, Ch1) and signal proportional to the current flowing in the circuit (blue, Ch0) in time plot. The graphs are taken from the actual program of the non-linear susceptometer

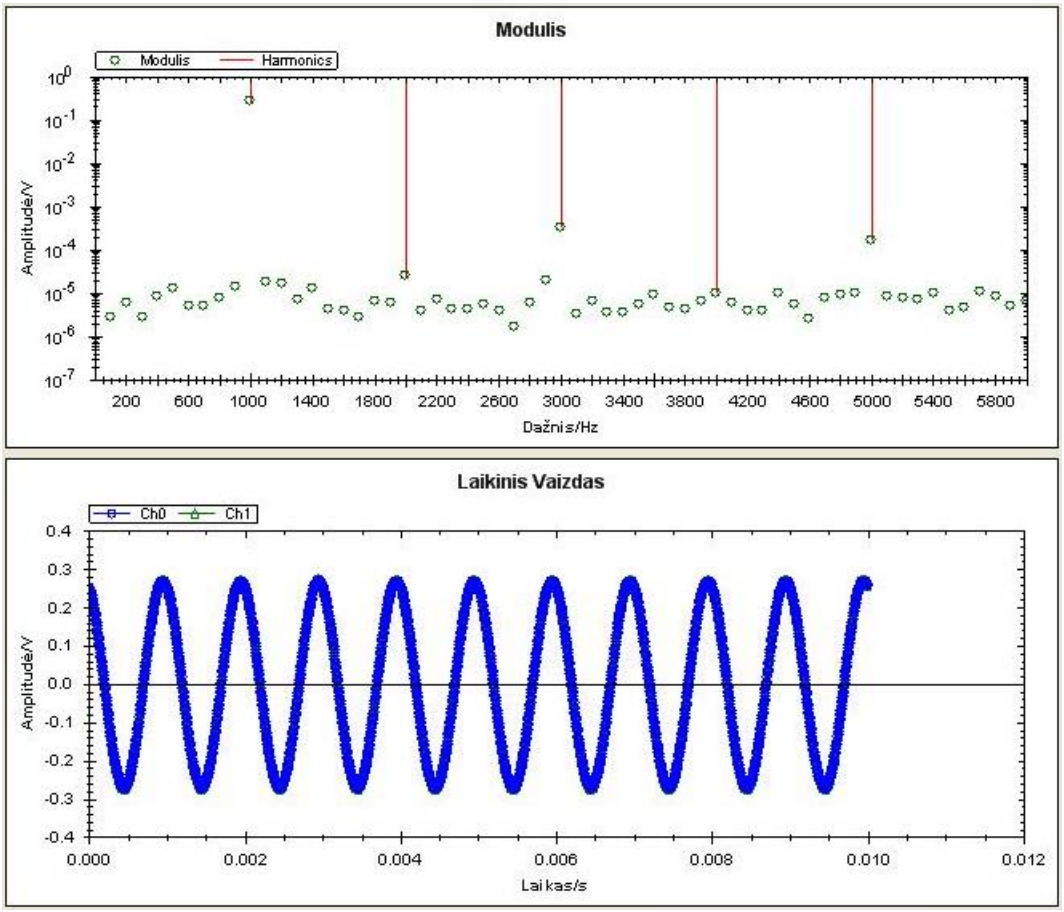

Figure 5.8 Response of a sample under test measured with the non-linear susceptometer. The generated voltage signal frequency is 1 kHz, amplitude 3 V. The higher graph is spectrum of absolute amplitudes. The sticks are only a guide for eyes to find the five harmonics, the amplitude of each harmonic is the green circle. The lower graph shows the signal proportional to the current flowing in the circuit. The generated voltage signal of 1 kHz is omitted here. The graphs are taken from the actual program of the non-linear susceptometer

The performance of the susceptometer is exhibited by an experiment performed on $0.4NaBi_{0.5}Ti_{0.5}O_3 - 0.45SrTiO_3 - 0.15PbTiO_3$ (0.4NBT-0.45ST-0.15PT) ceramic sample with silver paste contacts. The sample was heated up to a temperature of 460 K. The measurement of a non-linear susceptibility was performed on the cooling cycle down to 320 K. The frequencies of the generated signal were 80 Hz, 317 Hz, 1262 Hz and 5000 Hz. The amplitude of an alternating electric field was 160 V/cm. The sample was not additionally polarized in a constant electric field prior to the measurement.

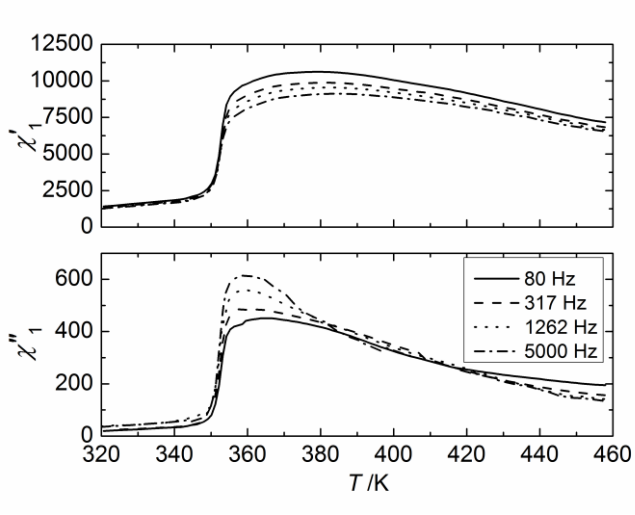

Figure 5.9 Temperature dependence of 1st order complex susceptibility of 0.4NBT-0.45ST-0.15PT ceramic

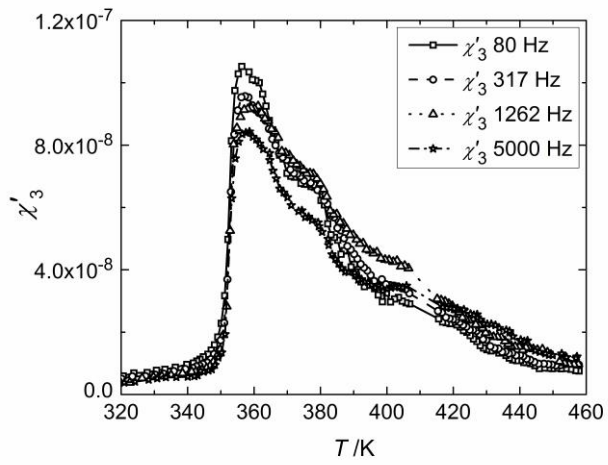

Figure 5.10 Temperature dependence of real part of 3rd order complex susceptibility of 0.4NBT-0.45ST-0.15PT ceramic

The results of the measurement are as follows. A temperature dependence of the 1st order complex susceptibility ($\chi'_1(T)$) is shown in Figure 5.9, where a specific behavior of the compound is revealed. In the temperature range above 360 K it behaves as a relaxor ferroelectric. Namely, the maximum of a real part of the complex susceptibility shifts towards the higher temperatures with increase of a frequency. In the vicinity of 350 K there is a susceptibility drop, which can be related to a discontinuous phase transition. Figure 5.10 shows a temperature dependence of the real part of 3rd order of complex susceptibility

($\chi'_3(T)$), which has a positive sign. That is a good indication of occurrence of the first order phase transition. Similar measurements were published by Svirskas et al. [49], only the measurements of the non-linear susceptibility presented there are made up to frequency of 1 kHz. Here we have shown, that our susceptometer is capable of measuring the non-linear dielectric response in frequencies higher than 1 kHz (5 kHz 1st harmonic in this particular case, which makes frequency of 15 kHz of the 3rd harmonic), primarily due to the additional calibration step, where frequency response of the system is evaluated.

Another example of the performance of our susceptometer was made by measuring PMN single crystal. The temperature behavior of $\chi'_1(T)$, $\chi'_3(T)$ and $a_3(T)$ are shown in Figure 5.11. $\chi'_1(T)$ shows a typical behavior of PMN. Here, $\chi'_3(T)$ may look as showing the first order phase transition, but it is well known, there are no structural phase transitions observed in the vicinity of the dielectric anomaly in PMN. Hence, $\chi'_3(T)$ shows a typical behavior of RFs, being positive in the vicinity of T_m. The obtained result is similar as published by Dec et al. [35]. As the authors wrote, so in our result, indeed, it cannot be spotted any anomalies in $a_3(T)$ in the vicinity of $T_f \approx 220$ K, as it was predicted by SRBRF glassy model of RFs [32,54,55]. However, it should be remarked, that the scaled non-linear susceptibility $a_3(T)$ can be considered as a static quantity [33] as it shows no sizable frequency dispersion [35]. The behavior of $a_3(T)$ on pure PMN is consistent with Glazounov-Tagantsev phenomenological model of dynamic non-linear response of RFs [33] and corresponds to typical RF behavior, that shows a single minimum of $a_3(T)$ close to T_m and steep increase for all the frequencies with cooling.

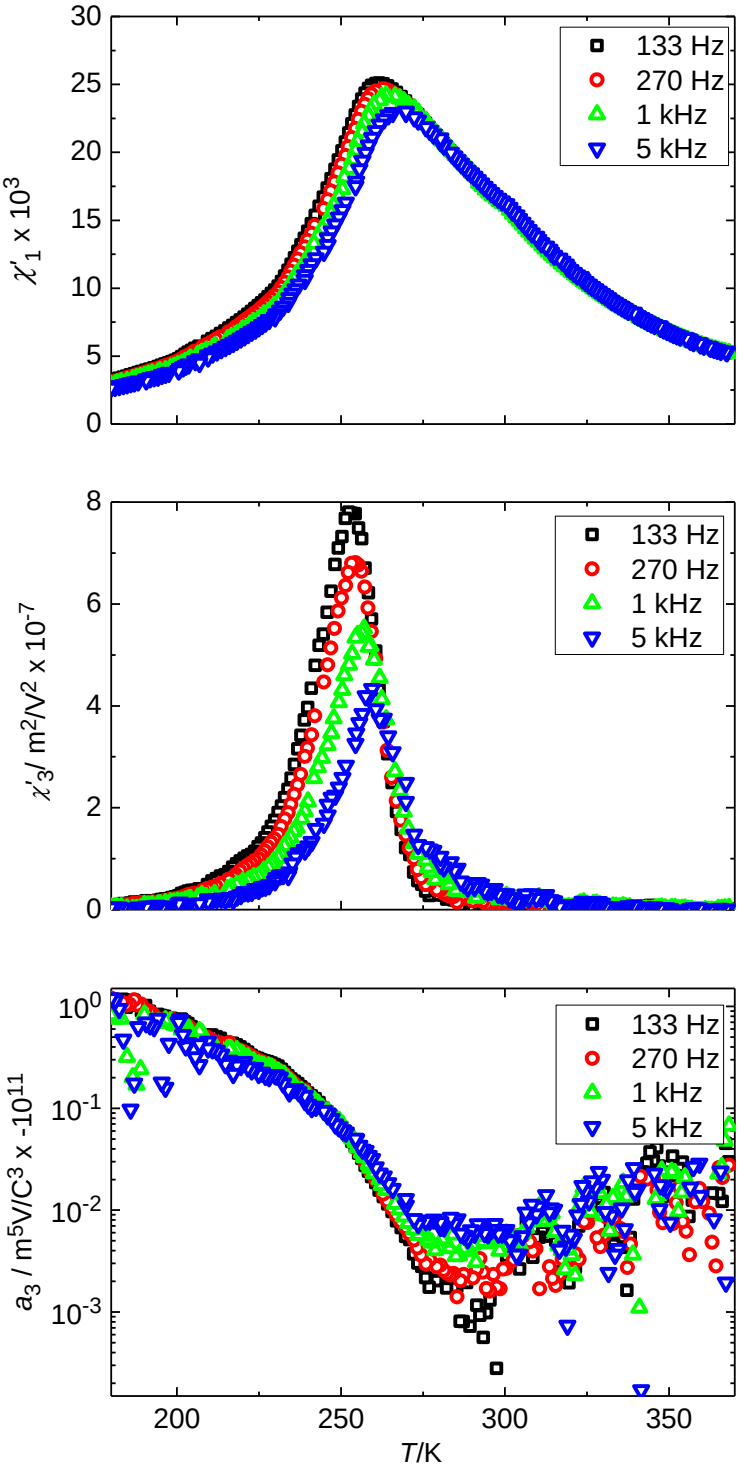

Figure 5.11 Temperature dependence of 1st order, 3rd order and scaled susceptibilities of PMN crystal

These two experimental examples confirm that we have constructed a powerful characterization setup. It allows characterizing the linear and non-linear macroscopic response of polar dielectrics simultaneously. High fields are not necessary, as in other non-linear experiments (e.g. determination of non-linearity from induced polarization). Furthermore, it is possible to obtain linear and non-linear response of material by a single experiment in wide temperature range. This opens a different perspective of analyzing polar dielectrics and characterizing phase transitions. Notably, such equipment is not available commercially and it exceeds other non-linear susceptometers constructed so far with expanded frequency range.

5.1.1 Summary

A powerful characterization setup was constructed. It allows measuring the linear and non-linear macroscopic response of polar dielectrics simultaneously, without requirement of high electric fields. Furthermore, it was shown that a phase shift calibration of the non-linear susceptometer allows expanding the frequency range of the measurement to the higher frequencies. The averaging algorithm helps to improve SNR. Combined with the phase shift calibration and proper filtering of the frequencies above the Nyquist limit, these improvements may allow measurements with fundamental frequency as high as 1/10 of the sampling frequency.

EXPERIMENTAL RESULTS

6.1 NON-LINEAR DIELECTRIC SUSCEPTIBILITY MEASUREMENTS OF (1-*x*)$PbMg_{1/3}Nb_{2/3}O_3$-*x*$PbTiO_3$ BASED MATERIALS

A strong piezoelectricity is found in solid solutions that show morphotropic phase boundary (MPB). The MPB is the boundary in a composition-temperature diagram, where the crystal structure changes abruptly [56]. One example of such interesting solid solutions is (1-*x*)$PbMg_{1/3}Nb_{2/3}O_3$-*x*$PbTiO_3$ (PMN-*x*PT). One compound, i.e. PMN, is a RF and PT is a normal ferroelectric. The PMN has a B-site charge disorder in a perovskite lattice, which creates random fields and supposed to promote the RF behavior, while the increase of PT supposed to decrease the strength of random fields. This is because the titanium ion has valence of 4+ and it is compatible in the $A^{2+}B^{4+}O_3$ perovskite lattice [31,57]. As well, PT has high T_C and combined with PMN shifts T_m to higher temperatures. The structural features near MPB of (1-*x*)PMN-*x*PT rise many discussions. At first, it was considered that the MPB distinguishes rhombohedral and tetragonal phases and that the material undergoes two consequent phase transitions: from cubic to tetragonal and from tetragonal to rhombohedral phase [58]. Later on, it was established that there is an intermediate monoclinic phase around the MPB [57]. According to what is written above, two interesting things can be pointed out. Firstly, it is known that from the certain value of PT concentration a spontaneous ferroelectric to RF phase transition should occur in the system. Hence, it is interesting to determine this concentration. Secondly, the mechanism of crossover from RF to ferroelectric is not determined so far.

Earlier investigations of the 0.83PMN-0.17PT single crystal (the middle composition between the PMN and MPB of PMN-*x*PT) showed that the mean relaxation time obtained by the broadband dielectric spectroscopy [59] undergoes a critical slowing down. This resembles an order-disorder phase transition. The critical slowing down of a central peak was also observed by the inelastic light scattering experiments [60,61]. It is worth noting that

inelastic light scattering experiments favor the existence of a phase transition in some lower content compositions [61–63].

It is obvious that the (1-*x*)PMN-*x*PT solid solution raises many scientific discussions and proves to be a fundamentally interesting solid solution. In order to increase the amount of knowledge about the compound non-linear dielectric susceptibility measurements were performed on the 0.83PMN-0.17PT single crystal. It was written above (section **4.1**) about the capabilities of this powerful research technique for polar dielectrics.

The 0.83PMN-0.17PT sample was received from prof. S. Kojima from Graduate School of Pure and Applied Sciences, University of Tsukuba, Japan. The single crystal was grown by the modified Bridgman technique [64]. Raw powders of PbO, MgO, Nb_2O_5 and TiO_2 with purity of more than 99.99% were used. The powders were mixed and a single crystal grown in a sealed platinum crucible to prevent the evaporation of PbO at high temperatures. The PMN seed crystal was used. The highest temperature was 1380°C and the temperature gradient was about 40-100°C/cm at a solid-liquid interface. The furnace temperature was controlled using a proportional integral differential (PID) controller. After soaking ≈ 10 h, the crucible was dropped at the rate of 0.1 to 1 mm/h. At the end of the process, the furnace temperature was cooled at the rate of 25°C/h to a room temperature.

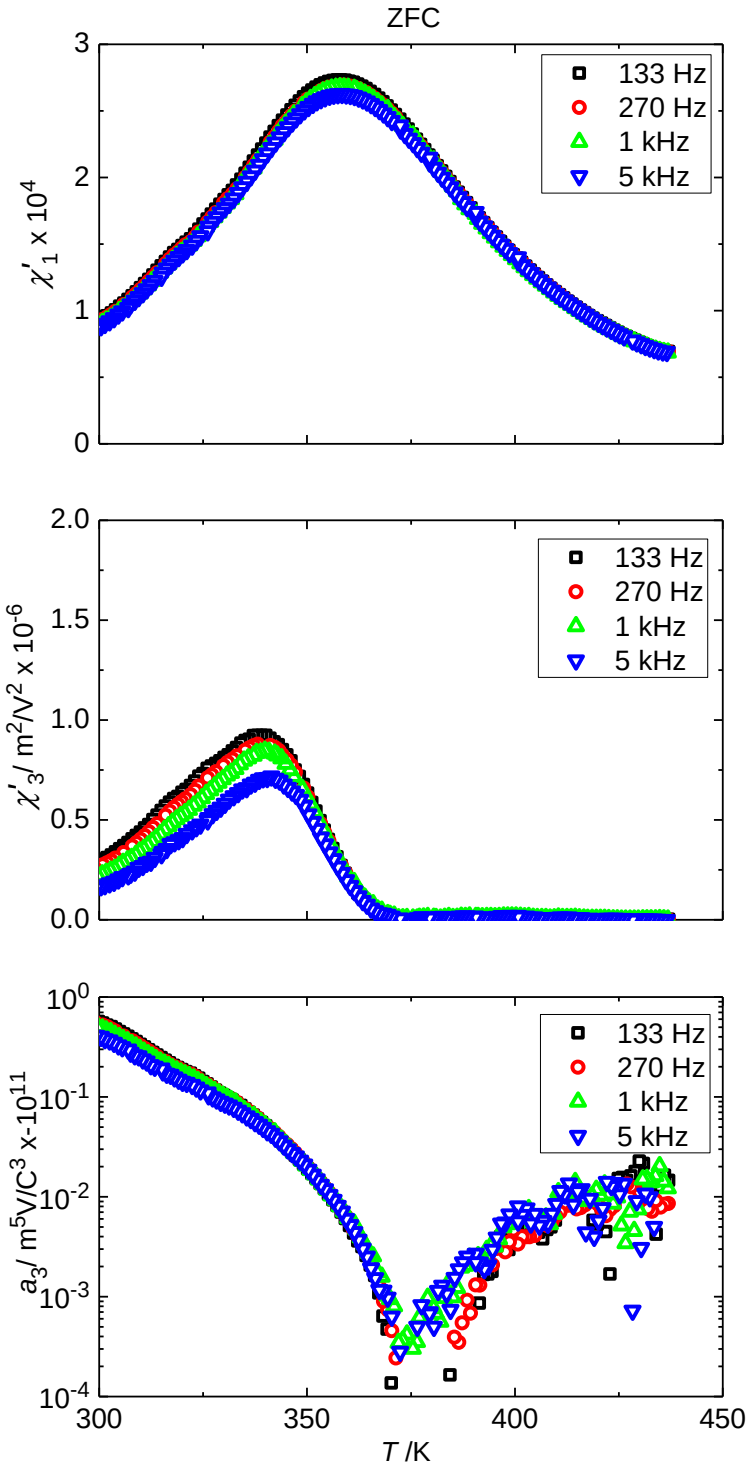

Figure 6.1.1 Temperature dependence of the first order susceptibility $\chi'_1(T)$ and the third order susceptibility $\chi'_3(T)$, as well as, scaled non-linear susceptibility $a_3(T)$ of ZFC PMN-0.17PT single crystal

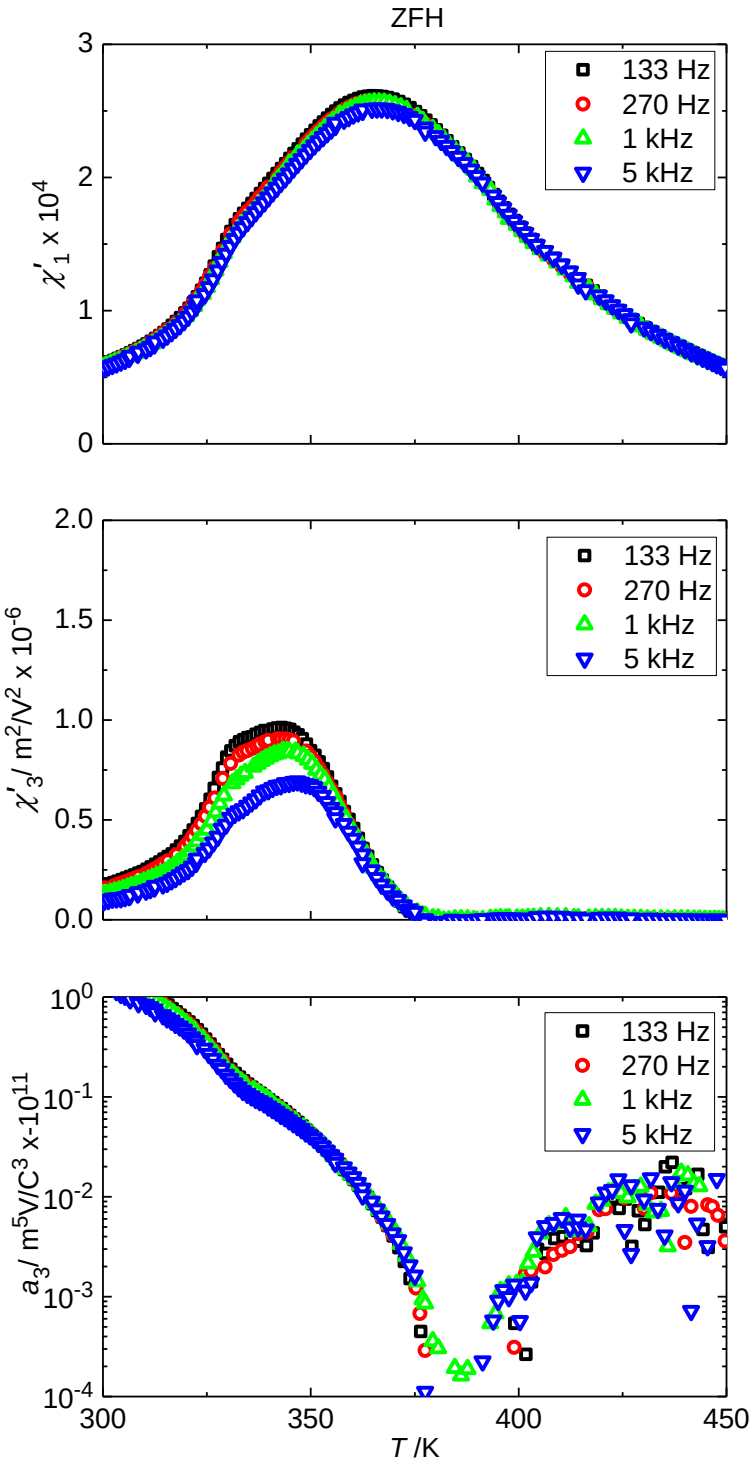

Figure 6.1.2 Temperature dependence of the first order susceptibility $\chi'_1(T)$ and the third order susceptibility $\chi'_3(T)$, as well as, scaled non-linear susceptibility $a_3(T)$ of ZFH PMN-0.17PT single crystal

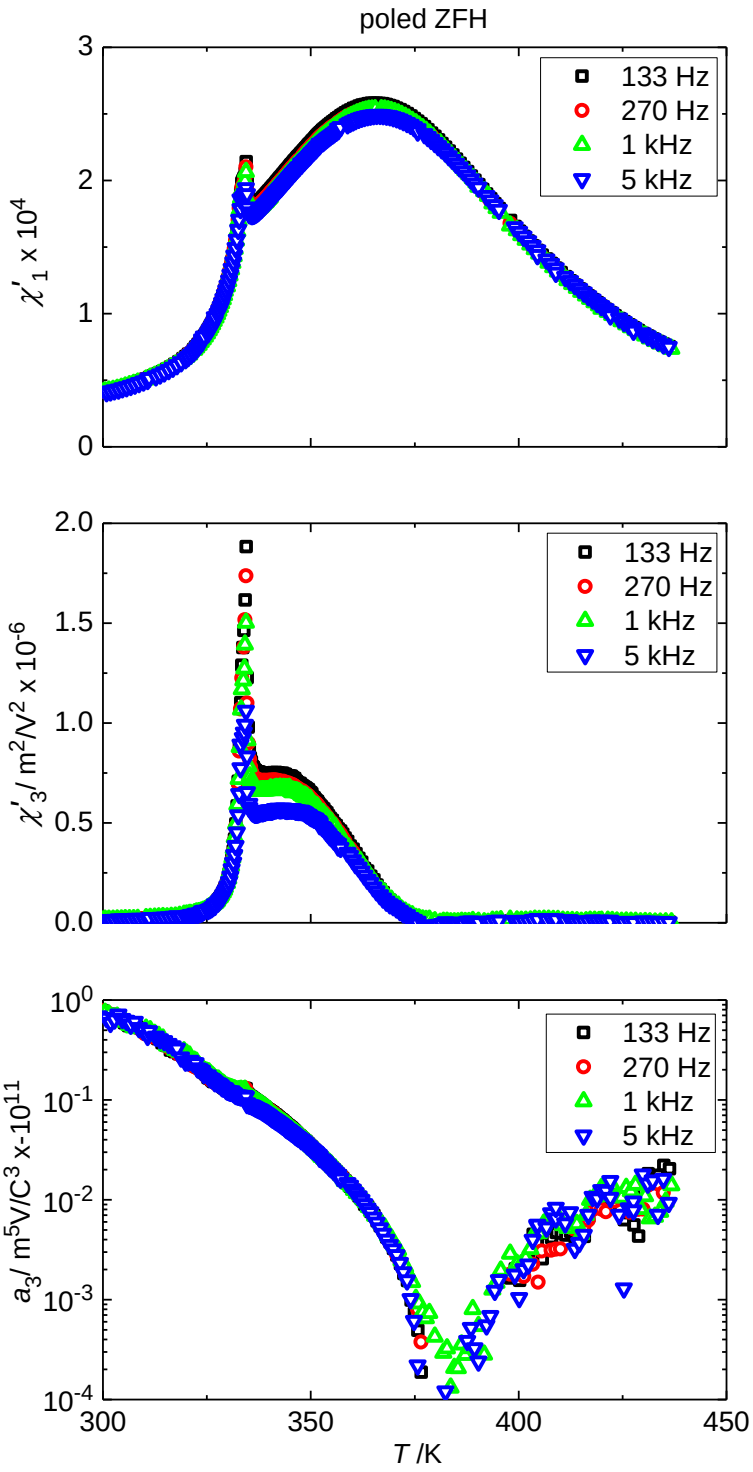

Figure 6.1.3 Temperature dependence of the first order susceptibility $\chi'_1(T)$ and the third order susceptibility $\chi'_3(T)$, as well as, scaled non-linear susceptibility $a_3(T)$ of ZFH poled PMN-0.17PT single crystal

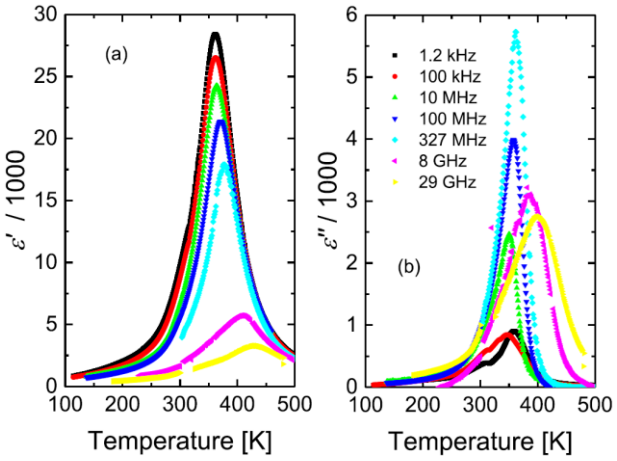

Figure 6.1.4 Temperature dependence of complex dielectric permittivity at different frequencies of a PMN-17PT single crystal [59].

Temperature dependences of the linear ($\chi'_1(T)$) and the third order non-linear ($\chi'_3(T)$), as well as, the scaled ($a_3(T)$) susceptibilities are shown in Figure 6.1.1. The linear part have a shape similar to any RFs, except in the frequency range presented the shift of peak towards the higher temperatures with increase of frequency is not pronounced. However, the shift is clearly seen in higher frequencies as published in [59] (Figure 6.1.4). If compared to pure PMN, the PMN-0.17PT has the temperature of maximum of dielectric susceptibility $T_m \approx$ 360 K, which is ≈ 100 K higher than in pure PMN (Figure 5.11). The T_m of PMN-0.17PT is increased, because of high phase transition temperature of ferroelectric PT addition, which is T_C = 763 K [65]. The nonlinear part of the dielectric susceptibility – $\chi'_3(T)$ is positive in the temperature range. Such behavior of $\chi'_3(T)$ hardly shows a phase transition. The response of $\chi'_3(T)$ and $a_3(T)$ is quite similar to the pure PMN [35] (Figure 3.2.8), hence PMN-0.17PT shows a RF behavior. The behavior of $a_3(T)$ is consistent with Glazounov-Tagantsev phenomenological model of dynamic non-linear response of RFs [33]. The obtained result shows quite a contrast to PZN-0.08PT [40], which has a change of sign in $\chi'_3(T)$, indicating occurrence of the 1st order phase transition. This structural phase transition was clarified by the powder neutron diffraction experiments [66].

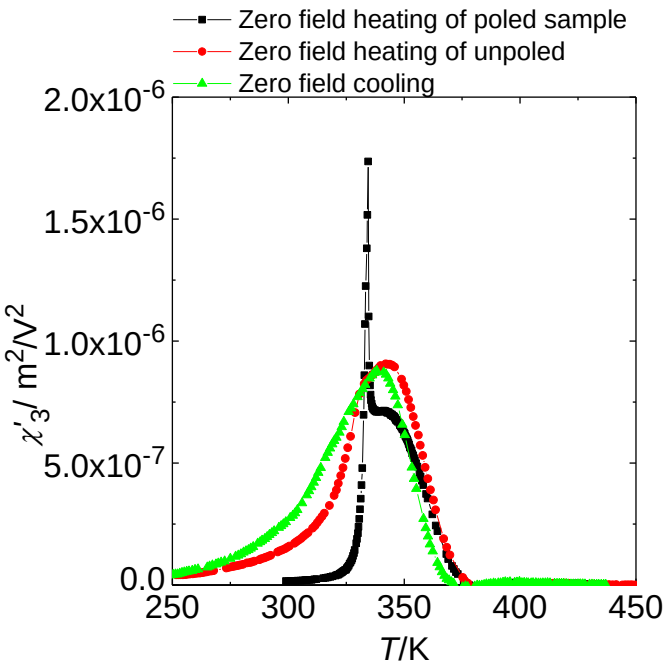

Figure 6.1.5 Temperature dependence of third order susceptibility of PMN-0.17PT single crystal measured in three different regimes

Non-linear susceptibility measurements on PMN-0.17PT were performed in a zero field cooling (ZFC) and a zero field heating (ZFH) regimes for both poled and unpoled sample. Obtained results of ZFH runs are shown in Figure 6.1.2 and Figure 6.1.3 of poled sample. The ZFC and ZFH curves are compared in Figure 6.1.5. It can be seen, that $\chi'_3(T)$ of an unpoled sample shows a temperature hysteresis. The hysteresis can be observed in the linear susceptibility, too. The interesting fact is that the increase of χ'_3 is much sharper during the ZFH compared to the ZFC experiment. This might be the hint of a slow spontaneous ordering and growth of PNRs to macroscopic ferroelectric domains in 300 – 340 K temperature region. As well, the critical slowing down was reported to be observable by the broadband dielectric spectroscopy in this temperature region [59]. ZFH curve of the poled sample shows a sharp peak at around 330 K temperature. This peak clearly indicates the 1st order phase transition. Above the phase transition temperature a $\chi'_3(T)$ shows a behavior similar to RFs (positive broad peak). Finally, in higher temperatures the curve converges with the ZFH curve of the unpoled sample.

The occurrence of the phase transition to a ferroelectric phase on cooling is confirmed by hysteresis loops measurements.

In closer observation of $\chi'_1(T)$ of ZFH measurement of PMN-0.17PT a hump can be observed in vicinity of $T \approx 330$ K. This hump manifests as a sharp peak in $\chi'_3(T)$ in the poled sample. This means, that the phase transition occurs not only in poled sample, but in unpoled sample, too. In other words, external electric field is not necessary for occurrence of the phase transition in PMN-0.17PT single crystal. Poling of the sample only produces an alignment of domains within the sample and promotes higher jump in $\chi'_3(T \approx 330$ K). However, the hump is not observed in the ZFC run. It is quite clear, that PMN-0.17PT is in RF state in $T > 330$ K. Maybe, in the ZFC run, PNRs are oriented quite chaotically in vicinity of $T \approx 330$ K. This gives a RF like response of $\chi'_1(T)$ and $\chi'_3(T)$. However, in lower temperature, motions of PNRs are slowing down and they tend to correlate their alignment to the polarization direction of domains, similarly as explained by G. Xu et al. [29] (section **3.2**, p. 30). Indirect evidence of this is the dependence of a sharpness of the hump on polarization of the sample. Then, upon heating, past the phase transition temperature, ferroelectric domains vanishes and only partly correlated motions of PNRs remains, that contribute to $\chi'_1(T, f)$ (RF like broad maximum is observed).

Another solid solutions measured were PMN-0.1PT ceramics doped with 0.5% and 1% Mn (PMN-0.1PT:0.005Mn, PMN-0.1PT:0.01Mn). The samples were made by R. Katiliūtė supervised by prof. B. Malič in Jožef Stefan Institute, Ljublijana, Slovenia. The ceramics were prepared by mechano-synthesis method [67–70]. Chemicals used were: PbO (99.9%), MgO (99.24%), Nb_2O_5 (99.9%), TiO_2 (99.8%), MnO_2 (99.01%). Firstly, MgO was milled in a planetary mill for 3 hours at 600 rpm rate. Yttrium stabilized Zirconium (YSZ) balls of 3 mm size were used. Milling process was performed in an isopropanol. Powders were dried in 358 K temperature after the milling. Then, all the powders were mixed together and homogenized in the

planetary mill for 2 hours at 200 rpm rate. This was performed in an isopropanol together with 10 mm sized YSZ balls. The homogenized powder was dried in 358 K temperature. After that, the main procedure of the mechano-synthesis took part. The homogenized powder was milled for 72 hours at 300 rpm rate in the planetary mill, in an isopropanol, together with Wolfram-Carbide (WC) balls of 20 mm diameter. At the very end, the milling rate was increased to 800 rpm and YSZ balls of 3 mm diameter were used. Again, the milling took part in an isopropanol. Then, the resultant powder was dried. Further on, the powder was pressed with a single-axis press under 50 MPa of pressure. After that, an isostatic pressure of 300 MPa was used. Lastly, the pressed powder was heated in a furnace. The temperature of 1473 K was reached, with a heating rate of 2 K/min. The cooling to room temperature took part in the same rate after keeping the ceramic sample in temperature of 1473 K for 2 hours.

Mn doping of ferroelectric materials supposed to pin down the domains, which could be polarized with a strong external electric field, below the temperature of the phase transition. This happens due to the acceptor behavior of Mn^{2+}, generating oxygen vacancies for a charge compensation and resulting in defect dipole pairs that pin the domains [71–73]. Pinning of PNRs of RF is probable, as well.

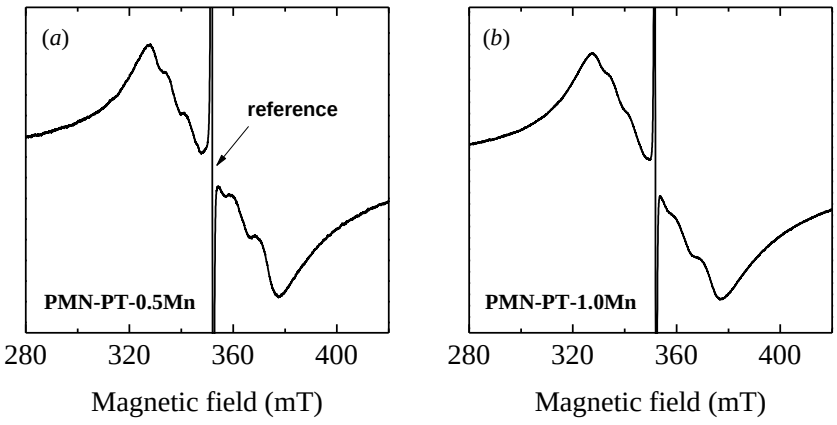

Figure 6.1.6 Room temperature X-band CW EPR spectrum of (a) PMN-0.1PT:0.005Mn (b) PMN-0.1PT:0.01

An EPR measurement on Mn-doped PMN-0.1PT (results unpublished) was supplied by a colleague M. Šimėnas. According literature, for Mn^{2+} ions one expects $g > 2$, while for Mn^{4+} the g-factor is slightly smaller than 2 [74]. EPR spectra of PMN-0.1PT:0.005Mn and PMN-0.1PT:0.01 (Figure 6.1.6) consist of broad line at the electron g-factor $g = 1.999(1)$ with poorly resolved hyperfine splittings of about 240 MHz. Thus, it is difficult to unambiguously determine the charge of the Mn ions from the current experimental data. Hence, results hint about appearance of Mn^{4+} and Mn^{2+} in Mn-doped PMN-0.1PT.

According to the defect chemistry of the perovskite structure, the introduction of charged impurities can change the concentration of oxygen or lead vacancies. Doping ions prefer to substitute the ions with equal valence and similar radii according to crystal chemistry principle. The radius of Mn^{2+} is close to that of Mg^{2+}, Nb^{5+} or Ti^{4+} [73]. So Mn^{2+} can be incorporated onto B sites, and oxygen vacancies are created for the charge compensation, resulting in defect dipole pairs [73].

The comparison of $\chi'_1(T)$, $\chi'_3(T)$ and $a_3(T)$ of PMN-0.1PT, PMN-0.1PT:0.005Mn, PMN-0.1PT:0.01Mn is shown in Figure 6.1.10, Figure 6.1.11 and Figure 6.1.12, accordingly. PMN-0.1PT shows a strong RFs behavior with a clear shift of maximum towards the higher temperatures with the increase of a frequency, in $\chi_1(T)$ plot (Figure 6.1.10). It is more difficult to spot the shift of the maximum of Mn-doped samples (Figure 6.1.11, Figure 6.1.12) or there is no shift of the maximum in the frequency range observed. However, the shift of the maximum is clearly visible in higher frequencies [67] (Figure 6.1.7). On the other hand, a clear decrease of maximum value of $\chi'_1(T)$ with the increase of Mn dopant concentration can be observed. As well, the maximum of $\chi'_1(T)$ shifts towards the higher temperatures with the increase of Mn dopant concentration (Figure 6.1.7). The behavior similar to that of the pure PMN single crystal [35] can be observed in $\chi'_3(T)$ of PMN-0.1PT, i.e. $\chi_3(T)$ shows

positive values in the temperature range observed with the frequency dispersion.

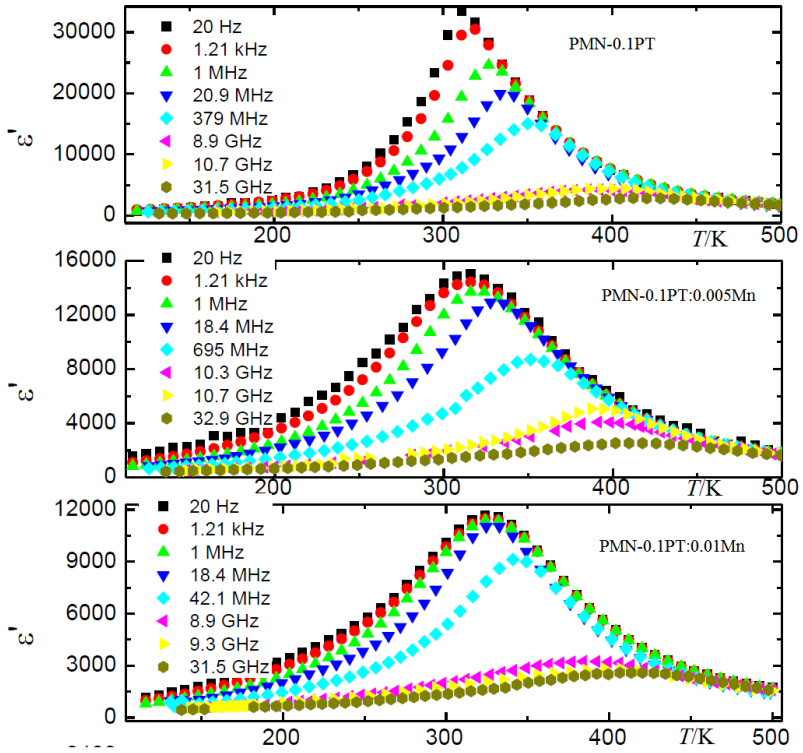

Figure 6.1.7 Broadband frequency dependence of dielectric permittivity of PMN-0.1PT (top), PMN-0.1PT:0.005Mn (middle) and PMN-0.1PT:0.01Mn (bottom) ceramics, showing a shift of maximum towards the higher temperatures with increase of frequency.

PMN-0.1PT:0.005Mn and PMN-0.1PT:0.01Mn shows a significant decrease of maximum of $\chi_3(T)$. Before discussing the temperature behavior of the scaled non-linear susceptibility $a_3(T)$, it should be remarked, that $a_3(T)$ can be considered as a static quantity [33] as it shows no sizable frequency dispersion [35]. The behavior of $a_3(T)$ of PMN-0.1PT:xMn can be compared with the one published by Dec et al. [35] on the pure PMN, which corresponds to a typical RF behavior, i.e. $a_3(T)$ shows small values in $T > T_m$ and it shows a rapid increase in $T < T_m$. Such behavior is consistent with Glazounov-Tagantsev phenomenological model of dynamic non-linear response of RFs [33]. However, in this case, it can be clearly observed, that the angle of the $a_3(T)$ curve in temperatures $T < 300$ K becomes more shallow with increase of Mn dopant concentration. Such behavior of $a_3(T)$ can be explained so, that the decrease of maximum of $\chi_1(T)$ is relatively much smaller, than the decrease of

maximum of $\chi_3(T)$, i.e. the decrease of $\chi_1(T)$ maximum in PMN-0.1PT:0.005Mn is ≈ 52%, if compared to the undoped PMN-0.1PT. The decrease of $\chi_3(T)$ maximum in PMN-0.1PT:0.01Mn ≈ 97%, if compared to the undoped PMN-0.1PT. The reason, why there is such a significant decrease in non-linear component of PMN-0.1PT:*x*Mn with increase of Mn dopant concentration is the most interesting. It is believed that higher order susceptibilities are more sensitive to dipolar order than the linear one [75,76]. Having this in mind, it seems that PMN-0.1PT doping with Mn indeed pins down PNRs, which are responsible for a huge susceptibility value of RFs.

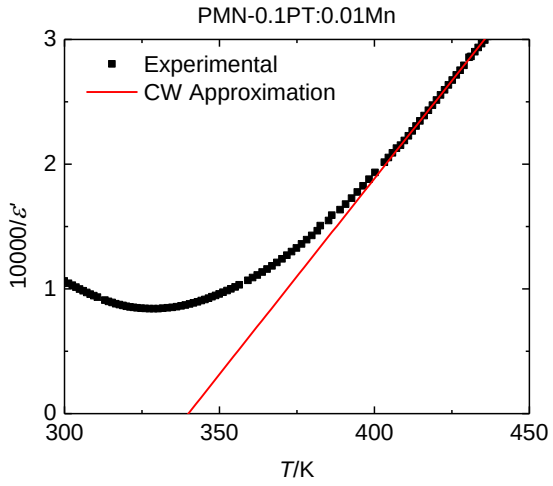

Figure 6.1.8 Curie-Weiss law (6.1.3) approximation above T_C on temperature dependence of inverse dielectric permittivity of PMN-0.1PT:0.01Mn ceramic

In order to find an explanation for the Mn impact on PMN-0.1PT behavior a temperature dependence of Edwards – Anderson parameter $q(T)$ was calculated. This parameter describes the tendency of nearby dipoles (in dielectric material) to have the similar orientation.

It is known that $\chi_1(T)$ is related with $q(T)$ with the following relation [32], in zero bias field:

$$\chi_1(T) = \frac{C(1-q(T))}{T - T_C(1-q(T))} \qquad (6.1.1)$$

Here T_C – is Curie temperature, C – is a constant. Given relationship allows deriving of expression of $q(T)$:

$$q(T) = 1 - \frac{T\chi_1(T)}{C + T_C\chi_1(T)} \qquad (6.1.2)$$

In order to find out the values of T_C and C, Curie-Weiss (CW) law (6.1.3) [77] approximations were applied on all three compositions of PMN-0.1PT:*x*Mn. Figure 6.1.8 shows the CW (6.1.3) approximation made on a temperature dependence of the inverse dielectric permittivity of PMN-0.1PT:0.01Mn ceramic.

$$\chi_1(T) = \frac{C}{T - T_C} \qquad (6.1.3)$$

This relationship is valid in temperatures above T_C. For approximation reasons, the inverse of the law was used, which allows linear approximation and easy expressions of C and T_C:

$$\frac{1}{\chi_1} = \frac{T - T_C}{C} \equiv kT + b \quad \Rightarrow \quad C = \frac{1}{k}; \quad T_C = -\frac{b}{k} \qquad (6.1.4)$$

Here k – is a slope coefficient and b – is an intercept of the linear function. The values of T_C and C are shown in Table 6.1.1. Equation (6.1.5) represents the physical meaning of the parameter q.

$$q_\mu = \frac{1}{N}\sum_i \langle S_{i\mu} \rangle^2 \qquad (6.1.5)$$

Table 6.1.1 CW approximation above T_C parameters of PMN-0.1PT:*x*Mn

	PMN-0.1PT	PMN-0.1PT:0.005Mn	PMN0.1-PT:0.01Mn
T_C/K	337 ± 1	327 ± 1	341 ± 1
$C/10^3$K	415 ± 10	525 ± 10	318 ± 10

The expression (6.1.5) says, that q of axis μ (where μ – is the axis in x, y, z three dimensional space) is equal to the average of a mean square of a dimensionless dipolar orientation S along the axis μ. N – is the number of PNRs. If all dipoles within the single dynamic PNR are oriented the same

direction (maximum correlation of the orientation) then q = 1. If none of the dipoles within the single PNR are oriented the same direction (orientations are not correlated), then q = 0. Assuming that surroundings of PNRs are non-polar, it is possible to talk about the overall correlation of orientation of dipoles within the crystal. To make this clearer, let's consider two publications discussed in the overview (section **3.1**). Xu et al. [12] come up with the idea that PNRs grow and/or smaller PNRs merge to larger ones with the decrease of temperature. Koreeda et al. [19] observed a fractal formation and percolation of PNRs with the decrease of temperature. This means, that just below T_B in charge disordered regions (because remaining regions are non-polar) of RF correlation of orientation of dipoles starts, with a very short radius of correlation. These dipole systems of correlated dipoles are PNRs. With decrease of temperature, the correlation radius increases. It should look like growth of PNRs. Now looking to Figure 6.1.9, it is possible to observe the increase of Edwards – Anderson parameter $q(T)$ with the decrease of temperature in PMN-0.1PT ceramics. This result is consistent with the assumption of growth of PNRs, i.e. the increase of radius of correlation of orientation of dipoles. This is, as well, consistent with $\chi'_1(T)$ (Figure 6.1.10), particularly with the shift of maximum of $\chi'_1(T)$ of PMN-0.1PT with the increase of frequency. The smaller PNRs are quick to flip and/or breath, hence they give contribution to high frequency curve of $\chi'_1(T)$. However, with the decrease of temperature PNRs grow and become more sluggish, i.e. larger ensemble of correlated dipoles require more time to flip. The frequency of flipping of PNRs become smaller, hence the contribution to $\chi'_1(T)$ of higher frequency starts to decrease. However, these slower PNRs are larger, hence they produce a larger peak of $\chi'_1(T)$ in lower frequency. Now looking again to Figure 6.1.9, the $q(T)$ of PMN-0.1PT:0.01Mn behaves the same, but it is shifted towards the higher temperatures, i.e. the $q(T)$ of PMN-0.1PT:0.01Mn has a higher value than undoped PMN-0.1PT at the same temperature. Firstly, let's discuss the behavior of $\chi'_1(T)$ of PMN-0.1PT:0.01Mn, which is presented

in Figure 6.1.12. The very first thing to notice, the maximum value of PMN-0.1PT:0.01Mn is smaller than in undoped ceramic, as well the maximum temperature is shifted towards the higher temperatures, if we compare to the undoped sample. However, the most important thing to observe is the absence of clearly visible shift of $\chi'_1(T)$ with increase of frequency. Broadband dielectric spectroscopy of PMN-0.1PT:0.01Mn showed the appearance of the clear shift the $\chi'_1(T)$ only in higher frequencies [67] (Figure 6.1.7). Considering earlier discussed relationship between the shift of maximum of $\chi'_1(T)$ with the increase of frequency and growth of PNRs, it seems that PMN-0.1PT:0.01Mn has a limit of length of correlation radius. The fact that the shift of maximum of $\chi'_1(T)$ is observed in higher frequencies [67] shows, that there is a growth of PNRs with decrease of temperature, but limited. At a certain frequency, the shift of maximum of $\chi'_1(T)$ vanishes and the maximum of $\chi'_1(T)$ of every lower frequency curve resides in the same temperature in PMN-0.1PT:0.01Mn. That means, the fixed size PNRs are flipping fast enough to give contribution to the lower frequency. It is known from literature, that Mn^{2+} pins down domains of a material [71–73]. It is possible, that dopant of Mn in PMN-0.1PT:0.01Mn pins some of dipoles, that otherwise could participate in collective motion. Furthermore, it is possible, that pinned static dipoles are spreading the correlation of orientation to other dipoles. Such behavior may be a reason, why there is a limit of growth of PNRs in PMN-0.1PT:0.01Mn ceramics. The explanation to $q(T)$ being higher than in undoped sample, then is quite simple, the volume of dynamic PNRs are limited by static surroundings, due to Mn-doping and in smaller PNRs dipoles orient easier. Furthermore, it is quite possible, that there is no percolation of PNRs in PMN-0.1PT:0.01Mn ceramics contrastingly to result published by Koreeda et al. [19].

The huge decrease of non-linear susceptibility $\chi'_3(T)$ of PMN-0.1PT:xMn with increase of Mn, can be explained using idea presented above. The expansions of PNRs are restricted in Mn doped compositions, i.e. the correlation of orientation of dipoles cannot spread to the PNRs that are pinned.

It means, that motions of dipoles within PNRs give contribution to the linear susceptibility $\chi'_1(T)$, while contribution to the non-linear susceptibility comes from the electric field driven spreading of PNRs.

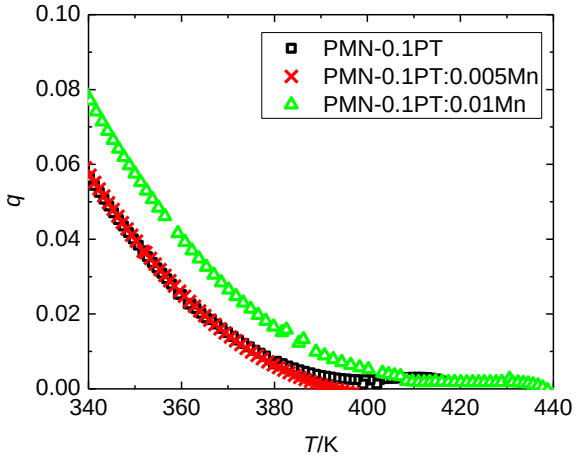

Figure 6.1.9 Temperature dependence of Edwards – Anderson parameter of PMN-0.1PT:*x*Mn above T_C

6.1.1 Summary

It was shown, that in PMN-0.17PT single crystal the phase transition of 1st order is observed, once performing non-linear dielectric spectroscopy on poled sample. It manifests as a sharp peak in $\chi_3(T)$ at $T \approx 330$ K.

PMN-0.1PT doping with Mn gives strong decrease of $\chi_1(T)$, as well as, $\chi_3(T)$. It is believed, that Mn^{2+} generates oxygen vacancies for a charge compensation [71–73] and results in pinning of otherwise dynamic PNRs. Hence, contribution to $\chi_1(T)$ is decreased.

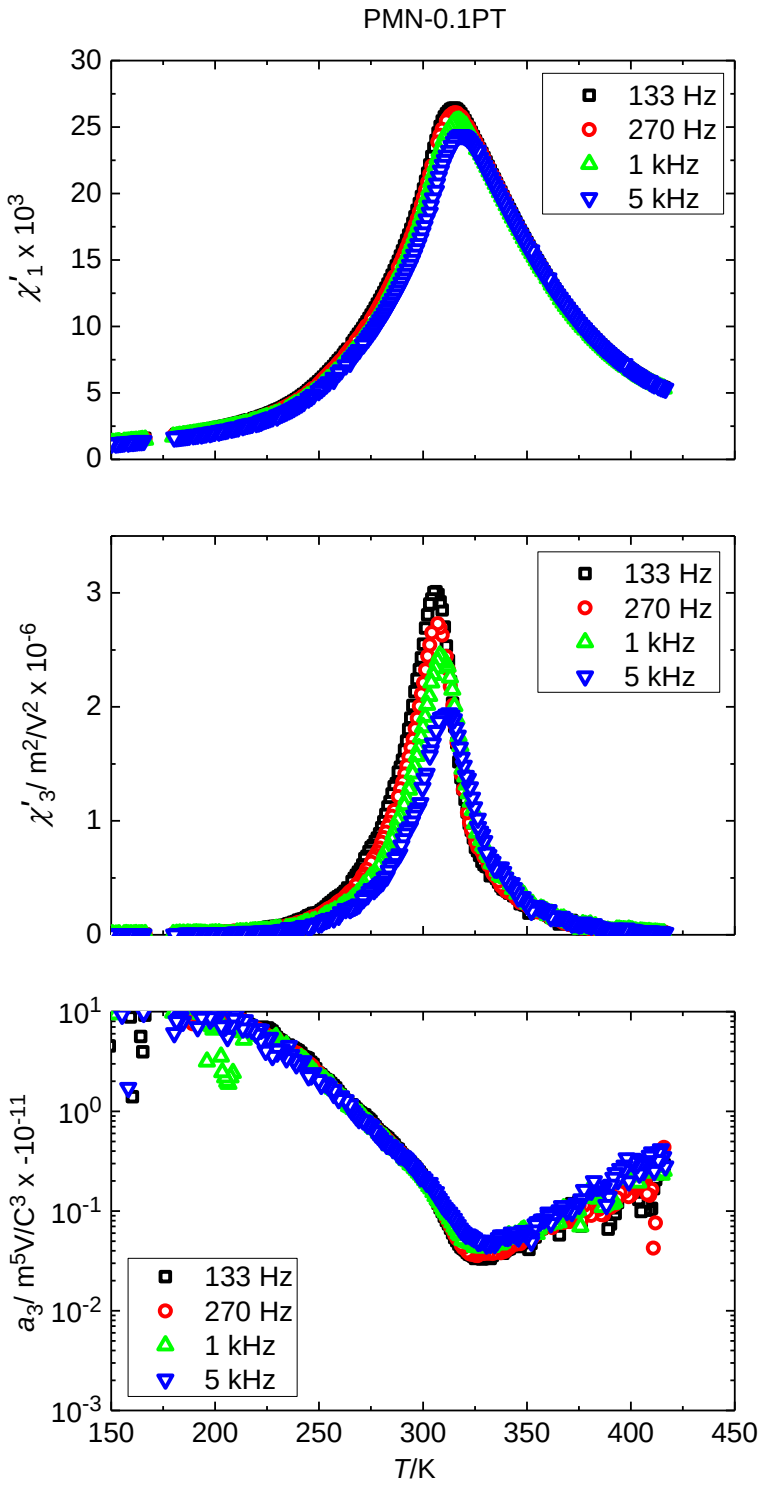

Figure 6.1.10 Temperature dependence of 1st order, 3rd order and scaled susceptibilities of PMN-0.1PT ceramic

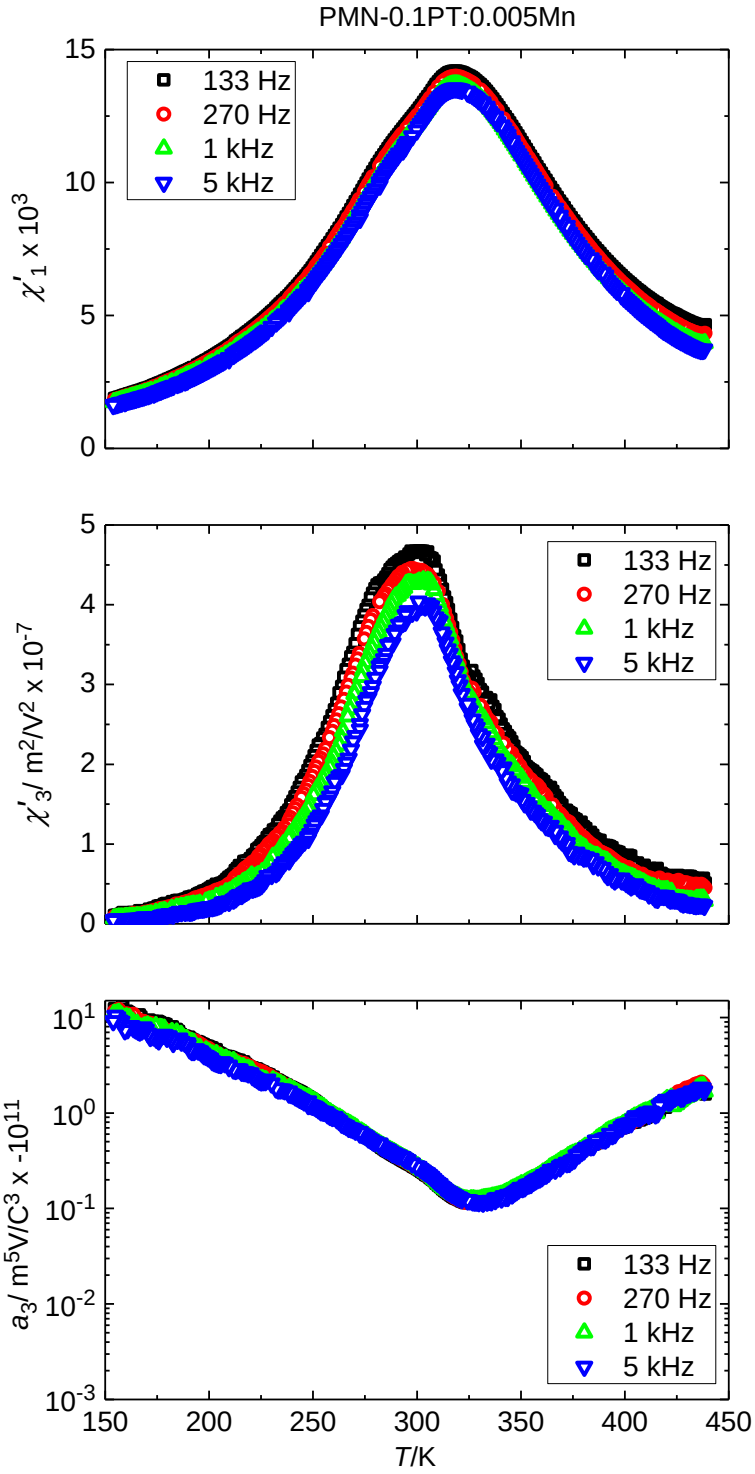

Figure 6.1.11 Temperature dependence of 1st order, 3rd order and scaled susceptibilities of 0.5% Mn-doped PMN-0.1PT ceramic

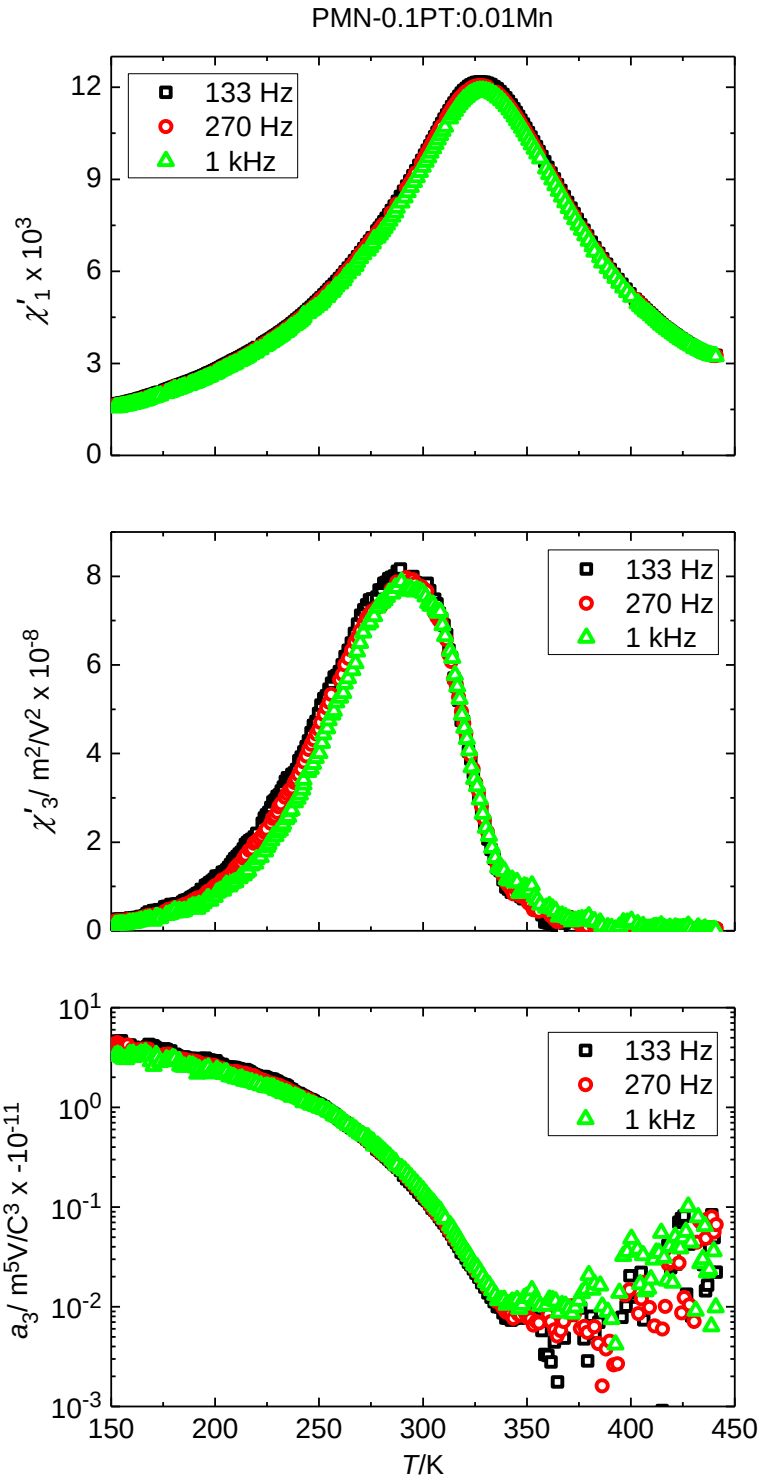

Figure 6.1.12 Temperature dependence of 1st order, 3rd order and scaled susceptibilities of 1% Mn-doped PMN-0.1PT ceramic

6.2 LINEAR DIELECTRIC SPECTROSCOPY OF PURE AND 2% La^{3+}-DOPED $Pb(Mg_{1/3}Nb_{2/3}O)_3$ SINGLE CRYSTAL

There are published works stating that the average size of the chemically ordered regions (regions, where Mg/Nb distribution in lattice is periodical – CORs) in pure PMN is smaller than 5 nm [78,79]. A-site La^{3+} doping can increase the size of the CORs [80–83]. Doping with 2% La^{3+} increases the size of the CORs in the PMN single crystal up to 100 nm [84]. The difference of physical properties of various relaxor ferroelectrics with enhanced B-site cation ordering has been widely studied [85–88]. Neutron and synchrotron radiation scattering analysis of pure and La^{3+}-doped PMN single crystal led to conclusion that the PNRs, which are in the CORs remain static, while those, which are in disordered matrix, tend to be dynamic [89]. Dielectric studies of X. Long et al. revealed that 2% La^{3+} doped PMN single crystal preserves Typical RF behavior [84]. Similar conclusion was drawn from subterrahertz relaxation results derived from Brillouin scattering measurements [90]. In comparison with the pure PMN, a La^{3+} doped crystal has lower dielectric constant maximum, which is slightly shifted towards lower temperatures [84,86,91]. In previous works, the Vogel-Fulcher fits for relaxation time, $\tau(T)$, revealed close values of relaxation parameters for PMN and $Pb(Mg_{1/3}Nb_{2/3})O_3$ – $0.02La(Mg_{2/3}Nb_{1/3})O_3$ (PLMN) crystals. Attempt time τ_0 was found to be in the order of 10^{-13} s for both crystals. Activation energy of pure PMN E_a = (0.07 ± 0.005) eV, PLMN E_a = (0.093 ± 0.008) eV. Freezing temperature of PMN T_{VF} = (213 ± 2) K, PLMN T_{VF} = (192 ± 8) K [84,92]. However, the dielectric response from which was determined the above data was studied at comparatively low frequencies, up to 1 MHz. With these data, the behavior of relaxation time and other parameters of relaxation spectrum can be determined only at comparatively low temperatures, where PNRs are comparatively large. Further is shown the dielectric response with the additional high-frequency dielectric data of PMN and PLMN single crystals that allow analyzing the response of PNRs at early stages of their development. As well, it allows calculating a distribution of relaxation times.

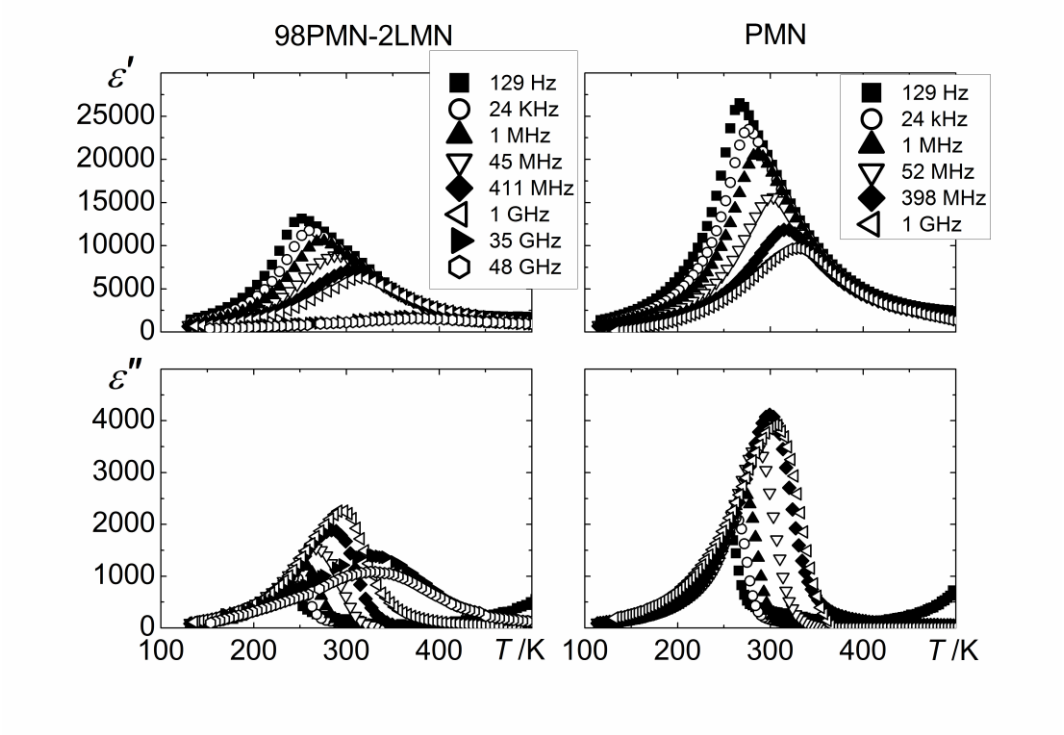

Figure 6.2.1 Temperature dependence of complex dielectric permittivity of PMN and PLMN single crystals

PMN and PLMN single crystals were grown from a high-temperature solution by the top-seeded solution growth (TSSG) method using a home-made tube furnace with a controlled temperature gradient field [84]. The samples were received from prof. Z.-G. Ye, from Department of Chemistry and 4D LABS, Simon Fraser University, Burnaby, Canada. The La dopant was incorporated through the solid solution and the charge neutrality was maintained by adjusting the Mg^{2+} and Nb^{5+} ration on the B-site. A mixture of PbO and B_2O_3 was used as a flux. The starting chemicals: PbO (99.99%), La_2O_3 (99.99%), MgO (99.9%), Nb_2O_5 (99.9%) and B_2O_3 (99.9%). The chemicals were weighted according to the stoichiometric composition of the PLMN and the flux to solute molar ration of 80:20. The chemicals were mixed and loaded into a platinum crucible, which was placed in a vertical furnace. A small PMN single crystal was used as a seed. The saturation temperature (a temperature, at which the seed crystal can retain and effectively grow from the solution) was found to be 1148°C for the PLMN-Pb/B_2O_3 flux system. The crystal growth took place upon cooling from 1150°C to 1080°C at a cooling

rate of 0.1°C/h. At the end of the slow cooling process, the grown crystal was pulled out of the melt surface and cooled down to room temperature at a rate of 15°C/h.

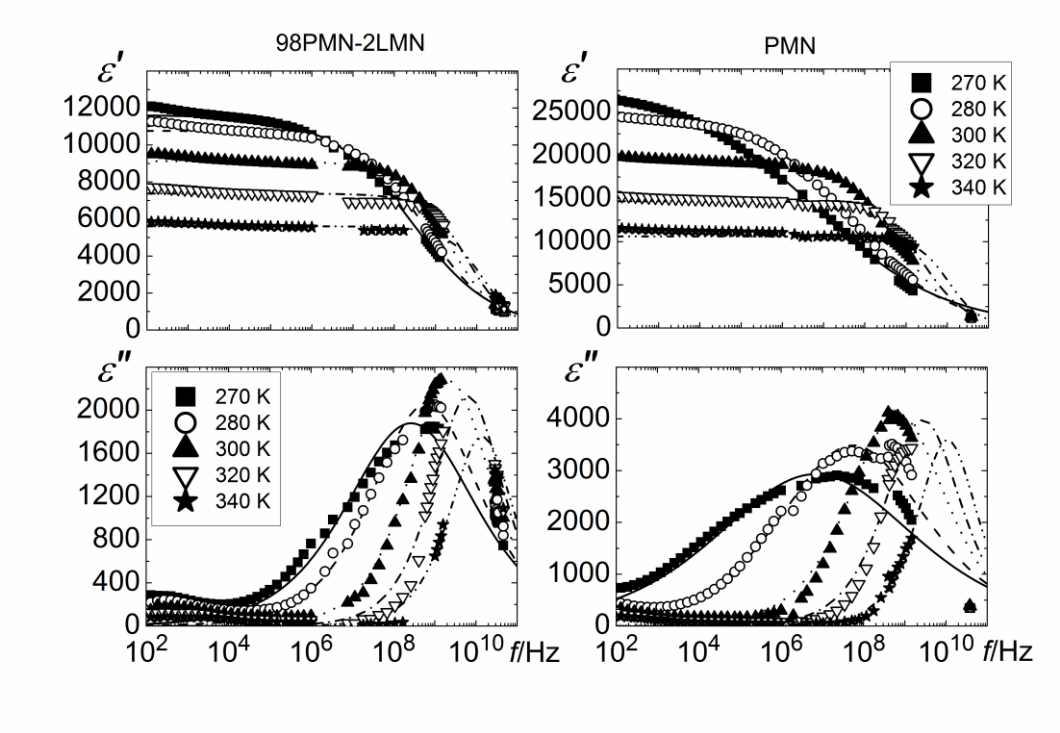

Figure 6.2.2 Frequency dependences of complex dielectric permittivity of PMN and PLMN single crystals. Lines show Cole – Cole fits

The temperature dependences of complex dielectric permittivity $\varepsilon^*(T)$ of PMN and PLMN single crystals are shown in Figure 6.2.1 for selected frequencies. Both dependences demonstrate typical behavior of relaxor ferroelectrics, i.e., the peak of the real part of the permittivity (ε') decreases and shifts towards the higher temperatures with the increase of frequency. An obvious difference between both crystals is the twice smaller peak of $\varepsilon'(T)$ in the PLMN crystal, which is ≈13 000 at the frequency of 129 Hz while for PMN it is ≈26 000 at the same frequency. The $\varepsilon'(T)$ peak of PLMN is not only lower in magnitude but also resides at 17 K lower temperature, i.e., at 129 Hz T_m = 250 K in PLMN and T_m = 267 K in PMN. At T < 220K the dielectric loss, $\varepsilon''(T)$, of both crystals decreases monotonically and becomes almost frequency independent, while at T > 400K the loss increases (this can be most clearly seen at 129 Hz frequency). This increase and related dispersion of ε' can be

tentatively related to the contribution of mobile charge carriers [92] and/or Maxwell – Wagner polarization. The temperature region where this process is clearly visible is too narrow to make a more detailed analysis of this phenomenon.

The frequency dependences of complex dielectric permittivity $\varepsilon^*(f)$ are shown in Figure 6.2.2 for PMN and PLMN crystals for selected temperatures. Both dependences display the narrowing of dispersion with the increase of temperature. An attempt was made to fit the data to Cole – Cole relation:

$$\varepsilon^*(\omega) = \varepsilon_\infty + \frac{\Delta\varepsilon}{1+(\mathrm{i}\omega\tau)^{1-\alpha}} \qquad (6.2.1)$$

The approximation curves in the temperature range of 270 K – 340 K are shown as lines in Figure 6.2.2. As we can see, the Cole – Cole relation is a reasonably good approximation at least in the frequency region of dipolar relaxation phenomenon.

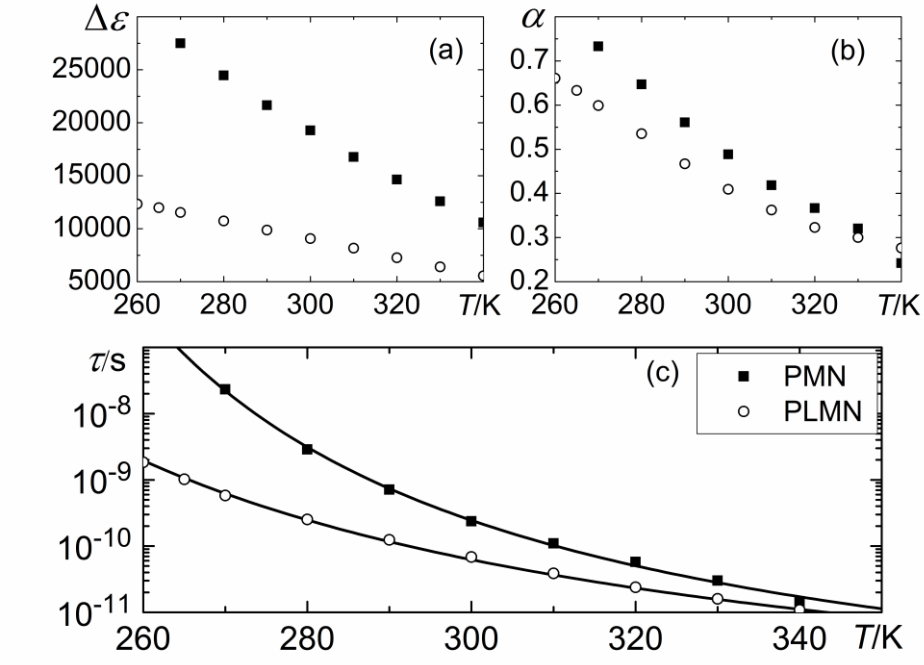

Figure 6.2.3 Temperature dependences of Cole – Cole parameters (a) $\Delta\varepsilon$, (b) α, (c) τ of PMN and PLMN single crystals. In (c) lines show the Vogel – Fulcher approximations

The temperature dependences of the best-fit Cole – Cole parameters are shown in Figure 6.2.3. The parameter $\alpha(T)$, which characterizes the width of

distribution of relaxation times, behaves very similarly for both single crystals, i.e. decreases monotonously with the increase of temperature. The same behavior is observed for the relaxation strength $\Delta\varepsilon(T)$ that is the difference between static dielectric permittivity and the permittivity at an infinitely high frequency (which may be temperature dependent in general case). This temperature behavior of the relaxation strength is associated with the shift of T_m and the narrowing of $\varepsilon^*(f)$ dispersion with an increasing temperature.

Temperature dependences of mean relaxation time (τ) are shown in Figure 6.2.3 (c). For both crystals $\tau(T)$ grows with the decrease of temperature in the whole temperature range of 260 K – 350 K available for the analysis. This behavior can be interpreted as slowing down of the dipolar dynamics of the system. The $\tau(T)$ dependences were fitted to the Vogel-Fulcher relation:

$$\tau = \tau_0 \exp\left(\frac{E_a}{k_B(T - T_{VF})}\right) \qquad (6.2.2)$$

The obtained parameter values are presented in Table 6.2.1. It reveals clear differences between temperatures T_{VF} of critical slowing down of dipolar dynamics (214 K for PMN and 180 K for PLMN, respectively). The similarity of activation energy, E_a, and attempt time, $\tau_{0,}$ suggests that the origin of the dynamics of PNRs in both crystals is the same. The relaxation parameters of PLMN obtained in this work are close to the values published earlier based on the analysis of low-frequency/low-temperature part of the spectrum [84]. Slight differences can be related to difference in La^{3+} concentration, which is difficult to control during crystal growth procedure.

Table 6.2.1 Vogel – Fulcher parameters of PMN and PLMN single crystals

Crystal	τ_0/s	E_a/eV	T_{VF}/K
PMN	5.9×10^{-14}	0.061 ± 0.009	214 ± 6
PLMN	6.3×10^{-14}	0.071 ± 0.007	180 ± 4

The dielectric permittivity data of pure PMN crystal was obtained in frequency range of 100 Hz – 1.6 GHz with additional data points at 37 GHz –

39 GHz range. Our results are comparable with the previously reported dielectric spectra of PMN crystal obtained in an extremely broad band of frequencies [93,94]. Namely, previously reported $E_a \approx 0.069$ eV and $T_{VF} \approx 200$ K are a good match to the values obtained in this work (Table 6.2.1).

To obtain a better description of relaxation processes in these materials, distributions of relaxation times were calculated by adopting Tikhonov regularization method [95,96]. The obtained distributions are shown in Figure 6.2.4 (a) for PLMN and (b) for PMN. The distributions of relaxation times of both crystals demonstrate a similar behavior, i.e. they broaden with the decrease of temperature, which is consistent with the expanding of the $\varepsilon^*(f)$ dispersion. In closer examination, one can notice that at all temperatures the edge of the distribution corresponding to the shortest relaxation time is located around 10^{-13} s and remains almost unchanged. With the decrease of temperature the distribution broadens only because of the increase of the longest relaxation time. The peak value of the distribution shifts towards longer times as well, i.e. mean relaxation time increases with the decrease of temperature, but not so rapidly. Besides the main maximum, additional anomalies appear in the low-frequency part of the spectrum at temperatures lower than about 300 K, both in PMN and PLMN. These anomalies suggest the development at low temperatures of additional relaxation processes which have not been resolved based on the analysis of $\varepsilon^*(f)$ spectra. Such a behavior may signify that at comparatively low temperatures the PNRs with slower dynamics appear, and an increase of amount of PNRs with slower dynamics causes an increase of the distribution function at higher time values. The edge of the distribution at the time value of 10^{-13} s remains intact, showing that a certain amount of relaxators with fast dynamics remains at low temperatures. This results agrees well with the fractal dynamics of PNRs as reported in [19].

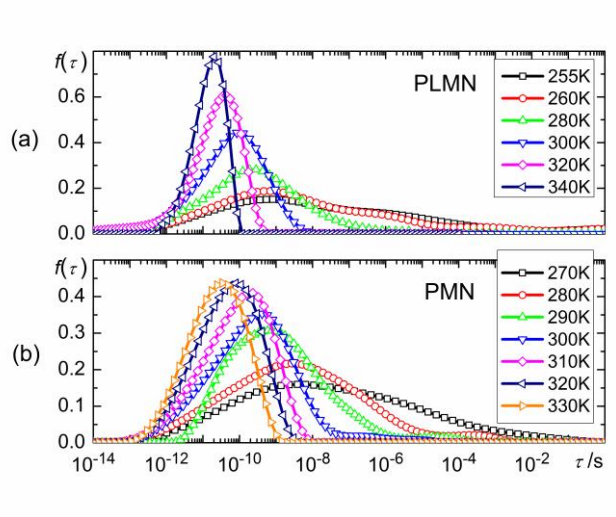

Figure 6.2.4 Distribution of relaxation times of (a) PLMN and (b) PMN single crystals

The distribution of relaxation times of PMN crystal has also been obtained in another research [28] (Figure 3.2.5) with few differences. Namely, in this work the maxima of $\varepsilon''(f)$ are slightly shifted towards higher frequencies. We believe this is because the previously measured crystal was grown using different method, i.e. flux technique [97]. Besides, in this work the range of calculations of relaxation times distribution was chosen just a little wider than the experimental results cover, leaving minimum range for extrapolation.

Earlier X-ray and electron diffraction studies of PLMN crystal showed that the doping with La^{3+} increases the size of chemically ordered regions [84]. As a result, we observed a twice smaller peak of $\varepsilon'(T)$ in PLMN showing that the amount of dynamic PNRs is smaller than in PMN. Besides, the T_{VF} in PLMN is lower and the peak of $\varepsilon'(T)$ is observed at slightly lower temperature, too. Nevertheless, the distribution of relaxation times in both crystals demonstrates similar behavior, which is consistent with the concept that the PNRs are growing and freezing with the decrease of temperature and percolate at some point.

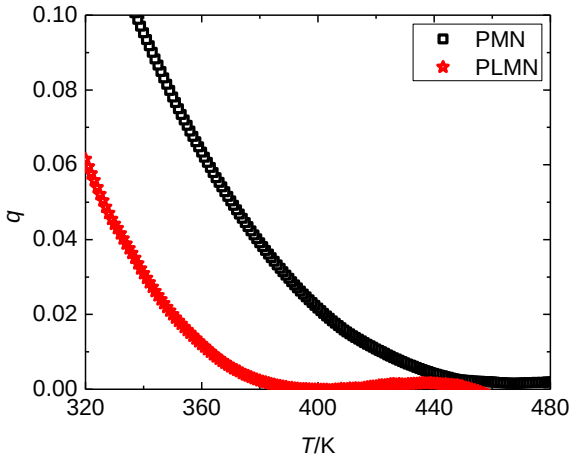

Figure 6.2.5 Temperature dependence of Edwards – Anderson parameter of PMN and PLMN single crystals

Therefore, the relaxation behaviour of PMN and PLMN is qualitatively the same in spite of the fact that chemical ordering is very different. Note that in perovskite relaxors with the $Pb(B'_{1/2}B''_{1/2})O_3$ structure, in which the number of orderable cations, B' and B'', is the same, and complete translational symmetry is possible in the ordered state, the chemical ordering leads to vanishing of relaxor behavior and emergence of a macroscopic ferroelectric or antiferroelectric phase transition [8,98]. In PMN and other known $Pb(B'_{1/3}B''_{2/3})O_3$ perovskite relaxors another type of chemical ordering is observed inside CORs, as discussed in the introduction. This ordering cannot lead to complete translational symmetry and does not influence significantly the relaxor behavior. This was shown previously in [84,99] for the low-frequency (1 Hz – 1 MHz) part of the dielectric spectrum and for subterrahertz relaxation derived from Brillouin scattering [90] and confirmed in this work for intermediate frequencies.

Table 6.2.2 CW approximation above T_C parameters of PMN and PLMN single crystals

	PMN	PLMN
T_C /K	334 ± 1	311 ± 1
$C/10^3$K	191 ± 10	232 ± 10

Additionally, the temperature dependence of Edwards – Anderson parameter $q(T)$ (6.1.2) was found for PMN and PLMN single crystals (Figure 6.2.5). Same procedure for extracting $q(T)$ is applied here as for PMN-0.1PT:*x*Mn ceramics (part **6.1**) and it provides Curie – Weiss approximation parameters (6.1.3) in Table 6.2.2. The increase of $q(T)$ with decrease of temperature is observed for both crystals. The discussion on the temperature behavior of $q(T)$ of PMN-0.1PT (part **6.1**) applies here, as well. The increase of $q(T)$ with decrease of temperature shows the increase of orientation correlation of dipoles within PNRs. However, $q(T)$ of PLMN crystal is smaller than $q(T)$ of PMN crystal at the same temperature, e.g. 360 K. It appears, that enhancement of chemically ordered regions of PLMN crystal prevents ordering of dipoles within a PNR. It is believed that local charge disorder is responsible for RF behavior. However, addition of La^{3+} reduces the local charge disorder, omitting part of the contribution of PNR to dielectric permittivity. That is the reason, why we observe lower values of $\varepsilon'(T)$ of PLMN. It is quite possible, that enhanced chemically ordered regions increases the percolation difficulty for PNRs. Hence, it is more difficult to spread the orientation correlation between dipoles and this gives decrease of $q(T)$ value. As well, this can be observed in $\varepsilon'(T)$ (Figure 6.2.1). There is quite strong shift towards higher temperatures of maximum of $\varepsilon'(T)$ with increase of frequency in both crystals. This means, that there is a wide distribution of sizes of PNRs in both crystals (as mentioned in **6.1** – larger PNRs give contribution to lower frequency value of $\varepsilon'(T)$). However, La^{3+} containing sites of PNRs give no contribution to polarization and to $\varepsilon'(T)$, because it has no charge disorder.

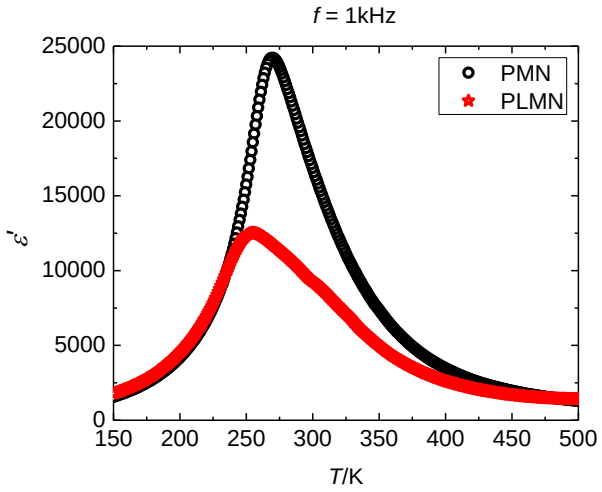

Figure 6.2.6 Temperature dependence of ε' at 1 kHz of PMN and PLMN single crystals illustrating the shift of maximum in La^{3+} doped material

La-doped PMN is quite a contrast to Mn-doped PMN-0.1PT. Both, La and Mn doping produces decrease of $\varepsilon'(T)$. On the other hand, La-doping produces a shift of maximum of $\varepsilon'(T)$ towards lower temperatures if compared to the undoped crystal (Figure 6.2.6), while Mn-doping produces shift of $\varepsilon'(T)$ maximum towards higher temperatures. The most interestingly, La-doped PMN crystal does have clearly visible RF like shift of maximum of $\varepsilon'(T)$ towards higher temperatures with increase of frequency (Figure 6.2.1), which witnesses the similar to pure PMN evolution of PNRs within the crystal and possible percolation of orientation of dipoles. Contrastingly, Mn-doped PMN-0.1PT ceramic does not show clearly visible RF like shift of maximum of $\varepsilon'(T)$ towards higher temperatures with increase of frequency, which witnesses a size limit of PNRs within the ceramic that contribute to $\varepsilon'(T)$, as dipoles are pinned. It is known, that the RF like shift of maxima of PMN-0.1PT:*x*Mn is observed in higher frequencies, however [67] (Figure 6.1.7). From the first perspective, both dopants decrease the value of $\varepsilon'(T)$, however the influence on temperature evolution of PNRs seems to be quite different.

6.2.1 Summary

In this work the dielectric properties of PMN and PLMN crystals were measured and compared. Being combined with the results of previous works

[84,90,99] our results show unambiguously that the relaxation dynamics and, therefore, the dipolar nanostructure are not influenced significantly by the size of chemically ordered regions. This experimental result is in sharp contrast with the conclusions of some theoretical works [8,100], which suggest a close relation between the scale of CORs and the relaxor behavior in PMN and other RFs. Furthermore, the same conclusion was obtained by analysis of Edwards – Anderson order parameter calculations. As well, the analysis provided interesting insights on temperature evolution of PNRs regarding different dopants on RFs. Namely, La-doping produces aggravation of correlation of dipolar orientation, while Mn-doping produces pinning of dipoles and prevents percolation of correlation of dipolar orientation, omitting their contribution to $\varepsilon'(T)$.

CONCLUSIONS

1. A non-linear dielectric susceptometer was constructed. Original software to control it was programmed. A calibration of a phase shift caused by equipment was implemented. It resulted in expanding the frequency range of the measurement to the higher frequencies, as high as 1/10 of the sampling frequency.
2. Poled PMN-0.17PT single crystal does show a 1st order phase transition from relaxor to ferroelectric phase. The phase transition manifests as a sharp peak in $\chi_3(T)$ at $T \approx 330$ K.
3. Mn-doping of PMN-0.1PT ceramics reduces the response of $\chi_3(T)$ significantly. This is an indication, that Mn-doping promotes appearance of defects, due to which the motionless dipoles are created and motions of PNRs are partially suspended.
4. The relaxation dynamics and, therefore, the dipolar nanostructure are not influenced significantly by the size of chemically ordered regions. Significantly increased size of chemically ordered regions by 2% La-doping of PMN single crystal did not quench relaxor behavior or promoted a spontaneous phase transition.
5. Calculations of Edwards – Anderson parameter show, that La and Mn doping produces different mechanisms for lowering the dielectric permittivity of relaxor materials. La-doping aggravates the growth of PNRs, while Mn-doping produces motionless dipoles.

REFERENCES

[1] A.A. Bokov, Z.-G. Ye, Recent progress in relaxor ferroelectrics with perovskite structure, J. Mater. Sci. 41 (2006) 31–52. doi:10.1007/s10853-005-5915-7.

[2] G. Burns, E. Burstein, "Dirty" displacive ferroelectrics, Ferroelectrics. 7 (1974) 297–299. doi:10.1080/00150197408238026.

[3] J. Dec, W. Kleemann, V. Bobnar, Z. Kutnjak, A. Levstik, R. Pirc, R. Pankrath, Random-field Ising-type transition of pure and doped SBN from the relaxor into the ferroelectric state, EPL Europhys. Lett. 55 (2001) 781. doi:10.1209/epl/i2001-00348-5.

[4] C.S. Pandey, J. Schreuer, M. Burianek, M. Mühlberg, Relaxor behavior of $Ca_xBa_{1-x}Nb_2O_6$ tuned by Ca/Ba ratio and investigated by resonant ultrasound spectroscopy, Phys. Rev. B. 87 (2013) 094101. doi:10.1103/PhysRevB.87.094101.

[5] G. Burns, F.H. Dacol, Glassy polarization behavior in ferroelectric compounds Pb(Mg13Nb23)O3 and Pb(Zn13Nb23)O3, Solid State Commun. 48 (1983) 853–856. doi:10.1016/0038-1098(83)90132-1.

[6] N. de Mathan, E. Husson, G. Calvarn, J.R. Gavarri, A.W. Hewat, A. Morell, A structural model for the relaxor PbMg1/3Nb2/3O3 at 5 K, J. Phys. Condens. Matter. 3 (1991) 8159. doi:10.1088/0953-8984/3/42/011.

[7] Z. Xu, M.-C. Kim, J.-F. Li, D. Viehland, Observation of a sequence of domain-like states with increasing disorder in ferroelectrics, Philos. Mag. A. 74 (1996) 395–406. doi:10.1080/01418619608242150.

[8] C.A. Randall, A.S. Bhalla, T.R. Shrout, L.E. Cross, Classification and consequences of complex lead perovskite ferroelectrics with regard to B-site cation order, J. Mater. Res. 5 (1990) 829–834. doi:10.1557/JMR.1990.0829.

[9] T.R. Shrout, W. Huebner, C.A. Randall, A.D. Hilton, Aging mechanisms in Pb(Mg1/3Nb2/3)O3-based relaxor ferroelectrics, Ferroelectrics. 93 (1989) 361–372. doi:10.1080/00150198908017368.

[10] M.A. Akbas, P.K. Davies, Domain Growth in Pb(Mg1/3Ta2/3)O3 Perovskite Relaxor Ferroelectric Oxides, J. Am. Ceram. Soc. 80 (1997) 2933–2936. doi:10.1111/j.1151-2916.1997.tb03214.x.

[11] M.A. Akbas, P.K. Davies, Processing and characterization of lead magnesium tantalate ceramics, J. Mater. Res. 12 (1997) 2617–2622. doi:10.1557/JMR.1997.0348.

[12] G. Xu, G. Shirane, J.R.D. Copley, P.M. Gehring, Neutron elastic diffuse scattering study of $Pb(Mg_{1/3}Nb_{2/3}O_3$, Phys. Rev. B. 69 (2004) 064112. doi:10.1103/PhysRevB.69.064112.

[13] S. Wakimoto, C. Stock, R.J. Birgeneau, Z.-G. Ye, W. Chen, W.J.L. Buyers, P.M. Gehring, G. Shirane, Ferroelectric ordering in the relaxor $Pb(Mg_{1/3}Nb_{2/3})O_3$ as evidenced by low-temperature phonon anomalies, Phys. Rev. B. 65 (2002) 172105. doi:10.1103/PhysRevB.65.172105.

[14] G. Xu, Z. Zhong, Y. Bing, Z.-G. Ye, C. Stock, G. Shirane, Ground state of the relaxor ferroelectric $Pb(Z_{1/3}Nb_{2/3})O_3$, Phys. Rev. B. 67 (2003) 104102. doi:10.1103/PhysRevB.67.104102.
[15] G. Xu, D. Viehland, J.F. Li, P.M. Gehring, G. Shirane, Evidence of decoupled lattice distortion and ferroelectric polarization in the relaxor system PMN-xPT, Phys. Rev. B. 68 (2003) 212410. doi:10.1103/PhysRevB.68.212410.
[16] S. Wakimoto, C. Stock, Z.-G. Ye, W. Chen, P.M. Gehring, G. Shirane, Mode coupling and polar nanoregions in the relaxor ferroelectric $Pb(Mg_{1/3}Nb_{2/3})O_3$, Phys. Rev. B. 66 (2002) 224102. doi:10.1103/PhysRevB.66.224102.
[17] P.M. Gehring, S. Wakimoto, Z.-G. Ye, G. Shirane, Soft Mode Dynamics above and below the Burns Temperature in the Relaxor $Pb(Mg_{1/3}Nb_{2/3})_3$, Phys. Rev. Lett. 87 (2001) 277601. doi:10.1103/PhysRevLett.87.277601.
[18] K. Hirota, Z.-G. Ye, S. Wakimoto, P.M. Gehring, G. Shirane, Neutron diffuse scattering from polar nanoregions in the relaxor $Pb(Mg_{1/3}Nb_{2/3})O_3$, Phys. Rev. B. 65 (2002) 104105. doi:10.1103/PhysRevB.65.104105.
[19] B. Dkhil, P. Gemeiner, A. Al-Barakaty, L. Bellaiche, E. Dul'kin, E. Mojaev, M. Roth, Intermediate temperature scale in lead-based relaxor systems, Phys. Rev. B. 80 (2009) 064103. doi:10.1103/PhysRevB.80.064103.
[20] B. Dkhil, J.M. Kiat, G. Calvarin, G. Baldinozzi, S.B. Vakhrushev, E. Suard, Local and long range polar order in the relaxor-ferroelectric compounds $PbMg_{1/3}Nb_{2/3}O_3$ and $PbMg_{0.3}Nb_{0.6}Ti_{0.1}O_3$, Phys. Rev. B. 65 (2001) 024104. doi:10.1103/PhysRevB.65.024104.
[21] A. Koreeda, H. Taniguchi, S. Saikan, M. Itoh, Fractal Dynamics in a Single Crystal of a Relaxor Ferroelectric, Phys. Rev. Lett. 109 (2012) 197601. doi:10.1103/PhysRevLett.109.197601.
[22] T. Nakayama, K. Yakubo, R.L. Orbach, Dynamical properties of fractal networks: Scaling, numerical simulations, and physical realizations, Rev. Mod. Phys. 66 (1994) 381–443. doi:10.1103/RevModPhys.66.381.
[23] J. Hlinka, Do we need the ether of polar nanoregions?, J. Adv. Dielectr. 02 (2012) 1241006. doi:10.1142/S2010135X12410068.
[24] P.M. Gehring, H. Hiraka, C. Stock, S.-H. Lee, W. Chen, Z.-G. Ye, S.B. Vakhrushev, Z. Chowdhuri, Reassessment of the Burns temperature and its relationship to the diffuse scattering, lattice dynamics, and thermal expansion in relaxor $Pb(Mg_{1/3}Nb_{2/3})O_3$, Phys. Rev. B. 79 (2009) 224109. doi:10.1103/PhysRevB.79.224109.
[25] A. Bosak, D. Chernyshov, S. Vakhrushev, M. Krisch, Diffuse scattering in relaxor ferroelectrics: true three-dimensional mapping, experimental artefacts and modelling, Acta Crystallogr. A. 68 (2012) 117–123. doi:10.1107/S0108767311040281.
[26] V. Westphal, W. Kleemann, M.D. Glinchuk, Diffuse phase transitions and random-field-induced domain states of the "relaxor''' ferroelectric

$PbMg_{1/3}Nb_{2/3}O_3$," Phys. Rev. Lett. 68 (1992) 847–850. doi:10.1103/PhysRevLett.68.847.
[27] V. Bovtun, S. Kamba, A. Pashkin, M. Savinov, P. Samoukhina, J. Petzelt, I.P. Bykov, M.D. Glinchuk, Central-Peak Components and Polar Soft Mode in Relaxor PbMg1/3Nb2/3O3 Crystals, Ferroelectrics. 298 (2004) 23–30. doi:10.1080/00150190490423057.
[28] R. Grigalaitis, J. Banys, A. Kania, A. Slodczyk, Distribution of relaxation times in PMN single crystal, J. Phys. IV Proc. 128 (2005) 127–131. doi:10.1051/jp4:2005128020.
[29] G. Xu, Z. Zhong, Y. Bing, Z.-G. Ye, G. Shirane, Electric-field-induced redistribution of polar nano-regions in a relaxor ferroelectric, Nat. Mater. 5 (2006) 134–140. doi:10.1038/nmat1560.
[30] X. Zhao, W. Qu, X. Tan, A.A. Bokov, Z.-G. Ye, Electric field-induced phase transitions in (111)-, (110)-, and (100)-oriented Pb(Mg1⁄3Nb2⁄3)O3 single crystals, Phys. Rev. B. 75 (2007) 104106. doi:10.1103/PhysRevB.75.104106.
[31] Z.-G. Ye, Y. Bing, J. Gao, A.A. Bokov, P. Stephens, B. Noheda, G. Shirane, Development of ferroelectric order in relaxor (1-x)$Pb(Mg_{1/3}Nb_{2/3})O_3$x$PbTiO_3$(0<~x<~0.15), Phys. Rev. B. 67 (2003) 104104. doi:10.1103/PhysRevB.67.104104.
[32] R. Pirc, R. Blinc, Spherical random-bond random-field model of relaxor ferroelectrics, Phys. Rev. B. 60 (1999) 13470–13478. doi:10.1103/PhysRevB.60.13470.
[33] A.E. Glazounov, A.K. Tagantsev, Phenomenological Model of Dynamic Nonlinear Response of Relaxor Ferroelectrics, Phys. Rev. Lett. 85 (2000) 2192–2195. doi:10.1103/PhysRevLett.85.2192.
[34] A.E. Glazounov, A.K. Tagantsev, Crossover in a non-analytical behaviour of dielectric non-linearity in PMN relaxor ferroelectric, J. Phys. Condens. Matter. 10 (1998) 8863. doi:10.1088/0953-8984/10/39/021.
[35] J. Dec, S. Miga, W. Kleemann, B. Dkhil, Nonlinear Dielectric Properties of PMN Relaxor Crystals within Landau-Ginzburg-Devonshire Approximation, Ferroelectrics. 363 (2008) 141–149. doi:10.1080/00150190802025947.
[36] A. Levstik, Z. Kutnjak, C. Filipič, R. Pirc, Glassy freezing in relaxor ferroelectric lead magnesium niobate, Phys. Rev. B. 57 (1998) 11204–11211. doi:10.1103/PhysRevB.57.11204.
[37] S. Ikeda, H. Kominami, K. Koyama, Y. Wada, Nonlinear dielectric constant and ferroelectric-to-paraelectric phase transition in copolymers of vinylidene fluoride and trifluoroethylene, J. Appl. Phys. 62 (1987) 3339–3342. doi:10.1063/1.339294.
[38] S. Miga, J. Dec, A. Molak, M. Koralewski, Temperature dependence of nonlinear susceptibilities near ferroelectric phase transition of a lead germanate single crystal, J. Appl. Phys. 99 (2006) 124107. doi:10.1063/1.2206267.

[39] S. Miga, J. Dec, K. Ćwikiel, Temperature dependences of nonlinear dielectric susceptibilities of triglycine sulphate near ferroelectric phase transition, Phase Transit. 80 (2007) 95–99. doi:10.1080/01411590601096010.
[40] M. Iwata, T. Ido, R. Nagahashi, Y. Ishibashi, Nonlinear dielectric susceptibility in relaxor ferroelectrics Pb(Zn1/3Nb2/3)O3-PbTiO3, Ferroelectrics. 498 (2016) 52–61. doi:10.1080/00150193.2016.1170420.
[41] Grigas, Microwave Dielectric Spectroscopy of Ferroelectrics and Related Materials, 1 edition, CRC Press, Amsterdam, the Netherlands, 1996.
[42] S. Miga, J. Dec, W. Kleemann, Computer-controlled susceptometer for investigating the linear and nonlinear dielectric response, Rev. Sci. Instrum. 78 (2007) 033902. doi:10.1063/1.2712792.
[43] A.K. Jonscher, Dielectric Relaxation in Solids, Chelsea Dielectric press, London. (1983).
[44] Y. Ishibashi, A phenomenological theory of nonlinear responses, Ferroelectrics. 195 (1997) 81–86. doi:10.1080/00150199708260493.
[45] V.L. Ginzburg, On the dielectric properties of ferroelectric (Segnette-electric) crystal and barium titanate, Zh. Exp. Theor. Phys. 15 (1945) 739–749.
[46] A.F. Devonshire, Theory of barium titanate, Part I, Phil. Mag. 40 (1949) 1040–1063.
[47] J. Dec, S. Miga, W. Kleemann, Dynamic nonlinear susceptibility in solid dielectrics, in: 2010 10th IEEE Int. Conf. Solid Dielectr. ICSD, 2010: pp. 1–5. doi:10.1109/ICSD.2010.5568203.
[48] R. Pirc, B. Tadić, R. Blinc, Nonlinear susceptibility of orientational glasses, Phys. B Condens. Matter. 193 (1994) 109–115. doi:10.1016/0921-4526(94)90001-9.
[49] S. Svirskas, M. Ivanov, S. Bagdzevicius, J. Macutkevic, A. Brilingas, J. Banys, J. Dec, S. Miga, M. Dunce, E. Birks, M. Antonova, A. Sternberg, Dielectric properties of solid solutions, Acta Mater. 64 (2014) 123–132. doi:10.1016/j.actamat.2013.11.040.
[50] Z. Kutnjak, B. Vodopivec, R. Blinc, Anisotropy of electric field freezing of the relaxor ferroelectric Pb(Mg1⁄3Nb2⁄3)O3, Phys. Rev. B. 77 (2008) 054102. doi:10.1103/PhysRevB.77.054102.
[51] R. Pirc, Z. Kutnjak, N. Novak, Compressible spherical dipolar glass model of relaxor ferroelectrics, J. Appl. Phys. 112 (2012) 114122. doi:10.1063/1.4769453.
[52] Y. Ishibashi, Nonlinear dielectric spectroscopy, J. Korean Phys. Soc. 32 (1998) 407–410. doi:http://dx.crossref.org/10.3938/jkps.32.407.
[53] C. Thibierge, D. L'Hôte, F. Ladieu, R. Tourbot, A method for measuring the nonlinear response in dielectric spectroscopy through third harmonics detection, Rev. Sci. Instrum. 79 (2008) 103905. doi:10.1063/1.2960564.
[54] R. Pirc, V. Bobnar, Nonlinear response of relaxor ferroelectrics, Ferroelectrics. 240 (2000) 1571–1578. doi:10.1080/00150190008227984.

[55] R. Blinc, J. Dolinšek, A. Gregorovič, B. Zalar, C. Filipič, Z. Kutnjak, A. Levstik, R. Pirc, Local Polarization Distribution and Edwards-Anderson Order Parameter of Relaxor Ferroelectrics, Phys. Rev. Lett. 83 (1999) 424–427. doi:10.1103/PhysRevLett.83.424.
[56] M. Ahart, M. Somayazulu, R.E. Cohen, P. Ganesh, P. Dera, H. Mao, R.J. Hemley, Y. Ren, P. Liermann, Z. Wu, Origin of morphotropic phase boundaries in ferroelectrics, Nature. 451 (2008) 545–548. doi:10.1038/nature06459.
[57] B. Noheda, D.E. Cox, G. Shirane, J. Gao, Z.-G. Ye, Phase diagram of the ferroelectric relaxor (1-x)$PbMg_{1/3}Nb_{2/3}O_3$-x$PbTiO_3$, Phys. Rev. B. 66 (2002) 054104. doi:10.1103/PhysRevB.66.054104.
[58] S.W. Choi, T.R. Shrout, S.J. Jang, A.S. Bhalla, Morphotropic phase boundary in Pb (Mg1/3Nb2/3)O3-PbTiO3 system, Mater. Lett. 8 (1989) 253–255. doi:10.1016/0167-577X(89)90115-8.
[59] Š. Svirskas, J. Banys, S. Kojima, Broadband dielectric spectroscopy of Pb-based relaxor ferroelectric (1-x)Pb(Mg1/3Nb2/3)O3-xPbTiO3 with intermediate random fields, J. Appl. Phys. 121 (2017) 134101. doi:10.1063/1.4979729.
[60] T.H. Kim, S. Kojima, J.-H. Ko, Electric field effects on the dielectric and acoustic anomalies of Pb[(Mg1/3Nb2/3)0.83Ti0.17]O3 single crystals studied by dielectric and Brillouin spectroscopies, Curr. Appl. Phys. 14 (2014) 1643–1648. doi:10.1016/j.cap.2014.09.014.
[61] M.A. Helal, M. Aftabuzzaman, S. Svirskas, J. Banys, S. Kojima, Temperature evolution of central peaks and effect of electric field in relaxor ferroelectric 0.83Pb(Mg1/3Nb2/3)O3–0.17PbTiO3 single crystals, Jpn. J. Appl. Phys. 56 (2017) 10PB03. doi:10.7567/JJAP.56.10PB03.
[62] A. Slodczyk, P. Daniel, A. Kania, Local phenomena of (1-x)$PbMg_{1/3}Nb_{2/3}O_3$-x$PbTiO_3$ single crystals studied by Raman scattering, Phys. Rev. B. 77 (2008) 184114. doi:10.1103/PhysRevB.77.184114.
[63] A. Slodczyk, A. Kania, P. Daniel, A. Ratuszna, Structural, vibrational and dielectric studies of 0.91PMN–0.09PT single crystals, J. Phys. Appl. Phys. 38 (2005) 2910. doi:10.1088/0022-3727/38/16/025.
[64] H. Luo, G. Xu, H. Xu, P. Wang, Z. Yin, Compositional Homogeneity and Electrical Properties of Lead Magnesium Niobate Titanate Single Crystals Grown by a Modified Bridgman Technique, Jpn. J. Appl. Phys. 39 (2000) 5581. doi:10.1143/JJAP.39.5581.
[65] A.M. Glazer, S.A. Mabud, Powder profile refinement of lead zirconate titanate at several temperatures. II. Pure PbTiO3, Acta Crystallogr. Sect. B. 34 (n.d.) 1065–1070. doi:10.1107/S0567740878004938.
[66] E.H. Kisi, J.S. Forrester, The phase transition sequence in the relaxor ferroelectric PZN–8% PT, J. Phys. Condens. Matter. 20 (2008) 165208. doi:10.1088/0953-8984/20/16/165208.
[67] R.M. Katilūtė, Mangano oksidu praturtintų PMN-10PT keramikų gamyba ir (di)elektrinis charakterizavimas, Master Thesis, Vilnius University, 2017.

[68] M. Sopicka-Lizer, High-Energy Ball Milling: Mechanochemical Processing of Nanopowders, Elsevier, 2010.
[69] D. Kuscer, J. Holc, M. Kosec, A. Meden, Mechano-Synthesis of Lead–Magnesium–Niobate Ceramics, J. Am. Ceram. Soc. 89 (2006) 3081–3088. doi:10.1111/j.1551-2916.2006.01221.x.
[70] D. Kuscer, J. Holc, M. Kosec, Formation of 0.65 Pb(Mg1/3Nb2/3)O3–0.35 PbTiO3 Using a High-Energy Milling Process, J. Am. Ceram. Soc. 90 (2007) 29–35. doi:10.1111/j.1551-2916.2006.01332.x.
[71] C. Molin, M. Sanlialp, V.V. Shvartsman, D.C. Lupascu, P. Neumeister, A. Schönecker, S. Gebhardt, Effect of dopants on the electrocaloric effect of 0.92 Pb(Mg1/3Nb2/3)O3–0.08 PbTiO3 ceramics, J. Eur. Ceram. Soc. 35 (2015) 2065–2071. doi:10.1016/j.jeurceramsoc.2015.01.016.
[72] J.-H. Park, J. Park, J.-G. Park, B.-K. Kim, Y. Kim, Piezoelectric properties in PMN–PT relaxor ferroelectrics with MnO2 addition, J. Eur. Ceram. Soc. 21 (2001) 1383–1386. doi:10.1016/S0955-2219(01)00023-1.
[73] L. Luo, W. Li, Y. Zhu, J. Wang, Growth and characteristics of Mn-doped PMN–PT single crystals, Solid State Commun. 149 (2009) 978–981. doi:10.1016/j.ssc.2009.04.018.
[74] A. Abragam, B. Bleaney, Electron Paramagnetic Resonance of Transition Ions, Oxford University Press, Oxford, New York, 2012.
[75] J. Dec, S. Miga, W. Kleemann, Ferroelectric Phase Transitions Viewed Via Nonlinear Dielectric Response, Ferroelectrics. 417 (2011) 82–92. doi:10.1080/00150193.2011.578500.
[76] B.E. Vugmeister, M.D. Glinchuk, Dipole glass and ferroelectricity in random-site electric dipole systems, Rev. Mod. Phys. 62 (1990) 993–1026. doi:10.1103/RevModPhys.62.993.
[77] M. Ivanov, J. Macutkevic, R. Grigalaitis, J. Banys, General view of ferroelectrics, in: Magn. Ferroelectr. Multiferroic Met. Oxides, Elsevier, 2018: pp. 5–33. doi:10.1016/B978-0-12-811180-2.00001-3.
[78] M.A. Akbas, P.K. Davies, Thermally Induced Coarsening of the Chemically Ordered Domains in Pb(Mg1/3Nb2/3)O3 (PMN)-Based Relaxor Ferroelectrics, J. Am. Ceram. Soc. 83 (2000) 119–23. doi:10.1111/j.1151-2916.2000.tb01158.x.
[79] A.D. Hilton, D.J. Barber, C.A. Randall, T.R. Shrout, On short range ordering in the perovskite lead magnesium niobate, J. Mater. Sci. 25 (1990) 3461–3466. doi:10.1007/BF00575371.
[80] S. Miao, J. Zhu, X.W. Zhang, X.H. Chen, High-energy electron irradiation study of relaxor ferroelectric $Pb(Mg_{1/3}Nb_{2/3})O_3$ and $Pb_{(1-x)}La_x[Mg_{(1+x)/3}Nb_{(2-x)/3}]O_3$ by transmission electron microscopy, J. Mater. Res. 17 (2002) 2615–2620. doi:10.1557/JMR.2002.0379.
[81] F. Jiang, S. Kojima, C. Zhao, C. Feng, Chemical ordering in lanthanum-doped lead magnesium niobate relaxor ferroelectrics probed by A1g Raman mode, Appl. Phys. Lett. 79 (2001) 3938–3940. doi:10.1063/1.1425957.

[82] S. Miao, X. Zhang, J. Zhu, Direct Compositional Analysis of Ordered Domains in Pure and La-Doped Pb(Mg1/3Nb2/3)O3 by Analytical Electron Microscopy Techniques, J. Am. Ceram. Soc. 84 (2001) 2091–2095. doi:10.1111/j.1151-2916.2001.tb00963.x.
[83] K.-M. Lee, H.M. Jang, W.-J. Park, Mechanism of 1:1 nonstoichiometric short-range ordering in La-doped Pb(Mg1/3Nb2/3)O3 relaxor ferroelectrics, J. Mater. Res. 12 (1997) 1603–1613. doi:10.1557/JMR.1997.0220.
[84] X. Long, A.A. Bokov, Z.-G. Ye, W. Qu, X. Tan, Enhanced ordered structure and relaxor behaviour of 0.98Pb(Mg1/3Nb2/3)O3–0.02La(Mg2/3Nb1/3)O3 single crystals, J. Phys. Condens. Matter. 20 (2008) 015210. doi:10.1088/0953-8984/20/01/015210.
[85] W. Qu, X. Zhao, X. Tan, In situ transmission electron microscopy study of the nanodomain growth in a Sc-doped lead magnesium niobate ceramic, Appl. Phys. Lett. 89 (2006) 022904. doi:10.1063/1.2219416.
[86] X. Zhao, W. Qu, H. He, N. Vittayakorn, X. Tan, Influence of Cation Order on the Electric Field-Induced Phase Transition in Pb(Mg1/3Nb2/3)O3-Based Relaxor Ferroelectrics, J. Am. Ceram. Soc. 89 (2006) 202–209. doi:10.1111/j.1551-2916.2005.00675.x.
[87] S. Kamba, D. Nuzhnyy, S. Veljko, V. Bovtun, J. Petzelt, Y.L. Wang, N. Setter, J. Levoska, M. Tyunina, J. Macutkevic, J. Banys, Dielectric relaxation and polar phonon softening in relaxor ferroelectric PbMg1/3Ta2/3O3, J. Appl. Phys. 102 (2007) 074106. doi:10.1063/1.2784972.
[88] F. Chu, N. Setter, A.K. Tagantsev, The spontaneous relaxor-ferroelectric transition of Pb(Sc0.5Ta0.5)O3, J. Appl. Phys. 74 (1993) 5129–5134. doi:10.1063/1.354300.
[89] S. Vakhrushev, a, Abstr. 11th Eur. Mtg Ferroelectr. (2007) 219.
[90] J.-H. Ko, T.H. Kim, S. Kojima, X. Long, A.A. Bokov, Z.-G. Ye, Effect of chemically ordered regions on the acoustic behaviors in Pb(Mg1/3Nb2/3)O3 studied by Brillouin scattering, J. Appl. Phys. 107 (2010) 054108. doi:10.1063/1.3346405.
[91] D.M. Fanning, I.K. Robinson, S.T. Jung, E.V. Colla, D.D. Viehland, D.A. Payne, Superstructure ordering in lanthanum-doped lead magnesium niobate, J. Appl. Phys. 87 (2000) 840–848. doi:10.1063/1.371951.
[92] A.A. Bokov, Z.-G. Ye, Double freezing of dielectric response in relaxor Pb(Mg1⁄3Nb2⁄3)O3 crystals, Phys. Rev. B. 74 (2006) 132102. doi:10.1103/PhysRevB.74.132102.
[93] V. Bovtun, S. Veljko, S. Kamba, J. Petzelt, S. Vakhrushev, Y. Yakymenko, K. Brinkman, N. Setter, Broad-band dielectric response of PbMg1/3Nb2/3O3 relaxor ferroelectrics: Single crystals, ceramics and thin films, J. Eur. Ceram. Soc. 26 (2006) 2867–2875. doi:10.1016/j.jeurceramsoc.2006.02.003.
[94] S. Kamba, M. Kempa, V. Bovtun, J. Petzelt, K. Brinkman, N. Setter, Soft and central mode behaviour in $PbMg_{1/3}Nb_{2/3}O_3$ relaxor ferroelectric, J.

Phys. Condens. Matter. 17 (2005) 3965–3974. doi:10.1088/0953-8984/17/25/022.
[95] A. Kajokas, A. Matulis, J. Banys, R. Mizaras, A. Brilingas, J. Grigas, Dielectric dispersion and distribution of the relaxation times of the relaxor PLZT ceramics, Ferroelectrics. 257 (2001) 69–74. doi:10.1080/00150190108016283.
[96] J. Macutkevic, J. Banys, A. Matulis, Determination of the Distribution of the Relaxation Times from Dielectric Spectra, Nonlinear Anal. Model. Control. 9 (2004) 75–88.
[97] A. Kania, A. Słodczyk, Z. Ujma, Flux growth and characterization of (1−x)PbMg1/3Nb2/3O3–xPbTiO3 single crystals, J. Cryst. Growth. 289 (2006) 134–139. doi:10.1016/j.jcrysgro.2005.11.009.
[98] N. Setter, L.E. Cross, The role of B-site cation disorder in diffuse phase transition behavior of perovskite ferroelectrics, J. Appl. Phys. 51 (1980) 4356–4360. doi:10.1063/1.328296.
[99] A.A. Bokov, B.J. Rodriguez, X. Zhao, J.-H. Ko, S. Jesse, X. Long, W. Qu, T.H. Kim, J.D. Budai, A.N. Morozovska, S. Kojima, X. Tan, S.V. Kalinin, Z.-G. Ye, Compositional disorder, polar nanoregions and dipole dynamics in Pb(Mg1/3Nb2/3)O3-based relaxor ferroelectrics, Z. Für Krist. Cryst. Mater. 226 (2011) 99–107. doi:http://dx.doi.org/10.1524/zkri.2011.1299.
[100] S. Tinte, B.P. Burton, E. Cockayne, U.V. Waghmare, Origin of the Relaxor State in $Pb(B'_xB''_{(1-x)})O_3$ Perovskites, Phys. Rev. Lett. 97 (2006) 137601. doi:10.1103/PhysRevLett.97.137601.

APPENDIX

9.1 PROGRAM FLOWCHART OF NON-LINEAR DIELECTRIC SUSCEPTOMETER

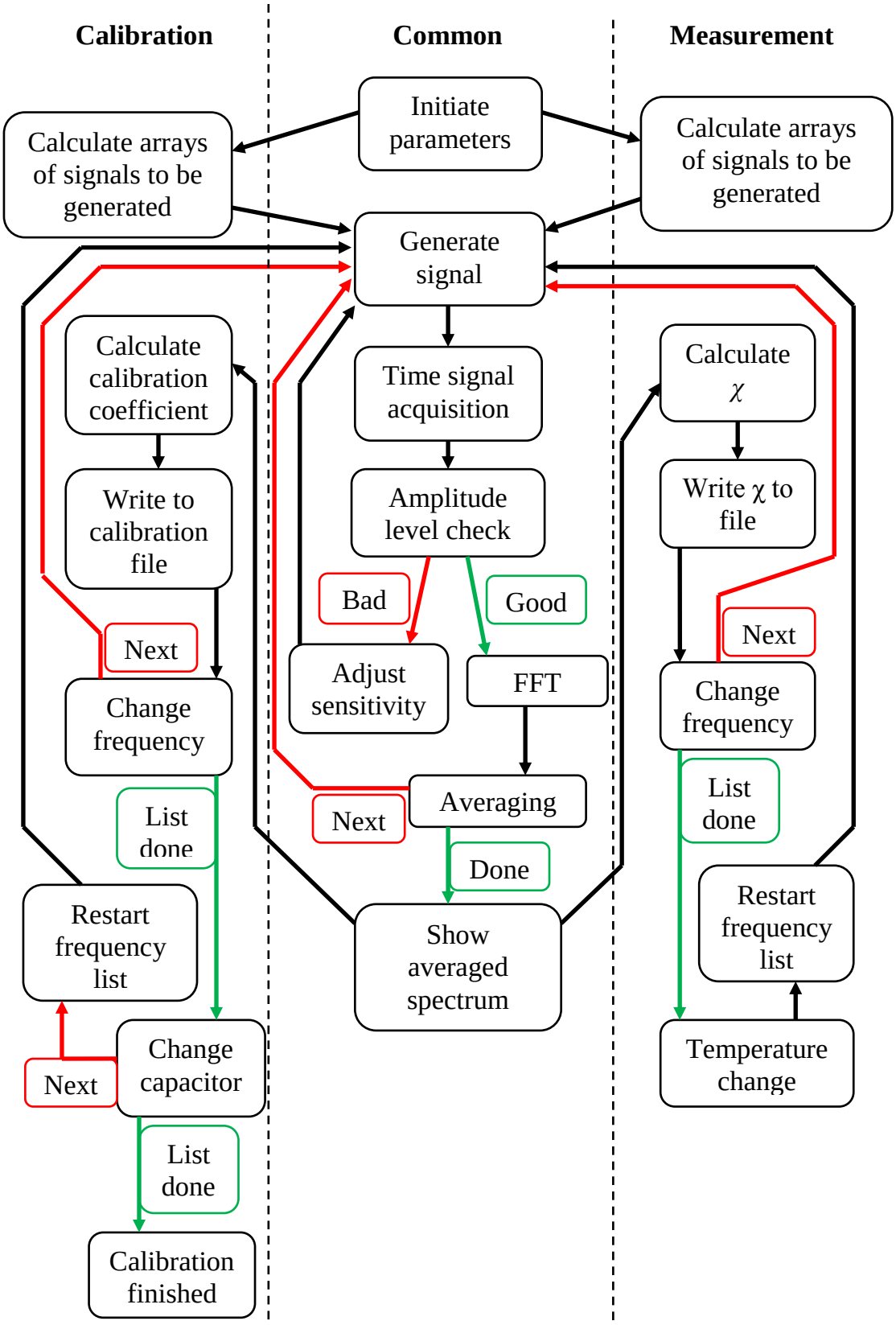

SANTRAUKA

Sutrumpinimai:

CV – Kiuri – Veiso;

CTS – chemiškai tvarki sritis;

FR – feroelektrinis relaksorius;

KR – kaitinimo režimas;

MFS – morfotropinė fazių sandūra;

PKR – poliarizavus bandinį kaitimo režimas;

PLMN – $Pb(Mg_{1/3}Nb_{2/3})O_3 – 0.02La(Mg_{2/3}Nb_{1/3})O_3$;

PMN – $Pb(Mg_{1/3}Nb_{2/3})O_3$;

PMN-*x*PT – $(1\text{-}x)PbMg_{1/3}Nb_{2/3}O_3\text{-}xPbTiO_3$;

PNS – polinė nano sritis;

PT – $PbTiO_3$;

VR – vėsinimo režimas;

PZN – $Pb(Zn_{1/3}Nb_{2/3})O_3$

10.1 ĮVADAS

Feroelektrinių relaksorių (FR) tyrimai yra patraukli sritis. Taikymams šios medžiagos žinomos kaip vieni geriausių pjezoelektrikų. Tačiau, šis darbas skirtas FR fundamentiniams tyrimams. Koncentruojantis į $Pb(Mg_{1/3}Nb_{2/3})O_3$ (PMN) pagrindo FR makroskopinių savybių tyrimus. PMN yra daugelio autorių laikomas kanoniniu FR. Šitai susiklostė istoriškai, nes pirmasis pagamintas FR buvo PMN. Nuo pat PMN tyrimų pradžios buvo ginčijamasi ar ši medžiaga turi fazinį virsmą, nes buvo pastebėtos anomalijos daugelio fizikinių parametrų temperatūrinėse priklausomybės, pvz.: lūžio rodiklio, dielektrinės skvarbos, garso greičio ir kt. Tačiau, neaptikta aiškių gardelės struktūrinių pakitimų, kuriuos būtų galima susieti su makroskopinių parametrų anomalijomis – medžiagos vidutinė struktūra išlieka kūbinė plačiame temperatūrų diapazone. Dar daugiau, nuo pat FR tyrimų pradžios, PMN temperatūrinei elgsenai bandyta pritaikyti fenomenologinę Landau-Ginzburgo-Devonšyro fazinių virsmų teoriją. Taip pat, buvo bandymų sukurti atskirą unikalios FR elgsenos teoriją. Plačiai priimta idėja, jog FR unikalią elgseną sukuria polinės nano sritys (PNS), t.y. dešimčių nanometrų dydžio polinės sritys, kurių dydis bei elgsena priklauso nuo temperatūros, slėgio ir įvairių priemaišų kristale. Yra laikoma, kad vienoje PNS visi dipoliai orientuoti ta pačia kryptimi, todėl neretai PNS vadinamos superdipoliais arba dipoliniu spiečiumi (klasteriu), kurie gali vartytis ir/arba kvėpuoti, esant nenuliniam elektriniam laukui ir temperatūrai. PNS atsiranda dėl netvarkingai pasiskirsčiusio vidinio krūvio medžiagoje. Kaip bebūtų, universalus teorinis modelis, galintis aprašyti FR nėra atrastas ir kiekvienas naujo modelio siūlymas sukelia daugybę diskusijų ir retorinių klausimų.

Šis darbas yra indėlis į FR medžiagų PMN pagrindu fizikinias žinias. Gauti rezultatai patvirtina, kad chemiškai tvarkių sričių praplėtimas nesusilpnina FR elgsenos ir nesukuria savaiminio fazinio virsmo. Taip, pat buvo sukonstruotas netiesinio dielektrinio jautrio tyrimo stendas, su tikslu išgauti daugiau informacijos apie FR ir pažvelgti į šias medžiagas iš kitokios

perspektyvos. Šis tyrimo metodas leidžia stebėti netiesinio dielektrinio jautrio temperatūrinę elgseną nedarant įtakos medžiagos vidiniams laukams. Taip pat, netiesinio dielektrinio jautrio tyrimai gali suteikti įdomios informacijos apie fazinius virsmus vykstančius medžiagoje. Yra žinoma, kad aukštesnės eilės dielektrinis jautris yra jautresnis medžiagos dipoliniam judesiui, nei įprasti tiesinio dielektrinio jautrio tyrimai. Šios unikalios medžiagų tyrimo technikos dėka buvo aptiktas fazinis virsmas $0.83Pb(Mg_{1/3}Nb_{2/3})O_3 - 0.17PbTiO_3$ kristale. Taip pat, metodas atvėrė galimybę stebėti dipolių elgseną Mn praturtintose $0.9Pb(Mg_{1/3}Nb_{2/3})O_3 - 0.1PbTiO_3$ keramikose. $PbTiO_3$ yra įprastas feroelektrikas, jį maišant su PMN, gaminami relaksoriaus – feroelektriko kietieji tirpalai. Daugelis mokslininkų bando atrasti ribinę relaksoriaus – feroelektriko kietojo tirpalo koncentraciją, kurią pasiekus stebimas fazinis virsmas. Tokia riba fazinėje diagramoje vadinama morfotropine fazių sandūra. Ji idomi tuo, jog tokios koncentracijos kietasis tirpalas turi geriausias piezoelektrines bei poliarizacines (eng. *tunability*) savybes.

Apibendrinant, šis darbas duoda indėlį į fundamentines žinias apie medžiagas PMN pagrindu. Taip pat, atveria galimybę kitaip tyrinėti šias medžiagas panaudojant unikalų netiesinio dielektrinio jautrio tyrimo metodą.

10.2 DISERTACIJOS TIKSLAI IR UŽDAVINIAI

Šio darbo pagrindinis tikslas yra gilinti fundamentines žinias apie medžiagas PMN pagrindu, kuris gali būti išskirstytas į šias užduotis:

1. Atlikti tiesinius $0.98Pb(Mg_{1/3}Nb_{2/3})O_3 - 0.02La(Mg_{2/3}Nb_{1/3})O_3$ monokristalo dielektrinius tyrimus ir palyginti jo fizikines savybes su gryno $Pb(Mg_{1/3}Nb_{2/3})O_3$ kristalo fizikinėmis savybėmis. Atlikti abiejų monokristalų relaksacijos trukmių pasiskirstymo skaičiavimus, tuo būdu įvertinant La įtaką polinių nano sričių elgsenai.
2. Sukonstruoti kompiuteriu valdomą netiesinio dielektrinio jautrio matuoklį. Tai yra unikalus ir naujoviškas tyrimų metodas, kuris

matuoja medžiagos netiesinį atsaką ir suteikia įdomios informacijos apie fazės bei kolektyvinę dipolių elgseną.

3. Išsiaiškinti ar $0.83Pb(Mg_{1/3}Nb_{2/3})O_3 - 0.17PbTiO_3$ monokristale yra fazinis virsmas.
4. Išsiaiškinti Mn įtaką $0.9Pb(Mg_{1/3}Nb_{2/3})O_3 - 0.1PbTiO_3$ keramikų elgsenai.

10.3 GINAMIEJI TEIGINIAI

1. Netiesinio dielektrinio jautrio matavimo rezultatų tikslumui užtikrinti didėjant dažniui, reikalingas fazės skirtumo, tarp srovės ir įtampos, kalibravimas.
2. $0.83Pb(Mg_{1/3}Nb_{2/3})O_3 - 0.17PbTiO_3$ kristale yra fazinis virsmas iš feroelektrinio relaksoriaus į normalaus feroelektriko fazę.
3. $0.9Pb(Mg_{1/3}Nb_{2/3})O_3 - 0.1PbTiO_3$ keramikų praturtinimas Mn kuria nejudrias polines nano sritis.
4. La praturtinimo dėka žymiai praplėstos chemiškai tvarkios sritys $Pb(Mg_{1/3}Nb_{2/3})O_3$ kristale nesusilpnina feroelektrinio relaksoriaus elgsenos ir nesukuria savaiminio fazinio virsmo.

10.4 DARBO NAUJUMAS IR AKTUALUMAS

Pirmą kartą ištirtas $0.98Pb(Mg_{1/3}Nb_{2/3})O_3 - 0.02La(Mg_{2/3}Nb_{1/3})O_3$ monokristalo dielektrinės skvarbos spektras dažnių diapazone > 1 MHz ir įvertintas relaksacijos trukmių pasiskirstymas. Rezultatai gauti tiriant $Pb(Mg_{1/3}Nb_{2/3})O_3$ ir $0.98Pb(Mg_{1/3}Nb_{2/3})O_3 - 0.02La(Mg_{2/3}Nb_{1/3})O_3$ monokristalus patvirtino faktą, jog chemiškai tvarkių sričių praplėtimas nesukuria spontaninio fazinio virsmo.

Sukurtas unikalus netiesinio dielektrinio jautrio matuoklis. Suprogramuota programa matuoklio valdymui. Fazės kalibravimo procedūra nebuvo paskelbta anksčiau.

Pirmą kartą atlikti poliarizuoto ir nepoliarizuoto $0.83Pb(Mg_{1/3}Nb_{2/3})O_3 - 0.17PbTiO_3$ monokristalo netiesinio dielektrinio jautrio tyrimai. Tai padėjo atpažinti savaiminį fazinį virsmą monokristale.

Pirmą kartą atlikti Mn praturtintų $0.9Pb(Mg_{1/3}Nb_{2/3})O_3 - 0.1PbTiO_3$ keramikų netiesinio dielektrinio jautrio tyrimai. Atrastas stiprus PNS judėjimo apribojimas dėl Mn įmaišymo.

10.5 AUTORIAUS INDĖLIS

Atlikta $Pb(Mg_{1/3}Nb_{2/3})O_3$ ir $0.98Pb(Mg_{1/3}Nb_{2/3})O_3 - 0.02La(Mg_{2/3}Nb_{1/3})O_3$ monokristalų plačiajuostė dielektrinė spektroskopija, dielektrinių spektrų analizė ir relaksacijos trukmių pasiskirstymo skaičiavimai.

Sukonstruotas netiesinio dielektrinio jautrio matavimo stendas. Įrangai valdyti parašyta programa konsultuojantis su doc. M. Ivanov. Atlikti įvairių medžiagų netiesinio dielektrinio jautrio matavimai.

Verta paminėti, jog autorius yra skysčių dielektrinės spektroskopijos bendraaše linija įrangos kūrėjas, kuri buvo sukonstruota pagal dr. S. Lapinsko daugiamodį matematinį modelį. Įraga panaudota birių bei skystų medžiagų matavimamas.

10.6 EKSPERIMENTINĖ METODIKA

Dielektrinės skvarbos tyrimai 10 Hz – 10 MHz atlikti impedanso analizatoriumi HP-4284A. Bandinys patalpintas kriostate, kaip dielektrikas tarp dviejų lygiagrečių plokščiojo kondensatoriaus plokštelių. Matuojama sistemos talpa ir nuostolių tangentas. Suskaičiuojama bandinio kompleksinė dielektrinė skvarba atimant sistemos įtaką į talpą.

Dielektrinės skvarbos tyrimai 1 MHz – 3 GHz atlikti vektoriniu analizatoriumi Agilent 8714 ET. Bandinys talpinamas į kriostatą suformuotą ant bendraašės linijos galo, kaip talpinė apkrova. Matuojamas atspindžio koeficientas nuo bendraašės linijos galo, kuris sutampa su kalibracine plokštuma. Bandinio kompleksinė dielektrinė skvarba apskaičiuojama iš kompleksinio atspindžio koeficiento. Reikia pridurti, jog didėjant dažniui

elektromagnetinio lauko pasiskirstymas bandinyje tampa nehomogeniškas ir norint gauti teisingus rezultatus, elektromagnetinio lauko pasiskirstymą bandinyje reikia įskaičiuoti.

Dielektrinės skvarbos tyrimai 35 Ghz ir 48 GHz dažniuose atlikti stačiakampiuose bangolaidžiuose. Adatos formos bandinys talpinamas į bangolaidžio centrą, kur yra didžiausias pagrindinės modos elektrinio lauko stipris, statmenai ilgosioms sienelėms. Mikrobangų generatoriumi kuriama elektromagnetinė banga. Kompleksiniai praėjusios ir atsispindėjusios bangos koeficientai matuojami analizatoriumi Elmika R2400. Bandinio kompleksinė dielektrinė skvarba apskaičiuojama sprendžiant netiesines lygtis $\varepsilon^* = f(R^*)$ arba $\varepsilon^* = f(T, R)$, kur R – atspindžio koeficientas, T – praėjimo koeficientas, ε^* – kompleksinė dielektrinė skvarba.

Netiesinio dielektrinio jautrio tyrimai atlikti savadarbiu stendu. Jo ypatybės apžvelgots skyrelyje **10.7**. Bandinys talpinamas į kriostatą tarp dviejų lygiagrečių kondensatoriaus plokštelių. Matavimai atliekami 100 Hz – 5 kHz dažnių diapazone. Signalo amplitudė parenkama nuo 0 V iki 10 V. Elektrinio lauko stipris, tuomet, priklauso nuo parenkamos signalo amplitudės ir bandinio storio. Netiesinis dielektrinis jautris suskaičiuojamas taip, kaip aiškina Miga et al. [42]. Bandinys patalpinamas į harmoniškai kintantį kampiniu dažniu ω elektrinį lauką $E(t)$:

$$E(t) = E_0 \sin \omega t \tag{10.6.1}$$

Tuomet, bandinio poliarizacija bendruoju atveju bus:

$$P(t) = \varepsilon_0 \sum_{i=1}^{n} \chi_i E^i(t) = \varepsilon_0 \sum_{i=1}^{n} \chi_i E_0^i \sin^i(\omega t) \tag{10.6.2}$$

Čia χ yra bandinio skaliarinis dielektrinis jautris. Šioje eilutėje yra lyginiai ir nelyginiai nariai. Paprastai eilutė skleidžiama iki nario $n = 3$. Mūsų matuoklis įskaito 5 narius, tuomet poliarizacija užrašoma taip:

$$P(t)=\varepsilon_0\sum_{i=0}^{5}\chi_i E_0^i\sin^i(\omega t)=\varepsilon_0[\frac{3}{8}\chi_4E_0^4+\frac{1}{2}\chi_2E_0^2+\left(\frac{5}{8}\chi_5E_0^5+\frac{3}{4}\chi_3E_0^3+\chi_1E_0\right)\sin(\omega t)-$$
$$-\left(\frac{1}{2}\chi_4E_0^4+\frac{1}{2}\chi_2E_0^2\right)\cos(2\omega t)-\left(\frac{5}{16}\chi_5E_0^4+\frac{1}{4}\chi_2E_0^3\right)\sin(3\omega t)+\left(\frac{1}{8}\chi_4E_0^4\right)\cos(4\omega t)+$$
$$+\left(\frac{1}{16}\chi_5E_0^5\right)\sin(5\omega t)] \qquad (10.6.3)$$

Čia galima pastebėti, kad netiesiniai dielektrinio jautrio nariai gauna indelį iš aukštesniųjų narių. Slinkties srovė gaunama iš poliarizacijos pokyčių:

$$I=S\frac{\partial D(t)}{\partial t} \qquad (10.6.4)$$

kur $D = \varepsilon_0 E + P$ ir S yra elektrodo plotas. Atsižvelgus į (10.6.3) ir (10.6.4), srovė užrašoma taip:

$$I(t)=\varepsilon_0S\omega\left(\frac{5}{8}\chi_5E_0^5+\frac{3}{4}\chi_3E_0^3+(\chi_1+1)E_0\right)\cos(\omega t)+\varepsilon_0S\omega\left(\chi_4E_0^4+\chi_2E_0^2\right)\sin(2\omega t)-$$
$$-\varepsilon_0S\omega\left(\frac{15}{16}\chi_5E_0^5+\frac{3}{4}\chi_3E_0^3\right)\cos(3\omega t)-\varepsilon_0S\omega\left(\frac{1}{2}\chi_4E_0^4\right)\sin(4\omega t)+$$
$$+\varepsilon_0S\omega\left(\frac{5}{16}\chi_5E_0^5\right)\cos(5\omega t) \qquad (10.6.5)$$

Čia galima pastebėti, kad slinkties srovė turi daug harmoninių narių. Kiekvienas jų tiesiškai priklauso nuo atitinkamos eilės dielektrinio jautrio χ_i. Jas išsprendus gaunama:

$$\chi_1=\frac{1}{\varepsilon_0S\omega}\left(\frac{d}{U_0}\right)(I_1+I_3+I_5)-1$$

$$\chi_2=\frac{1}{\varepsilon_0S\omega}\left(\frac{d}{U_0}\right)^2(I_2+2I_4)$$

$$\chi_3=\frac{1}{\varepsilon_0S\omega}\left(\frac{d}{U_0}\right)^3\left(-\frac{4}{3}I_3-4I_5\right)$$

$$\chi_4=\frac{1}{\varepsilon_0S\omega}\left(\frac{d}{U_0}\right)^4(-2I_4)$$

$$\chi_5=\frac{1}{\varepsilon_0S\omega}\left(\frac{d}{U_0}\right)^5\left(\frac{16}{5}I_5\right) \qquad (10.6.6)$$

čia $E_0 = U_0/d$, kur U_0 – signalo amplitudė ir d – bandinio storis. Tokiu būdu, sąryšis (10.6.6) leidžia suskaičiuoti tiesinį ir aukštesnių eilių dielektrinius jautrius iš pamatuojamų fizikinių dydžių, t.y. įtampos amplitudės ir srovės amplitudės. Tačiau, aukščiau pateikti sąryšiai galioja dielektrikams be nuostolių. Norint gauti išraišką dielektrikui su nuostoliais ar mažai laidžiam, reikia amplitudes pakeisti kompleksinėmis, įskaitant slinkties srovės fazės pokytį įtampos atžvilgiu. Reikia paminėti, jog slinkties srovės nelyginių harmonikų komponentės idealiame dielektrike (be nuostolių, nelaidus) yra paslinktos 90° įtampos atžvilgiu, o lyginės komponentės yra tos pačios fazės, kaip ir įtampa. Tuomet, (10.6.6) išraiškos kairiuosius narius pažymėsime Ψ_i*, tada nelyginės (mūsų atveju i = 1, 3, 5)) kompleksinio jautrio komponentės χ_i' ir χ_i" yra apskaičiuojamos taip:

$$\chi_i' = \mathrm{Im}\left(\Psi_i^*\right), \quad \chi_i'' = \mathrm{Re}\left(\Psi_i^*\right) \tag{10.6.7}$$

o lyginės komponentės (mūsų atveju i = 2, 4) apskaičiuojamos taip:

$$\chi_i' = \mathrm{Re}\left(\Psi_i^*\right), \quad \chi_i'' = \mathrm{Im}\left(\Psi_i^*\right) \tag{10.6.8}$$

Šis dielektrinio jautrio matuoklis gauna bandinio srovės laikinį atsaką išreikštą įtampa srovės priešstiprintuvio SR570 pagalba. Tuomet vykdoma greitoji Furje transformacija su gautais duomenimis. Dažninis vaizdas leidžia atlikti harmonikų analizę. Tačiau, toks spektras turi ir įrangos fazės postūmio dedamąją, kurią reikia atimti, norint gauti tikslius rezultatus. Dėl šios priežasties yra vykdomas fazės kalibravimas. Kalibraciniams koeficientams gauti naudojamas kondensatorių modulis Solartron 12961, kuriame sumontuoti 9.31 pF, 102 pF, 0.999 nF, 10.04 nF talpų, aukštos kokybės (tiesiniai, be nuostolių) kondensatoriai. Šie keturi kalibraciniai kondesatoriai apima visą matuoklio pamatuojamų talpų diapazoną. Taigi, jei kalibracinį kondensatorių C veikia harmoninis įtampos signalas $U^* = Ue^{j\omega t}$, gaunama srovė:

$$I^* = j\omega CU^* = j\omega CUe^{j(\omega t+\Delta\varphi)} = \omega CUe^{j\left(\omega t+\frac{\pi}{2}+\Delta\varphi\right)} \tag{10.6.9}$$

čia $\Delta\varphi$ – įrangos sukurtas fazės pokytis. Srovė idealiu atveju, kai įranga nesukelia parazitinio fazės postūmio, atrodytų taip:

$$I_{id}^{*} = \omega CUe^{j\left(\omega t+\frac{\pi}{2}\right)} \tag{10.6.10}$$

žinant šitai, dabar galima apskačiuoti kalibracinį koeficientą:

$$K^{*} = \frac{I_{id}^{*}}{I^{*}} = \frac{\omega CUe^{j\left(\omega t+\frac{\pi}{2}\right)}}{\omega CUe^{j\left(\omega t+\frac{\pi}{2}+\Delta\varphi\right)}} = \frac{1}{e^{j\Delta\varphi}} \tag{10.6.11}$$

Matuojant bandinį gaunama srovė atrodo taip:

$$I_{meas}^{*} = \omega C_b Ue^{j\left(\omega t+\frac{\pi}{2}+\varphi_b+\Delta\varphi\right)} \tag{10.6.12}$$

čia φ_b – bandinio sukeltas srovės fazes pokytis (lyginant su įtampa), C_b – bandinio talpa. Galima pastebėti, kad čia lieka $\Delta\varphi$ ir gadina matavimo rezultatus. Todėl, norint gauti teisingus rezultatus vykdoma fazės pataisa:

$$I_{result}^{*} = K^{*}I_{meas}^{*} = \omega C_b U\left(\frac{e^{j\left(\omega t+\frac{\pi}{2}+\varphi_b+\Delta\varphi\right)}}{e^{j\Delta\varphi}}\right) = \omega C_b Ue^{j\left(\omega t+\frac{\pi}{2}+\varphi_b\right)} \tag{10.6.13}$$

Tokiu būdu pašalinami įrangos sukelti fazės iškraipymai. Kalibraciniai koeficientai suskaičiuojami visoms harmonikoms vieną kartą prieš matavimą ir saugomi.

Visuose eksperimentuose temperatūra matuota multimetru Keithley Integra 2700. Platininis termorezistorius PT100 naudotas matavimuose 10 Hz – 1 MHz dažnių diapazone, bei netiesinio dielektrinio jautrio matavimuose. T-tipo termopora naudota aukštesnių dažnių matavimuose, t.y. bendraaše linija ir bangolaidžiais. Visų matavimo metodų kriostatuose yra įtaisyta kaitinimo viela, kuri šildoma valdomos galios įtampos šaltiniu. Šaldymui naudotas skysto azoto garų putimas.

Visiems eksperimentams atlikti buvo formuojami sidabro pastos kontaktai ant lygiagrečiųjų bandinio paviršių (išskyrus matavimus bangolaidžiais, kur bandinys daromas adatos pavidalo). Iš pradžių, bandinio paviršiai, ant kurių palnuojama suformuoti elektrinius kontaktus, šlifuojami.

Tuomet, bandinys nuplaunamas acetonu ir izopropanoliu ultragarsinėje vonelėje. Bandiniui išdžiūvus yra tepama sidabro pasta, ant vieno iš paviršių, plonu teptuku ir paliekama džiūti 10 minučių. Tuomet, bandinys apverčiamas ir sidabro pasta tepama ant kito paviršiaus, lygiagretaus pirmąjam. Po > 30 min. džiūvimo, bandinys dedamas į krosnelę ir kaitinamas iki 600°C, 4 K/min greičiu. Aukščiausioje temperatūroje bandinys palaikomas ≥ 2 valandas ir krosnelė išjungiama, kad atvėstų iki kambario temperatūros. Tada įvertinama susiformavusių kontaktų kokybė. Nustačius, jog kontaktai suformuoti gerai, bandinys naudojamas eksperimentams.

10.7 NETIESINIO DIELEKTRINIO JAUTRIO MATUOKLIS

Tiesiniai dielektrinio jautrio tyrimai atliekami mažu kintančios įtampos signalu. Sąryšis tarp medžiagos poliarizacijos P ir išorinio elektrinio lauko E yra gerai žinomas:

$$P = \varepsilon_0 \chi_1 E \qquad (10.7.1)$$

čia ε_0 – laisvosios erdvės elektrinė skvarba, χ_1 –dielektrinės medžiagos tiesinis dielektrinis jautris. Šis sąryšis nebegalioja stipresniuose elektriniuose laukuose. Tokiu atveju reikia įskaityti aukštesnės eilės narius:

$$P = \varepsilon_0 \left(\chi_1 E + \chi_2 E^2 + \chi_3 E^3 + ... \right) \qquad (10.7.2)$$

čia χ_i – yra netiesiniai dielektriniai jautriai (kur i – teigiami sveikieji skaičiai). Šios netiesinės komponentės rodo netiesinį indėlį į poliarizaciją [43]. Atsižvelgus į trečiosiosios eilės netiesinio dielektrinio jautrio χ_3 elgseną, galima vienareikšmiškai nustatyti fazinio virsmo rūšį. Feroelektrinėse sistemose, kuriose stebimas antrosios eilės fazinis virsmas, paraelektrinėje fazėje χ_3 yra neigiamas ir mažėjant temperatūrai, perėjus į feroelektrinę fazę, χ_3 šuoliškai keičia ženklą į teigiamą. Pirmosios rūšies fazinio virsmo atveju fazinio virsmo aplinkoje χ_3 išlieka teigiamas. Šitaip aiškina Landau-Ginzburgo-Devonšyro fenomenologinė fazinių virsmų teorija [45,46] bei buvo įrodyta tiraint triglicino sulfatą (antrosios eilės fazinis virsmas) ir bario titanatą (pirmosios eilės fazinis virsmas) [47]. Netiesinio dielektrinio jautrio tyrimai

atliekami siekiant išsisaiškinti esminius skirtumus tarp FR bei dipolinių stiklų [32,48,49].

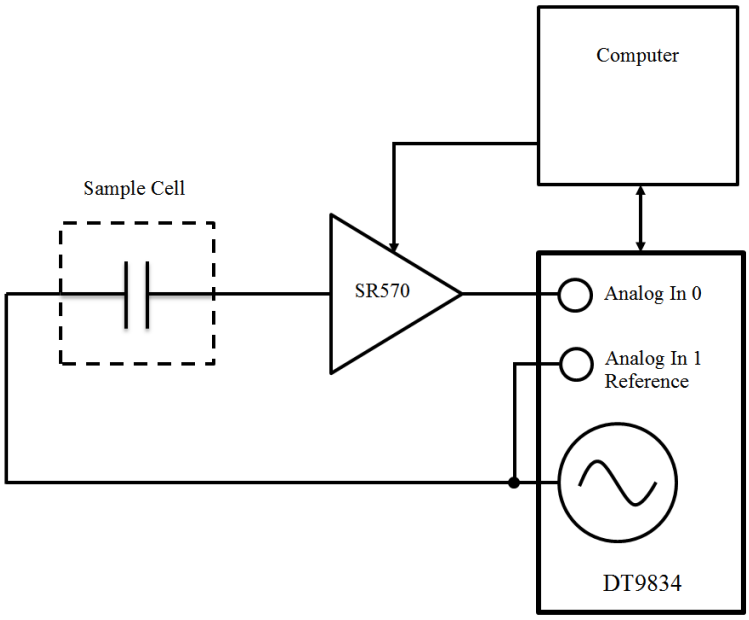

Paveikslas 10.7.1 Netiesinio dielektrinio jautrio matavaimo stendo blokinė schema

Netiesinio dielektrinio jautrio mokslinė vertė, tiriant fazinius virsmus įvairios medžiagose, yra pakankamai aiški. Žinomi keli sukurti metodai, leidžiantys atlikti tokius matavimus [37,42,52,53], tačiau nė vienas jų nėra gaminami komerciškai, todėl mums teko sukonstruoti savo variantą.

Mūsų netiesinio dielektrinio jautrio matavimo stendas sukonstuoruotas pagal S. Miga et al. [42] pateiktą variantą. Sistema susideda iš (Paveikslas 10.7.1): Data Translatios DT9834 skaitmeninio duomenų surinkimo modulio, Stanford Research Systems SR570 mažatriukšmio srovės priešstiprintuvio su valdomu jautriu, kompiuterio, bandinio kriostato. Bandinio matavimas atliekamas kintančios įtampos signalu be nuolatinės dedamosios. Signalo amplitudė yra pakankama stebėti medžiagos netiesinį dielektrinį jautri, tačiau žymiai mažesnė už medžiagos koercinį lauką. DT9834 naudojamas įtampos signalui generuoti ir bandinio atsakui matuoti. Priešstiptintuvis SR570 srovę, tekančią bandiniu, verčia įtampa, kurią gali matuoti modulis DT9834 kanalu „Analog In 0“. Kompiuteris vykdo programą, kuri valdo prietaisus, apdoroja duomenis ir įrašo į kietąjį diską. Kompiuterio programa – savadarbė. Su šia įranga galima matuoti bandinius, kurių talpa nuo 10 pF iki 10 nF. Matavimus

galima atlikti 8 Hz – 10 kHz dažnių diapazone. Maksimali signalo amplitudė ±10 V. Temperatūrų diapazoną apsprendžia kriostatas, kuriame talpinamas bandinys. Signalo-triukšmo santykis pasiekiamas iki 100 dB (10^5).

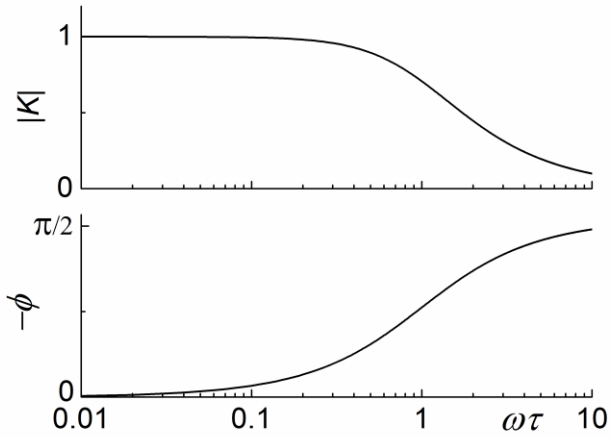

Paveikslas 10.7.2 RC grandinės tipinė dažninė charakteristika

Medžiagos kompleksiniam nietiesiniam dielektriniam jautriui gauti, matuojama per bandinį tekanti srovė, kuri yra kompleksinė (žr. [42] arba skyrių **10.6**). Norint gauti tikslius rezultatus, yra svarbu tiksliai matuoti fazės pokytį tarp generuojamo įtampos signalo ir bandiniu tekančios srovės. Tačiau sistemoje yra keli fazės iškraipymų šaltiniai: 1) DT9834 „Analog In“ kanalai surenka duomenis nevisai lygiagrečiai, tai yra neišvengiama, nes DT9834 modulis naudoja įprastą processorių, kuris nepalaiko tikro relaus laiko lygiagretaus duomenų surinkimo, dėl to tarp „Analog In“ ir „Analog In Reference“ atsiranda užlaikymas, sąlygojantis fazės iškraipymus; 2) SR570 turi riboto dažnio diskrečius stiprinimo diapazonus (diapazonai išskirstyti pagal signalo srovės stiprį), t.y. dažnių diapazonas apribotas RC grandinėmis. Yra žinoma, kad RC grandinė, veikinti kaip dažnių filtras, kartu ir pasuka fazę tarp signalo įtampos ir srovės (Paveikslas 10.7.2). Paveikslas 10.7.3 rodo tam tikro bandinio (čia medžiaga nekonkretizuojama, nes tai nėra esminė informacija) trečiosios eilės netiesinio dielektrinio jautrio priklausomybę nuo temperatūros $\chi_3(T)$. Taškais pateikti rezultatai yra matavimo, kuriame atlikta fazės poslinkio, tarp įtampos ir srovės, korekcija. Linija rodo rezultatus matavimo, kur fazės

korekcija neatlikta. Matavimai buvo atlikti vienu metu ir stebimas akivaizdus skirtumas. Paveikslas 10.7.4 leidžia aiškiau pastebėti įrangos sukurto fazės iškraipymo įtaką $\chi_3(T)$ matavimo rezultatams. Galima pastebėti, jog aukščiausio dažnio rezultatams sukuriama didžiausios vertės paklaida. Tai sutampa su RC filtro fazės priklausomybe nuo dažnio (Paveikslas 10.7.2), kur matoma, jog didėjant dažniui, RC filtro sukurtas fazės poslinkis didėja. Trūkis ties 400 K gali būti siejamas su srovės preišstiprintuvio stiprinimo koeficiento perjungimu. Srovės priešstiprintuvis SR570 turi diskrečias perjungiamas stiprinimo grandines.

Fazę iškraipančių šaltinių įtaka pašalinama atliekant kalibracinį matavimą (kaip aptarta skyriuje **10.6**). Tam tikslui naudojamas Solartron 12961 talpinių apkrovų modulis, sudarytas iš keturių labai aukštos kokybės (tiesinių, su mažais nuostoliais) kondensatorių – 9.31 pF, 102 pF, 0.999 nF, 10.04 nF talpų. Kalibraciniams koeficientamas gauti naudojamas ypatingos formos signalas, kurį galima aprašyti taip:

$$S(f)=\sum_{i=1}^{5}\frac{1}{i}\cos(2\pi ift+\varphi_i) \qquad (10.7.3)$$

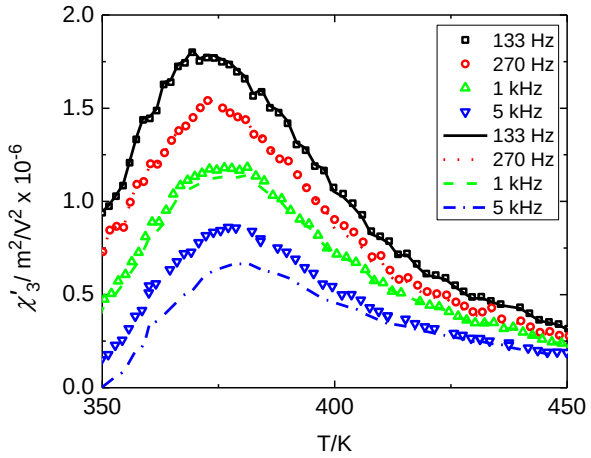

Paveikslas 10.7.3 Tam tikro bandinio trečiosios eilės netiesinio dielektrinio jautrio priklausomybė nuo temperatūros. Taškai rodo kalibruoto matavimo rezultatus, linijos rodo rezultatus, kur fazes poslinkis nekalibruotas. Legenda rodo pagrindinės harmonikos dažnį

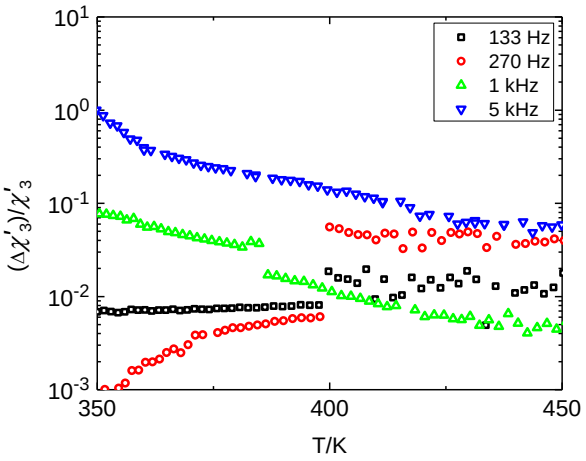

Paveikslas 10.7.4 Trečiosios eilės netiesinio dielektrinio jautrio priklausomybės nuo temperatūros (Paveikslas 10.7.3) santykinė paklaida, atsiradusi dėl matavimo įrangos sukurto fazės, tarp įtampos ir srovės, iškraipymo. Legenda rodo pagrindinės harmonikos dažnį

Signalas *S* susideda iš penkių harmonikų. Kiekvienos harmonikos amplitudė sumažinta harmonikos numerio skaičiu kartų. Tokiu būdu, signalo išvestinėje gaunamos vienodos amplitudės harmonikos. Tai svarbu todėl, kad bandiniu tekanti srovė yra proporcinga įtampos signalo išvestinei. Dar daugiau, kalibracinio signalo harmonikų pradinės fazės yra parenkamos taip, kad būtų efektyviai išnaudojamas tiek įtampos, tiek srovės signalo dinaminis diapazonas, t.y. rastas toks harmonikų pradinių fazių rinkinys, kad įtampos signalo, bei įtampos signalo išvestinės pagal laiką signalų RMS/pikinės vertės santykis būtų minimalus. Signalų palyginimas pateiktas aukščiau (Paveikslas 2.2.3 ir Paveikslas 2.2.4). Galima pastebėti, kad parinkus pradines įtampos signalo fazes išvengiama trumpų, aukštų įtampos šuolių bei signalas pasiskirsto vienodžiau nulio atžvilgiu.

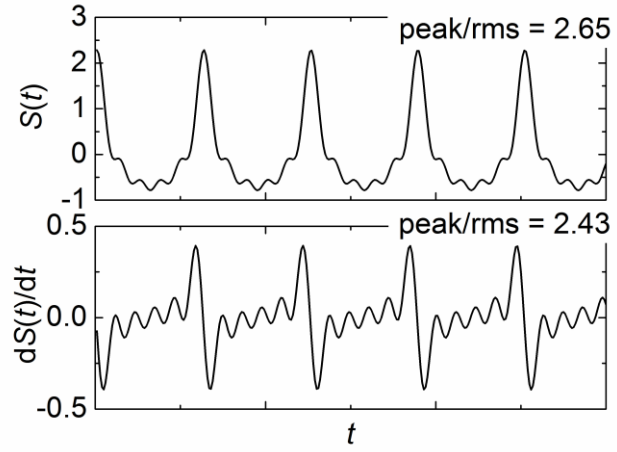

Paveikslas 10.7.5 Penkių harmonikų signalas ir jo išvestinė, kai pradinės įtampos fazės yra lygios

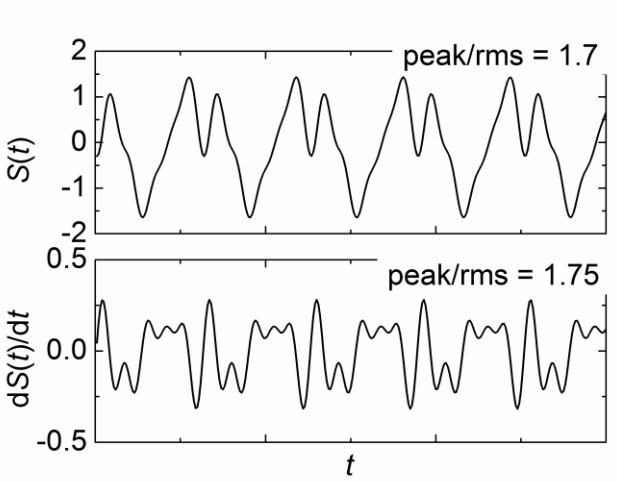

Paveikslas 10.7.6 Penkių harmonikų signalas ir jo išvestinė, kai pradinės įtampos fazės parinktos taip, kad būtų minimizuotas signalo ir jo išvestinės RMS/pikinės vertės santykis. Harmonikų fazes $\varphi_1 \approx 0.412$, $\varphi_2 \approx 3.443$, $\varphi_3 \approx 2.859$, $\varphi_4 \approx 3.602$, $\varphi_5 \approx 2.922$

Verta paminėti, kad netiesinio dielektrinio jautrio matavimo stendo programoje yra įdiegtas signalo vidurkinimo algoritmas, kuris padeda pasiekti 100 dB signalo/triukšmo santykį. Kitas svarbus aspektas – įtampos signalas yra generuojamas DT9834 moduliu, kuris yra skaitmeninis įtaisas. Nors ir prietaiso skiriamoji geba gan didelė (16 bit skaičius-analogas konverteris, 500kHz diskretizacijos dažnis), kvantuoti žingsneliai įtampos signale gali sukelti didelius per bandinį tekančios srovės šuolius. Dėl šios priežasties yra

naudojamas papildomas 30 kHz analoginis RC filtras DT9834 generuojamo signalo išėjime. 30 kHz atkirtos dažnis turėtų būti pakankamas, kad nuslopinti 500 kHz diskretizacijos dažnio sukeltus srovės šuolius.

Visos aukščiau paminėtos netiesinio dielektrinio jautrio matavimo sistemos savybės leidžia patikimai atlikti įvairių medžiagų netiesinio dielektrinio jautrio matavimus. Deka sistemos fazės iškraipymų kalibravimo, matavimo signalo pagrindinės harmonikos dažnio diapazonas praplėstas iki 1/10 diskretizacijos dažnio.

10.8 (1-*x*)$PbMg_{1/3}Nb_{2/3}O_3$-*x*$PbTiO_3$ PAGRINDO MEDŽIAGŲ NETIESINIO DIELEKTRINIO JAUTRIO TYRIMAI

(1-*x*)$PbMg_{1/3}Nb_{2/3}O_3$-*x*$PbTiO_3$ (PMN-*x*PT) yra kietas tirpalas, kur PMN yra FR, o PT yra normalus feroelektrikas. Tokie kietieji tirpalai įdomūs tuo, jog parinkus tam tikrą tirpalo dedamųjų koncentraciją galima gauti morfotropinės fazių sandūros (MFS) būseną reikiamoje temperatūroje. MFS yra riba fazinėje kompozicijos-temperatūros diagramoje, kurioje kristalo struktūra staigiai keičiasi. Medžiagos arti MFS turi stiprų pjezoelektrinį efektą. Yra žinoma, kad FR maišant su normaliu feroelektriku, pasiekus tam tikrą koncentraciją yra stebimas fazinis virsmas. Tačiau, nevisada lengva nustatyti, kurioje koncentracijoje fazinis virsmas jau vyksta. Taip pat, įdomu išsiaiškinti, kas vyksta junginyje maišant FR su normaliu feroelektriku.

0.83PMN-0.17PT monokristalas yra viduryje tarp PMN ir MFS. Ankstesni kitų mokslininkų tyrimai parodė požymius, bylojančių apie fazės kitimą šioje koncentracijoje [59,61]. Todėl įdomu išsiaiškinti ar tikrai 0.83PMN-0.17PT turi fazinį virsmą ir kokio tipo jis gali būti. Tuo tikslu atlikti kristalo netiesinio dielektrinio jautrio tyrimai. Tyrimams naudotas 0.83PMN-0.17PT (100) krypties monokristalas, užaugintas modifikuotu Bridžmano metodu [64].

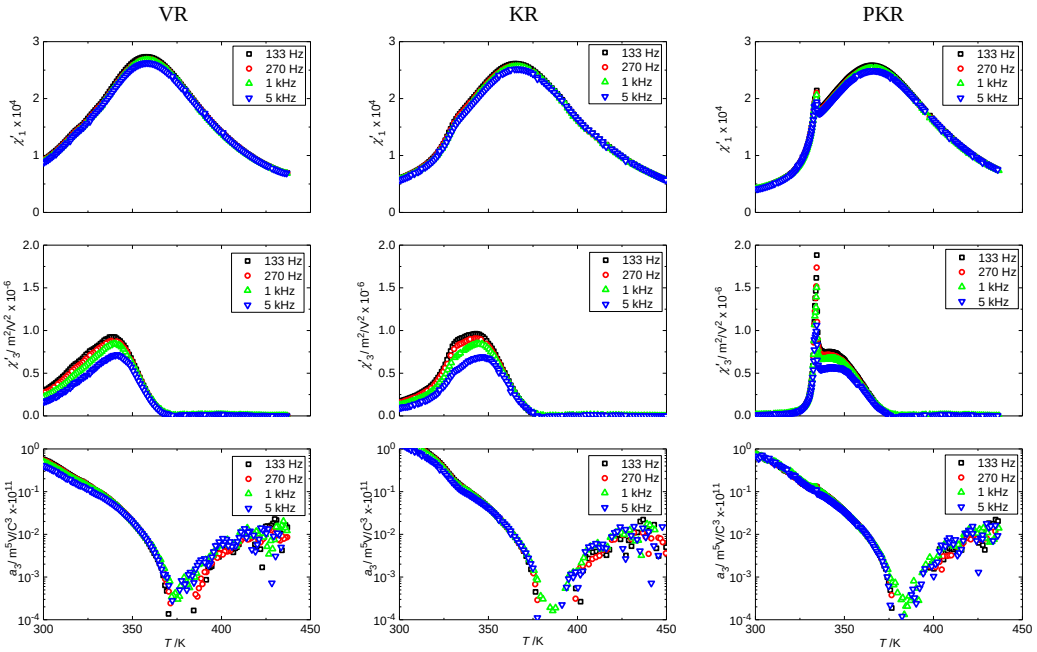

Paveikslas 10.8.1 PMN-0.17PT monokristalo tiesinio dielektrinio jautrio $\chi'_1(T)$, trečiosios eilės netiesinio dielektrinio jautrio $\chi'_3(T)$, santykinio dielektrinio jautrio koeficiento $a_3(T)$ priklausomybės nuo temperatūros, matuojant (iš kairės) vėsinant, kaitinant, kaitinant poliarizavus bandinį

Netiesinio dielektrinio jautrio matavimai atlikti trimis režimais: 1) vėsinimo režimu (VR) – bandinys užkaitinamas iki aukštos temperatūros, tada matavimas atliekamas bandiniui vėstant pastoviu greičiu; 2) kaitinimo režimu (KR) – bandinys atšaldomas iki žemos temperatūros ir matavimai atliekami bandinį kaitinant iki aukštos temperatūros pastoviu greičiu; 3) poliarizuoto bandinio KR (PKR) – bandinys poliarizuojamas kambario temperatūroje, aukštesniame nei koercinis, elektriniame lauke, ir matavimai atliekami kaitinant iki aukštos temperatūros pastoviu greičiu. Paveikslas 10.8.1 rodo visų trijų matavimo režimų palyginimą. Žvelgiant į VR, tiesinio dielektrinio jautrio priklausomybėje nuo temperatūros ($\chi'_1(T)$) nėra aiškiai matomas viršūnės slinkimas aukštesnių temperatūrų link, didėjant dažniui. Tačiau, aukštesniuose dažniuose ši elgsena yra stebima [59]. Trečiosios eilės dielektrinis jautris yra teigiamas visame temperatūrų diapazone ($\chi'_3(T)$) ir, kartu su santykiniu netiesinio dielektrinio jautrio koeficientu ($a_3(T)$), primena gryno PMN kristalo elgseną [35]. Taip pat, $a_3(T)$ atitinka Glazounovo-Tagantsevo FR

fenomenologinį dinaminio netiesinio atsako modelį [16]. Dėl paminėtų savybių, galima teigti, jog stebima įprasto FR elgsena. Gautas rezultatas yra gan kontrastingas panašiam kietąjam tirpalui PZN-0.08PT, kur stebimas pirmosios rūšies fazinis virsmas, tačiau $\chi'_3(T)$ keičia ženklą [40]. Fazinio virsmo buvimas patvirtintas neutronų sklaidos eksperimentu [66].

Žvelgiant į KR matavimo rezultatus, stebima temperatūrinė $\chi'_1(T)$ histerezė. Taip pat, kupra ties 330 K temperatūra, kuri matoma ir $\chi'_3(T)$. Staigesnis $\chi'_1(T)$ augimas kylant temperatūrai KR atveju, gali byloti apie lėtą spontaninį tvarkimąsį arba PNS augimą į makroskopinius feroelektrinius domenus. Įdomu tai, jog PKR režime, kupra virsta aštriu teigiamu šuoliu $\chi'_3(T)$ 330 K temperatūroje, kuris gali būti siejamas su pirmosios rūšies faziniu virsmu. Temperatūrų diapazone virš šio aštraus šuolio stebima FR elgsena.

Kita ištirta medžiaga yra PMN-0.1PT kietasis tirpalas praturtintas 0.5% ir 1% Mn (PMN-0.1PT:0.005Mn, PMN-0.1PT:0.01Mn). Šios keramikos buvo pagamintos mechano syntezės metodu [67–70].

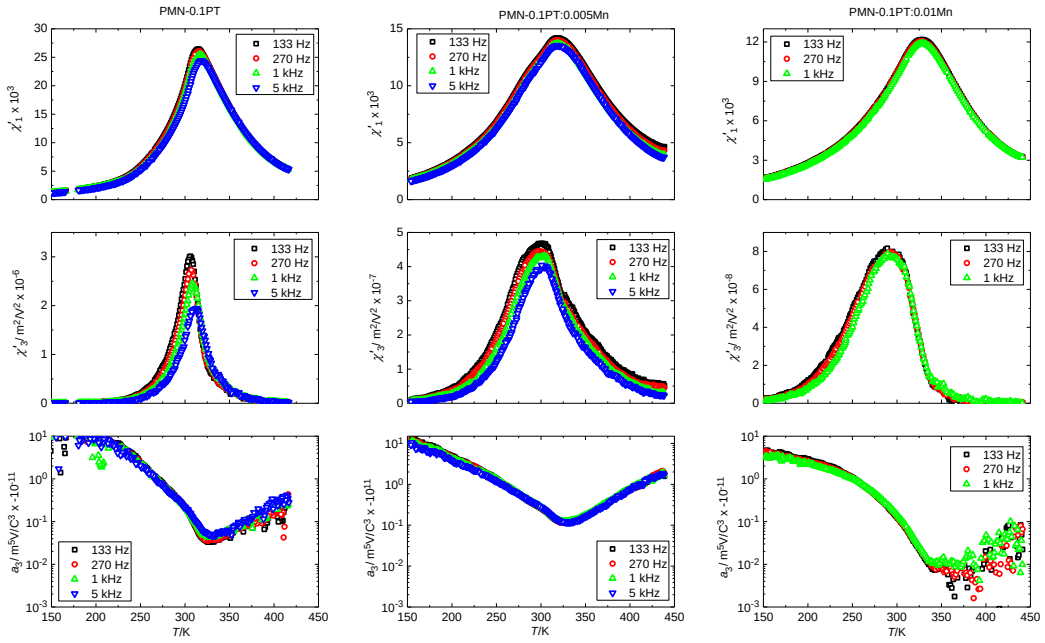

Paveikslas 10.8.2 (iš kairės) PMN-0.1PT, PMN-0.1PT:0.005Mn, PMN-0.1PT:0.01Mn keramikų tiesinio dielektrinio jautrio $\chi'_1(T)$, trečiosios eilės netiesinio dielektrinio jautrio $\chi'_3(T)$, santykinio dielektrinio jautrio koeficiento $a_3(T)$ priklausomybės nuo temperatūros

Feroelektrinių medžiagų praturtinimas Mn (kur Mn įgauna +2 oksidacijos laipsnį) mažina domenų reakciją į išorinį elektrinį lauką (domenai tampa neperorientuojami išoriniu elektriniu lauku). Taip atsitinka dėl akceptorinės Mn^{2+} elgsenos. Mn^{2+} patenka į B poziciją ABO_3 perovskitinėje struktūroje ir sukuria deguonies vakansijas kompensuoti krūviui, dėl kurių atsiranda stacionarios defekto dipolio poros [71–73]. Tikėtina, kad tokiu pat būdu gali būti sukuriamos nejudrios PNS.

Paveikslas 10.8.2 rodo PMN-0.1PT, PMN-0.1PT:0.005Mn, PMN-0.1PT:0.01Mn keramikų $\chi'_1(T)$, $\chi'_3(T)$ ir $a_3(T)$ temperatūrines priklausomybes. PMN-0.1PT rodo aiškią FR elgseną. $\chi'_1(T)$ maksimumas slenka aukštesnių temperatūrų link, didėjant dažniui. $\chi'_3(T)$ yra teigiamas visame temperatūrų diapazone, o $a_3(T)$ atitinka Glazounovo-Tagantsevo FR fenomenologinį dinaminio netiesinio atsako modelį [16]. Mn praturtintose keramikose, pateiktame dažnių diapazone, sunkiau stebimas $\chi'_1(T)$ maksimumo poslinkis didėjant dažniui, tačiau jis išryškėja aukštesniuose dažniuose [67]. Kitas svarbus aspektas yra tas, kad Mn praturtintose keramikose stebima sumažėjusi $\chi'_1(T)$ maksimumo vertė ir maksimumas paslinktas aukštesnių temperatūrų link. Labai įdomu tai, jog stebimas žymus $\chi'_3(T)$ sumažėjimas. $\chi'_3(T)$ PMN-0.1PT:0.005Mn keramikoje sumažėjo $\approx$ 52%, o PMN-0.1PT:0.01Mn net $\approx$ 97%, lyginant su keramika be Mn. Čia svarbu paminėti, jog aukštesnės eilės dielektrinis jautris yra jautresnis dipolių elgsenos pokyčiams [75,76] nei tiesinis. Toks žymus $\chi'_3(T)$ sumažėjimas padarė įtaką $a_3(T)$, tačiau net ir Mn praturtintose keramikose $a_3(T)$ atitinka Glazounovo-Tagantsevo FR fenomenologinį dinaminio netiesinio atsako modelį [16]. Verta paminėti, jog pasak Glazounovo-Tagantsevo [16], $a_3(T)$ yra bedispersinė ir, jei joje ir stebima dispersija, ji greičiausiai yra tikra $a_3(T)$ dispersija arba atsirado dėl to, jog $\chi'_3(T)$ skaičiavimui yra naudotas ribotas aukštesnės dielektrinio jautrio komponenčių skaičius.

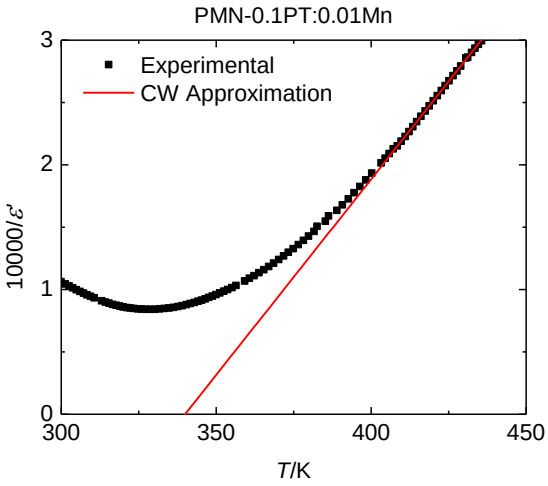

Paveikslas 10.8.3 PMN-0.1PT:0.01Mn keramikos atvirkštinės dielektrinės skvarbos priklausomybės nuo temperatūros CV (2.3.3) aproksimavimas

Norint išsiaiškinti Mn įtaką PMN-0.1PT elgsenai, buvo suskaičiuota Edvardso – Andersono parametro priklausomybė nuo temperatūros $q(T)$. Atvėju, kai nėra pastovaus išorinio elektrinio lauko, $\chi'_1(T)$ susietas su $q(T)$ tokiu sąryšiu,:

$$\chi_1(T) = \frac{C(1-q(T))}{T - T_C(1-q(T))} \qquad (10.8.1)$$

Čia T_C – Kiuri temperature, C – konstanta. Tuomet $q(T)$ galima išreikšti taip:

$$q(T) = 1 - \frac{T\chi_1(T)}{C + T_C\chi_1(T)} \qquad (10.8.2)$$

Norint surasti T_C ir C vertes, buvo panaudota Kiuri-Veiso (CV) aproksimacija (10.8.3) visoms PMN-0.1PT:xMn kompozicijoms. Vieną iš aproksimacijos CV pavyzdžių rodo Paveikslas 10.8.3.

$$\chi_1(T) = \frac{C}{T - T_C} \qquad (10.8.3)$$

Šis sąryšis galioja temperatūrų diapazone > T_C. Aproksimacijos tikslams naudota atvirkščia sąryšio forma, kuri leidžia daryti tiesinę aproksimaciją ir nesudėtingai suskaičiuti T_C ir C:

$$\frac{1}{\chi_1} = \frac{T - T_C}{C} \equiv kT + b \quad \Rightarrow \quad C = \frac{1}{k}; \quad T_C = -\frac{b}{k} \tag{10.8.4}$$

Čia k – yra tiesės krypties koeficientas ir b – konstanta. Gautas T_C ir C vertes rodo Lentelė 10.8.1.

Lentelė 10.8.1 PMN-0.1PT, PMN-0.1PT:0.005Mn, PMN-0.1PT:0.01Mn keramikų $\chi'(T)$ CV aproksimacijos virš T_C parametrai

	PMN-0.1PT	PMN-0.1PT:0.005Mn	PMN0.1-PT:0.01Mn
T_C/K	337 ± 1	327 ± 1	341 ± 1
$C/10^3$K	415 ± 10	525 ± 10	318 ± 10

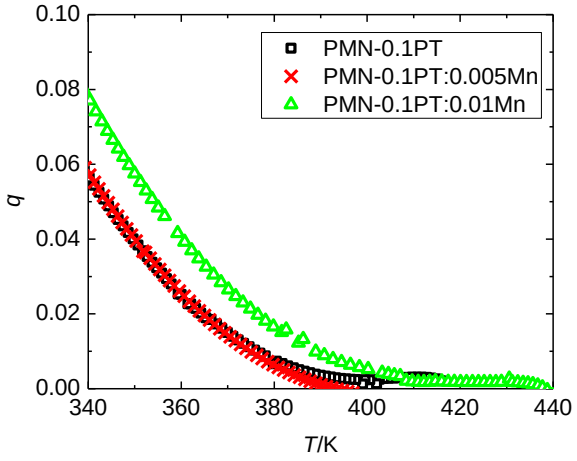

Paveikslas 10.8.4 PMN-0.1PT, PMN-0.1PT:0.005Mn ir PMN-0.1PT:0.01Mn keramikų Edvardso – Andersono parametro priklausomybė nuo temperatūros

Parametras q susijęs su dipolių orientacijos koreliacija PNSe. Vienoje PNS visi dipoliai orientuoti ta pačia kryptimi (dipolių orientacija koreliuota), jei q = 1. Dipoliai orientuoti atsitiktinai (dipolių orientacija nekoreliuota), jei q = 0. Padarius prielaidą, kad PNS aplinka yra nepolinė, galima kalbėti apie bendrą visų dipolių orientaciją. Čia reikia paminėti dvi publikacijas. Xu et al. [28] aiškina, kad mažėjant temperatūrai, PNS auga ir/arba susilieja į didesnes PNS. Koreeda et al. [29] pastebėjo, kad mažėjant temperatūrai PNS formuoja fraktalines struktūras ir perkoliuoja. Tai reiškia, kad T_B (PMN $T_B \approx 600$ K) temperatūroje atsiranda trumpas dipolių orientacijos koreliacijos radiusas. Šios korialiuotų dipolių sistemos yra PNS. Mažėjant temperatūrai koreliacijos

radiusas ilgėja, todėl stebimas PNS augimas. Paveikslas 10.8.4 rodo PMN-0.1PT Edvardso-Andersono parametro priklausomybę nuo temperatūros. Galime čia pastebėti, kad $q(T)$ auga mažėjant temperatūrai. Šis rezultatas sutampa su PNS augimo prielaida. Taip pat, tai padeda paaiškinti, kodėl stebimas $\chi'_1(T)$ viršūnės poslinkis didėjant dažniui. Mažesnės PNS persiorientavimo trukmė trumpesnė (mažesnis dipolių ansamblis), todėl aukštame dažnyje jos duoda indelį į $\chi'_1(T)$. Mažėjant temperatūrai, PNS auga ir persiorientavimas tampa ilgiau trunkančiu procesu (didėja dipolių ansamblis). Didesnės PNS nespėdamos persiorientuoti per aukšto dažnio signalo periodo trukmę, indelio į $\chi'_1(T)$ neduoda – jis stebimas žemesniame dažnyje ir maksimumas gaunamas žemesnėje temperatūroje. Paveikslas 10.8.4 rodo, kad PMN-0.1PT:0.01Mn $q(T)$ elgiasi taip pat, tačiau yra paslinktas aukštesnių temperatūrų link, t.y. toje pačioje temperatūroje PMN-0.1PT:0.01Mn $q(T)$ yra didesnis, nei PMN-0.1PT. Reiškia, PMN-0.1PT:0.01Mn dipoliai toje pačioje temperatūroje yra labiau koreliuoti nei PMN-0.1PT atveju. Norint išsiaiškinti to priežastis, panagrinėsime PMN-0.1PT:0.01Mn $\chi'_1(T)$ (Paveikslas 10.8.2). Čia svarbiausias požymis yra tas, kad šiuose žemuose dažniuose PMN-0.1PT:0.01Mn $\chi'_1(T)$ neturi aiškaus maksimumo poslinkio aukštesnių temperatūrų link, didėjant dažniui, skirtingai nei PMN-0.1PT. Reiškia, PNS augimas PMN-0.1PT:0.01Mn yra suvaržytas. Panašu, kad Mn veikia PNS panašiai kaip ir domenus, t.y. dėl praturtinimo Mn, dalis dipolių tampa nejudrūs. Įmanoma, kad mažėjant temperatūrai nejudrių dipolių orientacijos koreliacija perduodama šalia esantiems dipoliams. Todėl, lieka mažesnės judrių PNS „salos“, kurios duoda įtaką $\chi'_1(T)$. Taigi, mažesnis judrių dipolių ansamblis – greičiau auga orientacijos kereliacijos vektorius, todėl $q(T)$ didesnis nei gryname PMN-0.1PT. Taip pat, įmanoma, kad praturtinimas Mn užkerta kelia PNS perkoliacijai, nes PNS saloms užkertamas kelias susilieti dėl išplitusių stacionarių dipolių sričių.

Stiprus $\chi'_3(T)$ sumažėjimas didinant Mn koncentarciją PMN-0.1PT:xMn gali būti aiškinamas remiantis aukščiau pateiktomis prielaidomis. PNS

plėtimasis yra apribotas dėl praturtinimo Mn, t.y. įkaltų dipolių orientacija nėra koreliuota su judrių PNS. Reiškia, judrios PNS duoda indėlį į $\chi'_1(T)$, o $\chi'_3(T)$ gauna indėlį dėl PNS išsiplėtimo dėl išorinio elektrinio lauko poveikio.

Apibendrinant, netiesinio dielektrinio jautrio matavimai PMN-0.17PT padėjo aptikti fazinį virsmą 330K temperatūroje. PMN-0.1PT praturtinimas Mn sukuria nejudrių dipolių sritis, kurių orientacija nekoreliuota su judrių PNS. Dėl to, sumažėja $\chi'_1(T)$, stipriai sumažėja $\chi'_3(T)$ ir dingsta $\chi'_1(T)$ maksimumo poslinkis žemuose dažniuose.

10.9 GRYNO IR 2% La^{3+} PRATURTINTO $Pb(Mg_{1/3}Nb_{2/3})O_3$ KRISTALŲ TIESINĖ DIELEKTRINĖ SPEKTROSKOPIJA

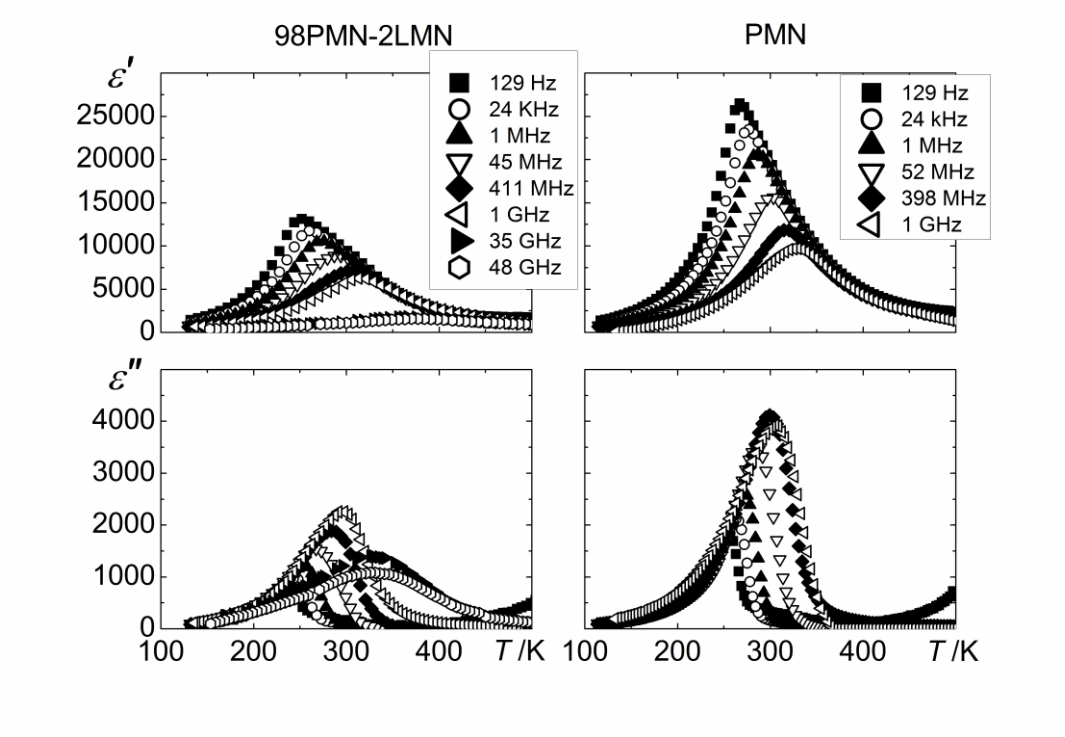

Paveikslas 10.9.1 PMN ir PLMN monokristalų kompleskinės dielektrinės skvarbos priklausomybė nuo temperatūros

Vidutinis chemiškai tvarkių sričių (sritys, kur Mg/Nb pasiskirstymas gardelėje yra periodiškas – CTS) dydis PMN monokristale yra mažesnis nei 5 nm [78,79]. PMN praturtinimas La^{3+}, kuris nukeliauja į A poziciją perovskito ABO_3 gardelėje, praplėčia chemiškai tvarkias sritis iki 100 nm [84]. Neutronų ir rentgeno spindulių sklaidos eksperimentai parodė, kad CTS yra statinės, o

dinaminės yra tik netvarkioje matricoje esančios PNS [89]. Toliau yra pateikta gryno PMN ir 2% La praturtinto monokristalų dielektrinės ($Pb(Mg_{1/3}Nb_{2/3})O_3$–$0.02La(Mg_{2/3}Nb_{1/3})O3$ – PLMN) spektroskopijos rezultatai, kurie papildo anksčiau publikuotus žemesnių dažnių rezultatus [84] ir leido suskaičiuoti relaksacijos trukmių pasiskirstymus.

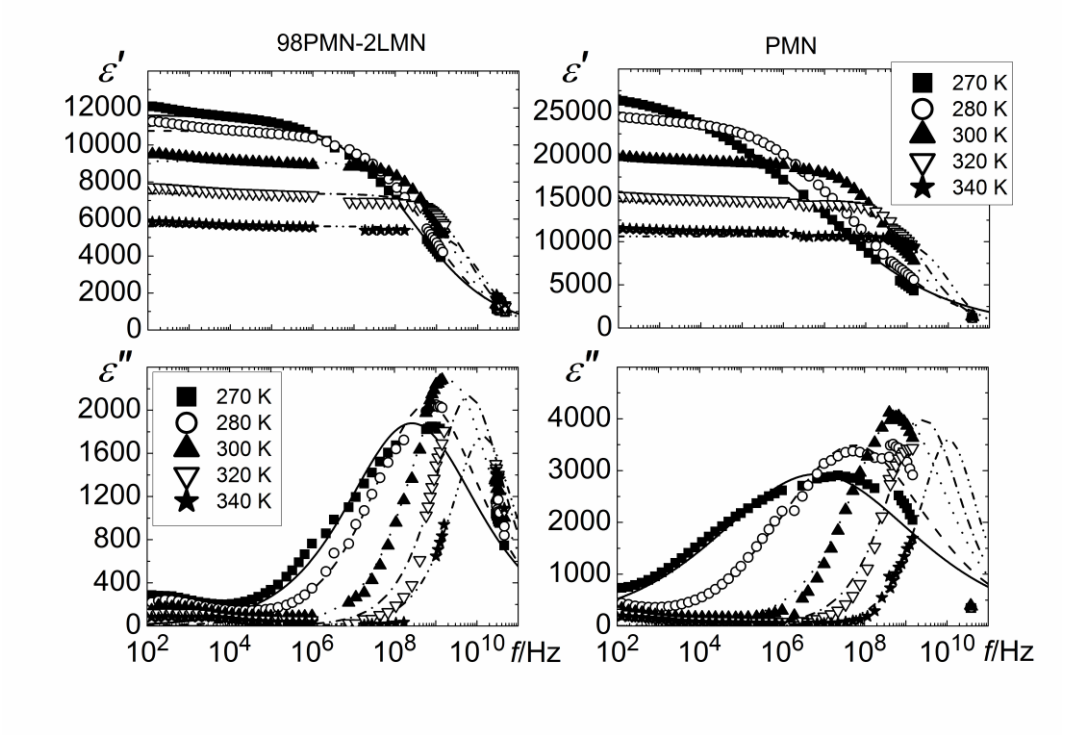

Paveikslas 10.9.2 PMN ir PLMN monokristalų kompleksinės dielektrinės skvarbos priklausomybė nuo dažnio. Linijos rodo Koulo – Koulo aproksimacijas

PMN ir PLMN monokristalai užauginti iš aukštos temperatūros tirpalo panaudojant kristalą – sėklą. Paveikslas 10.9.1 rodo jų kompleksinės dielektrinės skvarbos priklausomybę nuo temperatūros ($\varepsilon^*(T)$). Žinoma, kad PMN yra laikomas kanoniniu FR, tačiau panašu, jog PLMN, nors ir su praplėstomis CTS, vistiek rodo aiškią FR elgseną. Stebimas, $\varepsilon'(T)$ maksimumo poslinkis aukštesnių temperatūrų link, didėjant dažniui. Tačiau, PLMN to pačio dažnio maksimumas yra pasislinkęs į 17 K žemesnę temperatūrą ir yra apie 2 kartus mažesnės vertės, nei gryno PMN. Paveikslas 10.9.2 rodo PMN ir PLMN kristalų kompleksinės dielektrinės skvarbos priklausomybę nuo dažnio $\varepsilon^*(f)$. Abiejuose kristaluose stebimas dispersijos siaurėjimas didėjant temperatūrai.

Galima pastebėti, kad abiejų kristalų $\varepsilon^*(f)$ neblogai aproksimuojama Koulo – Koulo lygtimi:

$$\varepsilon^*(\omega) = \varepsilon_\infty + \frac{\Delta\varepsilon}{1+(\mathrm{i}\omega\tau)^{1-\alpha}} \qquad (2.4.1)$$

Paveikslas 10.9.3 rodo PMN ir PLMN kristalų $\varepsilon^*(f)$ Koulo – Koulo aproksimacijos parametrų priklausomybes nuo temperatūros. Parametras $\alpha(T)$ – charakterizuoja relaksacijos trukmių pasiskirstymo plotį ir rodo panašią elgseną abiejuose kristaluose. Panašią elgseną rodo ir relaksacijos stipris $\Delta\varepsilon(T)$ – tai yra skirtumas tarp statinės dielektrinės skvarbos ir dielektrinės skvarbos be galo aukštame dažnyje. Abiejų kristalų vidutinės relaksacijos trukmės priklausomybė nuo temperatūros $\tau(T)$ auga mažėjant temperatūrai ir neblogai aproksimuojama Vogelio – Fulčerio sąryšiu:

$$\tau = \tau_0 \exp\left(\frac{E_a}{k_B(T - T_{VF})}\right) \qquad (2.4.2)$$

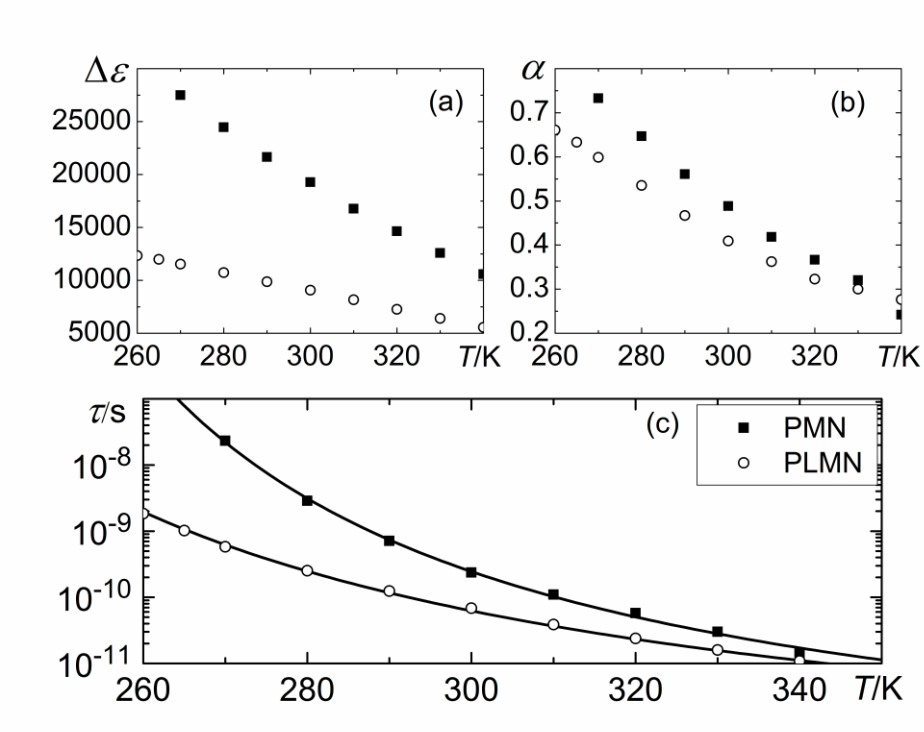

Paveikslas 10.9.3 PMN ir PLMN monokristalų $\varepsilon^*(f)$ Koulo – Koulo apriksimacijos parametrų priklausomybė nuo temperatūros. (c) linija atitinka Vogelio – Fulčerio aproksimacijas

Aproksimacija parodo aiškų kritinio lėtėjimo temperatūrų T_{VF} skirtumą abiejuose kristaluose (Lentelė 10.9.1). Aktyvacijos energijos E_a ir dipolio persiorientavimo trukmės aukštoje temperatūroje τ_0 vertės panašios ir byloja apie panašią dipolių elgsenos prigimtį abiejuose kristaluose. Čia gautos PMN ir PLMN kristalų Vogelio – Fulčerio aproksimacijos parametrų vertės beveik sutampa su anksčiau kitų mokslininkų publikuotomis [84,93,94].

Lentelė 10.9.1 PMN ir PLMN monokristalų $\tau(T)$ Vogelio – Fulčerio aproksimacijos parametrai

Kristalas	τ_0/s	E_a/eV	T_{VF}/K
PMN	5.9×10^{-14}	0.061 ± 0.009	214 ± 6
PLMN	6.3×10^{-14}	0.071 ± 0.007	180 ± 4

Su tikslu gauti geresnį relaksacinių procesų supratimą PMN ir PLMN kristaluose buvo apskaičiuoti relaksacijos trukmių pasiskirstymai (Paveikslas 10.9.4). Relaksacijos trukmių pasiskirstymai abiejose medžiagose atrodo panašiai – platėja mažėjant temperatūrai. Tai paaiškinama atsižvelgus į dispersijos platėjimą $\varepsilon^*(f)$. Tačiau, verta atkreipti dėmesį, kad mažėjant temperatūrai, pasiskirstymai plinta tik į ilgesnių trukmių pusę, o trumpiausių pasiskirstymo trukmių kraštas ties 10^{-13} s išlieka visose temperatūrose. Relaksacijos trukmių pasiskirstymo augimas ilgesnių trukmių link, gali būti susijęs su PNS augimu ir jų persiorientavimo lėtėjimu mažėjant temperatūrai. Tačiau tai, jog pasiskirstymas rodo nenulines vertes trumpų trukmių diapazone, net ir žemesnėse temperatūrose, gali būti siejamas su anksčiau minėta fraktaline PNS struktūra [29], t.y. žemesnėse temperatūrose, nors ir PNS susilieja augdamos, tačiau lieka sparčiau virpančios atšakos.

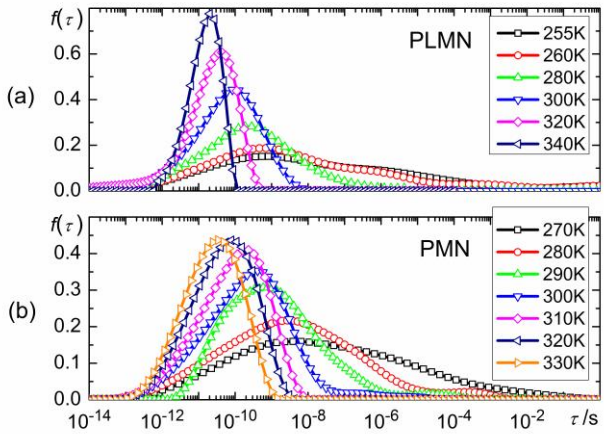

Paveikslas 10.9.4 (a) PLMN ir (b) PMN kristalų relaksacijos trukmių pasiskirstymas

Papildomai suskaičiuota PMN ir PLMN mono kristalų Edvardso – Andersono parametro $q(T)$ priklausomybe nuo temperatūros (Paveikslas 10.9.5) pagal (10.8.2). Tam pasiekti, atlikta CV aproksimacija (10.8.4), kurios deka gaunami parametrai T_C ir C (Lentelė 10.9.2). Diskusija apie $q(T)$ elgseną, pateikta dalyje **10.8** apie PMN-0.1PT:*x*Mn, galioja ir čia. Esminis skirtumas pastebėtas čia, yra tas, kad PLMN $q(T)$ vertė, toje pačioje temperatūroje, yra mažesnė nei gryno PMN (pvz.: 360 K). Abu kristalai, PMN ir PLMN, rodo stiprią FR elgseną, tačiau PLMN turi beveik 2 kartus mažesnę $\varepsilon'(T)$ maksimumo vertę, kuris yra apie 17 K žemesnėje temperatūroje, nei gryname kristale. Tokie elgsenos skirtumai stebimi todėl, kad didesnės CTS PLMN kristale apsunkina PNS perkoliaciją mažėjant temperatūrai, t.y. PNS dipolių orientacijos koreliacija apribota platesnėmis CTS salomis. CTSe esantys dipoliai yra statiški, todėl ilgesnis orientacijos koreliacijos radiusas nei PMN reikalingas PLMN, norint PNS augti, mažėjant temperatūrai.

Lentelė 10.9.2 PMN ir PLMN $\varepsilon'(T)$ CV aproksimacijos virš T_C parametrai

	PMN	PLMN
T_C /K	334 ± 1	311 ± 1
$C/10^3$K	191 ± 10	232 ± 10

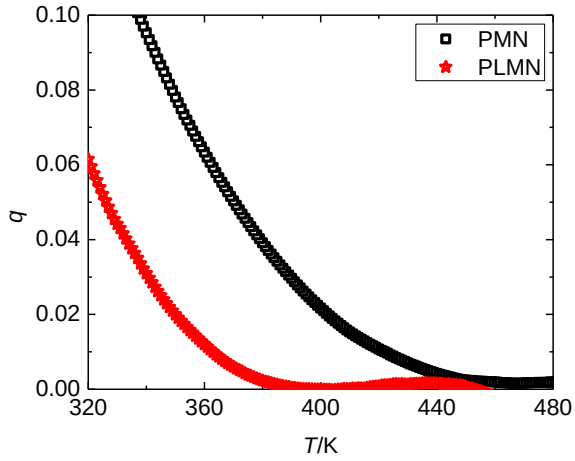

Paveikslas 10.9.5 PMN ir PLMN kristalų Edvardso – Andersono parametro priklausomybė nuo temperatūros

PMN praturtinimas La daro kitokią įtaką medžiagos elgsenai, nei PLMN-0.1PT praturtinimas Mn. Abi medžiagos yra FR. Abiejose medžiagose yra sumažinama $\varepsilon'(T)$, tačiau dėl skirting priežasčių. La PMN kristale praplečia chemiškai tvarkias sritis, todėl PNS orientacijos perkoliacija apsunkinama, tačiau ji vyksta ir stebima aiški FR elgsena. Mn PMN-0.1PT keramikoje sukuria defektus, dėl kurių yra įkalami dipoliai ir užkertamas kelias PNS perkoliacijai. Taip pat, ribojamas PNS dydis ir žemesniuose dažniuose nestebimas FR būdingas $\varepsilon'(T)$ maksimumo poslinkis.

10.10 DISERTACIJOS IŠVADOS

1. Sukonstruotas netiesinio dielektrinio jautrio matuoklis. Parašyta jį valdanti programa. Įdiegtas įrangos sukelto fazės poslinkio kalibravimas, kurio deka praplėstas pagrindinės harmonikos dažnių diapazonas iki 1/10 diskretizacijos dažnio.
2. Poliarizuotame PMN-0.17PT monokristale pastebėtas pirmosios rūšies fazinis virsmas iš relaksoriaus į normalų feroelektriką. Fazinis virsmas pasireiškia kaip aštrus pikas $\chi_3(T)$ $T \approx 330$ K temperatūroje.
3. PMN-0.1PT keramikų praturtinimas Mn ženkliai sumažina $\chi_3(T)$. Tai parodo, kad Mn sukurti defektai sumažina PNS judėjimą

4. FR elgsena nėra labai susilpninama, ženkliai praplėtus chemiškai tvarkias sritis. PMN kristale, praturtintame 2% La, neužgniaužta FR elgsena ir nestebemas spontaninis fazinis virsmas.
5. Edvardso – Andersono parametrų skaičiavimai parodė, kad FR praturtinimas La ir Mn sukuria skirtingus dielektrinės skvarbos sumažėjimo mechanizmus. Praturtinimas La apsunkina PNS augimą, o praturtinimas Mn sukuria nejudrius dipolius.

10.11 PUBLIKACIJOS

1. D. Jablonskas, R. Grigalaitis, J. Banys, A. A. Bokov, Z.-G. Ye, Broadband dielectric spectra in $PbMg_{1/3}Nb_{2/3}O_3$ crystals with chemical ordering modified by La doping, *Appl. Phys. Lett.*, vol. **107**, Issue 14, p. 142905, 2015, doi: 10.1063/1.4932656.
2. D. Jablonskas, M. Ivanov, R. Grigalaitis, J. Banys, Implementation of an improved non-linear susceptometer, *Ferroelectrics*, vol. **513**, Issue 1, p. 32-37, 2017, doi: 10.1080/00150193.2017.1350071.
3. Š. Svirskas, D. Jablonskas, V. Samulionis, S. Kojima, J. Banys, Is there a spontaneous ferroelectric phase transition in $0.83PbMg_{1/3}Nb_{2/3}O_3$-$0.17PbTiO_3$ single crystal?, *J. All. Comp.*, vol. **748**, p. 127-133, 2018, doi: 10.1016/j.jallcom.2018.03.130.
4. Š. Svirskas, D. Jablonskas, V. Samulionis, A. Kuprevičiūtė, J. Banys, S. J. Chin, T. McNally, Effect of $Mo_6S_3I_6$ nanowires on dielectric properties of poly(ε-caprolactone), *Phys. stat. sol. (a)*, vol. **210**, Issue 11, p. 2272-2277, 2013, doi: 10.1002/pssa.201329313.
5. D. Jablonskas, S. Lapinskas, S. Rudys, M. Ivanov, J. Banys, Full-wave finite space model of open-ended coaxial line for dielectric spectroscopy of liquids, *Rev. Sci. Instrum.*, vol. **88**, Issue 8, p. 084703, 2017, doi: 10.1063/1.4991312.
6. D. Jablonskas, M. Ivanov, J. Banys, G. A. Giffin, S. Passerini, Dielectric spectroscopy of Pyr_{14}TFSI and Pyr_{12O1}TFSI ionic liquids, *Electrochim. Acta*, 2018, doi: 10.1016/j.electacta.2018.04.104.

10.12 LITERATŪRA

[1] S. Miga, J. Dec, W. Kleemann, Computer-controlled susceptometer for investigating the linear and nonlinear dielectric response, Rev. Sci. Instrum. 78 (2007) 033902. doi:10.1063/1.2712792.

[2] A.K. Jonscher, Dielectric Relaxation in Solids, Chelsea Dielectric press, London. (1983).

[3] V.L. Ginzburg, On the dielectric properties of ferroelectric (Segnette-electric) crystal and barium titanate, Zh. Exp. Theor. Phys. 15 (1945) 739–749.

[4] A.F. Devonshire, Theory of barium titanate, Part I, Phil. Mag. 40 (1949) 1040–1063.

[5] J. Dec, S. Miga, W. Kleemann, Dynamic nonlinear susceptibility in solid dielectrics, in: 2010 10th IEEE Int. Conf. Solid Dielectr. ICSD, 2010: pp. 1–5. doi:10.1109/ICSD.2010.5568203.

[6] R. Pirc, R. Blinc, Spherical random-bond random-field model of relaxor ferroelectrics, Phys. Rev. B. 60 (1999) 13470–13478. doi:10.1103/PhysRevB.60.13470.

[7] R. Pirc, B. Tadić, R. Blinc, Nonlinear susceptibility of orientational glasses, Phys. B Condens. Matter. 193 (1994) 109–115. doi:10.1016/0921-4526(94)90001-9.

[8] S. Svirskas, M. Ivanov, S. Bagdzevicius, J. Macutkevic, A. Brilingas, J. Banys, J. Dec, S. Miga, M. Dunce, E. Birks, M. Antonova, A. Sternberg, Dielectric properties of solid solutions, Acta Mater. 64 (2014) 123–132. doi:10.1016/j.actamat.2013.11.040.

[9] S. Ikeda, H. Kominami, K. Koyama, Y. Wada, Nonlinear dielectric constant and ferroelectric-to-paraelectric phase transition in copolymers of vinylidene fluoride and trifluoroethylene, J. Appl. Phys. 62 (1987) 3339–3342. doi:10.1063/1.339294.

[10] Y. Ishibashi, Nonlinear dielectric spectroscopy, J. Korean Phys. Soc. 32 (1998) 407–410. doi:http://dx.crossref.org/10.3938/jkps.32.407.

[11] C. Thibierge, D. L'Hôte, F. Ladieu, R. Tourbot, A method for measuring the nonlinear response in dielectric spectroscopy through third harmonics detection, Rev. Sci. Instrum. 79 (2008) 103905. doi:10.1063/1.2960564.

[12] Š. Svirskas, J. Banys, S. Kojima, Broadband dielectric spectroscopy of Pb-based relaxor ferroelectric (1-x)Pb(Mg1/3Nb2/3)O3-xPbTiO3 with intermediate random fields, J. Appl. Phys. 121 (2017) 134101. doi:10.1063/1.4979729.

[13] M.A. Helal, M. Aftabuzzaman, S. Svirskas, J. Banys, S. Kojima, Temperature evolution of central peaks and effect of electric field in relaxor ferroelectric 0.83Pb(Mg1/3Nb2/3)O3–0.17PbTiO3 single crystals, Jpn. J. Appl. Phys. 56 (2017) 10PB03. doi:10.7567/JJAP.56.10PB03.

[14] H. Luo, G. Xu, H. Xu, P. Wang, Z. Yin, Compositional Homogeneity and Electrical Properties of Lead Magnesium Niobate Titanate Single Crystals Grown by a Modified Bridgman Technique, Jpn. J. Appl. Phys. 39 (2000) 5581. doi:10.1143/JJAP.39.5581.

[15] J. Dec, S. Miga, W. Kleemann, B. Dkhil, Nonlinear Dielectric Properties of PMN Relaxor Crystals within Landau-Ginzburg-Devonshire Approximation, Ferroelectrics. 363 (2008) 141–149. doi:10.1080/00150190802025947.
[16] A.E. Glazounov, A.K. Tagantsev, Phenomenological Model of Dynamic Nonlinear Response of Relaxor Ferroelectrics, Phys. Rev. Lett. 85 (2000) 2192–2195. doi:10.1103/PhysRevLett.85.2192.
[17] M. Iwata, T. Ido, R. Nagahashi, Y. Ishibashi, Nonlinear dielectric susceptibility in relaxor ferroelectrics Pb(Zn1/3Nb2/3)O3-PbTiO3, Ferroelectrics. 498 (2016) 52–61. doi:10.1080/00150193.2016.1170420.
[18] E.H. Kisi, J.S. Forrester, The phase transition sequence in the relaxor ferroelectric PZN–8% PT, J. Phys. Condens. Matter. 20 (2008) 165208. doi:10.1088/0953-8984/20/16/165208.
[19] R.M. Katilūtė, Mangano oksidu praturtintų PMN-10PT keramikų gamyba ir (di)elektrinis charakterizavimas, Master Thesis, Vilnius University, 2017.
[20] M. Sopicka-Lizer, High-Energy Ball Milling: Mechanochemical Processing of Nanopowders, Elsevier, 2010.
[21] D. Kuscer, J. Holc, M. Kosec, A. Meden, Mechano-Synthesis of Lead–Magnesium–Niobate Ceramics, J. Am. Ceram. Soc. 89 (2006) 3081–3088. doi:10.1111/j.1551-2916.2006.01221.x.
[22] D. Kuscer, J. Holc, M. Kosec, Formation of 0.65 Pb(Mg1/3Nb2/3)O3–0.35 PbTiO3 Using a High-Energy Milling Process, J. Am. Ceram. Soc. 90 (2007) 29–35. doi:10.1111/j.1551-2916.2006.01332.x.
[23] C. Molin, M. Sanlialp, V.V. Shvartsman, D.C. Lupascu, P. Neumeister, A. Schönecker, S. Gebhardt, Effect of dopants on the electrocaloric effect of 0.92 Pb(Mg1/3Nb2/3)O3–0.08 PbTiO3 ceramics, J. Eur. Ceram. Soc. 35 (2015) 2065–2071. doi:10.1016/j.jeurceramsoc.2015.01.016.
[24] J.-H. Park, J. Park, J.-G. Park, B.-K. Kim, Y. Kim, Piezoelectric properties in PMN–PT relaxor ferroelectrics with MnO2 addition, J. Eur. Ceram. Soc. 21 (2001) 1383–1386. doi:10.1016/S0955-2219(01)00023-1.
[25] L. Luo, W. Li, Y. Zhu, J. Wang, Growth and characteristics of Mn-doped PMN–PT single crystals, Solid State Commun. 149 (2009) 978–981. doi:10.1016/j.ssc.2009.04.018.
[26] J. Dec, S. Miga, W. Kleemann, Ferroelectric Phase Transitions Viewed Via Nonlinear Dielectric Response, Ferroelectrics. 417 (2011) 82–92. doi:10.1080/00150193.2011.578500.
[27] B.E. Vugmeister, M.D. Glinchuk, Dipole glass and ferroelectricity in random-site electric dipole systems, Rev. Mod. Phys. 62 (1990) 993–1026. doi:10.1103/RevModPhys.62.993.
[28] G. Xu, G. Shirane, J.R.D. Copley, P.M. Gehring, Neutron elastic diffuse scattering study of $Pb(Mg_{1/3}Nb_{2/3}O_3$, Phys. Rev. B. 69 (2004) 064112. doi:10.1103/PhysRevB.69.064112.

[29] A. Koreeda, H. Taniguchi, S. Saikan, M. Itoh, Fractal Dynamics in a Single Crystal of a Relaxor Ferroelectric, Phys. Rev. Lett. 109 (2012) 197601. doi:10.1103/PhysRevLett.109.197601.
[30] M.A. Akbas, P.K. Davies, Thermally Induced Coarsening of the Chemically Ordered Domains in Pb(Mg1/3Nb2/3)O3 (PMN)-Based Relaxor Ferroelectrics, J. Am. Ceram. Soc. 83 (2000) 119–23. doi:10.1111/j.1151-2916.2000.tb01158.x.
[31] A.D. Hilton, D.J. Barber, C.A. Randall, T.R. Shrout, On short range ordering in the perovskite lead magnesium niobate, J. Mater. Sci. 25 (1990) 3461–3466. doi:10.1007/BF00575371.
[32] X. Long, A.A. Bokov, Z.-G. Ye, W. Qu, X. Tan, Enhanced ordered structure and relaxor behaviour of 0.98Pb(Mg1/3Nb2/3)O3–0.02La(Mg2/3Nb1/3)O3 single crystals, J. Phys. Condens. Matter. 20 (2008) 015210. doi:10.1088/0953-8984/20/01/015210.
[33] S. Vakhrushev, a, Abstr. 11th Eur. Mtg Ferroelectr. (2007) 219.
[34] V. Bovtun, S. Veljko, S. Kamba, J. Petzelt, S. Vakhrushev, Y. Yakymenko, K. Brinkman, N. Setter, Broad-band dielectric response of PbMg1/3Nb2/3O3 relaxor ferroelectrics: Single crystals, ceramics and thin films, J. Eur. Ceram. Soc. 26 (2006) 2867–2875. doi:10.1016/j.jeurceramsoc.2006.02.003.
[35] S. Kamba, M. Kempa, V. Bovtun, J. Petzelt, K. Brinkman, N. Setter, Soft and central mode behaviour in $PbMg_{1/3}Nb_{2/3}O_3$ relaxor ferroelectric, J. Phys. Condens. Matter. 17 (2005) 3965–3974. doi:10.1088/0953-8984/17/25/022.

PUBLICATIONS OF THE DOCTORAL DISSERTATION

1. D. Jablonskas, R. Grigalaitis, J. Banys, A. A. Bokov, Z.-G. Ye, Broadband dielectric spectra in $PbMg_{1/3}Nb_{2/3}O_3$ crystals with chemical ordering modified by La doping, *Appl. Phys. Lett.*, vol. **107**, Issue 14, p. 142905, 2015, doi: 10.1063/1.4932656.
2. D. Jablonskas, M. Ivanov, R. Grigalaitis, J. Banys, Implementation of an improved non-linear susceptometer, *Ferroelectrics*, vol. **513**, Issue 1, p. 32-37, 2017, doi: 10.1080/00150193.2017.1350071.
3. Š. Svirskas, D. Jablonskas, V. Samulionis, S. Kojima, J. Banys, Is there a spontaneous ferroelectric phase transition in $0.83PbMg_{1/3}Nb_{2/3}O_3$-$0.17PbTiO_3$ single crystal?, *J. All. Comp.*, vol. **748**, p. 127-133, 2018, doi: 10.1016/j.jallcom.2018.03.130.

with a form for this purpose (Reuse of Previously Published Material). More specific information can also be found in the Author Permission FAQ.

Q: May I include my AIP Publishing article in my thesis or dissertation?

AIP Publishing permits authors to include their published articles in a thesis or dissertation. It is understood that the thesis or dissertation may be published in print and/or electronic form and offered for sale on demand, as well as included in a university's repository. Formal permission from AIP Publishing is not needed. If the university requires written permission, however, we are happy to supply it.

Permission to Reuse AIP Publishing Material

Q: How do I obtain permission to reuse AIP Publishing material?

Using RightsLink®: AIP Publishing has partnered with the Copyright Clearance Center to offer Rightslink, a convenient online service that streamlines the permissions process. Rightslink allows users to instantly obtain permissions and pay any related fees for reuse of material, directly from AIP Publishing's website. Once licensed, the material may be reused legally, according to the terms and conditions set forth in each unique license agreement.

To use the service, access the article you wish to license on Scitation and simply click on the Reprints & Permissions link in the abstract. If you have questions about Rightslink, click on the link as described, and then click the "Help" button located in the top right-hand corner of the Rightslink page.

Without using RightsLink: Send requests for permission for republication or other reuse of AIP Publishing journal or conference proceedings material to rights@aip.org.

Contact address:

Office of Rights and Permissions
AIP Publishing
1305 Walt Whitman Road
Suite 300
Melville, NY 11747-4502
Telephone: +1 516-576-2268

Q: What information does AIP Publishing require in a permission request?

Please provide as much information as possible when requesting permission. Be sure to include the following:

- Citation information for the article containing the material you wish to reuse.
- A description of the material you wish to reuse, including the figure and/or table number as it appears in the article.
- The title, authors, name of the publisher, and expected publication date of the new work.
- The format(s) the new work will appear in—print, electronic, CD-ROM, for example.
- Information as to how the new work will be distributed and whether it will be offered for sale.

Q: Is permission needed to adapt or redraw AIP Publishing material?

Yes. Permission is still needed if you are adapting or redrawing material. If you are significantly modifying the material so as to create a new and unique work that would be eligible for copyright protection on its own, then permission is not needed.

Q: Is permission needed for an image taken from the Internet?

Broadband dielectric spectra in $PbMg_{1/3}Nb_{2/3}O_3$ crystals with chemical order modified by La doping

D. Jablonskas,[1] R. Grigalaitis,[1] J. Banys,[1] A. A. Bokov,[2] and Z.-G. Ye[2]
[1]*Faculty of Physics, Vilnius University, Sauletekio str. 9 III 817, LT-10222 Vilnius, Lithuania*
[2]*Department of Chemistry and 4D LABS, Simon Fraser University, Burnaby, British Columbia V5A 1S6, Canada*

(Received 10 August 2015; accepted 27 September 2015; published online 6 October 2015)

$PbMg_{1/3}Nb_{2/3}O_3$ (PMN) is a well known ferroelectric relaxor. PMN crystal doped with La^{3+} has greatly enlarged chemically ordered regions (CORs) in the structure. It is interesting to know how the development of CORs influences physical properties of PMN crystal. In this work, dielectric properties and distribution of relaxation times of PMN and $0.98Pb(Mg_{1/3}Nb_{2/3})O_3$–$0.02La(Mg_{2/3}Nb_{1/3})O_3$ (PLMN) crystals are studied. The experiment was performed in 120–500 K temperature range and wide frequency range—up to 46 GHz. The results demonstrate that the relaxor behaviour of PMN and PLMN is qualitatively the same in spite of the fact that chemical ordering is very different. © *2015 AIP Publishing LLC*. [http://dx.doi.org/10.1063/1.4932656]

Lead magnesium niobate, $PbMg_{1/3}Nb_{2/3}O_3$ (PMN), is a well known and widely studied relaxor ferroelectric (RF). RFs are characterized by a broad peak and a strong frequency dispersion of dielectric permittivity as a function of temperature.[1] In contrast to ordinary ferroelectrics, the dielectric anomaly is not connected with any macroscopic structural changes and PMN remains macroscopically cubic down to cryogenic temperatures.[2] It is believed that the main cause of this peculiar behaviour in dielectric permittivity of PMN is the appearance of polar nano regions (PNRs)—small nanometer size regions with correlated dipole moments embedded in disordered matrix. They start to form at Burns temperature (T_B), which is well above the temperature range of maximum of dielectric permittivity (T_m). PNRs are responsible for the relaxor behavior of PMN.[3,4] PMN has perovskite ABO_3 structure, where A site is occupied by Pb^{2+} and B site has a distribution of Mg^{2+} and Nb^{5+} ions. It is widely accepted to use the random site model[5–7] to describe the distribution of B site ions, according to which PMN structure can be written as $Pb(\beta'_{1/2}\beta''_{1/2})O_3$, where β'' is occupied solely by Nb^{5+} and β' is occupied by 2:1 random distribution of Mg^{2+} and Nb^{5+}. Such a configuration in chemically ordered regions (CORs) is characterized by periodical distribution of ions in B site, so the ordered domain is overall electroneutral, and can be generally formulated as $Pb[(Mg^{2+}_{2/3}Nb^{5+}_{1/3})_{1/2}Nb^{5+}_{1/2}]O_3$. These CORs are embedded in disordered matrix, in which ions in B site are distributed randomly without any periodicity.[5]

Neutron elastic diffuse scattering study of PMN suggested that at Burns temperature, T_B, the soft TO phonon mode becomes overdamped near Brillouin zone centre and starts to condense into PNRs. The regions become polarized along (111) direction. With the decrease of temperature, the number and size of PNRs in the system increase and small PNRs merge into larger ones. The result of this behavior is the increase in the total volume of PNRs in the system. The related ferroelectric soft-mode lifetime increases below T_m, and overdamping near the Brillouin zone centre disappears. The temperature range of T_m is not related to a phase transition. At temperatures much lower than T_m, a large scale overall "freezing" occurs. Further increase in the volume of PNRs is prevented, because ferroelectric coupling between PNRs and surrounding lattices is not sufficiently strong. The resulting phase will have a polar lattice of average cubic structure, but with embedded (rhomohedrally) polarized PNRs.[8] Recently, it has been found that at temperatures around 240 K percolation transition of PNRs occur. Furthermore, PNRs form a fractal in the single crystal. The fractal dimension at low temperatures was estimated[9] to be 2.61. It was suggested that the temperature behavior of PMN could be broadly interpreted in terms of only two temperature scales. A high temperature scale ($T_B \approx 420$ K), which is characterized by the appearance of static polar correlations and the minimum in the soft mode energy, and a lower temperature scale ($T_C \approx 210$ K), where domains form and a long-range ordered ferroelectric phase can be induced through the application of a sufficiently strong electric field.[10]

Although a lot of information has been accumulated about relaxors, their properties are being investigated intensively in order to find out the origin of their unique behavior. It was found that the average size of the CORs in pure PMN is smaller than 5 nm.[11,12] A-site La^{3+} doping can increase the size of the CORs.[13–16] Doping with 2% La^{3+} increases the size of the CORs in the PMN single crystal up to 100 nm.[17] The difference of physical properties of various relaxor ferroelectrics with enhanced B-site cation ordering has been widely studied.[4,5,18–21] After neutron and synchrotron radiation scattering analysis of pure PMN and La^{3+} doped PMN crystals, it was proposed that the PNRs which are in the CORs are static, while those, which are in disordered matrix, are dynamic.[22] The dielectric studies revealed that 2% La^{3+} doped PMN single crystal preserves typical relaxor ferroelectric behavior.[17] Similar conclusion was drawn from subterrahertz relaxation results derived from Brillouin scattering measurements.[23] In comparison with pure PMN, a La^{3+} doped crystal has lower dielectric constant maximum, which is slightly shifted towards lower temperatures.[17,19,24] The Vogel-Fulcher fits for relaxation time,

$\tau(T)$, revealed close values of relaxation parameters for PMN and $Pb(Mg_{1/3}Nb_{2/3})O_3$–$0.02La(Mg_{2/3}Nb_{1/3})O_3$ (PLMN) crystals. Attempt time τ_0 is in the order of 10^{-13} s for both crystals. Activation energy of pure PMN $E_a = (0.07 \pm 0.005)$ eV, PLMN $E_a = (0.093 \pm 0.008)$ eV. Freezing temperature of PMN $T_{VF} = (213 \pm 2)$ K, PLMN $T_{VF} = (192 \pm 8)$ K.[17,25] However, the dielectric response of PLMN has been studied only at comparatively low frequencies up to 1 MHz. With these data, the behavior of relaxation time and other parameters of relaxation spectrum can be determined only at comparatively low temperatures, where PNRs are comparatively large. To analyze the response of PNRs at early stages of their development, the high-frequency dielectric data are needed. The aim of this work is to study the differences of dielectric properties of pure PMN and 2% La^{3+} doped PMN single crystals in the wide frequency range.

Single crystals of PMN and PLMN were grown from high-temperature solution by the top-seeded solution growth method as described in Ref. 17. Dielectric measurements were performed in 120–500 K temperature range. Three different methods for different frequency ranges were used. In the range from 20 Hz to 1 MHz, measurements were performed using a HP-4284A impedance analyzer. The crystal sample of direction (100) with silver paste contacts was mounted in a capacitor inside the cryostat and the capacity and loss tangent were measured. For temperature measurement the Pt100 RTD was used. In frequency range from 1 MHz to 1.6 GHz dielectric measurements were performed with the vector analyzer Agilent 8714ET. The same crystallographic direction crystal sample with silver paste contacts was mounted on the end of coaxial line, acting as a capacitive load. Then the complex reflectance was measured. In order to avoid the inhomogeneity of electromagnetic field inside the sample, specifically sized samples were used in specific ranges of frequency, dividing the measurement procedure into three separate intervals: 1 MHz–400 MHz, 400 MHz–1 GHz, and >1 GHz, respectively. For temperature measurement, the type T thermocouple was used.

For dielectric measurements at higher frequencies two sets of waveguides were used. The rod-like sample was mounted into a special frame, so that it was parallel to the electric field and located in the center of the cross-section of the waveguide, where the intensity of the electric field is the highest. For temperature measurement the type T thermocouple was used, as well. Readings of temperature were performed using Keithley multimeter.

The temperature dependences of complex dielectric permittivity $\varepsilon^*(T)$ of PMN and PLMN single crystals are shown in Fig. 1 for selected frequencies. Both dependences demonstrate typical behavior of relaxor ferroelectrics, i.e., the peak of the real part of the permittivity (ε') decreases and shifts towards higher temperatures with the increase of frequency. An obvious difference between both crystals is the twice smaller peak of $\varepsilon'(T)$ in the PLMN crystal, which is ≈13 000 at the frequency of 129 Hz while for PMN it is ≈26 000 at the same frequency. The $\varepsilon'(T)$ peak of PLMN is not only lower in magnitude but also resides at 17 K lower temperature, i.e., at 129 Hz $T_m = 250$ K in PLMN and $T_m = 267$ K in PMN. At $T < 220$ K the dielectric loss, $\varepsilon''(T)$, of both crystals decreases monotonically and becomes almost frequency-

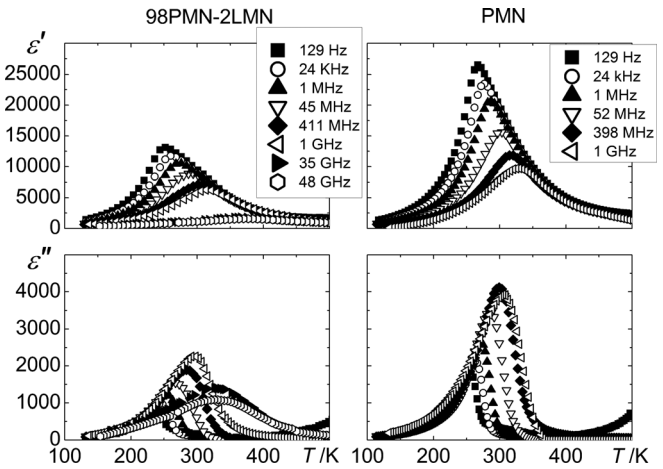

FIG. 1. Temperature dependences of complex dielectric permittivity of the PMN and PLMN crystals.

independent, while at $T > 400$ K the loss increases (this can be most clearly seen at 129 Hz frequency). This increase and related dispersion of ε' can be tentatively related to the contribution of mobile charge carriers[25] and/or Maxwell-Wagner polarization. The temperature region where this process is clearly visible is too narrow to make a more detailed analysis of this phenomenon.

The frequency dependences of complex dielectric permittivity $\varepsilon^*(f)$ are shown in Fig. 2 for PMN and PLMN crystals for selected temperatures. Both dependences display the narrowing of dispersion with the increase of temperature. An attempt was made to fit the data to Cole–Cole relation

$$\varepsilon^*(\omega) = \varepsilon_\infty + \frac{\Delta\varepsilon}{1 + (i\omega\tau)^{1-\alpha}}. \quad (1)$$

The fitting curves in the temperature range of 270 K–340 K are shown as lines in Fig. 2. As we can see, the Cole–Cole relation is a reasonably good approximation at least in the frequency region of dipolar relaxation.

The temperature dependences of the best-fit Cole–Cole parameters are shown in Fig. 3. The parameter $\alpha(T)$, which characterizes the width of distribution of relaxation times, behaves very similarly for both single crystals, i.e., decreases

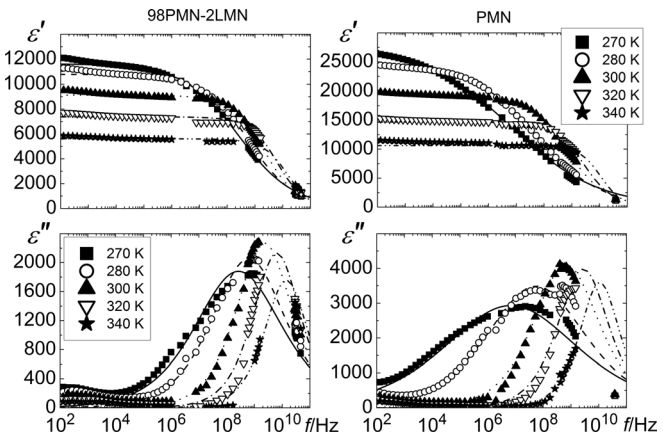

FIG. 2. Frequency dependences of complex dielectric permittivity of the PMN and PLMN crystals. Lines show Cole–Cole fits.

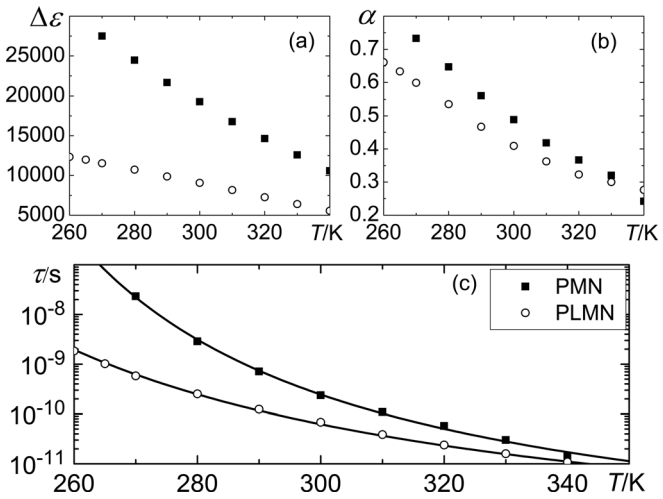

FIG. 3. Temperature dependences of Cole–Cole parameters (a) $\Delta\varepsilon$, (b) α, (c) τ of the PMN and PLMN crystals. In (c) lines show the Vogel–Fulcher fits.

monotonously with the increase of temperature. The same behavior is observed for relaxation strength $\Delta\varepsilon(T)$ that is the difference between static dielectric permittivity and the permittivity at infinitely high frequency (which generally changes with temperature). This temperature behavior of relaxation strength is associated with the shift of T_m and the narrowing of $\varepsilon^*(f)$ dispersion with increasing temperature.

Temperature dependences of mean relaxation time (τ) are shown in Fig. 3(c). For both crystals, $\tau(T)$ grows with the decrease of temperature in the whole temperature range of 260 K–350 K available for the analysis. This behavior can be interpreted as slowing down of the dipolar dynamics of the system. The $\tau(T)$ dependences were fitted to the Vogel-Fulcher relation characteristic of relaxors

$$\tau = \tau_0 \exp\left(\frac{E_a}{k_B(T - T_{VF})}\right). \quad (2)$$

The obtained parameter values are presented in Table I. It reveals clear differences between temperatures T_{VF} of critical slowing down of dipolar dynamics (214 K for PMN and 180 K for PLMN, respectively). The similarity of activation energy, E_a, and attempt time, τ_0, suggests that the origin of the PNRs dynamics in both crystals is the same. The relaxation parameters of PLMN obtained in this work are close to the values published earlier based on the analysis of low-frequency/low-temperature part of the spectrum.[17] Slight differences can be related to the difference in La^{3+} concentration, which is hardly controlled during crystal growth procedure.

The data of our dielectric measurements of pure PMN crystals were obtained in the frequency range of 100 Hz up to 1.6 GHz and few data points at 37 GHz–39 GHz were obtained besides. Our results are comparable with the previously reported dielectric spectra of PMN crystal obtained in an extremely broad band of frequencies.[26,27] Namely, previously reported $E_a \approx 0.069$ eV and $T_{VF} \approx 200$ K are a good match to the values obtained in this work (Table I).

TABLE I. Vogel–Fulcher parameters of the PMN and PLMN crystals.

Crystal	τ_0/s	E_a/eV	T_{VF}/K
PMN	5.9×10^{-14}	0.061 ± 0.009	214 ± 6
PLMN	6.3×10^{-14}	0.071 ± 0.007	180 ± 4

To obtain a better description of relaxation processes in these materials, distributions of relaxation times were calculated by adopting Tikhonov regularization method.[28,29] The obtained distributions are shown in Fig. 4(a) for PLMN and (b) for PMN. The distributions of relaxation times of both crystals demonstrate similar behavior, i.e., they broaden with the decrease of temperature, which is consistent with the expanding of the $\varepsilon^*(f)$ dispersion. In closer examination, one can notice that at all temperatures the edge of the distribution corresponding to the shortest relaxation time is located around 10^{-13} s and remains almost unchanged. With the decrease of temperature, the distribution broadens only because of the increase in the longest relaxation time. The peak value of the distribution shifts towards longer times as well, i.e., mean relaxation time increases with the decrease of temperature, but not so rapidly. Besides the main maximum, additional anomalies appear in the low-frequency part of the spectrum at temperatures lower than about 300 K, both in PMN and PLMN. These anomalies suggest the development at low temperatures of additional relaxation processes which have not been resolved based on the analysis of $\varepsilon^*(f)$ spectra. Such a behavior may signify that at comparatively low temperatures the PNRs with slower dynamics appear, and an increase in the amount of PNRs with slower dynamics causes an increase in the distribution function at higher time values. The edge of the distribution at the time value of 10^{-13} s remains intact, showing that a certain amount of relaxators with fast dynamics remains at low temperatures.

The distribution of relaxation times of PMN crystal has also been obtained in another research[30] with few differences. Namely, in this work the maxima of $\varepsilon''(f)$ are slightly shifted towards higher frequencies. We believe this is because the previously measured crystal was grown using different method, i.e., flux technique.[31] Besides, in this work the range of calculations of relaxation times distribution was chosen just a little wider than the experimental results cover, leaving minimum range for extrapolation.

Earlier X-ray and electron diffraction studies of PLMN crystal investigated here showed that the doping with La^{3+}

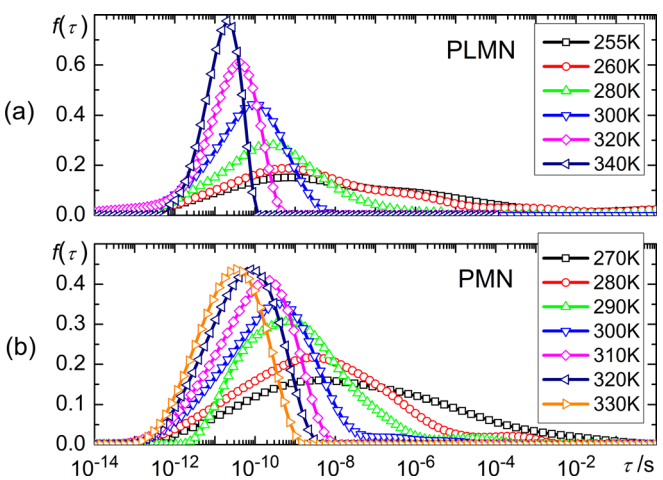

FIG. 4. Distribution of relaxation times of (a) PLMN and (b) PMN crystals.

increases the size of chemically ordered regions.[17] As a result, we observed a twice smaller peak of $\varepsilon'(T)$ in PLMN showing that the amount of dynamic PNRs is smaller than in PMN. Besides, the T_{VF} in PLMN is lower and the peak of $\varepsilon'(T)$ is observed at slightly lower temperature, too. Nevertheless, the distribution of relaxation times in both crystals demonstrates similar behavior, which is consistent with the concept that the PNRs are growing and freezing with the decrease of temperature and percolate at some point.

Therefore, the relaxation behaviour of PMN and PLMN is qualitatively the same in spite of the fact that chemical ordering is very different. Note that in perovskite relaxors with the $Pb(B'_{1/2}B''_{1/2})O_3$ structure in which the number of orderable cations, B′ and B″, is the same, and complete translational symmetry is possible in the ordered state, the chemical ordering leads to vanishing of relaxor behavior and emergence of a macroscopic ferroelectric or antiferroelectric phase transition.[4,32,33] In PMN and other known $Pb(B'_{1/3}B''_{2/3})O_3$ perovskite relaxors, another type of chemical ordering is observed inside CORs, as discussed in the introduction. This ordering cannot lead to complete translational symmetry and does not influence significantly the relaxor behavior. This was shown previously in Refs. 17 and 34 for the low-frequency (1 Hz–1 MHz) part of the dielectric spectrum and for subterrahertz relaxation derived from Brillouin scattering[23] and confirmed in this work for intermediate frequencies.

In this work, the dielectric properties of PMN and PLMN crystals were measured and compared. Being combined with the results of previous works,[17,23,34] our results show unambiguously that the relaxation dynamics, and therefore, the dipolar nanostructure are not influenced significantly by the size of chemically ordered regions. This experimental result is in sharp contrast with the conclusions of some theoretical models[4,35] which suggest a close relation between the scale of CORs and the relaxor behavior in PMN and other relaxors.

The work was supported by the Natural Science and Engineering Council of Canada (NSERC), the United State Office of Naval Research (ONR Grant No. N00014-12-1-1045) and the European Social Fund under the Global Grant measure (Project No. VP1-3.1-SMM-07-K-03-011).

[1]A. A. Bokov and Z.-G. Ye, J. Mater. Sci. **41**, 31 (2006).
[2]N. de Mathan, E. Husson, G. Calvarn, J. R. Gavarri, A. W. Hewat, and A. Morell, J. Phys. Condens. Matter **3**, 8159 (1991).
[3]Z. Xu, M.-C. Kim, J.-F. Li, and D. Viehland, Philos. Mag. A **74**, 395 (1996).
[4]C. A. Randall, A. S. Bhalla, T. R. Shrout, and L. E. Cross, J. Mater. Res. **5**, 829 (1990).
[5]M. A. Akbas and P. K. Davies, J. Am. Ceram. Soc. **80**, 2933 (1997).
[6]Z. Xu, S. M. Gupta, D. Viehland, Y. Yan, and S. J. Pennycook, J. Am. Ceram. Soc. **83**, 181 (2000).
[7]J. Chen, H. M. Chan, and M. P. Harmer, J. Am. Ceram. Soc. **72**, 593 (1989).
[8]G. Xu, G. Shirane, J. R. D. Copley, and P. M. Gehring, Phys. Rev. B **69**, 064112 (2004).
[9]A. Koreeda, H. Taniguchi, S. Saikan, and M. Itoh, Phys. Rev. Lett. **109**, 197601 (2012).
[10]C. Stock, P. M. Gehring, H. Hiraka, I. Swainson, G. Xu, Z.-G. Ye, H. Luo, J.-F. Li, and D. Viehland, Phys. Rev. B **86**, 104108 (2012).
[11]A. D. Hilton, D. J. Barber, C. A. Randall, and T. R. Shrout, J. Mater. Sci. **25**, 3461 (1990).
[12]M. A. Akbas and P. K. Davies, J. Am. Ceram. Soc. **83**, 119 (2000).
[13]S. Miao, J. Zhu, X. W. Zhang, and X. H. Chen, J. Mater. Res. **17**, 2615 (2002).
[14]F. Jiang, S. Kojima, C. Zhao, and C. Feng, Appl. Phys. Lett. **79**, 3938 (2001).
[15]S. Miao, X. Zhang, and J. Zhu, J. Am. Ceram. Soc. **84**, 2091 (2001).
[16]K.-M. Lee, H. M. Jang, and W.-J. Park, J. Mater. Res. **12**, 1603 (1997).
[17]X. Long, A. A. Bokov, Z.-G. Ye, W. Qu, and X. Tan, J. Phys. Condens. Matter **20**, 015210 (2008).
[18]W. Qu, X. Zhao, and X. Tan, Appl. Phys. Lett. **89**, 022904 (2006).
[19]X. Zhao, W. Qu, H. He, N. Vittayakorn, and X. Tan, J. Am. Ceram. Soc. **89**, 202 (2006).
[20]S. Kamba, D. Nuzhnyy, S. Veljko, V. Bovtun, J. Petzelt, Y. L. Wang, N. Setter, J. Levoska, M. Tyunina, J. Macutkevic, and J. Banys, J. Appl. Phys. **102**, 074106 (2007).
[21]F. Chu, N. Setter, and A. K. Tagantsev, J. Appl. Phys. **74**, 5129 (1993).
[22]S. Vakhrushev, in *Proceedings of Abstracts of the 11th European Meeting on Ferroelectricity*, Bled, Slovenia, September (2007), p. 219.
[23]J.-H. Ko, T. H. Kim, S. Kojima, X. Long, A. A. Bokov, and Z.-G. Ye, J. Appl. Phys. **107**, 054108 (2010).
[24]D. M. Fanning, I. K. Robinson, S. T. Jung, E. V. Colla, D. D. Viehland, and D. A. Payne, J. Appl. Phys. **87**, 840 (2000).
[25]A. A. Bokov and Z.-G. Ye, Phys. Rev. B **74**, 132102 (2006).
[26]V. Bovtun, S. Veljko, S. Kamba, J. Petzelt, S. Vakhrushev, Y. Yakymenko, K. Brinkman, and N. Setter, J. Eur. Ceram. Soc. **26**, 2867 (2006).
[27]S. Kamba, M. Kempa, V. Bovtun, J. Petzelt, K. Brinkman, and N. Setter, J. Phys. Condens. Matter **17**, 3965 (2005).
[28]A. Kajokas, A. Matulis, J. Banys, R. Mizaras, A. Brilingas, and J. Grigas, Ferroelectrics **257**, 69 (2001).
[29]J. Macutkevic, J. Banys, and A. Matulis, Nonlinear Anal. Modell. Control **9**, 75 (2004), available at: http://www.mii.lt/na/issues/NA_0901/NA09105.pdf.
[30]R. Grigalaitis, J. Banys, A. Kania, and A. Slodczyk, J. Phys. IV **128**, 127 (2005).
[31]A. Kania, A. Słodczyk, and Z. Ujma, J. Cryst. Growth **289**, 134 (2006).
[32]N. Setter and L. E. Cross, J. Appl. Phys. **51**, 4356 (1980).
[33]A. A. Bokov, I. P. Raevskii, and V. G. Smotrakov, Fiz. Tverd. Tela **26**, 2824 (1984), available at http://www.researchgate.net/publication/280611714 [Sov. Phys. Solid State **26**, 1708 (1984)].
[34]A. A. Bokov, B. J. Rodriguez, X. Zhao, J.-H. Ko, S. Jesse, X. Long, W. Qu, T. H. Kim, J. D. Budai, A. N. Morozovska, S. Kojima, X. Tan, S. V. Kalinin, and Z.-G. Ye, Z. Kristallogr. **226**, 99 (2011).
[35]S. Tinte, B. P. Burton, E. Cockayne, and U. V. Waghmare, Phys. Rev. Lett. **97**, 137601 (2006).

We encourage you to:

- Share your work (https://authorservices.taylorandfrancis.com/sharing-your-work/)Make printed copies of your article to use for lecture or classroom purposes.
- Include your article in a thesis or dissertation.
- Present your article at a meeting or conference and distribute printed copies of the article.
- Republish the article (making sure you cite the original article).
- Adapt and expand your published journal article to make it suitable for your thesis or dissertation.

Alternatively, any author publishing with us can opt to retain their own copyright and sign a licence to publish.

Useful definitions

()Version of Record (VoR)
"A fixed version of a journal article that has been made available by … a publisher by formally and exclusively declaring the article 'published.'

This includes any 'early release' article that is formally identified as being published even before the compilation of a volume issue and assignment of associated metadata, as long as it is citable via some permanent identifier(s).

This does not include any 'early release' article that has not yet been 'fixed' by processes that are still to be applied, such as copy-editing, proof corrections, layout, and typesetting."

(Defined by National Information Standards Organization (http://www.niso.org/publications/rp/RP-8-2008.pdf), in partnership with the Association of Learned and Professional Society Publishers.)

Useful links

- Creative Commons licences (https://creativecommons.org/licenses/)
- UK Intellectual Property Office's What is copyright? (https://www.gov.uk/government/organisations/intellectual-property-office) guide
- US Government's Copyright Office guide to copyright (http://www.copyright.gov/)
- World Intellectual Property Organization guide to copyright (http://www.wipo.int/cgi-bin/koha/opac-detail.pl?bib=14057)

Publishing agreements: your options » (https://authorservices.taylorandfrancis.com/publis agreements-your-options/)

FERROELECTRICS
2017, VOL. 513, 32–37
https://doi.org/10.1080/00150193.2017.1350071

Taylor & Francis
Taylor & Francis Group

Implementation of an improved non-linear susceptometer

D. Jablonskas, M. Ivanov, R. Grigalaitis, and J. Banys

Vilnius University, Faculty of Physics, Vilnius, Lithuania

ABSTRACT

Non-linear susceptibility measurements of ferroelectrics and related materials allows to unambiguously recognize the type of the phase transition. Although, such devices are not available commercially. We present here a non-linear susceptomer with few improvements, that allow to expand the frequency range of measurement to higher frequencies. Namely, this susceptometer is implemented with phase shift calibration procedure. Improvements described here may allow measurements with fundamental frequency as high as 1/10 of the sampling frequency.

ARTICLE HISTORY
Received 19 June 2016
Accepted 27 March 2017

Introduction

The relationship between polarization P and external electric field E, is well known:

$$P = \varepsilon_0 \chi_1 E, \tag{1}$$

where ε_0 – electric permittivity of the free space and χ_1 – the linear electric susceptibility of a dielectric material. Such relationship is valid, if condition of small external electric field applies. In experiments, where large electric field is introduced, the $P(E)$ relationship is no longer linear and higher order susceptibilities have to be taken into account:

$$P = \varepsilon_0 \left(\chi_1 E + \chi_2 E^2 + \chi_3 E^3 + \ldots\right), \tag{2}$$

here χ_i – are non-linear susceptibilities (where i – positive integers). These non-linear components show the non-linear contribution to the polarization [1]. The measurements of the non-linear dielectric susceptibility of polar dielectrics give useful information on phase transitions [2]. Namely, it is possible to unambiguously recognize the type of the phase transition. Ferroelectric systems, which display continuous or second order phase transition, have negative third order susceptibility (χ_3) in paraelectric state and, with decrease of temperature, χ_3 changes sign to positive at the temperature of the phase transition. In case of a discontinuous phase transition or a first order transition the sign of χ_3 is positive and remains unchanged throughout the vicinity of temperature of the phase transition. So is explained by the theory of Landau-Ginzburg-Devonshire [3, 4] and was proved by measurements of Triglycine Sulfate and Barium Titanate [5]. As well, it

CONTACT D. Jablonskas dziugas.jablonskas@ff.vu.lt Vilnius University, Faculty of Physics, Sauletekio av. 9/IIIb, LT-10222 Vilnius, Lithuania.

proves to be a useful tool to investigate essential differences between relaxor ferroelectrics and dipolar glasses [6–8]. A good example are works on PMN [9, 10], that helped to derive a more general model than Spherical Random Bond Random Field model [6] for behavior of relaxor ferroelectrics [11]. This model, the Compressible Spherical Dipolar Glass, takes into account the electrical polarization and the fluctuations of the strain tensor.

The usefulness of measurements of non-linear susceptibility in characterizing phase transitions of polar dielectrics is clear. There are a few methods developed, which allow to perform the measurements of non-linear susceptibility [12–15], but none of them are available commercially. Thus we present one, which we implemented ourselves.

Susceptometer

The concept of our susceptometer is based on equipment presented by S. Miga, et al. [14]. Our system consists of (Fig. 1): Data Translations DT9834 Data Acquisition Module, Stanford Research Systems SR570 Low Noise Current Preamplifier with controllable sensitivity, Computer, Sample Cell. DT9834 module is used to generate zero biased alternating voltage signal with amplitude, which allows to observe nonlinear response of the sample under test, but is rather small in comparison with coercive field of material of the sample. The signal drives the sample within the sample cell. The current of the sample response is converted to voltage by SR570 current preamplifier. And the Analog In channel of DT9834 module is used to gather the measurement data. As well, a separate Analog In channel is used to gather the data of the reference signal which drives the load (sample inside the cell/cryostat). Computer is used to control sensitivity of SR570 and to perform calculations with the data gathered with DT9834. Our equipment allows us to perform measurements of samples with capacitances in range of 10 pF up to 10 nF. Estimated frequency range of excitation signal is 8 Hz – 10 kHz. The maximum amplitude of the alternating signal is ± 10 V. As the sample is put in separate cryostat, it is possible to perform measurements in wide temperature range 100 K – 500 K. We are able to achieve Signal to Noise Ratio (SNR) of 100 dB (10^5).

Data extraction

The displacement current of the sample response is complex and contains phase shift in respect of the reference signal. This data is used to calculate complex linear and

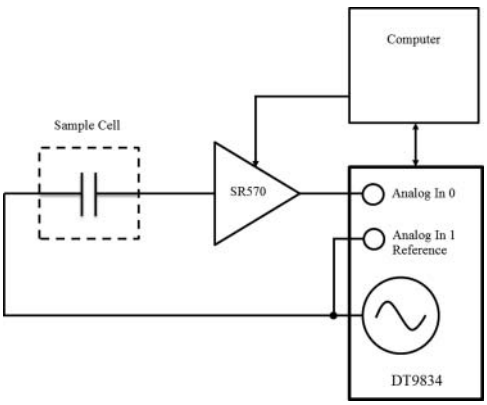

Figure 1. Block diagram of non-linear susceptibility measuring system.

non-linear susceptibilities, as explained in [14]. Here, couple of things should be considered: 1) DT9834 Analog In channels does not gather data exactly simultaneously, which is unavoidable, because the device uses semiconductor processor, which does not support real time parallel operations, thus there is an intrinsic delay between any two operations and that results in phase shift between measurement signal and reference signal gathered with separate Analog In channels; 2) SR570 has limited amplification band, i.e. the amplifier response is flat up to certain frequency. Furthermore with increase of frequency the phase shift increases. The amplification frequency band is limited by RC circuit. The frequency response of it is shown in Fig. 2. As well, the device has different sensitivities with different threshold frequencies. In order to acquire correct data at higher frequencies the phase shift caused by the equipment has to be taken into account. For this reason we perform phase calibration. The phase distortions of the system is gathered by measuring calibration capacitors. We use Solartron 12961 dielectric reference module, which contains four calibrated linear capacitors of 9.31 pF, 102 pF, 0.999 nF, 10.04 nF capacitances. As well, the calibration signal is of specific shape, it is described by [3]:

$$S(f) = \sum_{i=1}^{5} \frac{1}{i} \cos(2\pi i f t + \phi_i). \tag{3}$$

It consist of five harmonics, each harmonic has amplitude lowered by a number of harmonic in respect of the first harmonic. This is because the derivative of such signal would have equal amplitudes at every harmonic. And indeed, if we drive the calibration load, which is capacitive, with our voltage calibration signal, the resultant current will have the shape of a derivative of the original voltage signal. Furthermore, the phase of each harmonic is chosen such, that the peak/rms ratios of the signal and its derivative would be minimum. This helps to have the dynamic range of the signal symmetric in respect of 0. The comparison between signal, which have zero phases of each harmonic, and our specific signal is shown in Figures 3 and 4. The phase of each harmonic of the calibration signal: $\varphi_1 \approx 0.412$, $\varphi_2 \approx 3.443$, $\varphi_3 \approx 2.859$, $\varphi_4 \approx 3.602$, $\varphi_5 \approx 2.922$

It is important to notice that the amplitudes of higher harmonics of non-linear response of the sample are quite low and sensitive to noise. The noise level of the system is rather low, but additionally to obtain even better SNR the sample response averaging algorithm is

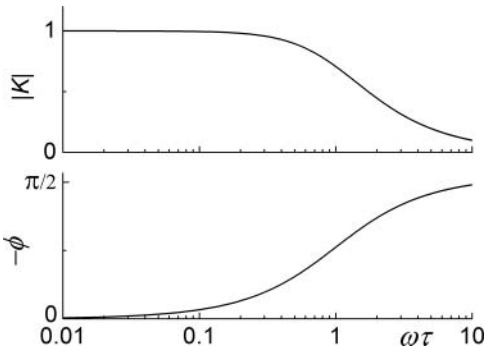

Figure 2. Frequency response of low-pass RC filter.

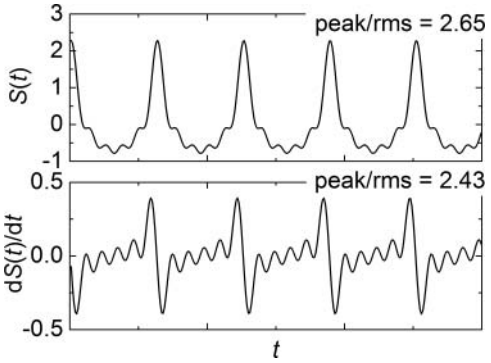

Figure 3. Shape of signal of sum of five harmonics and its derivative, where phases of each harmonic are equal.

implemented. Thanks to it, we are able to obtain signal to noise ratio up to 100 dB. Furthermore, it is worth to mention, that our excitation signal, as any digitally created signal tends to have quantization noise, which distorts the amplitude of the signal. Although, our voltage signal is rather linear (DT9834 uses 16bit DACs and 500 kHz sampling frequency), but the small quantized steps in voltage signal, may give rather large peaks in current response if capacitive load is driven. In order to prevent this uncontrollable phenomenon we use 1st order analog RC low pass filter, which has threshold frequency of 30 kHz, which is sufficient to prevent effects of quantization noise of 500 kHz sampling frequency. Moreover, to reduce the quantization distortions of generated signal we have implemented dithering. The features mentioned here makes our system capable to measure non-linear susceptibility of polar dielectrics.

Performance

The performance of the susceptometer is exhibited by an experiment performed on $0.4NaBi_{0.5}Ti_{0.5}O_3 - 0.45SrTiO_3 - 0.15PbTiO_3$ (0.4NBT-0.45ST-0.15PT) ceramic sample with silver paste contacts. The sample was heated up to temperature of 460 K. The measurement

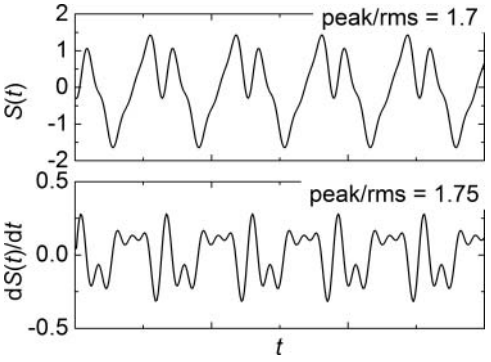

Figure 4. Shape of signal of sum of five harmonics and its derivative, where phases chosen to minimize Peak/RMS ratio of signal and its derivative. The phase of each harmonic: $\varphi_1 \approx 0.412$, $\varphi_2 \approx 3.443$, $\varphi_3 \approx 2.859$, $\varphi_4 \approx 3.602$, $\varphi_5 \approx 2.922$.

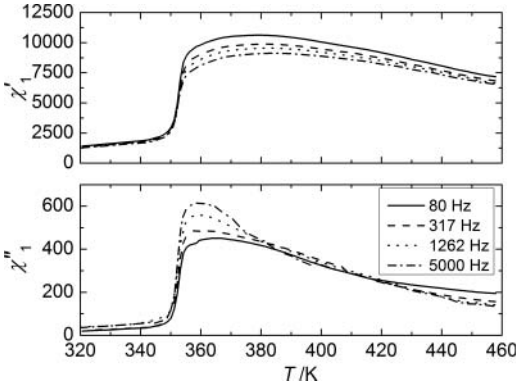

Figure 5. Temperature dependence of 1st order complex susceptibility of 0.4NBT-0.45ST-0.15PT ceramic.

of non-linear susceptibility was performed on cooling cycle down to 320 K. The frequencies of generated signal were 80 Hz, 317 Hz, 1262 Hz and 5000 Hz. The amplitude of alternating electric field was 160 V/cm. The sample was not additionally polarized in constant electric field prior to the measurement.

The results of the measurement are as follows. A temperature dependence of the 1st order complex susceptibility is shown in Fig. 5, where a specific behavior of the compound is revealed. In the temperature range above 360 K it behaves as relaxor ferroelectric. Namely, the maximum of real part of complex susceptibility shifts towards higher temperatures with increase of frequency. In the vicinity of 350 K there is a susceptibility drop, which can be related to a discontinuous phase transition. Figure 6 shows a temperature dependence of the real part of 3rd order of complex susceptibility, which has a positive sign. That is a good indication of occurrence of the first order phase transition. Similar measurements were published by Svirskas et al. [8], only the measurements of non-linear susceptibility presented there are made up to frequency of 1 kHz. Here we have shown, that our susceptometer is capable of measuring non-linear dielectric response in frequencies higher than 1 kHz (5 kHz 1st harmonic in this particular case, which makes frequency of 15 kHz of 3rd harmonic),

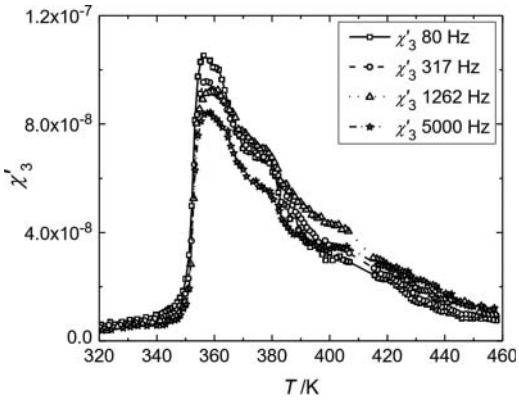

Figure 6. Temperature dependence of real part of 3rd order complex susceptibility of 0.4NBT-0.45ST-0.15PT ceramic.

primarily due to the additional calibration step, where frequency response of the system is evaluated.

Conclusions

In this work we have shown, that a phase shift calibration of the non-linear susceptometer allows to expand the frequency range of the measurement to the higher frequencies. The averaging algorithm helps to improve SNR. Combined with the phase shift calibration and proper filtering of the signals above the Nyquist limit, these improvements may allow measurements with fundamental frequency as high as 1/10 of the sampling frequency.

Acknowledgements

We thank Marija Dunce, Eriks Birks and Marija Antonova for making $0.4NaBi_{0.5}Ti_{0.5}O_3 - 0.45SrTiO_3 - 0.15PbTiO_3$ ceramics

References

1. A. K. Jonscher *Dielectric relaxation in solids*, London, Chelsea Dielectric Press, 1983
2. Y. Ishibashi A phenomenological theory of nonlinear responses. *Ferroelectrics.* **195**(1), 81–6 (1997 May 1).
3. V. L. Ginzburg. On the dielectric properties of ferroelectric (Segnette-electric) crystal and barium titanate. *Zh Exp Theor Phys.* **15**, 739–49 (1945).
4. A. F. Devonshire. Theory of barium titanate. *Part I. Phil Mag.* **40**, 1040–63 (1949).
5. J. Dec, S. Miga, W. Kleemann. Dynamic nonlinear susceptibility in solid dielectrics. In: *2010 10th IEEE International Conference on Solid Dielectrics (ICSD).* 1–5 (2010).
6. R. Pirc, R. Blinc. Spherical random-bond random-field model of relaxor ferroelectrics. *Phys Rev B.* **60**(19), 13470–8 (1999 Nov 15).
7. R. Pirc, B. Tadić, R. Blinc. Nonlinear susceptibility of orientational glasses. *Phys B Condens Matter.* **193**(2), 109–15 (1994 Feb 1).
8. S. Svirskas, M. Ivanov, S. Bagdzevicius, J. Macutkevic, A. Brilingas, J. Banys, et al. Dielectric properties of solid solutions. *Acta Mater.* **64**, 123–32 (2014 Feb).
9. J. Dec, S. Miga, W. Kleemann, B. Dkhil. Nonlinear Dielectric Properties of PMN Relaxor Crystals within Landau-Ginzburg-Devonshire Approximation. *Ferroelectrics.* **363**(1), 141–9 (2008 May 21).
10. Z. Kutnjak, B. Vodopivec, R. Blinc. Anisotropy of electric field freezing of the relaxor ferroelectric Pb(Mg1/3Nb2/3)O3. *Phys Rev B.* **77**(5), 54102 (2008 Feb 8).
11. R. Pirc, Z. Kutnjak, N. Novak. Compressible spherical dipolar glass model of relaxor ferroelectrics. *J Appl Phys.* **112**(11), 114122 (2012 Dec 1).
12. S. Ikeda, H. Kominami, K. Koyama, Y. Wada. Nonlinear dielectric constant and ferroelectric−to−paraelectric phase transition in copolymers of vinylidene fluoride and trifluoroethylene. *J Appl Phys.* **62**(8), 3339–42 (1987 Oct 15).
13. Y. Ishibashi Nonlinear dielectric spectroscopy. *J Korean Phys Soc.* **32**, 407–10 (1998).
14. S. Miga, J. Dec, W. Kleemann. Computer-controlled susceptometer for investigating the linear and nonlinear dielectric response. *Rev Sci Instrum.* **78**(3), 33902 (2007 Mar 1).
15. C. Thibierge, D. L'Hôte, F. Ladieu, R. Tourbot. A method for measuring the nonlinear response in dielectric spectroscopy through third harmonics detection. *Rev Sci Instrum.* **79**(10), 103905 (2008 Oct 1).

Table of Author's Rights

	Preprint version (with a few exceptions- see below *)	Accepted Author Manuscript	Published Journal Articles
Use for classroom teaching by author or author's institution and presentation at a meeting or conference and distributing copies to attendees	Yes	Yes	Yes
Use for internal training by author's company	Yes	Yes	Yes
Distribution to colleagues for their research use	Yes	Yes	Yes
Use in a subsequent compilation of the author's works	Yes	Yes	Yes
Inclusion in a thesis or dissertation	Yes	Yes	Yes
Reuse of portions or extracts from the article in other works	Yes	Yes with full acknowledgement of final article	Yes with full acknowledgement of final article
Preparation of derivative works (other than for commercial purposes)	Yes	Yes with full acknowledgement of final article	Yes with full acknowledgement of final article
Preprint servers	Yes	Yes with the specific written permission of Elsevier	No
Voluntary posting on open web sites operated by author or author's institution for scholarly purposes	Yes (author may later add an appropriate bibliographic citation, indicating subsequent publication by Elsevier and journal title)	Yes, with appropriate bibliographic citation and a link to the article once published	Only with the specific written permission of Elsevier
Mandated deposit or deposit in or posting to subject-oriented or centralized repositories	Yes under specific agreement between Elsevier and the repository	Yes under specific agreement between Elsevier and the repository**	Yes under specific agreement between Elsevier and the repository
Use or posting for commercial gain or to substitute for services provided directly by journal	Only with the specific written permission of Elsevier	Only with the specific written permission of Elsevier	Only with the specific written permission of Elsevier

** Voluntary posting of Accepted Author Manuscripts in the arXiv subject repository is permitted.

Journal of Alloys and Compounds 748 (2018) 127–133

Contents lists available at ScienceDirect

Journal of Alloys and Compounds

journal homepage: http://www.elsevier.com/locate/jalcom

Is there a spontaneous ferroelectric phase transition in $0.83PbMg_{1/3}Nb_{2/3}O_3$-$0.17PbTiO_3$ single crystal?

Š. Svirskas [a, *], D. Jablonskas [a], V. Samulionis [a], S. Kojima [b], J. Banys [a]

[a] Faculty of Physics, Vilnius University, Saulėtekio al. 9/IIIb, LT-10222, Vilnius, Lithuania
[b] Graduate School of Pure and Applied Sciences, University of Tsukuba, Tsukuba, Ibaraki, 305-8573, Japan

ARTICLE INFO

Article history:
Received 15 January 2018
Received in revised form
8 March 2018
Accepted 10 March 2018
Available online 12 March 2018

Keywords:
Relaxors
Phase transitions
PMN
Ferroelectricity
Nonlinear dielectric susceptibility

ABSTRACT

The macroscopic response of $0.83PbMg_{1/3}Nb_{2/3}O_3$-$0.17PbTiO_3$ (PMN-17PT) single crystals has been investigated in order to resolve existing controversy about the structural phase transition in the rhombohedral side of (1-x)$PbMg_{1/3}Nb_{2/3}O_3$-x$PbTiO_3$ phase diagram. The combination of nonlinear dielectric spectroscopy, temperature dependant polarization and strain hysteresis loop measurements and ultrasonic spectroscopy revealed that ferroelectric phase occurs spontaneously in PMN-17PT single crystals. The experimental techniques applied in this work probe the bulk of the sample and can unambigously determine the existence of a spontaneous ferroelectric phase.

The experiments showed that zero-field cooled sample has a normal ferroelectric hysteresis loop at room temperature. The electric-field dependence of induced polarization revealed that at a certain electric field the sample undergoes transformation from polydomain to monodomain-like states. The 1 s t order phase transition at 330 K was evidenced by the third order nonlinear dielectric susceptibility for monodomain sample. The nonlinear dielectric response of an unpoled sample does not show such abrupt jump and is more similar to the response of canonical relaxor $PbMg_{1/3}Nb_{2/3}O_3$.

Zero-field heating and zero-field cooling experiments also revealed very slow domain formation processes appearing at 300–320 K temperature. They are affected by the experimental conditions. There are evidences that on cooling the domains tend to grow in the sample.

1. Introduction

Lead magnesium niobate-lead titanate, (1-x)$PbMg_{1/3}Nb_{2/3}O_3$-x$PbTiO_3$ (PMN-xPT), is a solid solution system where one of the end members of phase diagram is relaxor ferroelectric and the other – normal ferroelectric. These compounds have a B-site charge disorder in the perovskite lattice. The charge disorder promotes the random fields which are the cornerstone of the relaxor phenomenon [1,2]. The strength of random fields can be altered by chemical substitution of ions in the perovskite lattice. In the case of PMN-xPT, the increase of PT concentration suppose to decrease the strength of random fields. This is due to the fact that titanium ion has a valence of 4+ and is electrostatically compatible in the $A^{2+}B^{4+}O_3$ perovskite lattice. This manifests as a crossover from relaxor to a classical ferroelectric [3,4] behaviour in the phase diagram of PMN-xPT. This crossover and its peculiarities makes the PMN-xPT one of the most intriguing phase diagrams in the solid state physics.

The most important feature of relaxor-ferroelectric solid solutions is the occurrence of the so called morphotropic phase boundary (MPB) in the phase diagram. The MPB is the boundary in a composition-temperature diagram where the crystal structure changes abruptly [5]. In the case of lead-based relaxor-ferroelectric solid solutions, the MPB is between rhombohedral (pseudocubic) and tetragonal symmetry [6]. There are a lot of discussions in the literature about the structural features of MPB region in PMN-xPT system. Firstly, it was considered that the MPB distinguishes rhombohedral and tetragonal phases and that the material undergoes two consequent phase transitions: from cubic to tetragonal and from tetragonal to rhombohedral phase [6]. Later on it was established that there is an intermediate monoclinic phase around the MPB [3]. The intermediate phase was found in other relaxor-ferroelectric solid solutions like PZN-xPT [8] as well.

The primary interest of MPB is closely related to the superior electromechanical and dielectric properties of these compositions.

* Corresponding author.
E-mail addresses: sarunas.svirskas@ff.vu.lt (Š. Svirskas), dziugas.jablonskas@ff.vu.lt (D. Jablonskas), vytautas.samulionis@ff.vu.lt (V. Samulionis), kojima@ims.tsukuba.ac.jp (S. Kojima), juras.banys@ff.vu.lt (J. Banys).

https://doi.org/10.1016/j.jallcom.2018.03.130
0925-8388/

Thus the compositions in the vicinity of the MPB are the main focus of the investigation. The various data on MPB compositions of PMN-xPT such as dielectric [9], ferroelectric [10], structural [3,11] can be found in the literature. The rhombohedral side of the phase diagram in PMN-xPT is less thoroughly studied. The knowledge about these compositions is important in order to understand the perovskite oxides with intermediary strength of random fields. The unique feature of this region is that from a certain value of PT concentration a spontaneous ferroelectric-to-relaxor phase transition should occur in the system. The most controversial question is the mechanism of this crossover from relaxor to ferroelectric phase. The value where a rhombohedral phase appears is not well determined and there are many debates in the literature which needs to be addressed. Lead magnesium niobate (PMN) is macroscopically cubic down to the low temperatures [12]. There are many evidences that the addition of lead titanate to PMN leads to enhancement of rhombohedral phase which should persist up to the MPB concentrations. The high resolution synchrotron x-ray diffraction experiments by Ye et al. showed that the rhombohedral phase appears in PMN-xPT for concentrations as low as 5 mol. % [4]. Neutron diffraction experiments, on the other hand, could not detect the macroscopic rhombohedral structure for a composition $x = 0.2$ down to 50 K [13]. There are further discrepancies concerning composition $x = 0.1$. X-ray diffraction showed the appearance of a ferroelectric phase [14], while neutron data revealed that the rhombohedral phase appears only at the surface of the sample [15]. Xu et al. suggested that the phase which is observed at $x < 20\%$ is not rhombohedral. There are even experiments showing that the compositions well below the MPB exhibit the monoclinic structure [16].

There are a lot of research devoted to the lattice dynamics of relaxor ferroelectrics. The canonical relaxors does not show a classical ferroelectric soft mode. The broad dielectric dispersion is due to the central mode which expands 15 orders of magnitude in frequencies [17,18]. This relaxation exhibits a glassy freezing phenomenon on cooling [19–21]. Such freezing can be observed in the broadband dielectric spectroscopy experiments. Some characteristic relaxation time undergoes slowing down and diverges at the freezing temperature T_f. The dielectric spectrum below the freezing temperature becomes infinitely broad. This is so called constant loss regime (dielectric loss is independent of frequency) [17,22]. Relaxors and dipolar glassess share the freezing phenomenon but the relaxational dynamics in the relaxors are much more complicated [23,24].

Earlier investigations of PMN-17PT single crystal (the middle composition between the PMN and MPB of PMN-xPT) showed that the mean relaxation time obtained by the broadband dielectric spectroscopy [25] undergoes critical slowing down. This resembles an order-disorder phase transition. The critical slowing down of a central peak was also observed by the inelastic light scattering experiments [26,27]. It is worth noting that inelastic light scattering experiments favours the existence of phase transition in some lower content compositions (i. e. PMN-10PT [28,29] and PMN-17PT [27]).

In this work we present our investigation on dielectric nonlinearities, polarization/strain hysteresis loops and ultrasonic properties of PMN-17PT. These experiments allow us to probe the macroscopic response of PMN-17PT single crystal and obtain the information from the bulk of the crystal. It should identify the ferroelectric phase transition (especially polarization switching experiments which are mandatory property for ferroelectrics [30]) unambigously.

2. Experimental

$0.83Pb(Mg_{1/3}Nb_{2/3})O_3$-$0.17PbTiO_3$ (PMN-17PT) single crystals were grown by a modified Bridgeman technique [31]. The pseudocubic [001] plate was used for the measurements. The same single crystal was also used in our previous dielectric spectroscopy studies [25].

The linear and third order nonlinear susceptibilities were measured simultaneously with custom made susceptometer according to the methodology reported by Miga et al. [32]. We used our improved version susceptometer [33]. Our system consists of Data Translations DT9834 data acquisition module, Standford Research SR570 low noise current amplifier and computer. Temperature measurements performed using 4 W-RTD PT100 temperature sensor connected to Keithley Integra 2700 multimeter. Sample with painted silver electrodes was used. The measurement was performed in a 120 V/cm alternating electric field. Such strength of electric field is well below coercive field strength, but it is enough to observe the non-linear response. Experiments were performed in 200 K–450 K temperature range and in 133 Hz, 270 Hz and 1 kHz frequencies.

Ferroelectric and strain hysteresis loops were measured with aixaCCT TF2000 analyzer. The measurements of displacement and polarization were carried out simultaneously by applying 10 Hz triangular wave pulses. The displacement was measurement with a help of a single beam interferometer. Unipolar triangular pulses were used for the measurement of displacement and polarization in order to determine the piezoelectric and electrostrictive coefficients.

The pyroelectric measurements were performed both on poled and unpoled samples. First the sample was heated up to 500 K and after it was cooled down to the lowest temperature the pyrocurrent was measured either on poled or unpoled sample. The heating rate was 10 K/min. The pyrocurrent was measured with the same aixaCCT TF2000 system. The temperature dependences of polarization was obtained by integrating the pyrocurrent [34].

The time of flight ultrasonic technique was used to measure longitudinal ultrasonic velocity at 10 MHz frequency. The custom made system with a z-cut $LiNbO_3$ transducers as a transmitter and receiver of ultrasonic waves were used. The wavevector of the ultrasonic wave was parallel to the [001] direction during the experiments. The sample was placed between two aluminum buffers. The temperature was measured with Keithley Integra 2700 multimeter. The T-type thermocouple was used as a sensor. The detailed description of the time of flight experimental configuration can be found in Ref. [35].

3. Results and discussion

3.1. Nonlinear dielectric susceptibility

Fig. 1 represents the temperature dependences of linear and third order nonlinear susceptibilities. The linear dielectric data is consistent with the previously published one for this crystal [25]. The temperature evolution of the susceptibilities possess similar features as a relaxor ferroelectric lead magnessium niobate [36,37]. The third order susceptibility is positive as is in the most relaxor ferroelectrics. The only difference is that the susceptibility does not exhibit well pronounced shift of permittivity maximum at different frequencies. Broadband dielectric spectroscopy revealed that the shift occurs only at microwave frequencies in PMN-17PT [25]. The 3rd order dielectric susceptibility is sensitive to the order of the phase transition. 1st and 2nd order ferroelectric phase transitions have a very distinct response [36,37]. The 1st order phase transition manifests as an abrupt jump in χ_3 (refer to the results of barium titanate [38] as an example of 1st order phase transition). The 1st order phase transition was evidenced from the third order nonlinear dielectric susceptibility in a relaxor ferroelectric PZN-8PT [39] (in this case the structural phase

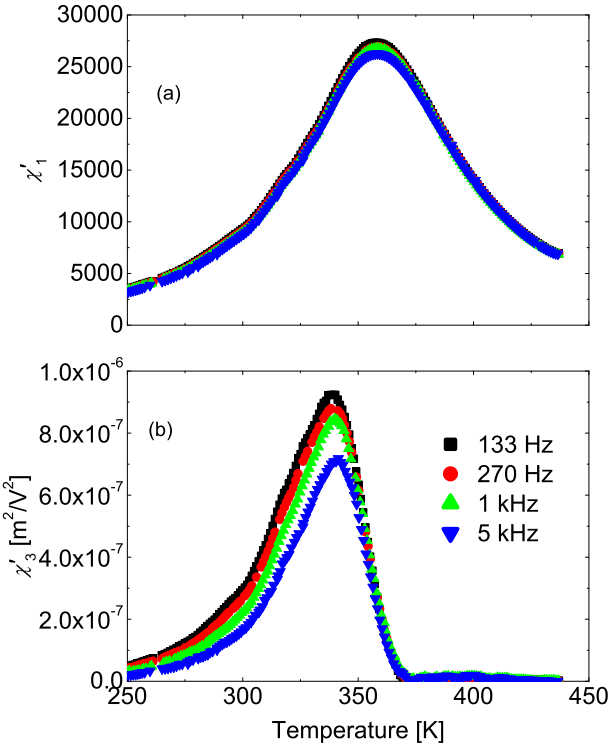

Fig. 1. Temperature dependence of the first order dielectric susceptibility (a) and the third order dielectric susceptibility (b).

transition was clarified by the powder neutron diffraction experiments as well [40]). It is evident from the Fig. 1 that such kind of jump is not observed in our case. Nonlinear susceptibility does not show spontaneous 1st order phase transition and supports the data obtained by the neutron scattering experiments. It seems that the polar nano regions (PNRs) are responsible for the dielectric anomaly. Although Kutnjak et al. reported the temperature-field-composition phase diagram of PMN-xPT (the samples with concentrations $x = 0$; 0.1; 0.25 and 0.295 were investigated) where they showed that the 1st order phase transitions are terminated by the line of critical end points [41]. They concluded that the giant electromechanical response is closely related to this critical phenomenon. In the case of PMN-17PT (which lies between $x = 0.1$ and 0.25) the same conclusions should be applied as stated in the paper by Kutnjak et al. [41]. Kim et al. reported the temperature dependences of the dielectric permittivity under DC bias [26] which clearly shows a 1st order phase transition on the field-cooling and the zero-field cooling (ZFC).

The measurements of nonlinear susceptibility were performed in a zero field heating (ZFH) regime for both poled (we assume it is a monodomain state) and unpoled sample (Fig. 2). The poled sample clearly exhibit a sharp peak at around 330 K temperature indicating a 1st order phase transition. Above the phase transition temperature a diffuse decrease of χ_3 characteristic to relaxor phase is observed. It eventually converges to a ZFH curve of the unpoled sample at higher temperatures. The ZFC and ZFH curves of an unpoled sample show quite large hysteresis. The hysteresis can be observed in linear susceptibility as well. The most interesting fact is that the increase of χ_3 is much sharper during ZFH compared to a ZFC experiment. This might be the hint of slow spontaneous ordering and growth of PNRs to macroscopic ferroelectric domains in 300–340 K temperature region. This is the region where the critical slowing down is observed by the broadband dielectric spectroscopy [25].

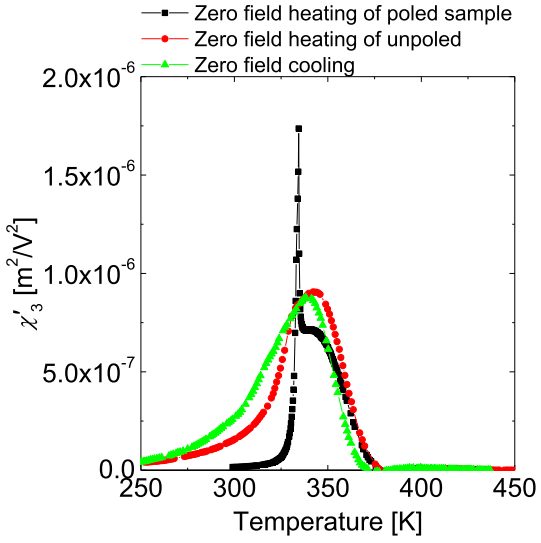

Fig. 2. Temperature dependence of the third order dielectric susceptibility.

3.2. Piezoelectric, ferroelectric and pyroelectric characterization

The nonlinear dielectric susceptibility experiments do not affect the structure of domains or PNRs since the probing electric field is much smaller than the coercive field of material under investigation. The most important feature of ferroelectrics is the possibility to switch the polarization. Thus, the investigation of polarization and strain hysteresis is mandatory to identify the ferroelectricity in the material. Fig. 3 represents hysteresis loops of PMN-17 PT at different temperatures. The sample was heated above the Burns temperature (600 K) and cooled down. The measurements were performed on heating cycle after ZFC. The ferroelectric hysteresis loop is observed at room temperature (the black curve represents the very first measurement after ZFC). This indicates that the ferroelectric phase in PMN-17PT condenses spontaneously on ZFC. The room temperature phase is non-cubic. One can argue that the ferroelectric phase is being induced by an external electric field. This phenomenon is well-known in the relaxor ferroelectrics. Our case does not show an electric field induced phase transition at room temperature. Only a single switching peak in the current-voltage characteristics is observed. In the case of electric field induced phase transition two peaks in current vs. voltage characteristics exist. The loop itself has a different shape (for example, compare hysteresis loops in PMN [42]). Furthermore, the strain vs. electric field has a piezoelectric character. The piezoelectricity cannot manifest in the cubic crystal so it is another justification of a non-centrosymmetric phase, since canonical relaxor ferroelectrics have an electrostrictive character at temperatures where the phase transition can be induced by an external electric field.

The temperature region in the vicinity of a permittivity maximum has rather slim polarization hysteresis loops. This interval also shows characteristic relaxor ferroelectric hysteresis loops where two peaks in voltamperic characteristics are observed. The electromechanical properties in this region show large hysteretic behaviour which is characteristic to an electric field induced phase transitions in relaxors. It also resembles electrostrictive behaviour. The highest temperature region shows the paraelectric behaviour in both polarization and strain hysteresis. The clear electrostrictive character is observed in the strain vs. field plot. This is usual behaviour for the cubic perovskite oxides.

Further investigations of polarization and strain hysteresis of the ZFC sample were carried out by applying unipolar electric field

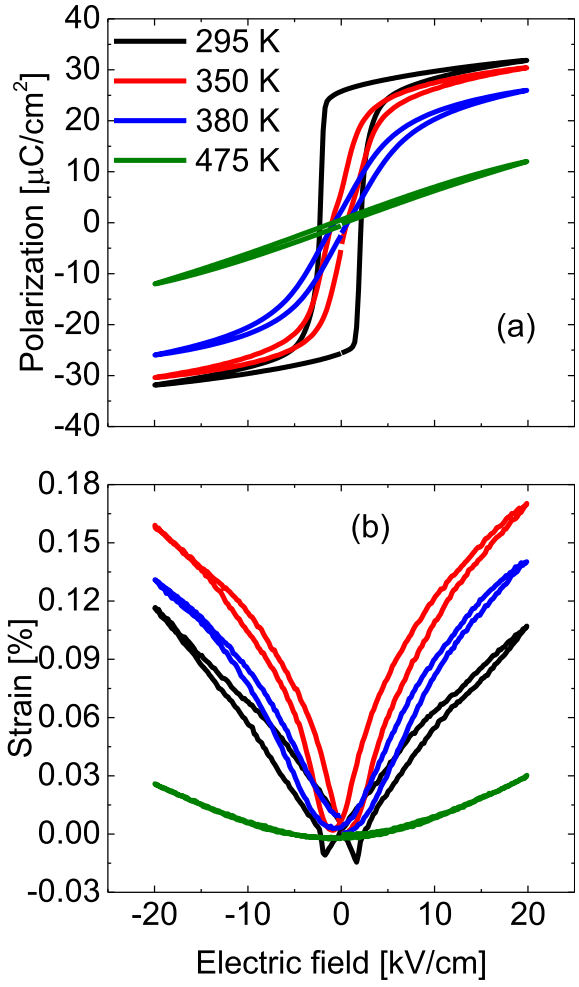

Fig. 3. Electric field dependence of polarization (a) and strain (b).

with a different amplitude in order to clarify the non-existence of an electric field induced phase transition. Fig. 4 represents the electric field dependence of polarization in PMN-17PT single crystal at 295 K. For the low electric field regime, the induced polarization should change linearly with the increase of an electric field. That was observed for the lowest amplitude curve, (initial and second curve after ZFC i. e.black and red curves). When the electric field of 1.5 kV/cm strength was applied, a nonlinear behaviour and an abrupt increase in maximum polarization was observed (see green curve in Fig. 4). The final curve (i. e. the largest amplitude, blue curve) again showed a nearly linear behaviour of polarization.

The change of induced polarization is steeper for the lower fields (i. e. below 1 kV/cm) compared to the highest field curve (≥ 2 kV/cm, blue curve). It might be related to the reversible (nano-) domain wall movement. The unpoled sample has many (nano-) domains and domain walls. These walls are very sensitive to an external electric field and thus can be moved easily. These kind of movements give a larger contribution to the induced polarization. Above the certain value of the electric field (> 1.5 kV/cm) the sample switches to a different kind of domain state. The field value of 1.5 kV/cm corresponds to the field value reported by Helal et al. where the single LA mode splits into two peaks [27]. They also reported another transition to macroscopic monodomain structure at higher fields, but it was not observed in our polarization experiment. We believe that the field of 1.5 kV/cm is sufficient for driving the sample to a single domain state. In this case the concentration of domain walls decreases drastically (or disappears completely). The absence of domain walls explains the change of slope of the induced polarization curve for monodomain sample. The contribution to the induced polarization solely comes from the lattice. This experimental result is a strong evidence that the phase transition is not being induced by the field but rather the field drives the sample to a single domain state.

Field dependence of electromechanical behaviour was investigated for a single domain sample. Fig. 5 represents the ratio of maximum strain to electric field amplitude. This ratio roughly represents the value of piezoelectric coefficient d_{33} (we will call this ratio as effective d_{33}) for certain amplitude of electric field E_{max} in a monodomain ferroelectric phase (black and blue curves in Fig. 5). The electric field dependence of effective d_{33} shows weak dependence on the electric field. This shows that there are no additional contributions to the strain and we can conclude that the poled sample is fully monodomain.

The electric field dependence of effective d_{33} becomes much more complicated above the 330 K. The function appears to have a maximum. This maximum is closely related to the electric field inducible phase transition. The long range ferroelectric order is lost above 330 K but still can be induced by an electric field. This is the true *E*-field inducible phase transition region in PMN-17PT and it

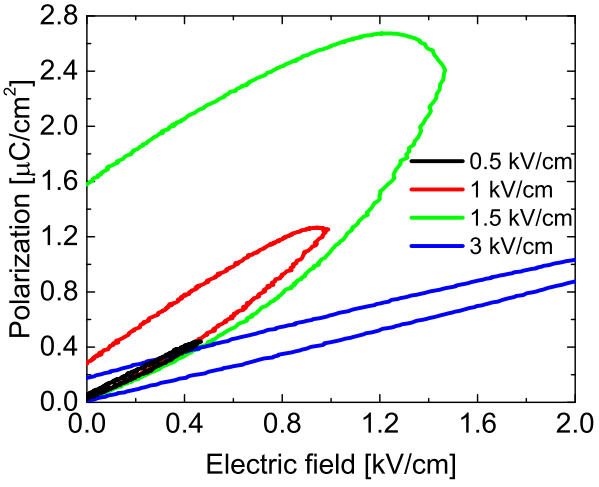

Fig. 4. Electric field dependence of polarization in PMN-17PT single crystal at 295 K temperature. Four consequent measurements were performed by increasing the amplitude of triangular pulse.

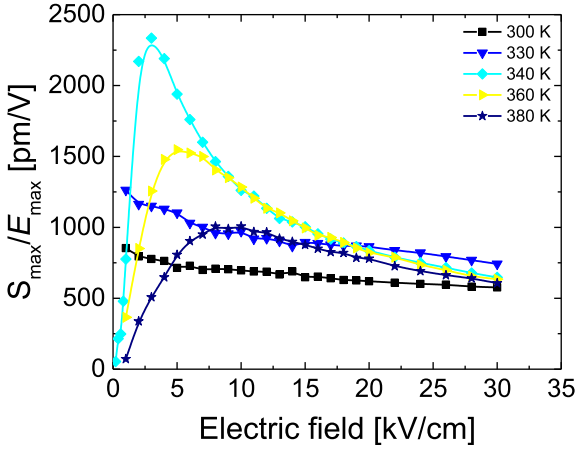

Fig. 5. Electric field dependence of effective d_{33} coefficient at different temperatures.

only appears above the 330 K. The strain vs. electric field has a different physical nature below and above this maximum. The strain at low field regime is due to the electrostriction. Above the maximum (after inducing ferroelectric phase), the electromechanical response can be considered as a piezoelectric effect. The convergence of the ratio S_{max}/E_{max} to the room temperature value (i. e. black curve) hints the same physical origin of the strain. The quadratic field dependence of strain at low fields (at low fields $P \sim E$) is evidenced in Fig. 6. The inset of Fig. 6 shows the linear behaviour of strain vs. square of polarization and unambiguously identifies the electrostrictive behaviour at the lowest field. The change of the slope can be observed at higher values of polarization. This is related to the electric field inducible phase transition and indicates the change of electromechanical response. Surprisingly, the dependence of strain is nearly linear at the highest fields. The strain at 340–400 K temperature interval can be described by two distinct electrostriction coefficients Q_{11}. One coefficient describes the region below E-field inducible phase transition and the other – above. The Q_{11} of high field region is larger by roughly 20% compared to the low field region. This is quite confusing result bearing in mind that ratio S_{max}/E_{max} at higher fields mimics the same behaviour as in a monodomain ferroelectric state. The *strain vs.* P^2 dependence suggests that the strain can be described by electrostrictive type behaviour in an E-field induced phase. The temperature dependence of small signal d_{33} and electrostriction coefficient Q_{11} is presented in the SUPPLEMENTARY MATERIAL (Fig. S1).

Temperature dependences of pyroelectric coefficient and remanent polarization are depicted in Fig. 7. The data which was obtained from the ferroelectric hysteresis loops (i. e. Fig. 2(a)) are consistent with the ones determined by the pyroelectric measurements. The poled PMN-17PT undergoes a first order phase transition. The abrupt polarization drop is observed at the temperatures which correlated with the permittivity maximum at low temperatures (see Fig. 1 (a)). Unfortunately, this temperature does not correlate with a critical slowing down temperature which was obtained from the dielectric spectra [25]. Furthermore, the phase transition peak of poled sample detected by the third order nonlinear susceptibility (Fig. 1 (c)) does not coincide with the pyrocoefficient peak (and the minima observed in longitudinal ultrasonic velocity – Fig. 8).

There was also an attempt to perform pyroelectric measurements for unpoled sample. The comparison of detected pyrocurrent

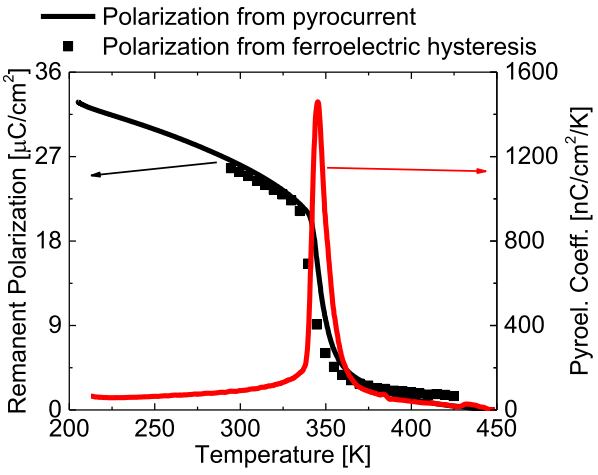

Fig. 7. Temperature dependence of remanent polarization and pyroelectric coefficient.

for both cases are represented in SUPPLEMENTARY MATERIAL (Fig. S2). Even in the unpoled sample the peak can be detected at the same temperatures as for the poled sample. Pyrocurrent measurements are very sensitive for the structural changes and the data on the unpoled sample supports the idea that the structural phase transition exists in PMN-17PT.

Above the 350 K temperature pyroelectric data show non-zero remanent polarization indicating that there are static PNRs which contribute to the pyrocurrent. The small remanent polarization above the permittivity peak maximum was observed in pure PMN [19] as well.

3.3. Ultrasonic properties

The temperature dependence of longitudinal ultrasonic velocity along pseudocubic [001] direction is depicted in Fig. 8. The minimum in the velocity indicates the presence of phase transition. The 10 MHz data correlates with the inelastic light scattering experiments. The minimum in both experiments are nearly at the same temperature [26]. Surprisingly, this result is nearly in agreement with the critical slowing down temperature which we obtained previously in these single crystals [25].

If we considered the phenomenological Landau theory, the ultrasonic data indicates that PMN-17PT single crystals have a linear

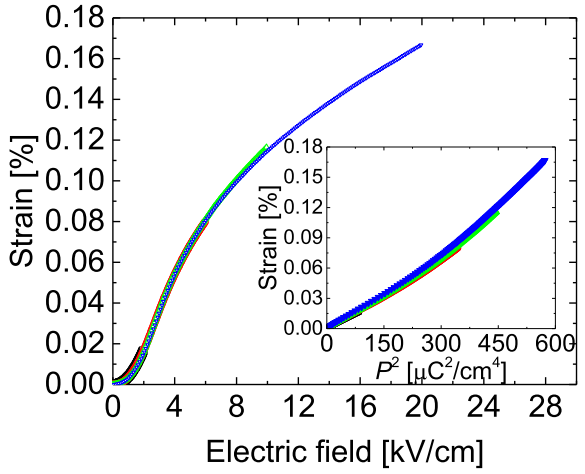

Fig. 6. Electric field dependence of strain at 360 K. The inset represents strain vs. the square of polarization curves.

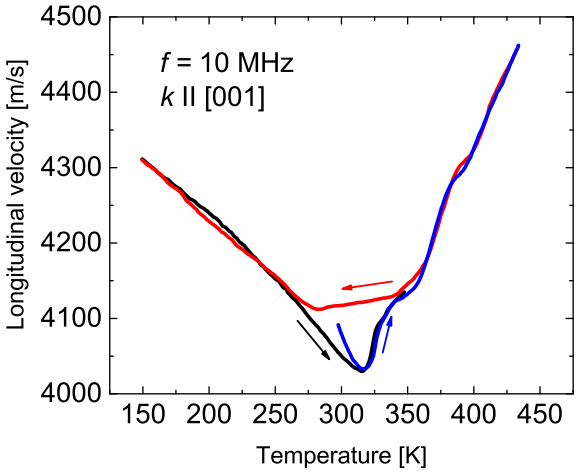

Fig. 8. Temperature dependence of longitudinal ultrasonic velocity on cooling and heating cycles.

coupling between order parameter and strain [43]. It is a significant indication of proper ferroelectric phase transition in this system. A very interesting feature can be observed on heating and cooling cycles of ultrasonic experiment. There is a significant thermal hysteresis associated to this anomaly. It is important to note that there is a time dependence of longitudinal velocity in the vicinity of the minimum. The cooling curve tends to relax to the heating curve. When the sample is cooled down way below the room temperature and then heated up, the initial temperature dependence is reproduced. If the sample is kept at room temperature, it slowly relaxes to the value corresponding to the heating curve. This is clearly related to some kind of slow kinetics of polar nano clusters under random fields. It hints that at room temperature the ferroelectric phase develops and PNRs might be nucleating to the larger sized domains. These larger domains persists at room temperature and can only be destroyed by heating the sample once again. This result is in agreement with the measurements of third order nonlinear susceptibility.

3.4. Peculiarities and the role of PNRs

Many experimental data were accumulated on the PMN-17PT single crystal. The dielectric data favours the relaxor picture since no well pronounced jump in temperature dependences of susceptibility can be observed. This means that the PNRs are still the key ingredient in the explanation of this anomaly. The role of PNRs in PMN-17PT above the maximum temperature T_m is probably the same as in pure PMN. Most of the experimental results are in agreement with this fact. Below the T_m, some mesoscale ordering takes place which stabilizes the ferroelectric phase. The PNRs become more correlated and thus sensitive to an external electric field. That is probably the reason why the normal hysteresis loops are observed at room temperature after ZFC. The time of flight ultrasonic experiments along with Brillouin scattering [26,27] hint that the ordering takes place at the mesoscale. Inelastic neutron scattering experiments also revealed anomalies in transverse acoustic phonon branches for PMN-20PT single crystals [44]. When the mesoscale order is broken, only pure relaxor properties persists. It might be the case that below ~330 K (the temperature below which the normal hysteresis can be observed) the coercive field of ferroelectric sublattice and the field required to induce ferroelectric order in relaxor sublattice coincide. We do not observe any double hysteresis loops. This means the PNRs and ferroelectric domains coexist below 330 K. PNRs can nucleate to normal domains with time and/or with the decrease of temperature.

4. Conclusions

The investigation of macroscopic properties in PMN-17PT single crystals were carried out. These experiments allowed us to obtain the information about the bulk of the sample. The presented data favours the idea that there is a spontaneous ferroelectric phase transition in PMN-17PT. The detailed investigation of electric field dependence of polarization and strain showed that the changes in the response of PMN-17PT single crystals are related to the nano-domain wall motion which can be switched off from the certain values of electric field (i. e. the sample becomes monodomain-like). The electric field dependence of effective d_{33} at room temperature (in poled sample) also supports the idea of a monodomain state.

Different experimental data revealed different temperatures which might be related to the phase transition. The investigation of a poled PMN-17PT single crystal revealed that the temperature around 330 K is related to the loss of a monodomain state (i. e. depolarization). This temperature is closely related to the critical slowing down identified by the broadband dielectric spectroscopy. From the order-disorder ferroelectric perspective, this might suggest that our system consists of different pseudospins which have a different length (probably can expand several unit cells). The spins (discrete polarization vectors of the PNRs/nanodomains) in the unpoled sample are randomly distributed and at least some of them are easily manipulated by an external electric field. They are responsible for the ferroelectricity in PMN-17PT.

These experiments also revealed a very slow growth of ferroelectric order after ZFC experiment. Further cooling far below the dielectric peak temperature enhances a ferroelectric phase which after heating persists at room temperature and can only be destroyed by a ZFH experiment at least up to 500 K. So, for the point of view of order-disorder phase transitions, it seems that the ordering in PMN-17PT is a very slow process.

Acknowledgements

This study was supported in part from JSPS Open Partnership Joint Research Projects No. 16039901 and by the Research Council of Lithuania (grant No. LJB-1/2016).

Appendix A. Supplementary data

Supplementary data related to this article can be found at https://doi.org/10.1016/j.jallcom.2018.03.130.

References

[1] V. Westphal, W. Kleemann, M.D. Glinchuk, Diffuse phase transitions and random-field-induced domain states of the "relaxor" ferroelectric $PbMg_{1/3}Nb_{2/3}O_3$, Phys. Rev. Lett. 68 (1992) 847–850, https://doi.org/10.1103/PhysRevLett.68.847.

[2] W. Kleemann, Random fields in relaxor ferroelectrics — a Jubilee review, J. Adv. Dielectr. 2 (2012) 1241001, https://doi.org/10.1142/S2010135X12410019.

[3] B. Noheda, D.E. Cox, G. Shirane, J. Gao, Z.-G. Ye, Phase diagram of the ferroelectric relaxor (1-x)$PbMg_{1/3}Nb_{2/3}$O3-x$PbTiO_3$, Phys. Rev. B 66 (2002), 054104, https://doi.org/10.1103/PhysRevB.66.054104.

[4] Z.-G. Ye, Y. Bing, J. Gao, A.A. Bokov, P. Stephens, B. Noheda, G. Shirane, Development of ferroelectric order in relaxor (1-x)$PbMg_{1/3}Nb_{2/3}O_3$-x$PbTiO_3$ (0<~x<~0.15), Phys. Rev. B 67 (2003), 104104, https://doi.org/10.1103/PhysRevB.67.104104.

[5] M. Ahart, M. Somayazulu, R.E. Cohen, P. Ganesh, P. Dera, H. Mao, R.J. Hemley, Y. Ren, P. Liermann, Z. Wu, Origin of morphotropic phase boundaries in ferroelectrics, Nature 451 (2008) 545–548, https://doi.org/10.1038/nature06459.

[6] S.W. Choi, T.R. Shrout, S.J. Jang, A.S. Bhalla, Morphotropic phase boundary in Pb ($Mg_{1/3}Nb_{2/3}$)O_3-$PbTiO_3$ system, Mater. Lett. 8 (1989) 253–255, https://doi.org/10.1016/0167-577X(89)90115-8.

[8] D.E. Cox, B. Noheda, G. Shirane, Y. Uesu, K. Fujishiro, Y. Yamada, Universal phase diagram for high-piezoelectric perovskite systems, Appl. Phys. Lett. 79 (2001) 400–402, https://doi.org/10.1063/1.1384475.

[9] T.R. Shrout, Z.P. Chang, N. Kim, S. Markgraf, Dielectric behavior of single crystals near the (1−x) Pb($Mg_{1/3}Nb_{2/3}$)O_3-(x) $PbTiO_3$ morphotropic phase boundary, Ferroelectrics Lett. 12 (1990) 63–69, https://doi.org/10.1080/07315179008201118.

[10] J.C. Ho, K.S. Liu, I.N. Lin, Study of ferroelectricity in the PMN-PT system near the morphotropic phase boundary, J. Mater. Sci. 28 (1993) 4497–4502, https://doi.org/10.1007/BF01154962.

[11] J. Han, W. Cao, Electric field effects on the phase transitions in [001]-oriented (1-x)Pb($Mg_{1/3}Nb_{2/3}$)O_3-x$PbTiO_3$ single crystals with compositions near the morphotropic phase boundary, Phys. Rev. B 68 (2003), 134102, https://doi.org/10.1103/PhysRevB.68.134102.

[12] N. de Mathan, E. Husson, G. Calvarn, J.R. Gavarri, A.W. Hewat, A. Morell, A structural model for the relaxor $PbMg_{1/3}Nb_{2/3}O_3$ at 5 K, J. Phys. Condens. Matter 3 (1991) 8159, https://doi.org/10.1088/0953-8984/3/42/011.

[13] G. Xu, D. Viehland, J.F. Li, P.M. Gehring, G. Shirane, Evidence of decoupled lattice distortion and ferroelectric polarization in the relaxor system PMN-xPT, Phys. Rev. B 68 (2003), 212410, https://doi.org/10.1103/PhysRevB.68.212410.

[14] B. Dkhil, J.M. Kiat, G. Calvarin, G. Baldinozzi, S.B. Vakhrushev, E. Suard, Local and long range polar order in the relaxor-ferroelectric compounds $PbMg_{1/3}Nb_{2/3}O_3$ and $PbMg_{0.3}Nb_{0.6}Ti_{0.1}O_3$, Phys. Rev. B 65 (2001), 024104, https://doi.org/10.1103/PhysRevB.65.024104.

[15] P.M. Gehring, W. Chen, Z.-G. Ye, G. Shirane, The non-rhombohedral low-temperature structure of PMN−10% PT, J. Phys. Condens. Matter. 16 (2004) 7113, https://doi.org/10.1088/0953-8984/16/39/042.

[16] A.K. Singh, D. Pandey, O. Zaharko, Powder neutron diffraction study of phase transitions in and a phase diagram of (1-x)[Pb($Mg_{1/3}Nb_{2/3}$)O_3]-$PbTiO_3$, Phys. Rev. B 74 (2006), 024101, https://doi.org/10.1103/PhysRevB.74.024101.
[17] V. Bovtun, S. Kamba, A. Pashkin, M. Savinov, P. Samoukhina, J. Petzelt, I.P. Bykov, M.D. Glinchuk, Central-peak components and polar soft mode in relaxor PbMg1/3Nb2/3O3 crystals, Ferroelectrics 298 (2004) 23–30, https://doi.org/10.1080/00150190490423057.
[18] V. Bovtun, S. Veljko, S. Kamba, J. Petzelt, S. Vakhrushev, Y. Yakymenko, K. Brinkman, N. Setter, Broad-band dielectric response of PbMg1/3Nb2/3O3 relaxor ferroelectrics: single crystals, ceramics and thin films, J. Eur. Ceram. Soc. 26 (2006) 2867–2875, https://doi.org/10.1016/j.jeurceramsoc.2006.02.003.
[19] D. Viehland, S.J. Jang, L.E. Cross, M. Wuttig, Freezing of the polarization fluctuations in lead magnesium niobate relaxors, J. Appl. Phys. 68 (1990) 2916–2921, https://doi.org/10.1063/1.346425.
[20] A. Levstik, Z. Kutnjak, C. Filipič, R. Pirc, Glassy freezing in relaxor ferroelectric lead magnesium niobate, Phys. Rev. B 57 (1998) 11204–11211, https://doi.org/10.1103/PhysRevB.57.11204.
[21] D. Viehland, M. Wuttig, L.E. Cross, The glassy behavior of relaxor ferroelectrics, Ferroelectrics 120 (1991) 71–77, https://doi.org/10.1080/00150199108216802.
[22] I. Rychetský, S. Kamba, J. Petzelt, Constant dielectric losses in PLZT relaxor at low temperatures, Ferroelectrics 291 (2003) 83–91, https://doi.org/10.1080/00150190390222574.
[23] J. Banys, R. Grigalaitis, A. Mikonis, J. Macutkevic, P. Keburis, Distribution of relaxation times of relaxors: comparison with dipolar glasses, Phys. Status Solidi C 6 (2009) 2725–2730, https://doi.org/10.1002/pssc.200982529.
[24] R. Grigalaitis, J. Banys, A. Sternberg, K. Bormanis, V. Zauls, Dynamics of polar clusters in PMN ceramics: comparison with PMN single crystal, Ferroelectrics 340 (2006) 147–153, https://doi.org/10.1080/00150190600889221.
[25] Š. Svirskas, J. Banys, S. Kojima, Broadband dielectric spectroscopy of Pb-based relaxor ferroelectric (1-x)Pb(Mg1/3Nb2/3)O3-xPbTiO3 with intermediate random fields, J. Appl. Phys. 121 (2017), 134101, https://doi.org/10.1063/1.4979729.
[26] T.H. Kim, S. Kojima, J.-H. Ko, Electric field effects on the dielectric and acoustic anomalies of Pb[(Mg1/3Nb2/3)0.83Ti0.17]O3 single crystals studied by dielectric and Brillouin spectroscopies, Curr. Appl. Phys. 14 (2014) 1643–1648, https://doi.org/10.1016/j.cap.2014.09.014.
[27] M.A. Helal, M. Aftabuzzaman, S. Svirskas, J. Banys, S. Kojima, Temperature evolution of central peaks and effect of electric field in relaxor ferroelectric 0.83Pb(Mg1/3Nb2/3)O3–0.17PbTiO3 single crystals, Jpn. J. Appl. Phys. 56 (2017) 10PB03, https://doi.org/10.7567/JJAP.56.10PB03.
[28] A. Slodczyk, P. Daniel, A. Kania, Local phenomena of (1-x)$PbMg_{1/3}Nb_{2/3}O_3$-x$PbTiO_3$ single crystals ($0 \leq x \leq 0.38$)$ studied by Raman scattering, Phys. Rev. B 77 (2008), 184114, https://doi.org/10.1103/PhysRevB.77.184114.
[29] A. Slodczyk, A. Kania, P. Daniel, A. Ratuszna, Structural, vibrational and dielectric studies of 0.91PMN–0.09PT single crystals, J. Phys. Appl. Phys. 38 (2005) 2910, https://doi.org/10.1088/0022-3727/38/16/025.
[30] N. Setter, What is a ferroelectric—a materials designer perspective, Ferroelectrics 500 (2016) 164–182, https://doi.org/10.1080/00150193.2016.1232104.
[31] H. Luo, G. Xu, H. Xu, P. Wang, Z. Yin, Compositional homogeneity and electrical properties of lead magnesium niobate titanate single crystals grown by a modified Bridgman technique, Jpn. J. Appl. Phys. 39 (2000) 5581, https://doi.org/10.1143/JJAP.39.5581.
[32] S. Miga, J. Dec, W. Kleemann, Computer-controlled susceptometer for investigating the linear and nonlinear dielectric response, Rev. Sci. Instrum. 78 (2007) 033902, https://doi.org/10.1063/1.2712792.
[33] D. Jablonskas, M. Ivanov, R. Grigalaitis, J. Banys, Implementation of an improved non-linear susceptometer, Ferroelectrics 513 (2017) 32–37, https://doi.org/10.1080/00150193.2017.1350071.
[34] B.A. Strukov, A.P. Levanyuk, Ferroelectric Phenomena in Crystals, first ed., Springer-Verlag, Berlin, 1998.
[35] V. Samulionis, Š. Svirskas, J. Banys, A. Sánchez-Ferrer, S.J. Chin, T. McNally, Ultrasonic properties of composites of polymers and inorganic nanoparticles, Phys. Status Solidi A 210 (2013) 2348–2352, https://doi.org/10.1002/pssa.201329294.
[36] J. Dec, S. Miga, W. Kleemann, Ferroelectric phase transitions viewed via nonlinear dielectric response, Ferroelectrics 417 (2011) 82–92, https://doi.org/10.1080/00150193.2011.578500.
[37] J. Dec, S. Miga, W. Kleemann, B. Dkhil, Nonlinear dielectric properties of PMN relaxor crystals within landau-Ginzburg-Devonshire approximation, Ferroelectrics 363 (2008) 141–149, https://doi.org/10.1080/00150190802025947.
[38] S. Miga, J. Dec, W. Kleemann, Non-linear dielectric response of ferroelectrics, relaxors and dipolar glasses, in: M. Lallart (Ed.), Ferroelectr. - Charact. Model., InTech, 2011. http://www.intechopen.com/books/ferroelectrics-characterization-and-modeling/non-linear-dielectric-response-of-ferroelectrics-relaxors-and-dipolar-glasses. (Accessed 23 April 2014).
[39] M. Iwata, T. Ido, R. Nagahashi, Y. Ishibashi, Nonlinear dielectric susceptibility in relaxor ferroelectrics Pb(Zn1/3Nb2/3)O3-PbTiO3, Ferroelectrics 498 (2016) 52–61, https://doi.org/10.1080/00150193.2016.1170420.
[40] E.H. Kisi, J.S. Forrester, The phase transition sequence in the relaxor ferroelectric PZN–8% PT, J. Phys. Condens. Matter. 20 (2008), 165208, https://doi.org/10.1088/0953-8984/20/16/165208.
[41] Z. Kutnjak, J. Petzelt, R. Blinc, The giant electromechanical response in ferroelectric relaxors as a critical phenomenon, Nature 441 (2006) 956–959, https://doi.org/10.1038/nature04854.
[42] D. Fu, H. Taniguchi, M. Itoh, S. Koshihara, N. Yamamoto, S. Mori, Relaxor $Pb(Mg_{1/3}Nb_{2/3})O_3$: a ferroelectric with multiple inhomogeneities, Phys. Rev. Lett. 103 (2009), 207601, https://doi.org/10.1103/PhysRevLett.103.207601.
[43] W. Rehwald, The study of structural phase transitions by means of ultrasonic experiments, Adv. Phys. 22 (1973) 721–755, https://doi.org/10.1080/00018737300101379.
[44] T.Y. Koo, P.M. Gehring, G. Shirane, V. Kiryukhin, S.-G. Lee, S.-W. Cheong, Anomalous transverse acoustic phonon broadening in the relaxor ferroelectric $Pb(Mg_{1/3}Nb_{2/3})_{0.8}Ti_{0.2}O_3$, Phys. Rev. B 65 (2002), 144113, https://doi.org/10.1103/PhysRevB.65.144113.